Entrained Flow Gasification of Victorian Brown Coals using CO_2 as Reactant

Tao Xu

Supervisors: Prof. Sankar Bhattacharya
Prof. Dr.-Ing. Klaus R.G. Hein

This thesis is presented in partial fulfilment for the degree of
Doctor of Chemical Engineering
at Monash University

September 2017

Statement of Authorship

List of Publications

Publications published or submitted to date from the project include:

Journal Papers

1. T. Xu, S.C. Srivatsa, S. Bhattacharya, In-situ synchrotron IR study on surface functional group evolution of Victorian and Thailand low-rank coals during pyrolysis. J Anal Appl Pyrolysis. 2016; 122:122-130.
2. P.P. Sripada, Xu, T., M. Kibria, S. Bhattacharya, Comparison of entrained flow gasification behaviour of Victorian brown coal and biomass. Fuel, 2016; 203:942-953.
3. T. Xu, and S. Bhattacharya, Entrained-flow Gasification of Victorian brown coals and chars using CO_2: gasification behaviour and pollutant gas emission, Applied Energy, 2017. (submitted to the Journal)
4. T. Xu, and S. Bhattacharya, Entrained flow gasification behaviour of Victorian Brown coal char at low temperatures, Fuel, 2017 (submitted to the Journal)

Conference Papers

1. T. Xu, and S. Bhattacharya, Entrained flow gasification behaviour of Victorian Brown coal at low temperatures, in The 40th International Technical Conference on Clean Coal & Fuel Systems 2015: Clearwater, Florida, USA.
2. T. Xu, and S. Bhattacharya, Entrained flow pyrolysis and gasification of Victorian Brown coal, in International Conference on Coal Science & Technology 2015 (ICCST & 2015), Melbourne, Australia.
3. T. Xu, and S. Bhattacharya, A study on Entrained Flow Gasification of Victorian Brown Coal, in 5th Annual Monash University Chemical Engineering Conference 2015

Thesis including published works declaration

I hereby declare that this thesis contains no material which has been accepted for the award of any other degree or diploma at any university or equivalent institution and that, to the best of my knowledge and belief, this thesis contains no material previously published or written by another person, except where due reference is made in the text of the thesis.

This thesis includes two original papers published in peer reviewed journals and two unpublished publications. The core theme of the thesis is entrained flow gasification. The ideas, development and writing up of all the papers in the thesis were the principal responsibility of myself, the student, working within the Chemical Engineering under the supervision of Prof. Sankar Bhattacharya.

In the case of chapter 4-6 and chapter 8, my contribution to the work involved the following:

Thesis Chapter	**Publication Title**	**Status** *(published, in press, accepted or returned for revision)*	**Nature and % of student contribution**	**Co-author name(s) Nature and % of Co-author's contribution***	**Co-author(s), Monash student Y/N***
4	In-situ synchrotron IR study on surface functional group evolution of Victorian and Thailand low-rank coals during pyrolysis	Published	70%, Concept and collecting data and data analysis and writing first draft	1) Srikanth Chakravatula Srivatsa, input into manuscript 10% 2) Sankar Bhattacharya, input into manuscript and editing 20%	Yes Yes
5	Entrained flow gasification behaviour of Victorian brown coal char at low temperatures	submitted	80%, Concept and collecting data and data analysis and writing first draft	1) Sankar Bhattacharya, input into manuscript and editing 20%	Yes
6	Entrained flow gasification of	submitted	80%, Concept and collecting data and	1) Sankar Bhattacharya, input	Yes

	Victorian brown coals using CO_2: gasification behaviour and pollutant gas emission		data analysis and writing first draft	into manuscript and editing 20%	
8	Comparison of entrained flow gasification behaviour of Victorian brown coal and biomass	Published	35%, Concept and collecting data and data analysis and writing first draft	1) Pavan Pramod Sripada, input into manuscript 35% 2) M.A. Kibria, input into manuscript 10% 3) Sankar Bhattacharya, input into manuscript and editing 20%	Yes Yes Yes

I have not renumbered sections of submitted or published papers in order to generate a consistent presentation within the thesis.

Student signature:  **Date: 10/09/2017**

The undersigned hereby certify that the above declaration correctly reflects the nature and extent of the student's and co-authors' contributions to this work. In instances where I am not the responsible author I have consulted with the responsible author to agree on the respective contributions of the authors.

Main Supervisor signature:  **Date: 17/09/2017**

Acknowledgements

Firstly, I acknowledge my supervisor, Professor Sankar Bhattacharya, for his guidance and support throughout the research project. His knowledge and feedback have been extremely useful in helping me to construct my experimental plan and final thesis, in addition to preparing us with essential skills that would be helpful for our future careers. He has been caring, wise, friendly and supportive, and my debt to him is enormous. I also gratefully acknowledge the support from China Scholarship Council (CSC), Brown Coal Innovation Australia (BCIA), and Monash University for their various contribution to this project.

Colleagues in schools and Chemical Engineering department have had a huge influence on my career, which is reflected in this study. In particular, I would acknowledge Joanne Tanner, Srikanth Chakravartula Srivatsa, and Kim Phu, who gave me a lot of valuable guildance and training on my project; Pavan Pramod Sripada, Mahmud Kibria, Xiaocheng Lin, and Yang Wang. Their wisdom, support, guidance and friendship over the years have been most important.

I would also like to thank Jane Moodie for her teaching and guidance on research writing. Jane also helped me proofread and edit my research papers and thesis. I have learnt so much on academic writing from her.

I have always valued the contribution of my parents, Xiangchun Xu and Wei Zhang, who made enormous sacrifices to give me the best education when I was younger, and for their unconditional love and support at all stages of my career.

Abstract

Victoria has abundant brown coal resource, but they are mainly used for mine-mouth power generation units with very low efficiency and high greenhouse gas emissions. Entrained flow gasification is a technology with great potential for Victorian brown coal utilization to produce high-value products. However, little is known about entrained flow gasification of Victorian brown coal. Therefore, the major objective of this study is to obtain a better understanding of entrained flow gasification of Victorian brown coal with CO_2 using different experimental and modelling approaches. The focus of this research is to examine:

1) the effect of a wide range of operational variables on gasification performance and emission of air pollutants,
2) the mineral transformation during coal pyrolysis and char gasification,
3) a comparison of entrained flow gasification behaviour of Victorian brown coal and biomass,
4) the kinetic modelling of char-CO_2 gasification of Victorian brown coal.

The experimental gasification work was performed with CO_2 using two entrained flow reactors (EFR), a low temperature reactor (up to 1000 °C) and a high temperature reactor (up to 1650 °C). The entrained flow gasification behaviour was examined, in particular, gasification performance (carbon conversion and gas composition) and the emission of air pollutants (H_2S, HCN, and NH_3). The mineral transformation was also investigated by measuring the char and gasification residue obtained from the experiments with XRD and SEM-EDX instruments.

The effect of five main factors (total gas flow rate, residence time, temperature, CO_2 concentration, and gasification process) on entrained flow gasification behaviour was investigated. All five factors had a significant effect on the gasification performance. The total gas flow rate significantly affected the gas velocity in the reactor and therefore influenced the gasification performance by changing the mode of gas-particle contact from gas-controlled entrained flow to solid-controlled falling flow. It was found that gasification under entrained flow condition achieved better gasification performance than gasification under falling flow condition. The longer residence time also improved gasification performance. At 1000 °C, the residence time of Victorian brown coal (Yallourn and Morwell) for complete carbon conversion was found to be around 20 s. This indicates that entrained flow gasification of Victorian brown coal should be undertaken above 1000 °C. Moreover, both the higher temperature and higher CO_2 concentration improved the gasification performance. Interestingly, higher temperature increased the H_2S and HCN emissions, but higher CO_2 concentration decreased

H_2S and HCN emissions. The different gasification processes, direct and two-step gasification, had little effect on the carbon conversion but had a strong effect on gas composition. Compared to two-step gasification, direct gasification generated little CH_4 and more CO because of the reverse water-shift reaction. It is clear that 1200 °C is sufficient to achieve high carbon conversion (~98%) for the Victorian brown coals (Yallourn, Loy Yang, and Maddingley) tested in this study for gasification using CO_2 up to 40% concentration.

Mineral transformations during coal pyrolysis and char gasification were observed at high temperatures between 1000 °C and 1400 °C. In addition, mineral transformation during coal pyrolysis and char gasification varied for parent coals (Yallourn, Loy Yang, and Maddingley). The decomposition of $CaSO_4$ and the formation of Fe_3O_4/ $MgFe_2O_4$ were found in Maddingley and Yallourn coal. Loy Yang coal mainly had one major mineral phase, quartz, and had no significant mineral transformation during coal pyrolysis and char gasification.

Victorian brown coals are low-rank fuels. Therefore, entrained flow gasification of one Victorian brown coal (Loy Yang) was compared with that of another low-rank fuel - a biomass (pine bark) - by direct gasification of the fuels. The Loy Yang coal and pine bark were found to have similar carbon conversion (>95%) at 1200 °C. The product gas of the two fuels was CO-rich because of the Boudouard reaction, and Loy Yang coal achieved higher H_2 and CO concentration than pine bark. The pollutant gas emission varied for the fuels. No NH_3 was observed for Victorian brown coal and no H_2S was observed for pine bark during entrained flow gasification in CO_2.

Kinetic modelling of Victorian brown coals (Yallourn and Maddingley) was investigated using thermo-gravimetric analyser and EFR data. A modified volumetric model was validated for Victorian brown coals by fitting the TGA data, and it was used to calculate the kinetic parameters. Using the kinetic parameters, a mathematical equation was developed for predicting the carbon conversion of Victorian brown coal chars at 1000-1400 °C. It showed good agreement with the experimental EFR data at high temperature.

This study presents a comprehensive investigation on entrained flow gasification of Victorian brown coal with CO_2. It offers an important understanding of the effects of operational variables on gasification performance, the emission of air pollutants, and mineral transformation during entrained flow gasification. The information generated in this study will advance the development of Victorian brown coal gasification for commercial applications.

Table of Contents

List of Abbreviations

ASAP	Accelerated Surface Area and Porosimetry analyzer
A-PFBC	Advanced Pressurized Fluidized Bed Combustion
BCIA	Brown Coal Innovation Australia
BET	Brunauer-Emmett-Teller
BGL	British Gas Lurgi
BSEM	Back-Scattered Electron Microscopy
CFD	Computational Fluid Dynamics
CHNS	Carbon Hydrogen Nitrogen Sulfur
CRC	Cooperative Research Centre
DAEM	Distributed Activation Energy Model
DTF	Drop Tube Reactor
EERC	Energy and Environmental Research Center
EDX	Energy dispersive X-ray analysis
EFR	Entrained Flow Reactor
FTIR	Fourier Transform Infrared Spectrometer
GC-MS	Gas Chromatograph with Mass Spectrometry
GM	Grain Model
HTW	High Temperature Winkler
IEA	International Energy Agency
IRM	Infrared Microspectroscopy
IDGCC	Integrated Drying and Gasification Combined-Cycle
IGCC	Integrated Gasification Combined Cycles
LY	Loy Yang
MD	Maddingley
MVM	Modified Volumetric Model
RPM	Random Pore Model
SEM	Scanning Electron Microscopy
TGA	Thermogravimetric Analyzer/Analysis
VM	Volumetric Model
XRD	X-Ray Diffraction
XRF	X-Ray Fluorescence
YL	Yallourn

List of Figures

List of Tables

Chapter 1 Introduction

A comprehensive study of entrained flow gasification of Victorian brown coals is presented in this thesis. In this chapter, an overview of the research problem is introduced, the objectives of the study are stated, and the structure of the thesis is outlined.

Overview of the research problem

Brown coal, often referred to as lignite in the literature, is considered as the lowest rank coal among different coals. Low-rank coals account for 28% of the coal reserve worldwide. In Australia, Victorian brown coal represents a significant, low cost energy resource but its use is limited to mine-mouth power generation at relatively low efficiencies and large green house emission. Therefore, there is great interest in the assessment and development of alternative utilisation strategies for this vast resource.

Gasification is a feasible technology with great potential for Victorian brown coal utilization towards high-value products. Gasification is a thermochemical conversion process which is divided into two fundamental processes: coal pyrolysis and char gasification. Gasification can convert coal to syngas by reacting the coal with gasifying agents such as air, oxygen, steam, and carbon dioxide. Moreover, the syngas obtained from gasification has numerous of applications such as producing fuels and chemicals. The low cost of Victorian brown coal has seen much of the interest focus on conversion of these coals via gasification to liquid fuels and chemicals.

Commercial gasification technologies can be divided into three major types: fixed bed gasifiers, fluidised bed gasifiers, and entrained flow gasifiers. Of these types, entrained flow gasifiers are the most attractive for commercial plants because of their flexibility in feedstock handling and high gasification efficiency. In particular, for syngas production, the entrained flow gasifiers dominate the world market, compared to the other two gasifier types. However, scientific and technical information on the entrained flow gasification of brown coal is scarce in the public domain.

Kinetic data of coal/ char gasification is required to understand the physical and chemical process during the reaction that will enable the design of coal gasifiers. The kinetic data also can be used in reaction models for analysing the gasification rate, this is much required for gasifier design. There is very limited kinetic data available for Victorian brown coal gasification. Only one study [1] has reported kinetic data of CO_2 and steam gasification of Victorian brown coals using random pore

model. Nonetheless, it is limited to one reaction model and the validity of the kinetic data for entrained flow gasification is still unknown.

There have been few studies (small to pilot scale) into the gasification of Victorian brown coal. Most laboratory scale gasification studies have mainly focused on the effect of alkali and alkaline earth metals on pyrolysis and gasification using fixed bed and fluidised bed reactors [2-5]. Pilot scale studies were carried out at low temperatures using the fluidised-bed and transport gasifiers, resulting in low carbon conversion and poor gas quality. Few studies have investigated the entrained flow gasification behaviour of Victorian brown coal using CO_2 as reactant through two-step gasification (pyrolysis followed by gasification of char) [6]. It was found that no tar was detected at high temperature pyrolysis and gasification, and gas yield of CO and H_2 increased with increasing temperature and CO_2 concentration. However, these studies are limited to one Victorian brown coal (Morwell) and two step gasification. The effect of another gasification process, direct gasification, and residence time on the gasification behaviour of Victorian brown coals is still unknown. The behaviour of mineral matters during pyrolysis and gasification is also unclear. Moreover, Victorian brown coal and biomass are both known as low rank fuel, but their differences in entrained flow gasification behaviour have not been investigated.

Objectives of the research

This thesis is a significant extension of the previous work carried out at Monash University on gasification of Victorian brown coal. One main objective of this research is, therefore, to expand entrained flow gasification data for Victorian brown coal in CO_2 and deepen the understanding of mineral transformation during gasification process. The specific objectives of this research are:

- to identify the evolution of functional groups in Victorian brown coal during the initial step of gasification-coal pyrolysis;
- to understand the effect of five main operational variables (total gas flow rate, residence time, temperature, CO_2 concentration, and gasification processes) on gasification performance (carbon conversion and gas composition) and emission of gas pollutants (HCN, NH_3 and H_2S) during entrained flow gasification;
- to identify the mineral transformation of Victorian brown coals during entrained flow pyrolysis and gasification over a wide range of temperatures from low (700 ^oC) to high (1400 ^oC);

- to understand the similarities and differences of entrained flow gasification behaviour of Victorian brown coal and biomass with respect to gasification performance, emission of gas pollutants, and mineral transformation;
- to develop a mathematical model for predicting the carbon conversion of Victorian brown coal during CO_2 gasification.

Structure of the thesis

This thesis describes the experimental and modelling work carried out to achieve these objectives. In this thesis, an overview of brown coal resources and properties, gasification background, and gasifier technologies, and a review of recent research into Victorian brown coal gasification are presented in Chapter 2. In Chapter 3, the sample properties and preparation used in this study are introduced, the experimental setups of pyrolysis and gasification studies are outlined, and the analysis methods of gasification behaviour and coal/char samples are described.

Chapter 4 presents the experimental results of the changes of functional groups of Victorian brown coal during coal pyrolysis obtained using in-situ synchrotron IR.

Chapters 5 and 6 present the results of an experimental investigation into the effect of total gas flow rate, residence time, temperature, CO_2 concentration, and gasification processes (direct using coal vs two-step by first pyrolysing the coal and then gasifying the char) on the gasification performance and the emission of gas pollutants of Victoria brown coals during entrained flow gasification.

Chapter 7 presents the results of an experimental investigation into mineral transformations of Victorian brown coals during pyrolysis and gasification obtained through XRD measurements for the chars and gasification residues collected from low temperature and high temperature entrained flow gasification experiments.

Chapter 8 presents a comparison of entrained flow gasification behaviour of Victorian brown coal and biomass in terms of gasification performance, emission of gas pollutants, and mineral transformation through direct gasification.

Chapter 9 presents the results of the kinetic modelling of char-CO_2 gasification of Victorian brown coals, and contains a comparison of the modelling results and entrained flow gasification results.

Chapter 10 presents the major findings obtained in this study, and provides recommendations for future work.

The structures and objectives of this thesis are presented in Figure 1.1.

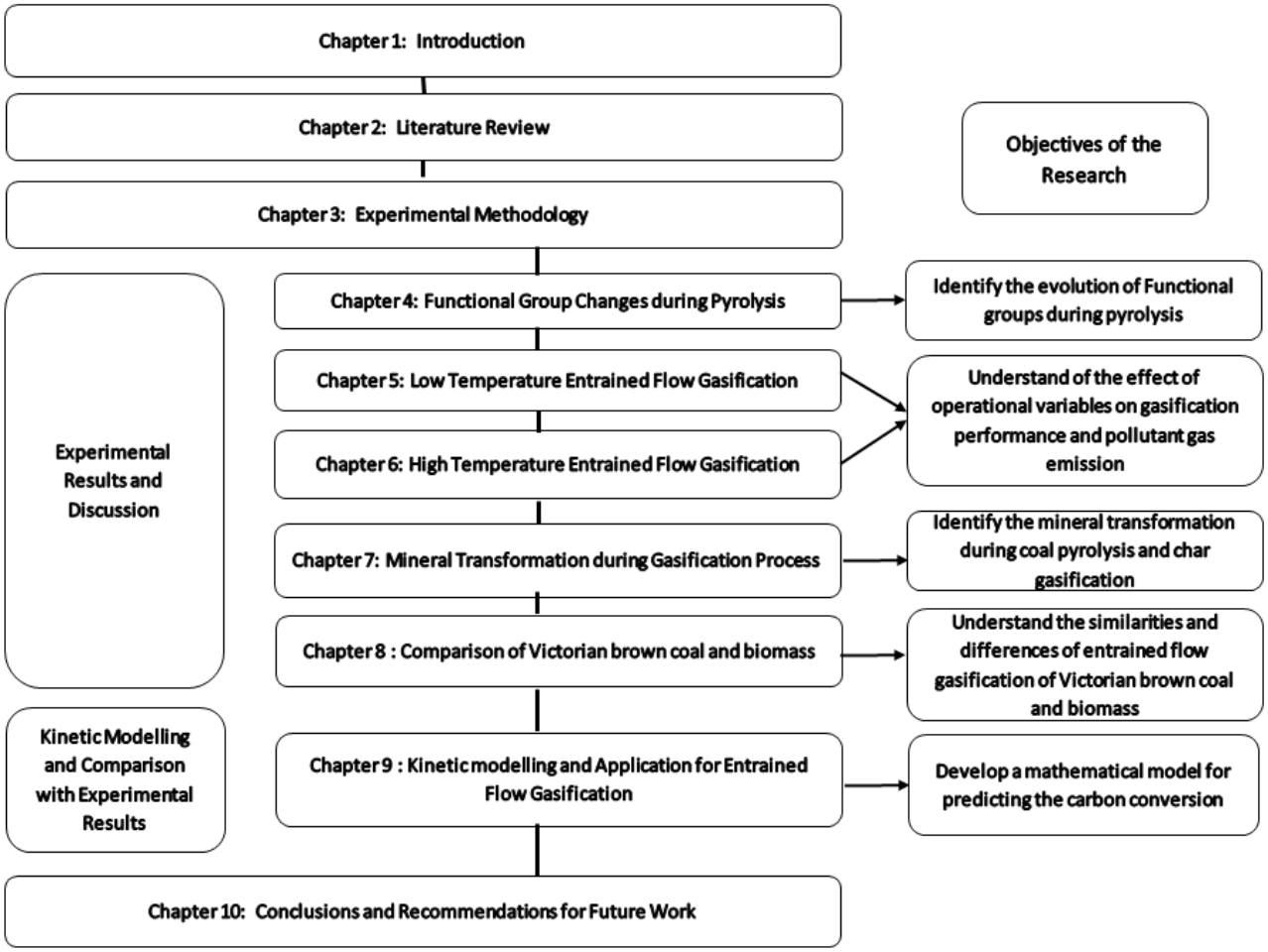

Figure 1.1: An overview chart of the thesis

Chapter 2 Literature review

Gasification is a thermochemical conversion process which can turn low-value feedstocks into high-value products. In practice, the use of CO_2 as gasifying agent is of interest as this has several advantages:

1) It can lower or avoid using steam which is expensive to produce;
2) The H_2/CO ratio in fuel gases can be easily adjusted to meet the specific requirement for chemical or fuel synthesis;
3) The gasification of CO_2, instead of air, can lead to flue gas with high percentage of CO_2, which is suitable for direct recovery and recycle of CO_2.

However, the reaction of CO_2 with carbon is highly endothermic, and therefore energy has to be supplied by partial combustion of carbon which will require some oxygen to be fed. The use of CO_2 allows the production of high-value products such as platform chemicals or fuels.

This chapter presents the background of this project and relevant previous studies. Firstly, the target of the project, brown coal, and the background of coal gasification are introduced. The gasification technologies for brown coal and kinetic studies of brown coal/char gasification with CO_2 are then described. The recent research into Victorian brown coal is also summarized. Moreover, current development of Victorian brown coal gasification is analysed.

2.1 Global and Victorian brown coal

This section briefly describes the quantity and quality of brown coal worldwide and in Australia.

2.1.1 Brown coal worldwide

Brown coal, often referred to as lignite in the literature, is considered as the lowest rank coal among different coals. Currently, brown coal is used primarily for electricity generation, but its use for other applications is expected to increase in the future because it does have a number of advantages over black coal. These advantages include low mining cost, high amount of volatiles, high reactivity, and low pollution-forming impurities such as sulphur, nitrogen, and heavy metals [7].

According to the BP Statistical Review of World Energy in 2017, there are 323 billion tons of brown coal reserves left, accounting for 28% of the coal reserve worldwide [8]. Current world brown coal reserves is sufficient to meet 153 years of global production based on current production rate 1024 million tonnes/ year. By country (Figure 2.1), 28.1% of worldwide brown coal reserves are located in

Russia (90.7 billion tonnes), 23.7% (76.5 billion tonnes) in Australia, 11.2% (36.2 billion tonnes) in Germany, 9.3% (30.1 billion tonnes) in US, 4.3% in the China (14 billion tonnes), 3.3% (10.9 billion tonnes) in Turkey, 2.5% (8.2 billion tonnes) in Indonesia, with 17.4% in the other countries [8]. It is evident that Australia has the second largest brown coal reserves in the world, and approximately 97% of its total brown coal resources are located in Victoria [9], as shown in Figure 2.2. The properties of Victorian brown coal are presented in the next section.

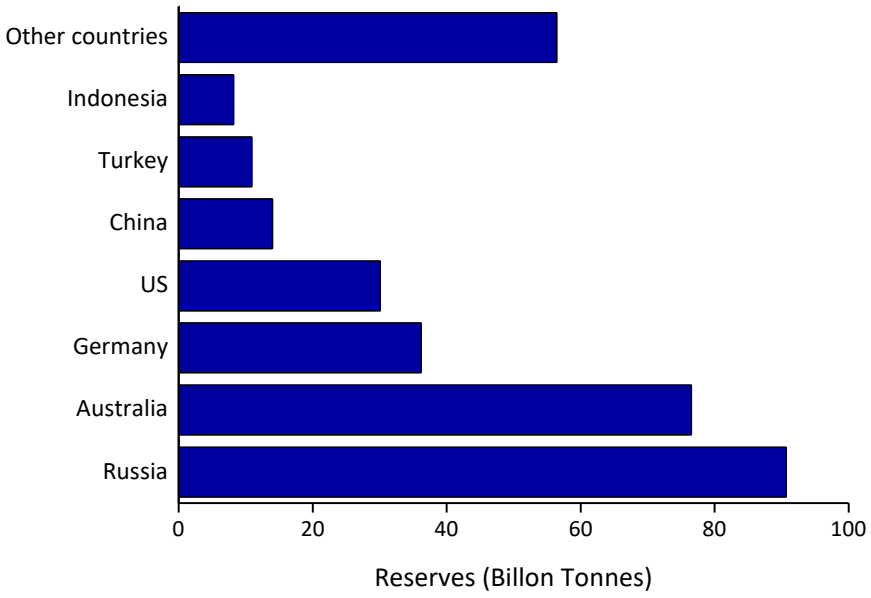

Figure 2.1: Distribution of proven reserves of brown coal worldwide 2017 by country [8]

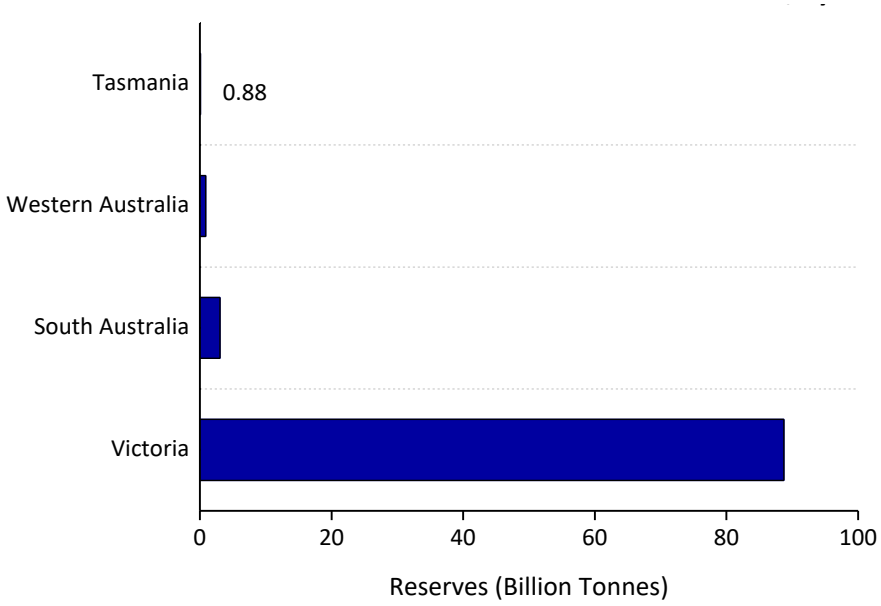

Figure 2.2: Distribution of brown coal reserves in Australia 2012 by state [9]

2.1.2 Victorian brown coal

Brown coal in the state of Victoria, Australia, is distributed in three major basins of the Latrobe Valley: the Murray Basin, Otway Basin and Gippsland Basin, as shown in Figure 2.3. The brown coal reserves in the Murray and Otway Basins are 19.6 and 15.5 billion tons, respectively. The Gippsland Basin is much larger than the other two, with an estimated reserve of 65 billion tons brown coal, which is account for more than 80% of Victoria's resource [10]. Seams of brown coal in the Gippsland basin are typically located under only 10-20 meters of overburden. The favourable lignite to overburden ratios in the Gippsland basin are between 0.5: 1 and 5:1, which indicates a high tonnage of resource for every cubic meter of non-coal material mined. This combines with easy digging characteristics, making it some of the lowest cost coal in the world [11].

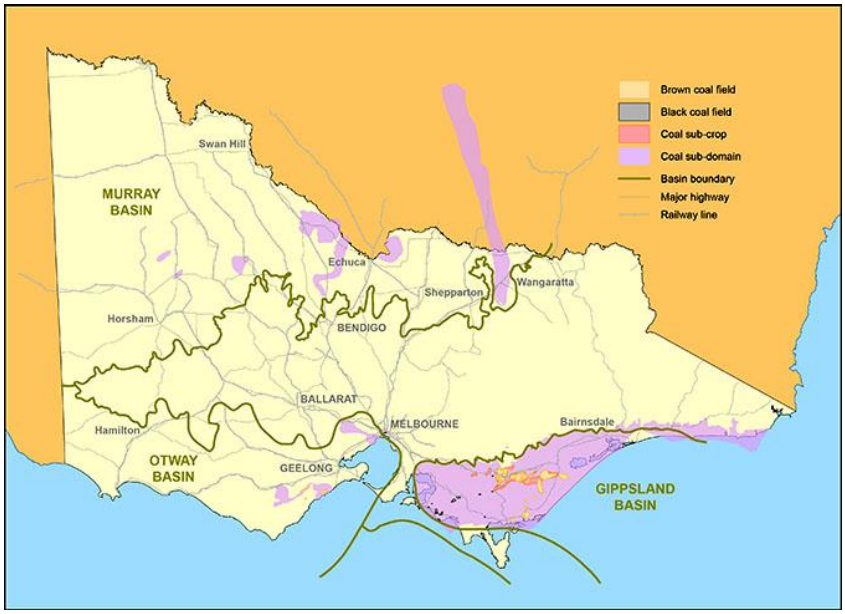

Figure 2.3: Victorian brown coal distribution in the Latrobe Valley [11]

Victorian brown coals have a low carbon content, 25–35% (65–70%, daf.) of raw coal. More than half of the carbon present in the coal is of aromatic nature, while the rest of the carbon is present in aliphatic chains and various functional groups. Brown coals have high oxygen content where oxygen is present as –COOH, −OH, ether or carbonyl forms. The sulphur content in as-mined Yallourn (YL) and Morwell (MW) coals ranges between 0.2 and 0.4% on a dry basis. The sulphur content in the Latrobe seam, one of the oldest coal seams near Morwell, averages 0.6% and exceed 1.5% in some locations. Sulfur present in Victorian brown coals is mostly organic [12]. Typical properties of Victorian brown coal are shown in Table 2.1 [13].

Table 2.1: Typical properties of Victorian brown coal [13]

Items	
Ultimate analysis (ash free basis, wt%)	
Carbon	65-70
Oxygen	25-30
Hydrogen	4.0-6.0
Nitrogen	0.36-0.85
Sulphur	0.14-5.36
Proximate analysis	
Ash (dry basis, wt%)	0.5-12.8
Moisture (wt%)	43.7-71.0
Calorific value	
Energy value (gross dry, MJ/kg)	25-29
Energy value (net wet, MJ/kg)	5.24-13.87

A comparison of different low-rank coals around the world including Victorian brown coals is shown in Figure 2.4 [14]. This figure shows the unique nature of Victorian brown coals with high moisture and low ash content compared to other low-ranked coals.

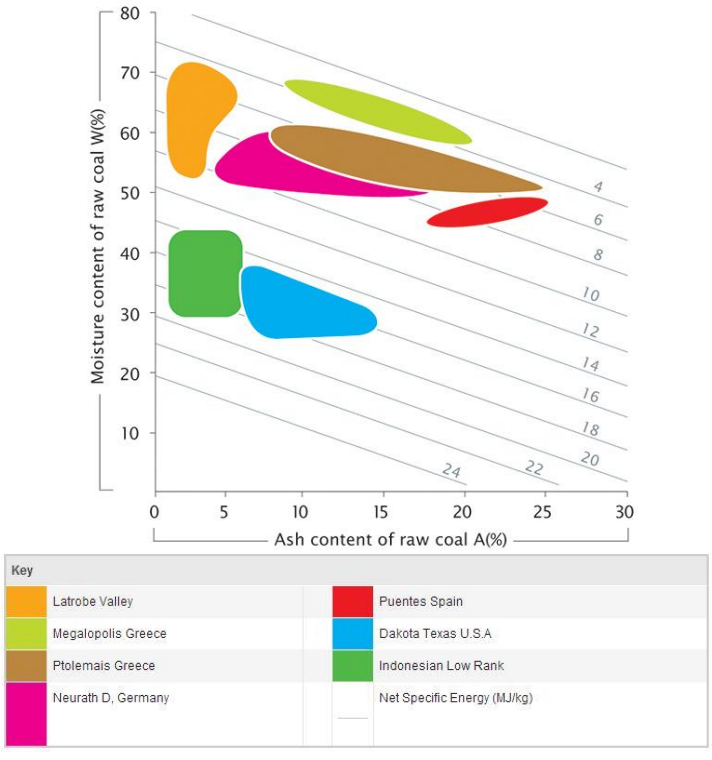

Figure 2.4: Comparison of different low rank coal [14]

Due to the special properties of Victorian brown coal- high moisture content and high reactivity, there are some real difficulties in coal transportation. As a result, Victorian brown coal is currently used in mine-mouth power generation plants, generating over 90% of electricity in Victoria [9]. However, it is also considered as a large contributor to greenhouse gas emissions because of this. Therefore, new applications towards high-value products are vital for the future of Victorian brown coal. Gasification, as one of the most potential and feasible technique for brown coal utilization, is investigated in this study, which can be used to generate syngas and value-added chemicals.

2.2 Background of coal gasification

This section introduces the background of coal gasification in terms of gasification process, gasification chemistry, and gasification applications.

2.2.1 Gasification process

Gasification is the reaction of a carbonaceous material, such as coal, with a gasifying agent, such as air, oxygen, carbon dioxide, or steam, to produce syngas (mainly of H_2 and CO) with fuel-dependent concentrations of CO_2, H_2O and CH_4 as well as trace amounts of various other permanent and non-permanent gases [15]. The gasification process can be divided into two fundamental processes: coal pyrolysis (also known as thermal decomposition or devolatilisation) and char gasification. The schematic gasification processes are shown in

Figure 2.5 and the general equations are given below:

Pyrolysis: coal → char + tars + gases

Gasification: char + reagent → gases + ash

First of all, combustion starts as soon as the fuel is introduced into the reactor and quickly consumes the majority of the available oxygen in the process to create the reducing atmosphere required for gasification.

Pyrolysis begins once the coal particles reach fuel-dependent temperatures, approximately 523 K [16]. The initial heating and devolatilisation of the coal takes place and results in the release of volatile matters and the breakage of covalent bonds and crosslinks, converting hydroaromatic groups into aromatic structures. This thermal decomposition also includes a series of complicated reactions

such as decarboxylation, cracking and repolymerisation, to release more volatile matters. It also results in the change of the mineral matter within the coal, for example, conversion of inorganic components to metal oxides.

After coal pyrolysis, the remaining char gasifies with a multiple of reactants including CO_2 and steam at approximately 1073 K [17]. This process produces the desired combustible syngas by a series of heterogeneous reactions. The product gases then react further among themselves and with the initial reagents to produce the final gas mixture.

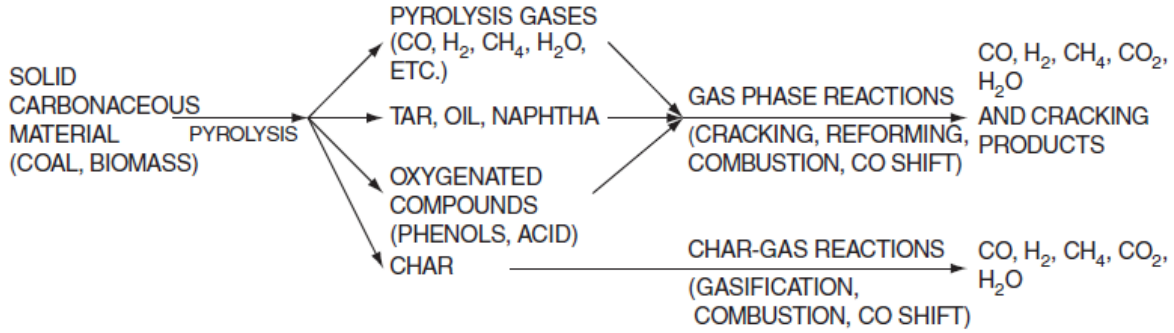

Figure 2.5: Schematic gasification processes [15]

2.2.2 Chemistry of gasification

Any gasification process can be divided into heterogeneous solid-gas reactions and homogeneous gas-phase reactions. The final gas product is composed mainly of CO, H_2, CO_2, and CH_4, but the composition of the final gas varies by the combination of heterogeneous solid-gas reactions and homogeneous gas-phase reactions. The heterogeneous and homogeneous reactions are shown as follows [18]:

Heterogeneous solid-gas reactions

Combustion	$C_{(s)} + O_2 \rightarrow CO_2$	(R 2.1)
Partial combustion	$C_{(s)} + \frac{1}{2}O_2 \rightarrow CO$	(R 2.2)
Boudouard reaction	$C_{(s)} + CO_2 \longrightarrow 2CO$	(R 2.3)
Water-gas reaction	$C_{(s)} + H_2O \rightleftharpoons CO + H_2$	(R 2.4)
Hydrogasification	$C_{(s)} + 2H_2 \rightleftharpoons CH_4$	(R 2.5)

Homogeneous gas-phase reactions

CO oxidation	$CO + \frac{1}{2}O_2 \rightarrow CO_2$	(R 2.6)
Water - gas shift	$CO + H_2O \rightleftharpoons CO_2 + H_2$	(R 2.7)
Steam reforming	$CH_4 + H_2O \rightleftharpoons CO + 3H_2$	(R 2.8)
Hydrogen combustion	$H_2 + \frac{1}{2}O_2 \rightarrow H_2O$	(R 2.9)
Methane dry reforming	$CH_4 + CO_2 \rightleftharpoons 2CO + 2H_2$	(R 2.10)

Of the five heterogeneous reactions (R 2.1)-(R 2.5), the first three are essentially complete under gasification conditions. Combustion reaction (R 2.1) is rapid and exothermic, which can provide heat for the later reactions and consumes the majority of oxygen in the gasifier. When the oxygen concentration falls and cannot meet the stoichiometry for combustion, partial oxidation (R 2.2) happens together with other heterogeneous reactions. The Boudouard reaction (R 2.3) is endothermic and is much slower than the partial oxidation under the same conditions. This is because that it is limited by a product gas (CO), and proceeds very slowly when the temperature is below 700°C [19].

In addition, the water-gas reaction (R 2.4) is endothermic and favoured by low pressure and high temperature [20]. It proceeds slowly below 900°C without catalyst but faster than the Boudouard reaction under the same conditions [19]. This reaction produces CO and H_2 by consuming carbon, which is an important source for syngas generation in the gasifier. The hydrogasification reaction (R 2.5) proceeds very slowly unless at high pressure (i.e. 70 bar).

The final gas composition is also affected by gas-phase reactions (R 2.6) – (R 2.10). The water-gas shift reaction adjusts the H_2/CO ratio, which is important for syngas applications into corresponding chemicals. The dry methane reforming reaction (R 2.10) can produce CO and H_2 by consuming CH_4. However, it occurs very slowly without using catalyst or high pressures [21].

2.2.3 Coal to products

As discussed in section 2.2.1, coal gasification converts coal to syngas, which is predominately a mixture of carbon monoxide and hydrogen. Syngas is a precursor to a wide range of energy and chemical products: it can be combusted in a combined cycle turbine system for efficient production of electricity, fed into a Fischer-Tropsch plant for the production of liquid fuels, reformed to methane to provide synthetic natural gas (SNG), converted to methanol to produce gasoline, or used as a

precursor for the production of a range of fertilisers, explosives and other chemicals [22-24]. Generic applications of coal-derived syngas are presented in Figure 2.6.

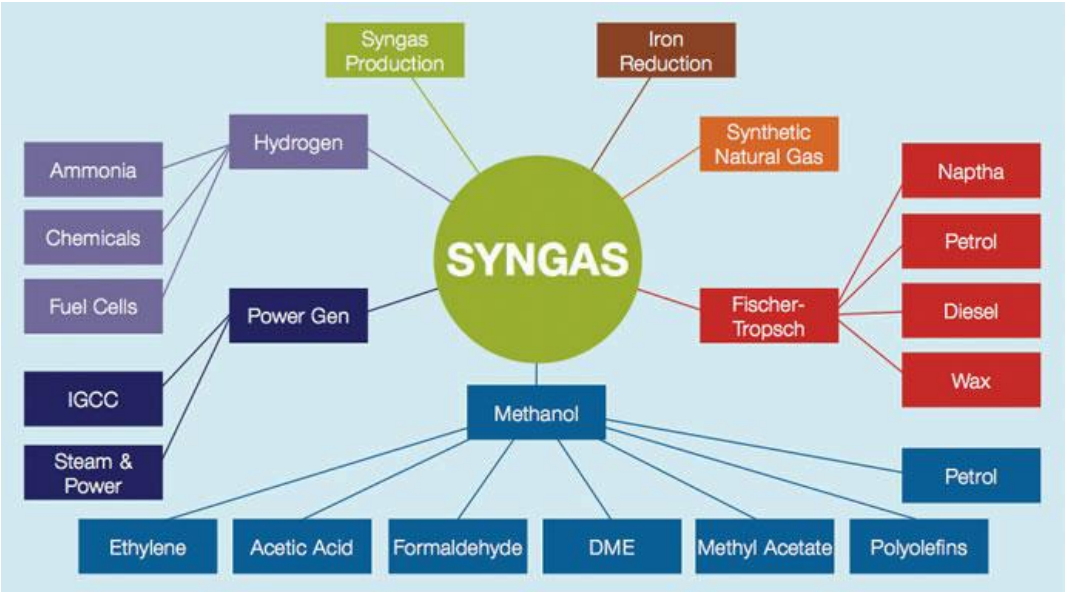

Figure 2.6: Applications of coal-derived syngas [25]

Most of these downstream processes are based on technologies that have a long history of development and improvement, requiring very little R&D to support their implementation into coal-to-products processes. However, the variability in the properties of the feedstocks and the different requirements of downstream processes mean that there is a range of gasification technologies, each one having particular requirements in terms of feedstock properties and producing syngas of varying quality and composition. The common gasification technologies are presented in the next section.

2.3 Gasification technologies

This section gives an overview of the main gasification technologies in use around the world, and provides some context for the traditional approaches to gasification of Victorian brown coal for power generation, and it also outlines the likely implications of a shift towards gasification of these materials for the production of liquid fuels, chemicals, hydrogen, and other.

Gasification technologies are generally classified based on bed types as listed in Table 2.2:

- Fixed bed gasifiers (also known as moving bed, dry ash or slagging)
- Fluidised bed gasifiers (dry ash or agglomerating)
- Entrained flow gasifiers (slagging)
- Transport gasifiers (modified fluidised bed, dry ash)

Table 2.2: Characteristics of different gasification technologies

Category	Fixed bed		Fluidised bed		Entrained flow	Transport
Ash condition	Dry	Slagging	Dry	Agglomerating	Slagging	Dry
Typical processes	Lurgi, SEDIN	BGL	Winkler, HTW, CFB,TRIG	KWR, U-Gas, AFB	Shell, GE,E-Gas, Simens,KT, and others	KBR,HRL
Feed characteristics						
Preferred coal rank	Any	High	Low	Any	Any	Low
Coal particle size (mm)	5-80	5-80	<6	<6	<0.1	<6
Gas velocity	Low to moderate	Low to moderate	Low to moderate (3-8m/s)	Moderate	High	High (11-18m/s)
Operating characteristics						
Typical operating temperature	900-1200ºC	900-1200ºC	800-900ºC	850-1100ºC	1200-1600ºC	950-1065ºC
Pressure	Moderate(20-35 bar)	Moderate (20-35 bar)	Moderate (25-30 bar)	Moderate (25-30 bar)	Moderate to high (20-70 bar)	Moderate (11-18 bar)
Outlet gas temperature	Low(450- 650 ºC)	Low(450- 650ºC)	Moderate (900-1050ºC)	Moderate (900-1050ºC)	High (1250-1600ºC)	Moderate (900-1050ºC)
Scale	Small	Small	small to medium	small to medium	Large	small to medium
Ash content	No limitation	<25%	No limitation	No limitation	<25% prederred	No limitation
Tars produced	Moderate to high	Moderate to high	Intermediate	Intermediate	Absent	Low
Key technical issues	Utilisation of fines and hydrocarbon liquids	Utilisation of fines and hydrocarbon liquids	Lower carbon conversion	Lower carbon conversion	Raw gas cooling	Commercial application

2.3.1 Fixed bed gasifiers

Fixed bed gasifiers, also called moving bed gasifiers, operate in a manner similar to blast furnaces, where lump coal is fed from the top and air or oxygen is supplied from the bottom [26]. The residence times of solids are high (1–2 hours) and coal mineral matter is removed either dry, as in the Lurgi FBDB^{TM} gasifier, or as a slag, as in the slagging BGL/Envirotherm technology. Dry-ash fixed beds usually have a rotating grate system at the bottom of the bed to facilitate removal of the ash. There are no moving parts at the bottom of the BGL gasifiers, as shown in Figure 2.7 (a). These characteristics mean that fixed bed gasifiers are relatively easy to operate but they have high maintenance requirements: this is why fixed-bed gasifier installations typically have two or more gasifiers with at least one idled for maintenance as part of the operation. The Lurgi FBDB^{TM} Mk Plus^{TM} gasifier is the most recent offering from this technology suite, operating at higher pressures (up to 60 bar) and with greater throughputs, as shown in Figure 2.7 (b).

Fixed-bed gasifiers have specific requirements of coal properties: structural stability of the slowly moving bed of coal and char is important, as is the ability for gas to permeate uniformly through the coal and char bed. The formation of fines, therefore, is not favourable as they significantly reduce this permeability. These gasifiers have relatively low throughput per unit, low degree of fuel flexibility and the tendency for the syngas to contain relatively high levels of methane, liquor, and tars. This makes them generally better suited to specific applications such as SNG production than for large scale FT or IGCC power generation applications. Considerable scale and reliability, however, can be achieved through the use of banks of many gasifiers, such as the Sasol plant in South Africa which uses more than 80 Lurgi gasifiers in a parallel configuration.

Fixed bed gasifiers can be attractive for high moisture coals because the coal is dewatered and heated by the hot gas moving countercurrently with the downward moving lump coal, resulting in low oxygen consumption. However, the use of lump coal immediately poses the problem of what to do with the fines that are usually present. Furthermore, dirty gases leave the gasifier at temperatures below 500 °C. This relatively low temperature and the presence of tars and liquor means that waste heat boilers or syngas coolers cannot be used.

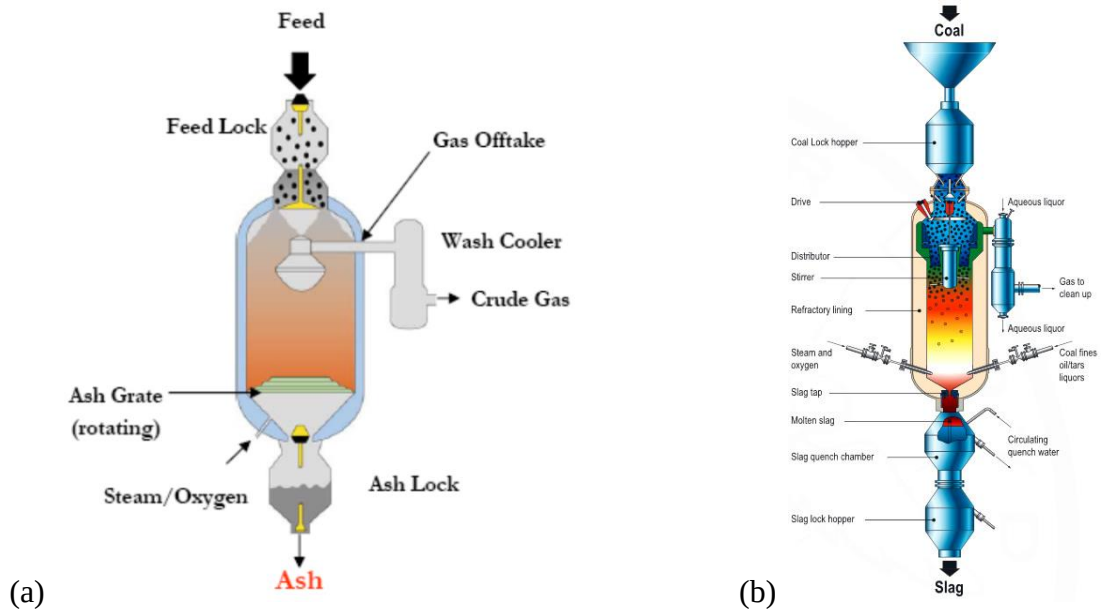

Figure 2.7: (a) The Lurgi FBDB™ fixed-bed, dry-bottom gasifier[26] and (b) the BGL (Envirotherm) slagging gasifier (www.netl.doe.gov, accessed May 2014).

The Great Plains Synfuels plant in the US gasifies lignite in an oxygen-blown dry-bottom fixed bed Lurgi gasifier producing about 153 million cubic feet of synthetic natural gas each year, as well as CO_2 which is sent to EOR applications in Canada. Current expansion of the facility to produce 1,100 tpd of urea will be completed by 2017, demonstrating the success of the operation as well as the flexibility afforded by gasification-based systems to respond to market changes. The Vresova IGCC plant in the Czech Republic gasifies approximately 2000 tonnes per day of lignite, also using Lurgi fixed-bed dry-bottom gasifiers, to produce power in an IGCC configuration. Clearly, lignites can be successfully gasified using fixed-bed technologies, provided that an adequate understanding of their structural and fragmentation properties shows them to be suitable.

2.3.2 Fluidised bed gasifiers

Fluidised bed gasifiers require coarse (1–10 mm) and dry coal (or biomass) particles in a bed fluidised by air or oxygen and steam [27]. To minimise agglomeration and prevent defluidisation of the bed, the operating temperature is usually kept below the ash softening temperature which for most coals is around 1000 °C. The gasifiers are known to operate at atmospheric or higher pressures.

There are two variants of fluidised bed gasifiers that have been commercialised: High Temperature Winkler (HTW) and U-Gas gasifiers. The HTW gasifier, shown in Figure 2.8(a), is a circulating fluidised bed gasifier operating at 3–5 m/sec fluidisation velocity and pressure up to 30 bar. A mix of incoming feed, partially converted coal and dry ash constantly circulates inside the bed maintaining a constant temperature in the bed. To keep the bed fluidised and minimise agglomerates, a part of the

mix is also constantly discharged from the bed. This discharge from the bed and low operating temperature also result in low carbon conversion (80-90%) in the gasifier. While Rhinebraun AG (now RWE) developed the process in 1926, ThyssenKrupp Uhde acquired the HTW technology in 2010.

The U-Gas gasifier, shown in Figure 2.8(b), is also a circulating fluidised bed gasifier but with air/O_2 and steam injection at the conical bottom to improve the carbon conversion to about 95%. It can operate up to 1100 °C, and large agglomerated ash is discharged from the bottom of the gasifier. The U-Gas gasifier was developed by the Gas Technology Institute in Chicago, while commercial licensing rights were acquired by Synthesis Energy Systems. In 2013, three plants were in operation at Hennan, Shandong and Inner Mongolia in China, all for chemicals production.

In the air-blown mode, fluidised bed gasifiers are known to produce low-calorific value fuel gas (around 5 MJ/kg), while oxygen-blown mode operation will result in medium calorific value fuel gas (around 9 MJ/kg). Because of lower operating temperature, fluidised bed gasifiers are inherently more suited for reactive coals, such as brown coal. However, low carbon conversion does remain a problem due to the low operating temperature.

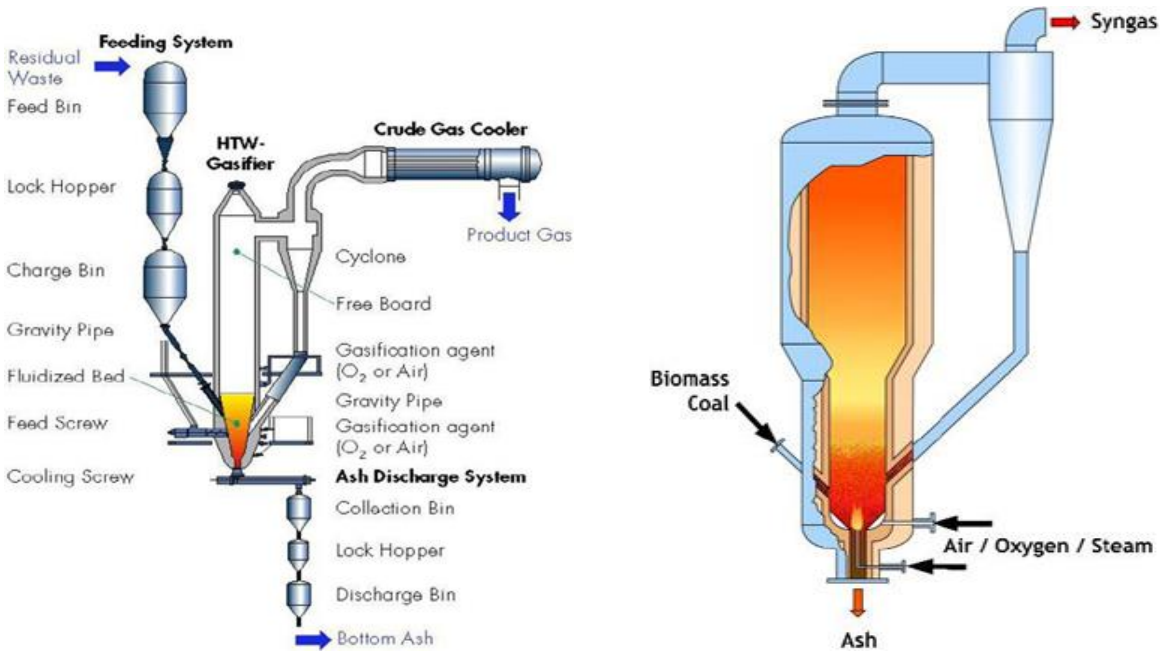

(a) (b)

Figure 2.8: Fluidised bed gasifiers - (a) High temperature Winkler type (b) U-Gas type (www.netl.doe.gov, accessed April 2014)

2.3.3 Transport gasifiers

The transport gasifier (Figure 2.9) is another circulating fluidised bed gasifier, but it operates at a higher velocity than a HTW gasifier promoting better mixing between the coal and the reactants. The main body of the gasifier has two sections: a larger-diameter mixing zone on the bottom, and a smaller-diameter riser section on the top. The larger diameter of the mixing zone lowers a gas velocity promoting solids mixing and consequently increasing solids retention time and therefore carbon conversion.

The transport gasifier can handle lower feed particle size compared to HTW gasifiers. Air or O_2 and steam addition at the bottom of the larger diameter mixing zone also improves carbon conversion. Due to low operating temperatures, the transport gasifier is also inherently more suited for reactive coals, such as brown coals and lignites. Since the operating temperature of the transport gasifier is under 1000 °C, the calorific value of a fuel gas produced is similar to that from fluidised bed gasifiers.

The transport gasifier technology has been developed by Kellog, Brown and Root and Southern Company at the Power System Development Facility at Wilsonville, Alabama and the EERC at the University of North Dakota. This has formed the basis for the 582 MW Transport Reactor Integrated Gasification powered IGCC plant at Kemper County in Mississippi. At the time of drafting this chapter (September 2017), this project has been kept on hold for cost reasons. The gasifier will operate in air-blown mode for the production of power and fertiliser, as well as CO_2 for enhanced oil recovery. Designs are known to be available for oxygen-blown operation. Another plant is known to be under negotiation for construction in Dongguan, China.

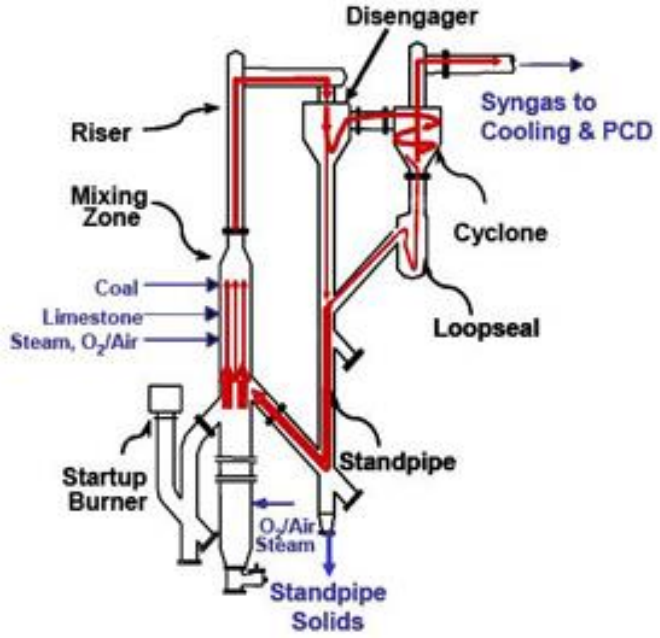

Figure 2.9: Transport Gasifier (www.netl.doe.gov, accessed August 2017).

2.3.4 Entrained flow gasifiers

Entrained flow gasifiers require pulverised coal at high pressures into a chamber where temperatures and pressures are high (up to, and possibly over 1800–2000 K and 2.0–4.0 MPa) and residence times are low (usually several seconds). Due to these intense reaction conditions, entrained flow gasifiers offer high throughput and conversion for a wide range of feedstocks, making them the most commonly used gasification technology for large-scale IGCC and coal-to-products applications (Table 2.2). Entrained flow gasification is currently feasible only at large scale. Some example schematics of common entrained flow gasifiers are given in Figure 2.10.

Table 2.3: Characteristics of the leading commercial entrained flow gasification technologies [28].

Technology	Stages	Oxidant	Feed	Configuration	Gasifier Wall
Shell, PRENFLO	1	O_2	Dry	Up-flow*	Water-wall
GE	1	O_2	Slurry	Down-flow	Refractory
CB&I E-Gas	2	O_2	Slurry	Up-flow	Refractory
MHI	2	Air	Dry	Up-flow	Refractory & Water-wall
Siemens	1	O_2	Dry	Down-flow	Water-wall

*More recently a down flow variant of this technology has been developed.

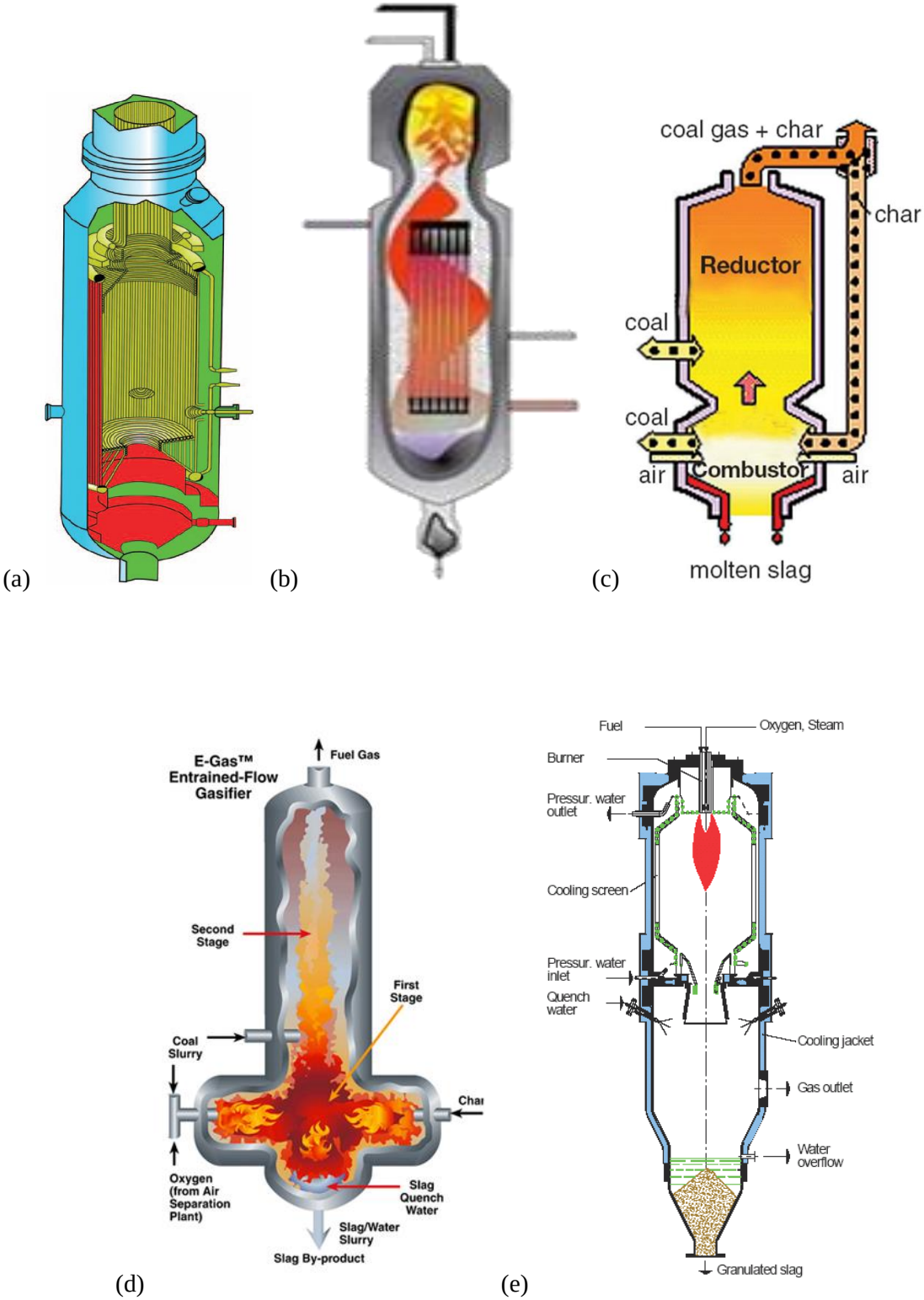

Figure 2.10: Examples of entrained flow gasifier technologies: (a) Shell, (b) GE, (c) MHI, (d) E-Gas, (e) Siemens [29].

The available commercial entrained flow gasification technologies are differentiated by particular combinations of the feeding method and oxidant type, gasifier configuration, construction material, and mode of syngas quench. The impacts of these variations on fuel requirements and syngas quality mean that most technology vendors are continually exploring variants to their gasifier design and syngas processing configuration. For example, Shell now offers a partial quench system and Siemens are developing a radiant syngas cooler configuration to suit specific applications.

Slurry-fed gasifiers, such as the GE and E-gas gasifiers, overcome issues associated with feeding powdered solids into pressure vessels and can operate at very high pressures; however, the increased reliability and decreased capital cost comes at the expense of a greater oxygen demand due to the increased thermal load. Refractory-lined slagging gasifiers, such as GE and E-Gas, are sensitive to the quality and quantity of the ash and slag, and are more susceptible to ceramic liner erosion and corrosion than water-wall gasifiers. Water-wall gasifiers, such as Shell and Siemens, require a protective slag layer to form, which is strongly dependent on the properties of the coal used.

Two-stage gasifiers, such as the MHI and E-Gas, gasifiers have two coal injection points: one in the 'combustion' stage, where heat is generated to melt the mineral matter and to drive the gasification reactions, and one in the second stage, where coal and char is 'gasified' using the heat and gaseous products from the combustion stage. The second stage also serves as a 'chemical quench', whereby the progress of the gasification reactions partially cools the syngas and stores this heat as chemical energy in the syngas. They consequently have greater cold gas efficiencies than single-stage gasifiers; however, this can be offset by higher rates of unconverted carbon and the possible production of some tar species. Two-stage gasifiers often have a char recycling capability, which increases the total carbon conversion but also increases the capital cost.

Most entrained flow gasifiers are oxygen blown, as the presence of significant amounts of N_2 is detrimental to the downstream chemicals and liquid fuels production processes. Furthermore, for gasification-based IGCC power plants which are designed for integrated carbon capture and storage, oxygen blown systems are favoured for similar reasons. In oxygen blown gasification, air is separated in an air separation unit and high purity O_2 (usually over 99%) is used as the oxidant, usually with steam to manage the temperature and enhance the production of syngas. There are significant capital and operating costs associated with operating an air-separation unit: the ASU can comprise up to 15% of the capital cost of an IGCC plant, and consume up to 20% of the power generated [30].

It is not common for air-blown gasifiers to be used in chemical and liquid fuel production processes. Air blown gasifiers are typically used in applications in which lower cost is important, such as some IGCC applications. The Nakoso IGCC plant in Japan, for example, was designed for high-efficiency power generation and was not initially designed for use with integrated carbon capture [31]. The greater gas volumes associated with air-blown gasification are significant: gasifiers must be larger, and downstream syngas cooling and cleaning plants must also be larger [32]. For IGCC applications, therefore, there is a trade-off between capital and operating cost and reliability.

The need for higher efficiencies and lower cost entrained flow gasification systems, particularly for Victorian brown coal utilisation, is driving new initiatives in gasifier design.

2.4 Kinetics studies of brown coal/char gasification with CO_2

Kinetics data of brown coal/char gasification is required to design coal gasifiers. Many research have been conducted for coal/char gasification kinetics. In this section, the mechanism, reaction rate, and reaction models for brown coal/char gasification with CO_2 are introduced.

2.4.1 Char-CO_2 mechanism

Different mechanisms for the char-CO_2 reaction have been proposed and reviewed [33-35]. They are interpreted by either an oxygen exchange mechanism [36], or a combination of oxygen exchange and CO inhibition [37]. The surface mechanism is based on the following reactions:

$$C + CO_2 \underset{k_{-1}}{\overset{k_1}{\rightleftharpoons}} C(O) + CO \quad \text{(R 2.11)}$$

$$C(O) \xrightarrow{k_2} CO + C( ) \quad \text{(R 2.12)}$$

$$C( ) + CO \overset{k_3}{\rightleftharpoons} C(CO) \quad \text{(R 2.13)}$$

Where $C( )$ represents available active sites on the surface of a char particle, C(O) and C(CO) are the occupied sits, and k_1, k_{-1}, k_2, and k_3 are rate constants.

Initially, CO_2 reacts with an active carbon on the surface (R 2.11) to generate CO and form a complex of the oxidised surface. Secondly, it is carbon gasification (R 2.12), where CO and new active sites are generated. It is widely acknowledged that the second step, carbon gasification, determines the reaction rate.

Later, some researchers [38] have found the inhibition influence of CO, the product of the CO_2 gasification, on the reaction by adsorbing and occupying active sites (R 2.13). Therefore, the reaction rate (r_s) is expressed as follows:

$$r_s = \frac{k_1 p(CO_2)}{1+\frac{k_{-1}}{k_2}p(CO)+\frac{k_1}{k_2}p(CO_2)} \quad \text{(E 2.1)}$$

Where p(CO) and $p(CO_2)$ are the partial pressure of each gas.

2.4.2 Gasification reaction rate

There are two gasification rate equations for CO_2 gasification: the nth order reaction rate equation and the Langmuir-Hinshelwood (L-H) reaction rate equation [34, 39]. The nth order reaction rate equation assumes that the overall gasification rate is proportional to the partial pressure of the reagent gas (CO_2), and it follows Arrhenius equation:

$$\mathrm{k} = A_0 \exp(-\frac{E_a}{RT}) P^n \quad \text{(E 2.2)}$$

where A_0 is a pre-exponential factor, E_a is activation energy, R is gas constant, T is temperature, P is the partial pressure of the gasifying agent, and n is reaction order.

According to the Arrhenius equation, the temperature has the greatest effect on reaction rate, and the effective reaction rate is controlled by the following three temperature regimes, shown in Figure 2.11:

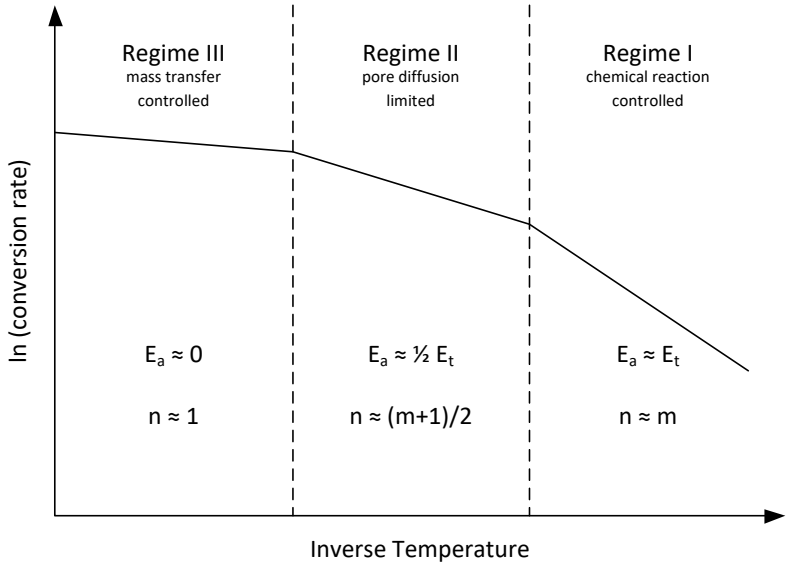

Figure 2.11: The effective reaction rate at different temperature regimes [40]

- Regime I (a low temperature zone, approximate < 1000 °C). The overall rate is controlled by the chemical reaction, and the gasification occurs throughout the particle [35]. In this temperature zone, the activation energy and all other kinetic parameters determined are the intrinsic values for the reaction [20]. Therefore, the kinetic parameters should be determined by the chemical reaction controlled temperature range, Regime I, to obtain the true values.
- Regime II (a medium temperature zone). The chemical reaction rate increases exponentially and gets higher, but it is limited by the gas diffusion within the pores [35]. In this regime, the measured activation energy is approximately the half of the true activation energy and the reaction order is approximately the half of the true order plus 1 [41].
- Regime III (a high temperature zone). The reaction rate is limited by the mass transfer within the boundary layer around the particle. The concentration of gaseous reactant at the external surface of the char particle is essentially zero and the reaction is controlled by external mass transfer. The activation energy in Regime III is negligible (~ 0) [35] and the char properties has no effect on the reaction rate.

The partial pressure of reactive gases has significant effect on char gasification rate. It is found that the gasification rate increases with pressure, and its effect is more marked in low pressure zone. At high pressure above 1 MPa, the enhancement of pressure on gasification rate diminishes with increasing pressure because of the inhibition effect of CO formed [42]. Hence, the Arrhenius equation is more applicable to low pressure gasification, and gasification rate (Ink) is a linear function of reaction order.

The L-H reaction rate equation is applied in order to explain the change in the dependence of the partial pressure on gasification rate:

$$\mathrm{k} = \mathrm{S}\frac{k_1 p(CO_2)+k_4 p^2(CO_2)}{1+k_2 p(CO_2)+k_3 p(CO)} \quad \text{(E 2.3)}$$

where S is the surface area of the char particle. The following elementary reactions were considered in this equation and the reaction rate constants k_j (j=1, 2, 3, 4) follows Arrhenius equation

$$CO_2 \xrightarrow{i_1} CO + (O) \quad \text{(R 2.14)}$$

$$CO \underset{i_2}{\overset{i_3}{\leftrightarrows}} (CO) \quad \text{(R 2.15)}$$

$$C + (O) \xrightarrow{i_4} CO \quad \text{(R 2.16)}$$

$$CO_2 + (CO) \xrightarrow{i_5} 2CO + (O) \quad \text{(R 2.17)}$$

$$CO + (CO) \xrightarrow{i_6} CO_2 + C \quad \text{(R 2.18)}$$

$$k_1 = i_1;\ k_2 = \frac{i_1}{i_4} + \frac{i_5}{i_3};\ k_3 = \frac{i_2}{i_3} + \frac{i_6}{i_3};\ k_4 = \frac{i_1 i_5}{i_3} \quad \text{(R 2.19)}$$

The L-H equation has been successfully used for the intrinsic kinetics of the CO_2 gasification by many researchers [43-46]. Compared to the nth order equation, the L-H expression has three important characteristics [47]:

1) The intrinsic reactivity of the CO_2 gasification is a non-linear function of CO_2 partial pressure and the reaction order, n, is not used.
2) The mechanism of the expression considers an adsorption – desorption reaction.
3) It includes the inhibition effect of CO, the product gas.

However, the main problem for the L-H equation is to evaluate the large number of the adsorption and kinetic constants when various gases are present.

Table 2.3 shows the kinetic parameters presented in previous kinetic studies for char-CO_2 gasification using the Arrhenius equation and L-H type equation. As seen, there are clear differences in both the activation energy and pre-exponential factor for low-rank coals, which could be a result of a combination of sample properties and preparation, experimental reactors, and gasification conditions.

Table 2.4: Kinetic parameters for char-CO_2 gasification

Coal type	Char sample	Ea (kJ/mol)	Pre-Exponential Factor (s^{-1})	Reference
Lignite	Victoria	146.4	n.r.	[48]
Lignite	Turkish coals	29-124.8	n.r.	[49]
Lignite	Utrillas	169.5	n.r.	[42]
Lignite	n.r.	149.1	8.21×10^2	[50]
Lignite	Yallourn	170	6.60×10^3	[51]
Lignite	Loy Yang	160	1.31×10^3	[52]
Densified Lignite	Morwell	230	n.r.	[53]
Bituminous coal	Australian coal	283	1.09×10^9	[54]
Bituminous coal	Pittsb. and Illinois	247.9	n.r.	[55]
Bituminous coal	n.r.	171	n.r.	[43]
Bituminous coal	Australian coal	257	2.54×10^7	[56]
Bituminous coal	American and Chinese coal	240-280	1.12×10^8-1.19×10^9	[57]

n.r. = not reported

2.4.3 Reaction models

Different models have been proposed to describe the coal char gasification reaction with CO_2. Models without considering coal structural changes during reaction are most simple. The volumetric model (VM) and the grain model (GM) are examples of this type of models. Other than these models, modified volumetric model (MVM) and random pore model (RPM) are introduced here as well.

2.4.3.1 Volumetric model

This model is the simplest, it reduces the heterogeneous gas-solid reaction of coal gasification to a homogeneous reaction by assuming that the gas is reacting with char in all possible places, both outside and inside the particle surface [58]. The kinetic expression for the reaction rate is given below:

$$\frac{dX}{dt} = k_{VM}(1 - X) \quad \text{(E 2.4)}$$

$$3[1 - (1 - X)^{1/3}] = k_{GM}t \quad \text{(E 2.5)}$$

Where k_{VM} is the kinetics reaction constant and X is the conversion.

2.4.3.2 Grain model

The grain model assumes that the reaction occurs at the external surface of char particle [59, 60]. As the reaction gradually moves inside the particle, only ash layer remains. At the intermediate conversion of a sample particle, there is a shrinking core of unreacted solid, which diminishes with the course of the reaction, the reactivity expressions are given below:

$$\frac{dX}{dt} = 3k_{GM}(1-X)^{2/3} \quad \text{(E 2.6)}$$

$$3[1-(1-X)^{1/3}] = k_{GM}t \quad \text{(E 2.7)}$$

Where k_{GM} is the kinetics reaction constant.

2.4.3.3 Random pore model

The random pore model was found by Bhatia and Perlumutter [61] who considered the random overlapping of pores' surface, which reduced the area available for reaction. Those changes are expressed with the structural parameter, ψ, which is the characteristic for this model. The RPM can predict the occurrence of the maximal rate in the course of the reaction. The ψ parameter can be calculated by (E 2.8) when initial porosity, ε_0, surface area, S_0 , and pore length, L_0, of the solid are known:

$$\psi = \frac{4\pi L_0(1-\varepsilon_0)}{S_0^2} \quad \text{(E 2.8)}$$

In addition, the structural parameter can be calculated by means of maximal conversion degree of solid, X_{max}, for which maximal reaction rate is observed. The value of ψ can be estimated according to relation (E 2.9). As a result, the basic kinetic expressions are shown in (E 2.10) and (E 2.11).

$$\psi = \frac{2}{2ln(1-X_{max})+1} \quad \text{(E 2.9)}$$

$$\frac{\mathrm{dX}}{\mathrm{dt}} = (1-\mathrm{X})\sqrt{1-\psi\ln(1-\mathrm{X})} \quad \text{(E 2.10)}$$

$$\frac{2}{\psi}(\sqrt{1-\psi\ln(1-X)}-1) = k_{RPM}t \quad \text{(E 2.11)}$$

2.4.3.4 Modified Volumetric model

This model is first developed by Kasaoka et al [62] and it modifies the equation of volumetric model by adding a new parameter-the time power (b). The reaction rate can be expressed by (E 2.12)- (E 2.14):

$$\frac{dX}{dt} = k_{MVM}(1 - X) \quad \text{(E 2.12)}$$

$$k_{MVM} = a^{\frac{1}{b}} b[-ln(1 - X)]^{\frac{b-1}{b}} \quad \text{(E 2.13)}$$

$$-\ln(1 - X) = at^{b} \quad \text{(E 2.14)}$$

Where a and b are empirical constants. This model applies a reaction order (b) to the volumetric model. It seems that the expressions of the volumetric model get closer to the random model by applying this order.

There are several other models developed for coal-char gasification and they are shown in Table 2.5. The efficiency of kinetic models in predicting the reaction rate during the coal gasification mainly depends on the type of coal, the experimental conditions, and the purpose of char reactivity evaluation.

However, the work for kinetics study of Victorian brown coal gasification is limited in the open literature. Only Tanner et al. reported kinetic data on CO_2 and steam gasification of Victorian brown coal chars generated from entrained flow pyrolysis using random pore model [1]. It suggests that other reaction models, i.e. grain model and volumetric model, could be applicable for Victorian brown coals. Moreover, the kinetic modelling results have not been compared with the experimental data in an entrained flow gasifier for their validity.

Table 2.5: Characteristics of different reaction models

Models	Equations	Comments	Applications
Volumetric model	$\frac{dX}{dt} = k(1-X)$	A homogeneous reaction model by assuming the gas is reacting with the char in all possible places.	X verse t, dX/dt verse t, kinetic constants
Grain model	$\frac{dX}{dt} = 3k(1-X)^{2/3}$	Char particles are considered as spherical grains.	X verse t, dX/dt verse t, kinetic constants
Random pore model	$\frac{dX}{dt} = (1-X)\sqrt{1-\psi\, ln(1-X)}$ $\psi = \frac{4\pi L_0(1-\varepsilon_0)}{S_0^2}$	This model considers the random overlapping of surfaces of pores. It assumes the pores are cylindrical and they are enlarged with the progress of the reaction and eventually merge together.	X verse t, dX/dt verse t, kinetic constants
Modified Volumetric model	$\frac{dX}{dt} = a^{\frac{1}{b}} b(1-X)[-ln(1-X)]^{\frac{b-1}{b}}$ $-\ln(1-X) = at^b$	This model applies a reaction order b (time power) and modified volumetric model. This model gets closer to RPM, in which a two order polynomial is the power of time.	X verse t, dX/dt verse t, kinetic constants
The Adschiri and Furusawa model [63]	$\frac{dX}{dt} = S_{(X)}k = k(1-X)$ $S_{(X)}$ is the surface area	This model considers the volumetric model is enough for high porosity (>0.5) char and includes the value of surface area.	X verse t, dX/dt verse t
Unification theory model [64]	$\frac{dX}{dt} = R_{CO}(1-X)^m$ $X = 1-[1-R_{CO}(1-m)t]^{\frac{1}{1-m}}$ m is the reaction order of gas	This model is based on the fact that when conversion (x) is plotted against dimensionless time $\gamma = t/t_{1/2}$, where $t_{1/2}$ is the half time for char-gas reaction, irregardless of temperature, pressures, gasifing agents and coals, all the experimental plots can be described by only one curve for conversion <0.7.	X verse t, kinetic constants

2.5 Recent gasification research into Victorian brown coal

Between 1994 and 2006, the CRC for Clean Power from Lignite carried out a considerable amount of research on the pyrolysis and gasification of Victorian brown coals and South Australian lignites. The work involved both modelling and experimental work at laboratory and pilot scale at facilities of the CRC partners (Monash University, University of Adelaide and CSIRO) and external collaborators (HRL Limited and the Energy and Environmental Research Centre (EERC) at the University of North Dakota, USA). Most of the experimental work was carried out at low temperatures, up to 900 ºC, relevant to the fluidised bed or transport gasifier.

This section summarises some of the important work and its major findings. The intention is to demonstrate the breadth and nature of the research that has been undertaken into gasification of Victorian brown coals.

2.5.1 Laboratory-scale studies

Considerable laboratory-scale experimental research into brown coal gasification was carried out at Monash University, the University of Adelaide, and Swinburne University of Technology. These studies have mainly focused on assessing alkali and alkaline earth metal (AAEM) emissions and their catalytic effects during pyrolysis and gasification of Victorian brown coals and South Australian lignites. Table 2.4 gives an overview of this work. Some highlights from work are discussed in this section, noting that the experimental conditions used make many of the outcomes difficult to apply to O_2-blown gasification conditions.

The volatilisation of sodium and other alkali and alkali earth metal (AAEM) species during pyrolysis was extensively studied during the CRC program and beyond [2, 3]. During the gasification of coal at conditions characteristic of a fluid bed process, the sodium species formed will depend on the initial form of sodium present in coal on gas atmosphere. This dependence on the gas atmosphere is particularly apparent for organically bound sodium, with CO_2 atmosphere favouring the formation of sodium carbonate (Na_2CO_3) although oxygen levels and temperature–time histories make the ultimate fate of sodium complex.

The release behaviour of sodium is temperature- and heating rate-dependent. Under fast heating conditions, the volatilisation of sodium from raw and NaCl-loaded coal samples increase monotonically until almost total volatilisation occurred at 900°C. Under slow heating rate conditions,

the volatilisation of Na from raw coal also increases monotonically although <20% of the total sodium is volatilized at 900°C. Sodium and chlorine does not show evidence of volatilisation together as NaCl molecules, as they show different trends in their volatilisation during pyrolysis.

The volatilisation of sodium from char during pyrolysis/gasification can reach a plateau due to the formation of a stable form of sodium. This lower 'retention limit' is independent of the level of loaded sodium in the coal. More sodium can be stabilised in the char at lower temperature compared to high temperature: this is believed to be related to the level of oxygen in the char. Significant volatilisation of calcium and magnesium occurs during CO_2 gasification of coal. This contrasts to its stability in inert atmosphere. Calcium and magnesium does not show a great difference in volatility between inert and steam atmospheres.

Most of this fundamental work was carried out at low temperatures relevant to fluidised bed pyrolysis and gasification under air-blown conditions. While these studies provide a strong scientific foundation that can be useful for understanding the AAEM behaviour during low temperature stages of gasification, their usefulness for oxygen-blown, high temperature (>1000 °C) gasification is likely to be limited.

Table 2.6: Australian laboratory-scale experimental work at Monash University, Swinburne University, and the University of Adelaide

Year	Coals &Size	Temperature	Pressure	Medium	Sample	Reactor	Key Findings:
2000 [65]	Lochiel coal, South Australia 106-150 µm	650-850°C	Atmospheric	Steam, CO, CO_2, H_2	Containing 1% NaCl and 10% Si	Horizontal tube furnace	1. Under inert gas environment, Na transformed to Na_2CO_3 , and further reduced by the char to element sodium and evaporated. 2. Under a steam environment, the melting point temperature of sodium carbonate found to decrease.
2000 [5]	Bowman coal, Morwell, Loy Yang, Yallourn Char 180-350µm	750-950°C	Atmospheric	Steam, CO_2, O_2	0.28-0.3kg/hr	Fluidised-bed reactor	1. Bed temperature, oxygen concentration, particle size, moisture content and coal rank were found to influence the devolatilisation time. 2. The devolatilisation time was found to be directly proportional to the particle diameter $t_v=Ad_p^n$. 3. A new theoretical treatment to distinguish between heat transfer and chemical kinetically controlled regimes of coal devolatilisation has been used.
2005 [66]	Loy Yang, Yallourn coal 0.5-2.0 mm	850°C	Atmospheric	Air, Air/steam	7.2-8.7 kg/hr	Fluidised-bed Reactor	1. 21 vol% CO for air gasification, 21 vol% H_2 for air/steam gasification. 2. Air gasification only yielded syngas richer in CO compared with air/steam gasification
2002 [4]	NaCl-loaded, Na-exchanged and Ca-exchanged Loy	Pyrolysis: 500-900°C Gasification:	Atmospheric	Ar /CO_2 Ar /steam	1.0-2.0g	Fluidised-bed/fixed-bed reactor	1. The valency and the chemical/physical form of the AAEM* species in the coal can affect their volatilisation during pyrolysis. 2. Na present as NaCl in the coal could exhibit good

	Yang coal 106-150 µm	900°C					catalytic activity during gasification. The differences in char structural changes between the two atmospheres also have a effect on reactivity.with steam atmosphere having a larger positive effect. 3. Longer exposure to temperature makes the char less reactive to subsequent gasification
2004 [67]	Loy Yang coal 106-150 µm	500-600°C	Atmospheric	O_2 in Ar	10-390 mg/min	Fluidised-bed/fixed-bed reactor	1. Increased yields of HCN and NH_3 during gasification in Oxygen at 500°C. 2. During gasification, NO_2 is formed from NO via reactions with HO_2 radical.
2005 [68]	H-Form and Fe-loaded Loy Yang coal 106-150 µm	Pyrolysis: 400-600°C Gasification: 800°C	Atmospheric	Steam	1.5-2.0g	Fluidised-bed/fixed-bed reactor	1. In the presence of iron species, the production of hydrogen during the gasification of chars from iron-loaded brown coal is greatly enhanced. 2. Both reduced-iron and magnetite finely dispersed in chars are strong catalysts for char gasification with steam.

2.5.2 Bench-scale studies in a fluidized bed gasifier

As part of the Lignite CRC research program, an experimental investigation on gasification of Victorian brown coal was performed at EERC, University of North Dakota [69]. In this study, the experimental rig had a maximum capacity of 2 kg/hr, operating pressure up to 10 bar and temperature up to 1000 °C. Pyrolysis and gasification tests of air dried Loy Yang coal were undertaken over a range of temperatures (400–800°C) and two pressures (1 and 10 bar) at low fluidisation velocity of around 0.3 m/sec representative of bubbling fluidised beds.

The study has generated data on the pyrolysis and gasification of large (~2 mm) low-rank coal particles over a range of temperatures and two pressures (1 and 10 bar) under pyrolysis and gasification conditions relevant to bubbling fluidised bed conditions. The data include the yield and composition of the char, tar, and gas. These data allow the efficiency and gas phase concentration of alkali and tar to be estimated when the advanced pressurised fluidised bed combustion (A-PFBC) process was investigated.

The salient features of the study are summarised below:

- The char yield decreased with temperature under both pyrolysis and gasification conditions. The gasification tests at 10 bar showed the char yield was about 34% at 700°C and 27% at 800°C. The energy content of the dry fuel gas was estimated to be in the range 3.5–4.0 and 3.5–4.6 MJ/kg respectively. The yield and heating value of the gas were found to be adequate for an A- PFBC process with the carboniser operating at 800°C. At higher pressures, the char yield decreased and the heating value of the gas increased.
- The gas yield from the 700°C gasification test at 10 bar was about 64% which was not sufficient to achieve a temperature at the topcombustor of 1270°C.
- A solid residence time of about 55 minutes appeared to yield about 30% char yield at 800°C. To obtain the same yield using a smaller size of particles, it was expected that lower steam/coal ratio and shorter residence time should be required.
- During the process of pyrolysis and gasification, chlorine and sulphur were depleted preferentially to sodium. Under gasification conditions at 800°C and 10 bar, retention of Na, Cl, and S in char was found to be about 65%, 20%, and 30% respectively. However, the gas phase alkali concentration estimated from this data was an order of magnitude above the currently acceptable limits for gas turbine operation. It was concluded that low temperature

carbonisation alone could not limit the concentration of gas phase alkali to an acceptable level. To achieve this, separate means such as gas cooling and/or use of alkali sorbents would be required.

- The tar yield under pressurised gasification condition was low (<3%) and was not expected to be a problem for the hot gas filters.

The information generated during these tests was relevant to part of the A-PFBC process that the CRC was assessing at the same time. The gaseous environment, fluidization velocity, particle size, and particle residence time used in the tests generated information that cannot be directly related to oxygen blown, CO_2-rich, high temperature (>1000°C) gasification.

2.5.3 Pilot-scale studies in a transport gasifier

The pilot scale studies in a transport gasifier were part of a collaborative project between the EERC and the CRC for Clean Power from Lignite [70]. In the project, the gasification performance of U.S. and Australian lignites was compared in two variants of fluidised-bed gasifiers, the transport gasifier and the high-temperature Winkler (HTW) gasifier, through short-duration (4–8 hr) tests under similar conditions of temperature and pressure.

The Transport Reactor Development Unit (TRDU) was modified to accommodate oxygen-blown operation that could produce power, chemicals, and fuel. These modifications consisted of changing the loop seal design from a J-leg to an L-valve configuration, thereby increasing the mixing zone length and residence time. In addition, the standpipe, dipleg, and L-valve diameters were increased to reduce slugging caused by bubble formation in the lightly fluidised sections of the solid return legs. A seal pot was added to the bottom of the dipleg so that the level of solids in the standpipe could be operated independently of the dipleg return leg. A separate coal feed nozzle was added that could inject the coal upward into the outlet of the mixing zone, thereby precluding any chance of the fresh coal feedback-mixing into the oxidizing zone of the mixing zone; however, difficulties with this coal feed configuration led to a switch back to the original downward configuration. Instrumentation to measure and control the flow of oxygen and steam to the burner and mix zone ports was added to allow the TRDU to be operated under full oxygen-blown conditions. A schematic of the TRDU is shown in Figure 2.12.

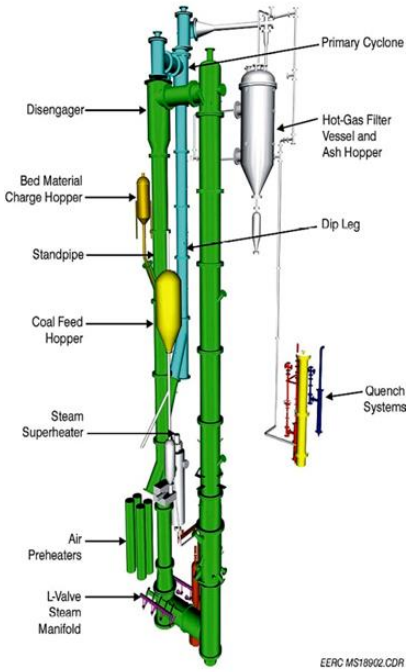

Figure 2.12: TRDU in the EERC gasification tower [70]

In total, five test were conducted and the data compared for this particular comparative study. These tests were conducted under both air blown and oxygen blown conditions. During these tests, 335 hours of operation on low rank coals such as North Dakota lignite and an Australian brown coal were performed. Data from these tests indicated that the transport gasifier performed better on the lower rank feedstock because of their higher char reactivity with the gasification reactions.

Test data indicated that these low rank feedstock provided similar fuel gas heating values; however, in general, the brown coals had lower carbon conversions than the North Dakota lignite. The high sodium levels in all of these coals led to lower operating temperatures in order to avoid bed agglomeration and deposition problems. This lower operating temperature resulted in lower than desired carbon conversions; however, the brown coal seemed to be more affected by the lower temperatures than the lignite, possibly due to its high thermal friability. Tests of a brown coal with fines removed suggested that removal of all of the fines resulted in lower carbon conversions and lower syngas heating value than the coals with the fines left in. For all fuels, the carbon conversion tended to increase and the heating value of corrected dry product gas decreased with an increasing oxygen/maf coal ratio. Comparable carbon conversions were achieved at similar oxygen/coal ratios for both air-blown and oxygen-blown operation. The fuel gas under oxygen-blown operation was high in hydrogen and carbon dioxide concentration since the high steam injection rate drives the water-gas shift reaction to produce more CO_2 and H_2 at the expense of the CO and water vapour.

However, the high steam and CO_2 partial pressures also greatly retarded the reaction of hydrogen sulphide with the calcium based sorbents.

The TRDU tests generated key performance data on carbon conversion, fuel gas calorific value, and some information on pollutant gases in the temperature range 800-900°C at pressure up to 10 bar. While these results could be representative of low temperature dry ash gasification, low carbon conversion (around 75%) means higher temperature or longer residence times will be required to obtain high carbon conversion.

2.5.4 Pilot-scale studies in a Winkler gasifier

A pressurised fluidised bed gasifier process development unit (PDU) was leased from HRL Ltd as part of the CRC research program [71]. The facility was designed as a high temperature Winkler (HTW) unit, built and commissioned by the State Electricity Commission of Victoria in 1992, and used in their test program. It was capable of operating at pressures up to 10 bar, temperatures up to 1000°C, and feed rates up to 300 kg/hr of dried coal. As the PDU had not been operated for a number of years, it was re-commissioned by the CRC in August 2001 following three tests.

The objective of the project was to provide data for the development of gasification based technologies using lignites, and for use in the validation of gasifier mathematical and process models. The data were generated under both air-blown (air and steam as gasification agents) and oxygen-enriched air-blown conditions through short-duration (approximately 2–4 hours steady-state condition) and longer-duration tests. Coals used were pre-dried by evaporative drying.

A schematic of the PDU plant is shown in Figure 2.13. In its original configuration, it consisted of an air blown gasifier based on the High Temperature Winkler (HTW) process. In 2002, HRL fitted its own O_2-enhanced system with a facility for oxygen injection up to level 3. The CRC decided to lease this system, and based on its tests, decided to retrofit oxygen and steam supply at freeboard level 4. The system requirements for oxygen-enhanced gasification were identified in conjunction with Air Liquide, who were also the suppliers of nitrogen and nitrogen storage system for the PDU use.

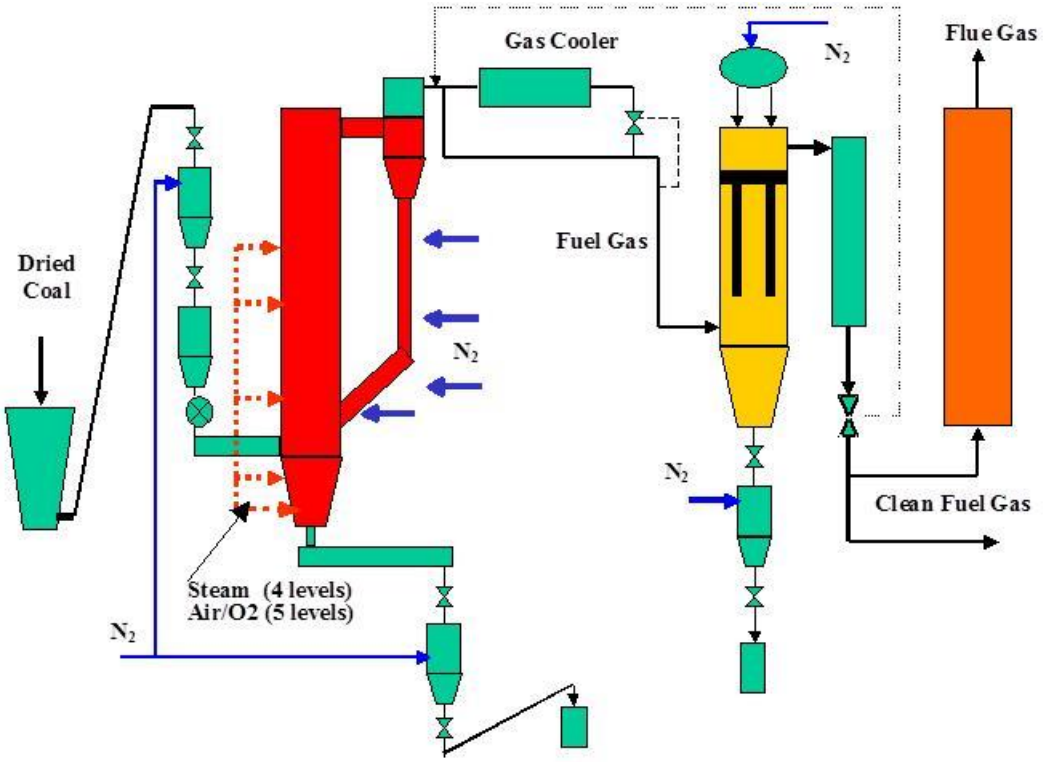

Figure 2.13: Schematic of the HTW Process Development Unit [71].

In this project, 140 tests were conducted at different pressures (2–8 bar), different temperatures (750–900 °C), with different gasification agents (air and oxygen) and feedstocks (10 Australian brown coals). It expected that carbon conversion would improve with the following:

- a narrower size distribution of the coal feed with little or no fines
- use of multiple efficient cyclones
- longer residence time (as in taller or commercial scale gasifiers, as well as gasifiers with expanded freeboard)

Additionally, it was expected that an acceptable fuel gas with LHV of 4 MJ/kg would be attained during commercial-scale gasification of these lignites. Tar was not a problem in any of the tests. There was no sign of any tar deposition on the filter elements in the gas filter, or any tar in the condensate from the fuel gas during the sampling period. During the tests, the fuel gas was cooled down to 400°C before being filtered of the dust. Based on the analysis, the majority of the alkali in the coal was transferred to the bed char and filter dust, rather than to the fuel gas.

Based on the test results, it was concluded that it would be difficult to obtain C-conversion in excess of 90% with Victorian and South Australian lignites on a consistent basis in fluidised bed gasifiers of a HTW type, which required coarse particles as feed material. This was due to the friable nature of

these coals which generate fines when dried. Fines lead to elutriation problems, but at the same time were also more amenable to gasify more quickly than coarse particles. It is, therefore, worthwhile assessing the gasification performance of these lignites in higher temperature gasifiers, which would convert carbon faster and also can use fine particles better, such as entrained flow gasifier or transport reactor gasifier.

2.5.5 Large-scale studies in an entrained flow gasifier

The large-scale studies in an entrained flow gasifier were conducted at Monash University [6, 72-74]. In this project, the experimental rig has a maximum capacity of 2 g/min, residence time up to 15s, and temperature up to 1600°C. Two step gasification (coal pyrolysis followed by the gasification of char) of dry Mowell coal and Rhenish lignite was carried out over a range of temperature (800-1400°C) and CO_2 concentration (10-80%) at a high gas flow rate of 16 L/min in an atmospheric entrained flow gasifier.

The study has generated data on pyrolysis and gasification of low rank coals at a wide range of temperatures (800-1400°C) under entrained flow conditions. The gasification performance, emission of air pollutants, yield and composition of char, tar, and gas were included in the data generated. The major findings from this project are summarized below:

- Few tar was generated during entrained flow pyrolysis and gasification below 1000°C, and no tar was detected at high-temperature pyrolysis and gasification above 1100°C.
- Entrained flow pyrolysis generated high surface and reactive chars for the subsequent gasification. However, the char yield generally decreased with increasing pyrolysis temperature at a high temperature between 1100°C and 1400°C.
- The gas yield of CO and H_2 increased with increasing temperature and CO_2 concentration.
- Morwell char required around 6 s for complete conversion at 1000 °C and 20% CO_2.
- The yield of hydrocarbon contaminants decreased with gasification temperature increases. No NH_3 was detected at high temperature pyrolysis and gasification. By contrast, H_2S and HCN were detected at ppmv level which requires gas cleaning.

However, the data generated from these tests are limited to one Victorian brown coal and two step gasification process. The information on other Victorian brown coals, direct gasification process, and effect of residence time is still missing, which needs to be further investigated. Moreover, biomass

and Victorian brown coal are both known as low rank fuel, but the similarities and differences of the two fuels in entrained flow gasification behaviour have never been studied.

2.6 Analysis of Victorian brown coal gasification

Although some gasification research of Victorian brown coal using different gasifiers and technologies has been performed, the related design requirements for the different gasifiers and the effects on conversion behaviour and syngas volumes for the different technologies are not well understood for Victorian brown coals. Moreover, these technologies for Victorian brown coal have their challenges and difficulties.

Bubbling fluidised beds are expected to pose particular challenges with localised hot spots potentially arising from the significantly greater concentration of O_2 at air inlets. These hot spots may lead to alkali vaporisation or agglomeration of the mineral matter in the coal particles. Agglomeration in a bubbling fluidised bed has significant impacts on operability and stability. Steam can be added to try and manage these temperature effects; however, knowledge of the fuel and technology specific requirements is needed to ensure that the addition of steam does not have an adverse impact on the overall gasification process. This is particularly relevant to very high moisture coals such as Victorian brown coals.

Recirculating fluidised beds and transport gasifiers are affected by the reduced syngas volume and also the low ash content managing the 'solids inventory' and gas velocities are seen as issues that need particular consideration. This is especially relevant for the transport gasifier (and entrained flow gasifiers which rely on char recycling systems, such as the two-stage entrained flow variants) given the importance of cyclone filtration to effective operation.

Fixed bed gasification has been successfully used to convert lignites to synfuels using oxygen blown gasification (e.g. at the Great Plains Synfuels plant). However, fixed bed technologies have very specific requirements for feedstock properties, in particular regarding coal and char strength, structure, and permeability. There is very little knowledge of how Victorian brown coals perform within such requirements and therefore their suitability for this kind of technology.

Compared with these gasification technologies, entrained flow gasifiers obtain high carbon conversion and tar-free product gas by requiring very short residence time (several seconds) and high temperature. Moreover, entrained flow gasifiers have the flexibility of feedstock handling especially

for coal, and no specific requirements for coal type [27]. Entrained flow gasification is the technology with the most potential for Victorian brown coals because of these advantages.

Little research has been conducted on gasification of Victorian brown coals using entrained flow technologies. Only Tanner et al. reported the gasification behaviour and mineral reactions during gasification for one Victorian brown coal (Morwell) using a high temperature entrained flow reactor [6, 72-75]. However, their studies are limited to one coal and two-step gasification process in which char is firstly produced from coal and then used for gasification. In practice, the majority of gasification companies, such as Shell, GE, and Siemens, use coal directly in their commercial entrained flow gasifiers [76].

In this study, we investigate entrained flow gasification of four Victorian brown coals at both laboratory and large scale. The two gasification processes, direct and two-step are studied and the gasification performance of Victorian brown coals is compared. Furthermore, the mineral matter behaviour of Victorian brown coals during pyrolysis and gasification is examined. This study offers new comprehensive understandings of entrained flow gasification of Victorian brown coals and provides valuable experimental data for industry to design gasifiers for low-rank coal.

2.7 Chapter summary

Victoria has abundant brown coal resources but these are mainly used for mine-mouth power generation units with large greenhouse gas emissions and low energy efficiency. Gasification is one of the most potential and feasible technologies for Victorian brown coal utilization into high-value products. Using gasification can convert Victorian brown coal to syngas for multiple applications. Therefore, there need to be a study of gasification of Victorian brown coal to require a deeper understanding of the gasification of brown coal for syngas generation.

Currently, there are three main types of gasifier: the fixed bed gasifier, the fluidized bed gasifier, and the entrained flow gasifier. The entrained flow gasifier can achieve higher carbon conversion with short residence time (a few seconds) and handle different types of coal feed from dry to slurry, and from low-rank to high-rank. In practice, commercial gasification technologies are almost all based on entrained flow technology. Furthermore, most entrained flow gasifiers are oxygen-blown because these gasifiers result in the absence of significant amounts of N_2, which is disadvantageous to the processes of CO_2 capture or downstream production of chemicals and liquid fuels. Hence, there is a need for higher efficiencies and lower cost entrained flow gasification systems, in particular for Victorian brown coal utilisation.

For coal gasifier design, kinetics of coal/char gasification is necessary in order to understand the physical and chemical process during the reaction. Moreover, the kinetic data can be used for the existing models which can be adapted for brown coal gasification process. Currently, the kinetic data for entrained flow gasification of Victoria brown coals is very limited, and only one study [1] has reported on Victorian brown coal chars. However, this study is limited to one reaction model and the validity of kinetic data for experimental entrained flow gasification is still unclear.

Some research has been performed on the gasification of Victorian brown coals and South Australian lignites. These research involve experimental work at both laboratory and pilot scale at facilities of the CRC for Lignite. However, most of the experimental work was carried out at low temperatures, up to 900°C, relevant to the fluidised bed or transport reactor pyrolyser or gasifier, which results in low C-carbon conversion and poor quality of gas. Few investigations on entrained flow gasification of Victorian brown coal can be found in open literature. Tanner et al. reported the data of entrained flow pyrolysis and gasification using an atmospheric entrained flow reactor including gasification performance and emission of air pollutants [6]. However, their studies are limited to one Victorian brown coal and two step gasification. Moreover, there is no study to compare entrained flow gasification behaviour between Victorian brown coal and another low rank fuel- biomass.

Therefore, this PhD project study is a significant extension of the previous work on Victorian brown coals and major objective is to expand the entrained flow gasification data of Victorian brown coal. In this project, the entrained flow gasification behaviour of four Victorian brown coals through direct and two step gasification was examined. The behaviour of mineral matters during entrained flow pyrolysis and gasification was also investigated. Victorian brown coal was compared with another low rank fuel- biomass- with respect to gasification performance, emission of gas pollutants, and mineral transformation. Furthermore, kinetics data of CO_2 gasification of Victorian brown coals using modified volumetric model was generated to develop a mathematic model for predicting carbon conversion of Victorian brown coal. This study would advance the development of the utilisation of Victorian brown coal in higher value product processes by generating fundamental experimental and modelling data at the laboratory and large scale.

Chapter 3 Experimental methodology

This chapter introduces the coal samples used in this study, main experimental setups for the research, and the analysis method for gasification behaviour and coal/char samples.

3.1 Coal samples

In this study, four Victorian brown coals have been selected for entrained flow gasification. The four Victorian brown coals are Morwell (MW), Loy Yang (LY), and Yallourn (YL) coal from Latrobe Valley, and Maddingley (MD) from Maddingley mine in Victoria. The coal samples were air dried and sieved with a particle size of 90-106 μm. The sieved coals were oven dried overnight before gasification experiments. As these dried coals can reabsorb moisture to some extent, the moisture content was determined immediately prior to the experiments. The properties of these coals were presented in Table 3.1.

Table 3.1: The properties of coal samples selected in this study

Items	**MW**	**MD**	**LY**	**YL**
Moisture (oven-dried, wt.%)	0.56-2.35	1.01-1.50	0.49-1.50	0.8-1.25
Proximate analysis (dry basis, wt.%)				
Volatile matter	49.31	47.50	48.00	48.18
Fixed carbon	48.65	37.26	43.58	51.82
Ash	2.04	15.24	8.42	2.32
Ultimate analysis (dry basis, wt.%)				
Carbon	60.42	50.91	60.01	62.99
Hydrogen	4.59	4.56	4.68	4.98
Nitrogen	1.54	0.51	0.58	0.54
Sulfur	0.86	3.34	0.70	0.40
Ash	2.04	15.24	8.42	2.32
Oxygen (by difference)	30.55	25.44	25.61	28.77

3.2 Experimental equipment

Four analytical and experimental equipment were used in this project: synchrotron infrared micro-spectroscopy, thermo-gravimetric analyzer, low temperature entrained flow reactor (up to 1000°C), and high temperature entrained flow reactor (up to 1650°C).

3.2.1 Synchrotron infrared micro-spectroscopy

The infrared microspectroscopy (IRM) at the Australia Synchrotron is utilized in this project for in-situ FTIR experiments to investigate the change of surface functional groups during pyrolysis, as shown in Figure 3.1. The IRM beamline is composed of a Bruker V80v Fourier transform infrared (FTIR) spectrometer and a Hyperion 2000 IR microscope, which offers high signal-to-noise ratios at between 3-8 μm diffraction limited spatial resolutions. It is perfect for the analysis of microscopic samples and is able to focus on a single small particle. In addition, the microscope attached to the system allows users to observe the morphology change of their samples during the experiment. The facility can be heated up to 550 °C with different heating rates, up to 150 °C/min, in N_2.

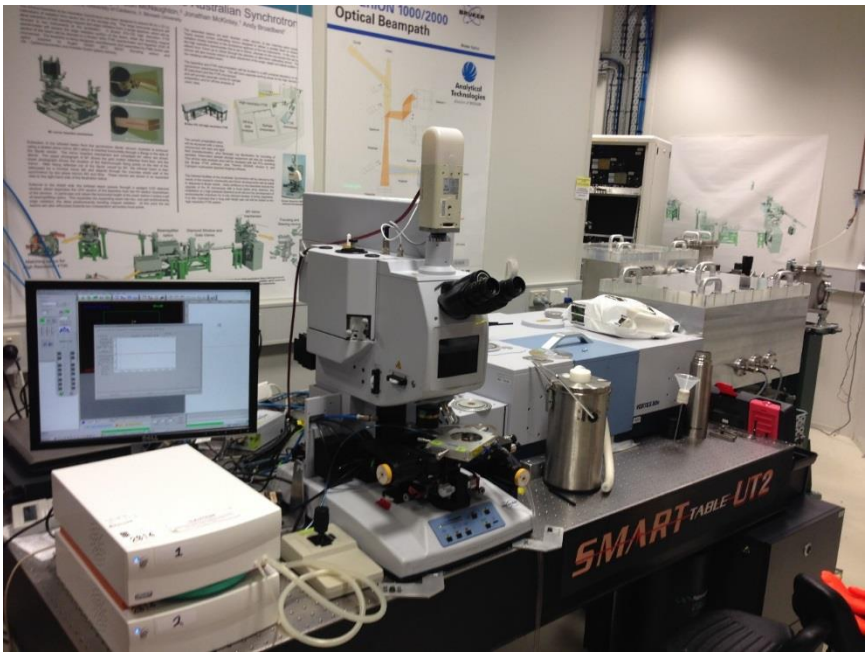

Figure 3.1: The picture of the synchrotron infrared micro-spectroscopy

3.2.2 Thermo-gravimetric analyzer (TGA)

A thermo-gravimetric analyzer (Netzsch STA model 449 F3 Jupiter) is utilized in this project for thermo-gravimetric analysis to investigate the gasification reactivity, as shown in Figure 3.2. Thermo-gravimetric analysis allows high precision measurements of mass change and temperature under various environment-pyrolysis, combustion or gasification. The furnace can be programed

either for a constant heating rate with various temperature, or the time for an isothermal reaction. In the experiments, a small amount of sample (around 10 milligrams) is placed in a small crucible inside an electrically heated furnace equipped with a mass balance and thermocouple for accurate measurements of temperature and mass loss. The maximum temperature of the TGA used in this project is 1250 °C.

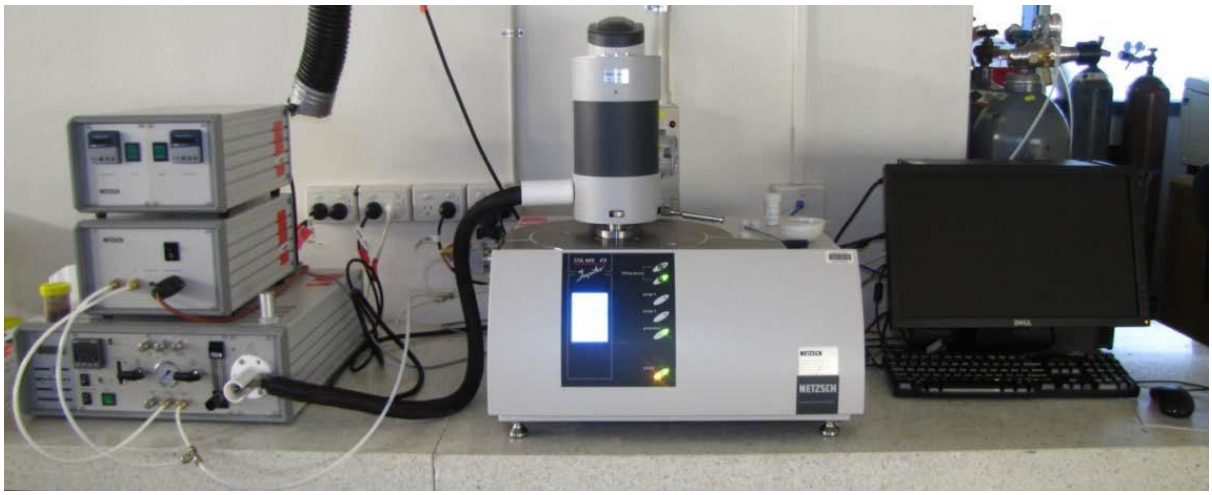

Figure 3.2: The picture of the Thermo-gravimetric analyzer (Netzsch STA model 449 F3 Jupiter)

3.2.3 Low temperature entrained flow reactor

An electronically heated entrained flow reactor was employed for low temperature char gasification, as shown in Figure 3.3. Variations in temperature, gasification medium and residence time allow the gasification process to be examined in terms of carbon conversion, gas composition and quality, char properties. The facility can be operated at wall temperature up to 1000 °C using pulverised coal or char (~100 μm). The input CO_2 gas flowrate between 0.25 and 1.5 L/min can generate CO_2 concentration of between 5% and 30%. The residence times of ~ 6 s can be achieved.

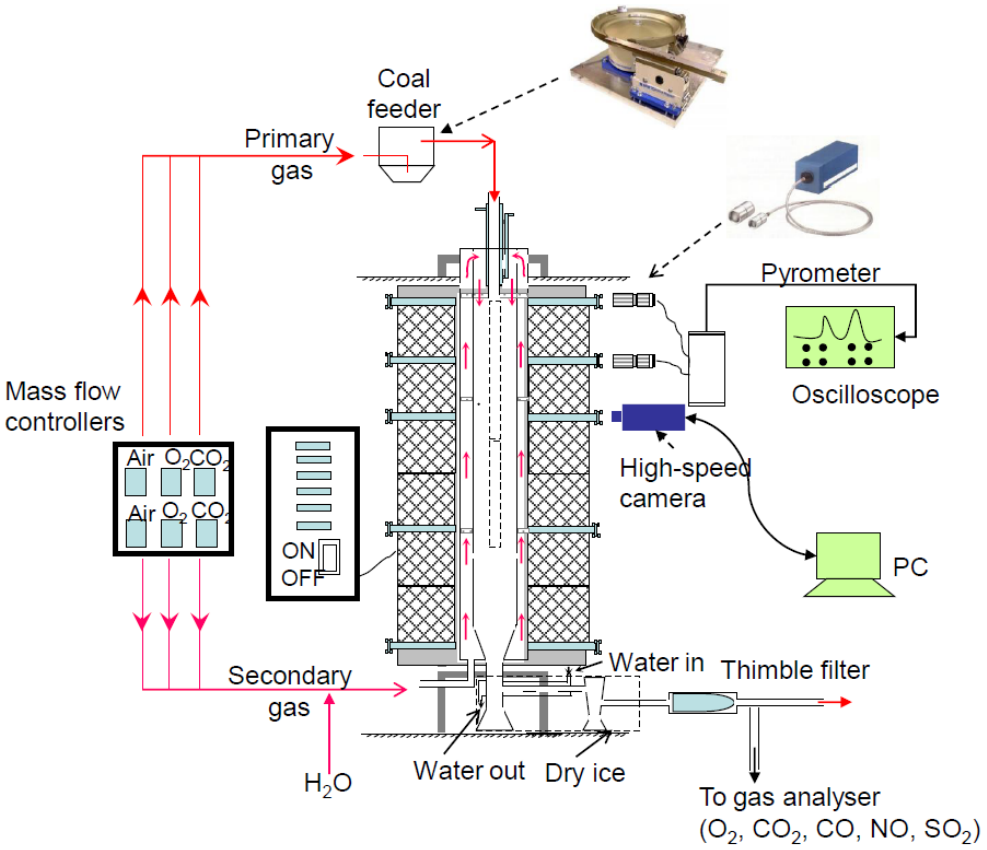

Figure 3.3: Schematic diagram of low temperature entrained flow reactor [77]

3.2.4 High-temperature entrained flow reactor

A high temperature electrically heated entrained flow reactor was employed to investigate the entrained flow gasification behaviour of low-rank coals at a variety of temperatures, CO_2 concentrations and residence time. The facility can be operated at wall temperature up to 1650 °C, is fed with pulverised coal or char at a feeding rate up to 2 g/min. Input CO_2 gas flowrate between 1.6 and 6.4 L/min can generate CO_2 concentration of between 10% and 40%. The residence times of between ~5 and 9s can be achieved. A schematic drawing of the entrained flow reactor is shown in Figure 3.4 [78].

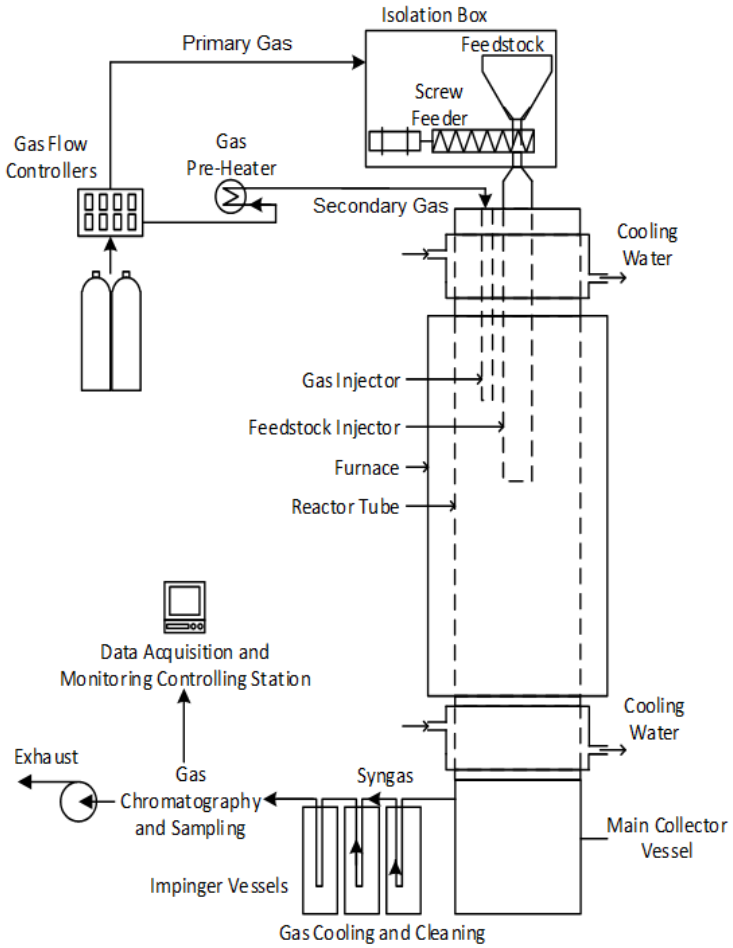

Figure 3.4. The schematic diagram of the high temperature entrained-flow gasifier [78]

3.3 Gasification behaviour

In this project, the gasification behaviour of coal is characterised in terms of carbon conversion, gas composition, and emission of air pollutants.

3.3.1 Carbon conversion

Carbon conversion represents the amount of carbon in the feedstock that has reacted to gas phase. It can be calculated using ash as a tracer (solid phase) or carbon balance between feed solid and gas phase (gas phase), and their calculations are given below:

Solid-phase carbon conversion: $\mathrm{X}(\%) = \frac{m_{C,feed} - m_{C,ash}}{m_{C,feed}} \times 100$

Gas-phase carbon conversion: $\mathrm{X}(\%) = \frac{(X_{CO} + X_{CO_2} + X_{CH_4}) \times 12}{m_{C,feed+CO_2}} \times 100$

Where $m_{C,feed}$ is the mass of carbon in the feeding inlet, $m_{C,ash}$ is the mass of carbon in solid residuce collected from the outlet, X_{CO}, X_{CO2}, X_{CH4} is the molar flowrate of CO, CO_2 and CH_4 in the outlet gas, $m_{C,feed+CO_2}$is the mass flowrate of the carbon including the feed coal/char and feed CO_2 in the inlet.

However, both the calculations have their own uncertainty. The uncertainty of sold-phase method includes the incomplete solid recovery at the outlet and due to ash evaporation; the uncertainty of gas-phase method is mainly from the inaccuracy of the gas analysis by the gas analyzer. The variations in results of the two methods ranged 0.4-7.6%. In this study, the carbon conversion was calculated in both solid and gas basis.

3.3.2 Gas composition

The gas composition of the product gas was analyzed using a micro-GC. The micro-GC is capable of online sampling the gas from the the downstream every three minutes to measure the concentration of the H_2, O_2, N_2, CO, CH_4, and CO_2. Before the experiments, the micro-GC was calibrated using external standard gases to ensure its accuracy. At least 20 data points, when the system is in the steady state after coal feeding, were collected for each run. Those gas composition data were normalized, averaged and presented in the study.

3.3.3 Pollutant gas emission

The NH_3, HCN, and H_2S emission level during gasification were measured three times respectively using a Dräger-Tube during steady state. The concentration of NH_3, HCN, and H_2S was averaged from measurements and presented in the study. The measurement accuracy of NH_3 is ± 10-15%, HCN is ± 10-15%, and H_2S is ± 5-10%.

3.4 Coal and char properties

In this project, the coal and char samples from pyrolysis and gasification experiments were characterised for chemical composition, particle size, morphology, and mineral matter.

3.4.1 Chemical composition

The chemical composition was measured by proximate analysis and ultimate analysis. The proximate analysis was carried out in a Thermo-Gravimetric Analyser (Model STA 449 F3 Jupiter®,

NETZSCH-Gerätebau GmbH, Germany) , according to Australian standards of low rank coal-AS 2434.2, 2434.7-2434.8. The moisture content is determined from the mass loss that a sample undergoes after it has been heated to 110 °C under N_2 atmosphere and the final mass stabilised. The volatile content of sample corresponds to the volatile products evolved between 110-900 °C under N_2 as a result of thermal decomposition. Ash is the residue that after the sample has lost moisture and volatile and fixed carbon has undergone combustion at 815 °C in air. The fixed carbon was determined by difference between sample weight after losing the volatile and ash content [79].

Ultimate analysis was conducted by CHNS/O analyser (Model 2400, Perkin-Elmer, USA). To determine carbon, hydrogen, nitrogen, and sulfur, the sample was combusted at 975 °C to obtain CO_2, H_2O, N_2, and SO_2, and analyzed through a chromatographic column. The system detects the gases by matching their thermal conductivity and directly gives the concentration of C, H, N, and S in weight percent by comparing with calibration standards. Ash content was determined by combustion the sample at 800 °C. The oxygen content was calculated by difference.

3.4.2 Particle size distribution and morphology

The particle size distribution of samples was examined by the Malvern Mastersizer 2000. The Mastersizer 2000 is a practical and reliable technique for a broad range of particle sizes based on the physics of light scattering. During the measurement, the loaded particles are passed through a focused laser beam. Particle scatter light at an angle that is intensively proportional to their size. The angular intensity of the scatter light is then measured by a series of photosensitive detectors to give a result on the particle size distribution of the samples. Special methods were required to prevent particle agglomeration whilst ensuring that the fragile coal and char particles were not damaged. Therefore, the coal and char samples were dispersed in ethanol, and analysed with no ultrasonic agitation.

Scanning Electron Microscope images of samples were generated on a Field-emission scanning electron microscope (FE-SEM) (Hitachi SU8010). SEM has been extensively used to study the morphology and cross section of coal and coal char. Analysis of the SEM image can provide valuable information such as particle size, swelling of the particles during conversion, and structure of char or ash.

3.4.3 Mineral matter

The mineral matter of coal and char samples was assessed by the X-ray powder diffraction. The X-ray diffraction (XRD) analysis is the widely used method for identifying mineral phases and minerals in coal and char. XRD of coal and char reveals important qualitative and quantitative information on the mineral matter composition in coal and the interaction of mineral matter during conversion process. It is a rapid and nondestructive technique, in most cases, it provides an unambiguous mineral determination[80].

In this study, a MiniFlex 600 XRD instrument was used to record X-ray intensities from the examined coal or char samples. Copper K radiation (30 kV, 30 mA) was used as an X-ray source. Samples were packed in to a round cavity in an aluminium holder and scanned in a step-scan mode (0.1^{o}/step) over the angular range of 5 to 100^{o} (2θ). The spectrum was then collected and analysed by the XRD software.

Chapter 4 Functional group evolution during pyrolysis

The gasification is a heterogeneous reaction where the devolatilization, also known as pyrolysis, and gasification steps occur. As the initial step in the coal gasification process, pyrolysis is important, accounting for up to 70% weight loss of coal. What happens during the pyrolysis process affects the structure of the residual solids (char) and their gasification behaviour, including emission of gaseous pollutants during the subsequent gasification step. Pyrolysis reactions might be more dominant at lower temperatures while gasification reactions at high temperatures. Therefore, it is important to understand the pyrolysis behaviour as a function of temperature, which improves understanding of any gasification process, either direct gasification or two step gasification (pyrolysis followed by char gasification). Moreover, the gas yield and char characteristics of pyrolysis are largely affected by the change of surface functional groups during coal pyrolysis. However, studies on the behaviour of functional groups during pyrolysis of low rank coals are very limited in the literature, especially for Victorian brown coals.

In this chapter, the evolution of surface functional groups of four Victorian brown coals (MW, YL, LY, and MD) and one Thailand lignite during pyrolysis was investigated at Australian Synchrotron. The change of functional groups during coal pyrolysis from 30 °C to 550 °C (the maximum capacity of the synchrotron IR) was in-situ examined by the synchrotron IR. To further explore the change of functional groups at a higher temperature (>550 °C), chars pyrolysed at 700-1000 °C in an entrained flow reactor were prepared in advance and then analysed by the synchrotron IR at room temperature. This study for the first-time presents important information on the behaviour of surface functional groups during coal pyrolysis by the synchrotron IR.

This chapter reproduces the following published paper in Journal of Analytical and Applied Pyrolysis.

Journal of Analytical and Applied Pyrolysis 122 (2016) 122–130

Contents lists available at ScienceDirect

Journal of Analytical and Applied Pyrolysis

journal homepage: www.elsevier.com/locate/jaap

In-situ synchrotron IR study on surface functional group evolution of Victorian and Thailand low-rank coals during pyrolysis

Tao Xu, Srikanth Chakravartula Srivatsa, Sankar Bhattacharya*

Department of Chemical Engineering, Monash University, VIC 3800, Australia

ARTICLE INFO

Article history:
Received 26 May 2016
Received in revised form 11 October 2016
Accepted 12 October 2016
Available online 13 October 2016

Keywords:
Synchrotron beamline
In-situ FTIR low-rank coals
TGA

ABSTRACT

In-situ synchrotron FTIR studies were conducted using four Victorian brown coals and one Thailand lignite to examine the evolution of functional groups from the surface of the sample during pyrolysis from room temperature to 550 °C. TGA data showed that the pyrolysis of all coals is comprised of a drying stage (30–200 °C) and devolatilization stage (200–900 °C). FTIR data showed that compared to Victorian brown coals, less surface functional groups were found in Thailand lignite. The loss of functional groups from Thailand lignite was observed during drying, and the devolatilization consisted of two stages. For Victorian brown coals, the concentration of oxygen contained hydroxyl and carboxyl groups decreased during the drying stage, due to the removal of water, and breakdown of weakly bonded alkene and alkyne. When temperature gradually increased during devolatilization stage, more functional groups were released. However, by 550 °C, the groups at the wavenumber of 1700–1340 cm^{-1} (carbonyl, carboxylate, aromatic ring, CH_3 and CH_2 groups) remained in the sample. Based on the spectra taken of two chars from the same brown coals, these groups were not completely removed until 1000 °C.

1. Introduction

Coal currently provides 40% of global electricity needs [1]. Brown coals are of the lowest rank among the coals, but the vast reserves of economically recoverable brown coal make it a large source of fuel for several countries. Victoria has over 430 billion tonnes of brown coal reserves, which account for over 20% the world's low-rank coal reserves. The shallow depth of overburden combined with high coal to overburden ratio (between 0.5:1 and 5:1) make it one of the lowest cost energy sources in the world [2]. The conversion of brown coals into fuel can be carried out through different processes such as pyrolysis, combustion, gasification, and liquefaction. As the initial step in any coal conversion process pyrolysis is important, accounting for up to 70% weight loss of coal [3]. What happens during the pyrolysis process affects the structure of the residual solids (char) and their gasification behaviour, including emission of gaseous pollutants during the subsequent gasification step.

During pyrolysis when the coal particle is heated up, functional groups on the surface of coal decompose and generate gases such as H_2, CO, CO_2, CH_4, and liquid products, leaving the char at the end [4]. The gas yield and char characteristics are largely affected by the change of surface functional groups during pyrolysis of coal. Pyrolysis process is influenced by several factors such as temperature, heating rate, pressure and coal rank. These factors have a significant effect on the char properties and kinetics of the devolatilization process [3,5].

Studies are available on the loss of functional groups on coal coalification process [6,7], oxidation [8], and drying process [9], but on pyrolysis of Victorian brown coal, it is limited. Ibarra et al. investigated the coal structure changes in peat and low-rank coals during the coalification process using Fourier transform infrared (FTIR) spectroscopy [7]. However, this study did not involve the functional group change with temperature. Calemma et al. used FTIR spectroscopy to study the chemical changes during dry oxidation of a sub-bituminous coal at low temperatures from 200 °C to 275 °C [8]. Tahmasebi et al. used FTIR to study the chemical structure changes during drying of Chinese lignite in hot air [9]. Nonetheless, their study did not evaluate the loss of the functional groups during pyrolysis.

In another study, Lin et al. studied the functional group transformation in a Chinese brown coal as a function of temperature up to 700 °C in N_2. The decomposition of aliphatic groups and release of a large amount of oxygen-containing functional groups (heterocyclic, phenolic hydroxyl, and crystalline hydrates) were observed when temperature increased [10]. Zhang et al. investigated the chemical structure change of Victorian Loy Yang coal and Western Australian

* Corresponding author.
E-mail address: Sankar.Bhattacharya@monash.edu (S. Bhattacharya).

http://dx.doi.org/10.1016/j.jaap.2016.10.009
0165-2370/

Table 1
Proximate and ultimate analysis of coal samples.

Items	Yallourn	Loy Yang	Morwell	Maddingley	Thailand lignite
Proximate analysis (wt%)					
Moisture (a.d.)	8.92	3.72	11.17	6.63	5.34
Volatile matter (d.b.)	48.18	48.26	49.31	41.33	45.20
Fixed carbon (d.b.)	45.70	45.59	48.65	33.80	3.99
Ash (d.b.)	6.12	6.15	2.04	24.87	50.81
Ultimate analysis (d.b., wt%)					
Carbon	66.35	66.15	60.42	40.08	23.19
Hydrogen	4.92	4.62	4.59	4.53	2.83
Nitrogen	0.39	0.64	1.54	0.32	0.95
Sulfur	0.30	0.31	0.86	1.66	4.00
Ash	6.12	6.15	2.04	24.87	50.81
Oxygen (by difference)	21.92	22.13	30.55	28.54	18.22

a.d. = air dry basis, d.b. = dry basis.

Collie sub-bituminous coal during fast pyrolysis to 600 °C. Aromatic ring system in these coals was not found to significantly change when the temperature increased to 600 °C [11]. However, in their studies, the functional group changes are measured from ex-situ samples. In other word, coal samples firstly pyrolysed in a wire-mesh reactor at a selected temperature, then cooled down to room temperature before taking IR analysis, where the effect of cooling on samples is unknown.

The results in the existing literature are mainly from ex-situ laboratory FTIR spectroscopy, where the sample was subjected to the desired temperature in a gaseous environment and cooled down before taking any measurement. For the laboratory based FTIR, coal samples are required to be crushed to a fine size and dispersed in a Potassium Bromide (KBr) disk and pressed at very high pressure. Hence, a bulk of samples, not any single distinct particle, are measured based on the assumption that particles are uniformly dispersed in the disk [12]. However, because of the high pressure applied during pressing the KBR pellet, the sample can also get destroyed. Another limitation of laboratory-based IR is that samples only can be measured at room temperature, so functional group changes during the pyrolysis process can not be directly observed. In contrast, at synchrotron IR beam line a single particle can be focused, and functional group evolution can be tested as a function of temperature in situ at high resolution. Thereby, the variation and error from heterogeneous differences among particles can be detected, and more precise information on surface functional groups can be obtained. Moreover, the synchrotron IR is capable of observing the particle morphology change during IR measurements [13]. Thus, in-situ synchrotron IR is a useful tool to determine the decomposition steps during the pyrolysis process.

The application of in-situ FTIR on coal is limited to the determination of the strength distribution of hydrogen bond up to 500 °C [14], or the examination of spontaneous combustion at low temperature [15–17]. There is one study to examine the decomposition of the functional groups for Huolinhe brown coal up to 500 °C [18]. They found the groups of methyl and carboxyl decomposed with temperature, whereas the intensity of ester and anhydride initially increased and then decreased. However, the application of in-situ FTIR for the high-temperature pyrolysis of low-rank coals has not been reported so far.

This study for the first-time presents information on the surface functional group evolution during coal pyrolysis by in-situ synchrotron IR. In this study, the effect of temperature on surface functional group evolution of four Victorian brown coals and one Thailand lignite during pyrolysis was investigated at the Infrared Microscopy beamline facility at Australian Synchrotron. To further explore the effect of char preparation temperature, chars pyrolysed at 700–1000 °C in a drop tube reactor were prepared in advance and analysed in the same beamline.

Table 2
Proximate and ultimate analysis of Yallourn and Maddingley char.

Fuel	Pyrolysis Temperature (°C)	Proximate analysis (dry basis)		
		Volatile matter	Fixed carbon	Ash
Yallourn	700	17.79	72.45	9.76
	800	8.29	83.37	8.33
	900	5.18	84.28	10.54
	1000	8.18	81.63	10.19
Maddingley	700	16.24	49.53	34.21
	800	13.08	52.27	34.21
	900	10.91	53.44	34.63
	1000	9.94	54.31	35.73

2. Experimental

2.1. Coal samples

Four Victorian brown coals (Morwell, Loy Yang, Yallourn, and Maddingley), and a Thailand lignite were used in this study. Thailand lignite is from the Mae Moh mine in Thailand. All samples were firstly air-dried and sieved between 20 μm and 38 μm. The proximate and ultimate analysis of the coal samples were given in Table 1.

Coal chars of Yallourn brown coal and Maddingley brown coal were also used to investigate the functional group evolution at different char preparation temperature. These coal chars are derived from coal pyrolysis in a drop tube furnace at four different temperatures – 700 °C, 800 °C, 900 °C and 1000 °C. The proximate analysis of Yallourn and Maddingley char pyrolysed at 700–1000 °C is presented in Table 2.

2.2. Apparatus and procedure

In situ FTIR experiments were conducted using the infrared Micro spectroscopy (IRM) beamline at the Australia Synchrotron. The IRM beamline consists of a Bruker V80v Fourier transform infrared (FTIR) spectrometer and a Hyperion 2000 IR microscope, which offers high signal-to-noise ratios at between 3 and 8 μm diffraction limited spatial resolutions. Because of this, the beamline is perfect to analyse microscopic samples. In a specially designed Linkam cell with BaF_2 window, the microscope attached to the system allows to pick the particle of interest and focus on it to obtain the information on a single particle during the course of the experiment.

About 0.5 mg sample was used for each run in the experiments and dispersed on BaF_2 disk. The sample chamber was initially purged at 30 °C for 10 min in a flowing nitrogen stream. Then these were heated at the rate of 10 °C/min up to 550 °C, in the presence of ultra-high purity nitrogen to maintain a pyrolysis atmosphere

and prevent combustion. The transmission spectra were collected by the acquisition of 100 scans at 100 °C intervals. After the samples had been analysed at 550 °C, and these were cooled down to room temperature at a rate of 10 °C/min. At each run, at least four particles were chosen for comparison.

To relate the functional group evolution to the stages of the pyrolysis, the infrared spectra at each temperature is compared with the weight loss measured by a thermo-gravimetric analyser (Model STA 449 F3 Jupiter®, NETZSCH-Gerätebau GmbH, Germany). Under ultra-high purity N_2 atmosphere, the temperature was raised to 200 °C at a slow heating rate of 5 K/min and then to 1000 °C at a heating rate of 10 K/min.

2.3. Data analysis

Since the majority of the functional groups were observed in the wavenumbers between 1200 and 3700 cm^{-1}, this range was chosen for data analysis. The spectral data were then analysed by Bruker Opus 7.2 software. Based on the analysis method of Kirtania et al. [12], the data were corrected for baseline and then the peaks were identified.

3. Results and discussion

3.1. Chemical functional group identification of raw coals

The identification of chemical functional group from the room temperature spectra of various coal samples was performed, and the results were listed in Table 3 for comparison. The functional groups listed were identified on the surface of the particles before the in-situ pyrolysis started.

As shown in Table 3, chemical functional groups observed in Thailand lignite were fewer than the Victoria brown coals. Only four main functional groups were identified in the Thailand lignite, and they are followed by alkyne (2100–2260 cm^{-1}), C═O stretching (1700 cm^{-1}), COO^- and aromatic ring (1560–1490 cm^{-1}), and cyclic —CH_2 (1370 cm^{-1}). Compared to Thailand lignite, Victoria Brown coals have more functional groups observed at the wavelength between 3030 and 3700 cm^{-1}. Furthermore, compared with other 3 Victoria brown coals, the aromatic C—H stretching (3030 cm^{-1}), methyl (C—H) (2896 cm^{-1}) was limited in the Morwell brown coal.

3.2. Thermogravimetric analysis of the pyrolysis process

Fig. 1 shows the thermogravimetric curves (TG and DTG curve) during pyrolysis of the Victorian and Thailand coals. TG profile shows the weight loss of the sample with temperature, and DTG profile presents the derivatives of the TG profile, which represents the weight loss rate as a function of temperature. Both these curves provide a precise mapping of the thermal process of the sample. The weight loss profile in Fig. 1 can be divided into two stages. The first stage is the drying phase, occurring at 50–200 °C, where the moisture within the sample is released. The pyrolysis mainly took place in the second stage from 200 to 900 °C – termed as devolatilization. This stage would form tar, light hydrocarbon, and char condensation because of the primary pyrolysis and secondary pyrolysis [21]. The third stage was of temperature over 900 °C. There is no further weight lost at this stage, and the curve becomes nearly flat. Comparing Victorian coals and Thailand coal, the initial pyrolysis temperature for all coals was similar up to 200 °C. However, the third stage of the Victorian coals started at a lower temperature (800 °C) than that of Thailand coal(at 920 °C), as shown in the TG curve in Fig. 1(a).

From the DTG curve in Fig. 1(b), firstly, a peak can be seen around 95–175 °C in the drying stage. In this stage, loss of adsorbed water in the sample is expected to release. Some coals may undergo reduction of oxygen-containing functional groups, including carboxyl, hydroxyl, and carbonyl [22]. The oxygen-containing functional groups are decomposed to generate carbon dioxide at elevated drying temperatures [23]. The second peak is at around 400 °C during the devolatilization stage. The general trend related to the functional group change in this stage was discussed by Serio et al. [3] and Solomon and Hamblen [24]. Firstly, depolymerisation happened on the weakest aliphatic bridges between aromatic and hydro aromatic clusters to release hydrogen, or to increase the aromatic hydrocarbon concentration, or to generate tar. During the primary pyrolysis, CO_2, CH_4, H_2O and light aliphatic gas are released because of the decomposition of functional groups. During secondary pyrolysis, CH_4, HCN, CO and H_2 would be formed from methyl groups, ring nitrogen compound, ether links, and ring condensation, respectively. Based on these observations, the functional group evolution during pyrolysis is further discussed in this study. It is interesting that there is a DTG peak around 800 °C for the Thailand coal, not for other Victorian coals, which is due to the mineral decomposition of silicon content present in the sample. However, the surface functional group change is the focus of this

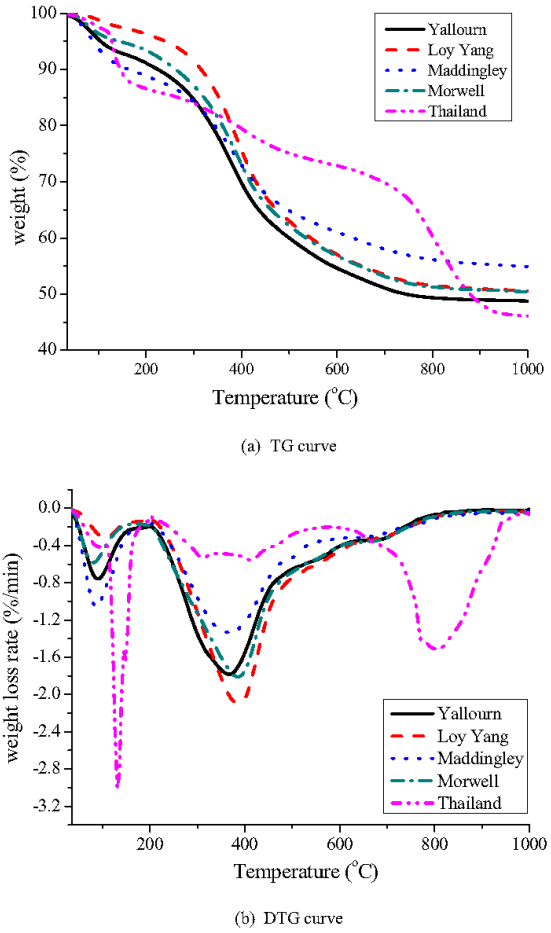

Fig. 1. Thermogravimetric curves of Australian and Thailand coals: (a) TG curve, (b) DTG curve.

Table 3
Functional groups identification of different coals.

Wavelength (cm^{-1})	Functional Groups	Thailand Lignite	Morwell coal	Loy Yang coal	Yallourn coal	Maddingley coal	Reference
3700–3300	—OH and —NH stretching	N	Y	Y	Y	Y	[14,19]
3030	aromatic C—H stretching	N	Y	N	N	N	[19]
2955	asymmetric methyl ($—CH_3$)	N	N	N	N	Y	[9]
2922	methylene ($—CH_2—$)	N	N	Y	Y	Y	[9]
2896	methyl(C—H)	N	Y	N	N	N	[9]
2850	methylene ($—CH_2—$)	N	Y	Y	Y	Y	[9]
2640	COOH dimers	N	N	N	N	Y	[14]
2509–3010	COOH dimers	Y	Y	Y	Y	Y	[20]
2370	atmospheric CO_2 interference	Y	Y	Y	Y	Y	[19]
2100–2260	alkyne	Y	Y	Y	Y	Y	[20]
1850–2000	alkene	N	N	Y	Y	Y	[20]
1772	esters, anhydrides second band	N	Y	Y	Y	Y	[6,8]
1748–1715	ester and aliphatic COOH	N	N	Y	Y	Y	[9]
1700	C═O stretching	Y	Y	Y	Y	Y	[8,19]
1660	conjugated C═O, ketones	N	Y	Y	N	N	[6,8,9]
1560–1490	COO—, aromatic ring	Y	Y	Y	Y	Y	[9]
1427–1437	CH_3,CH_2 groups (bending)	N	Y	Y	Y	Y	[8]
1370	CH_3 symmetric deformation, cyclic $—CH_2$	Y	Y	Y	Y	Y	[8,19]

Y- observed; N- not observed.

study, not the mineral decomposition. Hence it is not discussed further.

3.3. Effect of temperature on in situ pyrolysis

Fig. 2(a) shows the evolution of functional groups on Thailand lignite during in-situ pyrolysis using synchrotron FTIR. The fresh sample shows the presence of functional groups such as alkyne at 2165 cm^{-1}, C═O stretching at 1700 cm^{-1}, and COO^-/aromatic ring at 1577 cm^{-1}. The intensity of these functional groups decreased with the pyrolysis temperatures from 30 to 200 °C, indicating the loss of oxygen-containing functional groups with temperature in the drying stage (stage 1). This also results in the decrease of moisture holding capacity and spontaneous combustion tendency [9,25]. These oxygen-containing functional groups progressively lost with the increasing pyrolysis temperature to 550 °C in the devolatilization stage (stage 2). At 550 °C, fewer alkyne, and C═O stretching were observed, whereas, COO^- and aromatic ring at 1577 cm^{-1} were completely disappeared from the spectra. For alkene at 1790 cm^{-1}, the intensity dropped significantly until 200 °C and reached a plateau beyond that. At 550 °C, most of the functional groups became quite low or invisible. However, the peak at CH_3 symmetric deformation and cyclic $—CH_2$ at 1370 cm^{-1} were not affected much by temperature. Alternatively, all the spectra show a peak at 2300–2400 cm^{-1} which represent gas phase CO_2. This peak appears consistently suggesting to be atmospheric CO_2 but not the CO_2 released from the coal. As a result, this peak is not discussed for other coals.

Fig. 2(b) shows the profile at which functional groups present on coal either disappeared or their intensity decreased during pyrolysis to 550 °C. The arrows pointing above the curve indicate that the functional groups are completely removed, whereas the arrows pointing downwards indicate these functional group still remain in coal but their intensities decreased with temperature. In the drying stage, most of the oxygen-containing functional groups (C═O stretching, and COO^-/aromatic ring) in the Thailand coal decreased significantly from 30 to 200 °C, suggesting the removal of water. Interestingly, it also can be seen in TG and DTG curve of Thailand coal, a sudden and substantial decrease happening at 112 °C in the weight loss and weight loss rate, suggesting devolatilization stage initiated from this temperature and volatile released from this coal. The results indicate that alkene, alkyne, C═O stretching, and COO^-/aromatic ring in Thailand are weakly bonded functional groups and start decreasing at as low as 112 °C. These functional groups gradually kept evolving with temperature in the devolatilization stage and became of quite low concentration or completely released by 550 °C. TGA curves also show a second weight loss curve at 640 °C, which is estimated to be from the release of the strongly bonded functional groups—CH_3 symmetric deformation and cyclic $—CH_2$. This peak was not observed in Victorian coals.

Fig. 3 shows the functional group change in Morwell brown coal during in situ pyrolysis. The majority of the functional groups present in Morwell coal decreased steadily with temperature. During the drying stage up to 200 °C, hydroxyl groups at 3580 cm^{-1} decreased with the temperature, suggesting the removal of water and the release of CO_2 from the decomposition of carboxyl functional groups. In stage 2(devolatilization), The —OH stretching vibrations at 3580 cm^{-1} observed at room temperature vanished from the spectra at 300 °C. When the temperature increased to 400 °C, the intensity of methylene stretching vibration ($—CH_2—$) at 2850 cm^{-1}, and bending vibrations of CH_3 and CH_2 groups at 1427 cm^{-1} completely disappeared from the spectra. The peak due to methyl(C—H) at 2896 cm^{-1}, alkyne at 2132 cm^{-1}, esters and anhydrides second band at 1772 cm^{-1} were not observed at 500 °C. The intensity of conjugated C═O and ketones at 1660 cm^{-1}, and COO- and aromatic ring at 1524 cm^{-1} also became quite low at 500 °C. The results suggest that Morwell coal requires relatively low pyrolysis temperatures for the preparation of char.

Fig. 4 shows the functional group change in Loy Yang brown coal during in situ pyrolysis. Loy Yang brown coal exhibits similar effects to Morwell brown coal shown in Fig. 3. The spectra at room temperature show very weak intensity for hydroxyl groups at 3447 cm^{-1} suggesting very low moisture content in the sample. The spectra also show peaks for the symmetric and asymmetric stretching of methyl $—CH_3$ groups at 2980, 2933, and 2850 cm^{-1}. In the finger print region, the spectra show a range of functional groups nitrile group at 2160 cm^{-1}, conjugated double bonds of C═C═C at 1970–2015 cm^{-1} followed by C═O functional groups of esters and carboxylic and aldehydes at 1732, 1700 and 1660 cm^{-1}. Further at lower wavenumbers the spectra shows peaks for epoxide at 1245 cm^{-1}, C—N stretching in secondary amides at 1370 cm^{-1}, alkyl bending vibrations at 1425 cm^{-1} and COO^- skeletal vibrations at 1460, 1555 cm^{-1} and benzene ring vibrations at 1505 cm^{-1}. During pyrolysis, with an increase in temperature, the hydroxyl groups were initially lost at 200 °C in the drying stage. When the temperature gradually increased in stage 2, alkyl stretching vibrations disappeared from the sample at 300 °C. At 400 °C, the hydroxyl groups disappeared from the sample. However, the functional groups present in the fingerprint region did not show major

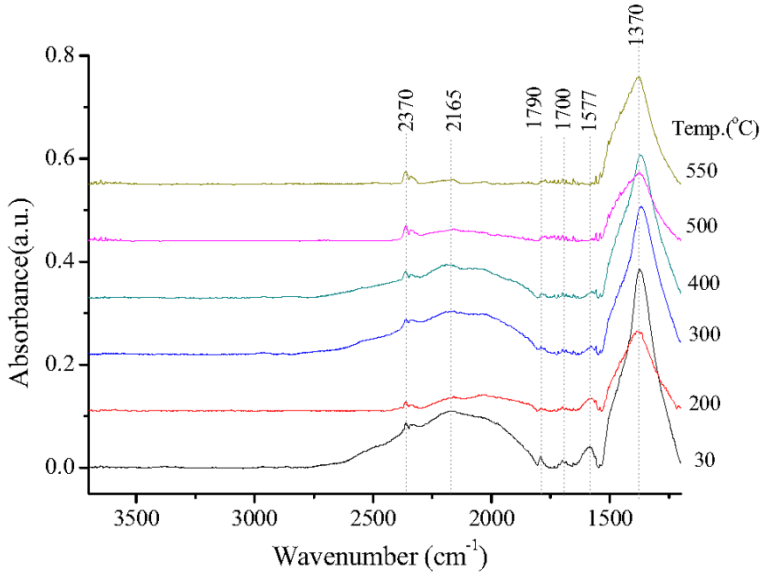

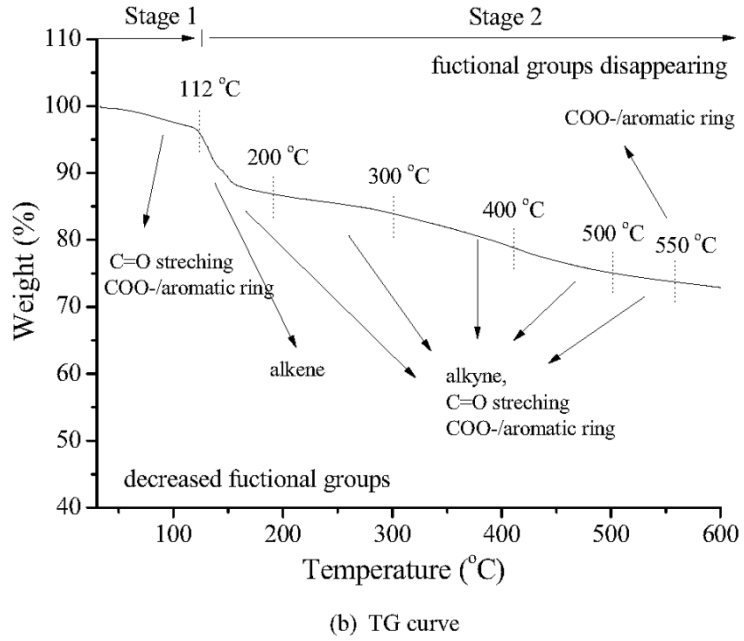

Fig. 2. Effect of temperature on functional group evolution of the Thailand lignite: (a) IR spectrum (b) TG curve.

changes suggesting higher temperature is required for the removal of these functional groups from the sample. At 550 °C, except —OH stretching at 3580 cm^{-1}, and methylene (—CH_2—) at 2922 cm^{-1}, other groups were still found to be present in the spectra. This indicates the temperature of 550 °C is not high enough for Yallourn coal pyrolysis, as there are many functional groups left.

Fig. 5 shows the evolution of functional group during in situ pyrolysis of another Victorian brown coal, Yallourn. The spectra of the sample at 30 °C shows peaks due to CH_2 groups at 2930 and 2850 cm^{-1} along with OH functional groups at 3565 cm^{-1}, albeit, at a smaller intensity. In the finger print region, the spectra show multiple peaks related to alkyne at 2153 cm^{-1} and alkene

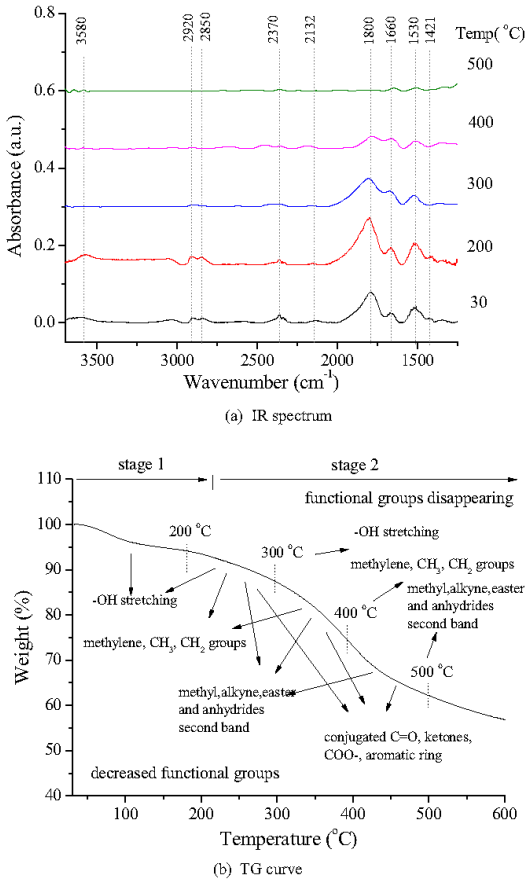

Fig. 3. Effect of temperature on functional group evolution of the Morwell coal: (a) IR spectrum (b) TG curve.

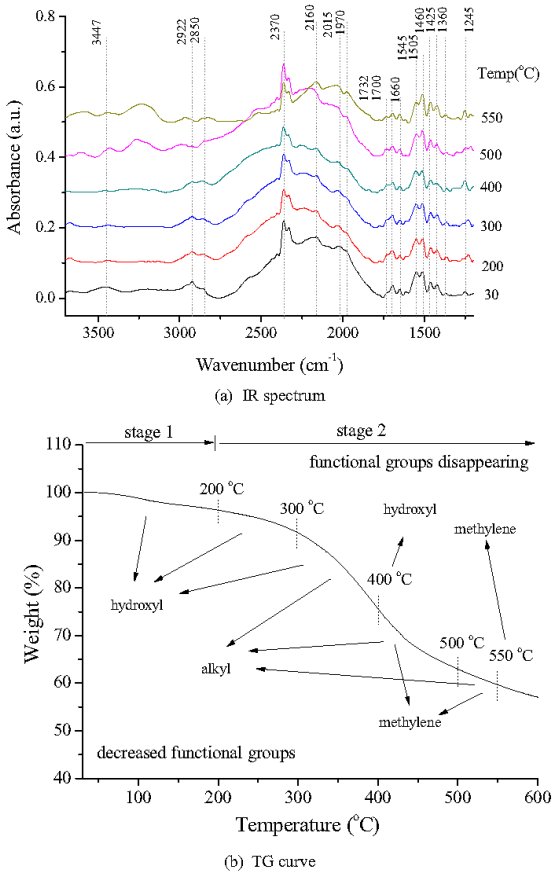

Fig. 4. Effect of temperature on functional group evolution of the Loy Yang coal: (a) IR spectrum, (b) TG curve.

at 1968 cm^{-1} C—C. When the pyrolysis temperature increased in stage 1, the intensity of alkyne and alkene groups significantly decreased. These observations suggest that the sample contains a lot of unsaturated compounds present as volatiles in the sample. During stage 2, with an increase in temperature, the methyl CH_2 groups, and OH groups tend to disappear and completely removed at 400 °C whereas alkene and alkyne functional groups leave the surface steadily with temperature. Interestingly, the intensity of the functional groups at 2032 and 1936 cm^{-1} continuous to grow with temperature and start to lose beyond 500 °C. These peaks can be attributed to the presence or formation of nitrile and conjugated C═C═C functional groups. However, at 550 °C, the functional groups at the whole wavelength of 1200–2400 cm^{-1} were still left, and they were alkyne at 2100–2260 cm^{-1}, alkene at 1968 cm^{-1}, esters, anhydrides second band at 1772 cm^{-1}, ester and aliphatic COOH at 1748–1715 cm^{-1}, COO— and aromatic ring at 1560–1490 cm^{-1}, bending CH_3 and CH_2 groups at 1427–1437 cm^{-1}, and CH_3 symmetric deformation and cyclic —CH_2 at 1370 cm^{-1}. The results suggest Yallourn coal also require higher pyrolysis temperature if complete removal of functional groups on the coal surface is required.

Fig. 6 shows the in situ FTIR spectra on pyrolysis of Maddingley brown coal. The room temperature spectra showed methylene CH_2 groups at 2922 and 2850 cm^{-1} but did not show any peaks due to surface hydroxyl or water peaks above 3500 cm^{-1}, suggesting very low moisture content in the coal. In the finger print region, the spectra show peaks at 2160 cm^{-1} which can be assigned to nitrile group and 1859 cm^{-1} for C═C═C conjugated double bonds in carbon. The peak at 1679 cm^{-1} was assigned to C═C mono, di or tri substituted bonds and 1550 cm^{-1} or benzene ring vibrations. The peaks at 1415 cm^{-1} are assigned to C═O groups in carbonyl and skeletal vibration of COO^- carboxylic functional groups and 1352 cm^{-1} C—N stretching in amides. From the spectra, it can be observed the functional groups remain intact until 300 °C beyond which the peaks tends to show a decrease in the intensity and majority of the peaks displaced from the spectra at 550 °C. In stage 1, the intensity of hydroxyl at 3595 cm^{-1} slightly decreased, whereas the carboxyl at 2640 cm^{-1} was observed to be significantly decreased and completely disappeared at 200 °C, suggesting the removal of free water and combined water. When the pyrolysis temperature increased in stage 2, the hydroxyl functional group disappeared from the spectrum at 300 °C. Interestingly, the majority of the peaks including methylene at 2922 and 2850 cm^{-1}, alkyne at 2160 cm^{-1}, alkene at 1859 cm^{-1}, and COO^- and aromatic ring at 1550 cm^{-1} just started to decrease from 300 °C onwards. With the increasing temperature, the alkene and methylene functional group vanished at 400 °C and 500 °C, respectively. The spectra at 550 °C show few more functional groups remained in the sample suggesting higher pyrolysis

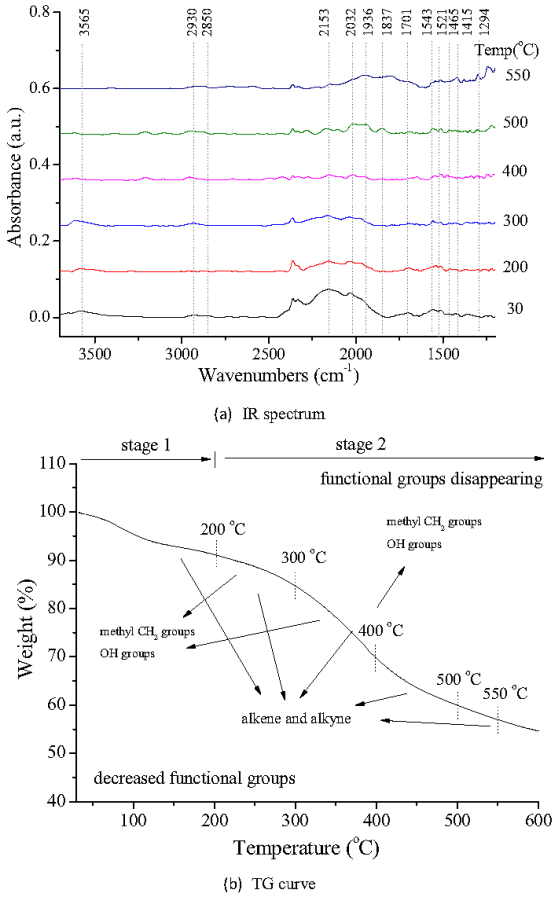

Fig. 5. Effect of temperature on functional group evolution of the Yallourn coal: (a) IR spectrum (b) TG curve.

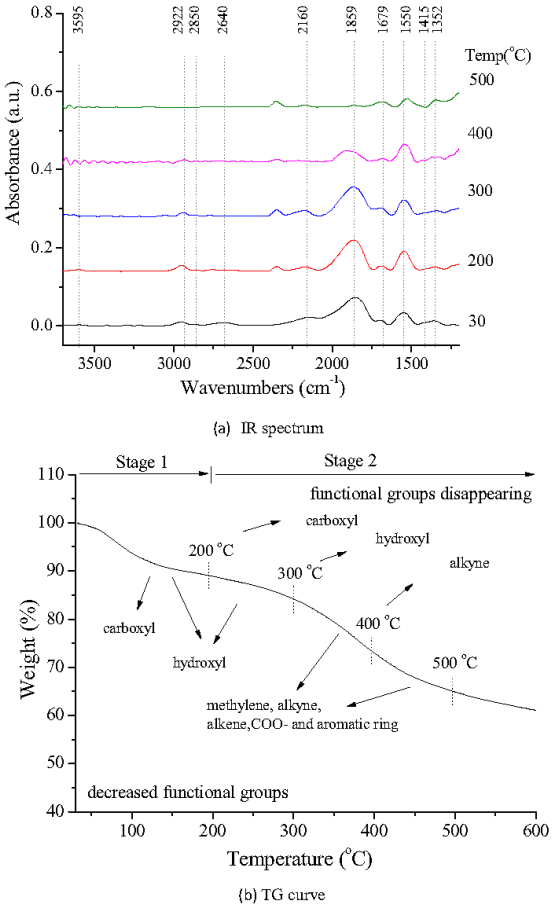

Fig. 6. Effect of temperature on functional group evolution of the Maddingley coal: (a) IR spectrum, (b) TG curve.

temperatures are required for the removal of volatiles from the Maddingley coal.

3.4. Effect of char preparation temperature

According to the results of the in-situ experiments, some functional groups were still left at 550 °C. This is because the Victorian and Thailand coals require temperatures over 900 °C for the entire pyrolysis process to take place which can be seen in Fig. 1. Below 550 °C, the primary pyrolysis is mainly taking place, whereas secondary pyrolysis happens at a higher temperature. During the secondary pyrolysis, the char would undergo ring condensation which will influence the char reactivity towards gasification because of the inhibition of the edge carbon sites [3]. As a result, char prepared at higher temperature was used here to investigate the functional group change with temperature after 550 °C and the relationship between char property and pyrolysis temperature. The coal char was pyrolysed at various temperatures (700–1000 °C) in a drop tube reactor. The functional groups observed in the infrared spectra of 700 °C pyrolysis coal char (Yallourn and Maddingley) were presented in Table 4.

As seen in Fig. 7, compared to the in-situ Yallourn char pyrolysed at 500 °C, more functional groups, hydroxyl at 3300–3700 cm^{-1}, alkyne at 2165 cm^{-1}, carbonyl at 1700 cm^{-1}, ketones at 1660 cm^{-1}, Benzene ring at 1530 cm^{-1}, and CH_3 and CH_2 groups at 1430 cm^{-1}, were found in the ex-situ Yallourn char pyrolysed at 700 °C. This is likely due to tar from the coal pyrolysis condensing on the surface of char when the temperature dropped to room temperature [26]. Also, the secondary pyrolysis can contribute to the increase in the concentration of the benzene ring at 1530 cm^{-1}, and CH_3

Table 4
Functional groups of Yallourn and Maddingley coal chars pyrolysed at 700 °C.

Wavenumbers (cm^{-1})	Functional Groups	Yallourn char	Maddingley char
3700–3300	—OH and —NH stretching	N	Y
2370	atmospheric CO_2 interference	Y	Y
2100–2260	alkyne	Y	Y
1850–2000	alkene	Y	Y
1835	Benzene ring overtone	Y	N
1748–1715	ester, aliphatic COOH	Y	Y
1700	C═O stretching	Y	Y
1660	Conjugated C═O, ketones	Y	N
1530	Benzene ring	Y	Y
1430	CH_3,CH_2 groups	Y	Y

Y = observed; N = not observed.

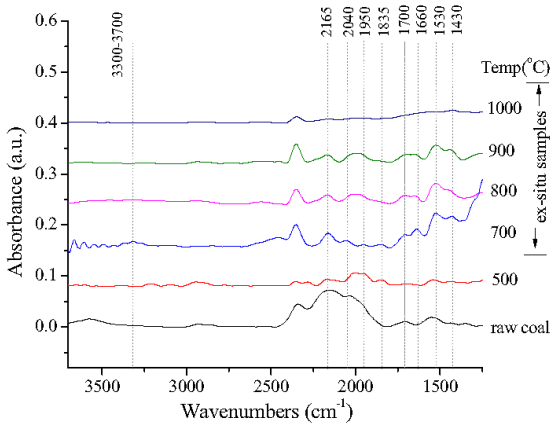

Fig. 7. Infrared spectra of Yallourn coal char pyrolysed at higher temperature.

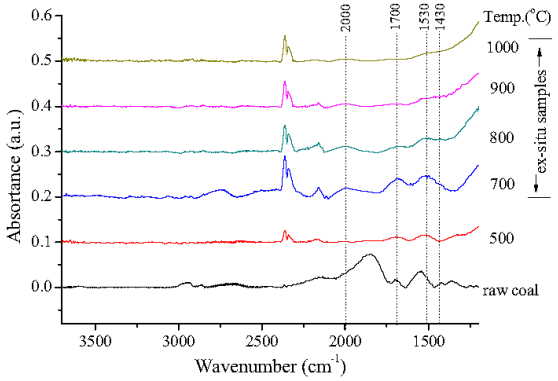

Fig. 8. Infrared spectra of Maddingley coal char pyrolysed at higher temperature.

and CH_2 groups at 1430 cm^{-1}. CH_3 and CH_2 groups can be from the cross-linking reaction between char and the secondary gas (mainly CO and H_2), and the Benzene ring can be from ring condensation. When the temperature is increased to 800 °C, hydroxyl at 3300–3700 cm^{-1} was lost in the spectra, suggesting more water is removed at higher char preparation temperature. The peak sat the wavelength of 1430–2165 cm^{-1} was also significantly decreased. At 1000 °C, few peaks were visible, and the intensity was considerably low, indicating Yallourn coal nearly lost all the surface functional groups at this temperature. The reasons for this are: (i) high temperature can accelerate the loss of the functional groups within the samples (ii) high temperature is beneficial to the cracking of tar from primary pyrolysis, leading to less volatile condensation on the char surface; (iii) high temperature also can improve the cross-linking reaction between char and primary gases towards the decrease of the functional groups. The results also suggest the high temperature can reduce the ring condensation from secondary pyrolysis. The condensation has an influence on the char reactivity towards gasification or combustion by eliminating carbon edge sites [3]. To sum up, the general trend shows that higher preparation temperature can result in less-functional group char with better gasification reactivity.

For Maddingley coal char in Fig. 8, a similar temperature effect was found in the functional group changes. The intensity of all the functional groups decreased, with the increasing temperature from 700 to 1000 °C. This can be attributed to the tar cracking at a higher temperature in the secondary pyrolysis. At 1000 °C, there was no further peak to be observed, expect the atmospheric CO_2 at 2350 cm^{-1}. This also confirms that at 1000 °C all the surface functional groups were lost from the char.

3.5. Comparison of victorian and Thailand coals on surface functional groups during pyrolysis

The in-situ synchrotron FTIR is used to examine the functional groups change during the pyrolysis up to 550 °C for four Victorian brown coal and a Thailand lignite. The comparison of results for these five coals on surface functional groups is given below:

- Compared to low-ash (2.6%) Victorian brown coals, high-ash (50%) Thailand lignite has less functional groups at wavenumbers of 2509–3700 cm^{-1} (No alkyl and hydroxyl groups).
- Relatively less functional groups were released from high-ash Thailand lignite during pyrolysis.
- Among the four Victorian brown coals, Morwell coal released larger fraction of functional groups as observed during in situ FTIR pyrolysis below 500 °C with only a fraction of functional groups like conjugated C═O, ketones, COO^- and aromatic ring remaining.
- In contrast, Loy Yang coal released very small fraction of functional groups during pyrolysis although it has a wide variety of functional groups among Victorian coals. No significant decrease was found in the functional groups at the wavenumber of 2500–1200 cm^{-1} below 550 °C. However alkyl functional groups started their release beyond 400 °C.
- Compared to other low-ash (2–6%) Victorian brown coal the carboxyl group was solely found to be released in high-ash (20%) Maddingley coal, and disappeared by 200 °C. Moreover, unlike other coals, the alkyne group in Maddingley coal released and disappeared between 300 and 400 °C.

Also, there are some common and general changes on functional groups found in the samples:

- The hydroxyl of five Victorian brown coals started to decrease in the drying stage below 200 °C and disappeared at 300–400 °C.
- The peaks for alkyne in all coals initially decreased between 200 and 300 °C, and significantly decreased with increasing temperature. The alkyne peaks of Maddingley and Morwell coals disappeared at 400 °C and 500 °C respectively. The other coals still have alkyne functional groups above 500 °C.
- The functional group of cyclic—CH_2 is difficult to release in all the coals, and the peak does not change at temperatures below 550 °C.
- By 550 °C, a significant number of functional groups (carbonyl, carboxylate, aromatic ring, CH_3 and CH_2 groups) remained in samples, suggesting that Victorian brown coals and Thailand lignite need to be pyrolyzed at a higher temperature. The ex-situ FTIR results of Yallourn and Maddingley char verify that the functional groups were completely released by 1000 °C.

4. Conclusions

The surface functional group evolution of Victorian and Thailand coals with temperature during in-situ pyrolysis up to 550 °C was studied using in situ synchrotron IR. For Thailand lignite, less surface functional groups were found, compared to Victoria brown coals. The group of the alkyne, alkene, C═O stretching, and COO— and aromatic ring started to lose from 112 °C in the drying stage and were almost removed when the temperature increased to 550 °C in the devolatilization stage. CH_3 symmetric deformation and cyclic

–CH_2 is estimated to release from 640 °C, based on the thermogravimetric curves.

The intensity of all the surface functional groups from Victoria brown coals decreased with temperature. During the drying stage, the concentration of oxygen contained species – hydroxyl and carboxyl- decreased due to the removal of water, with the breakage of the weak bonds such as alkene and alkyne. When temperature gradually increased in the devolatilization stage, more functional groups started to decrease and gradually disappear. More specifically, for Morwell coal, hydroxyl groups decreased significantly at 200 °C, and eventually vanished at 300 °C. Methylene and CH_3/CH_2 groups didn't change until 200 °C and got disappeared at 400 °C. Regarding Loy Yang coal, hydroxyl decreased at 200 °C and disappeared at 400 °C. Alkyl concentration decreased with increasing temperature from 300 °C, whereas the methylene decreased from 400 °C and completely disappeared by 550 °C. For Yallourn coal, the alkene and alkyne gradually decreased with temperature from 30 °C. Methyl CH_2 groups and OH groups decreased from 200 °C and disappeared at 400 °C. By 550 °C, the functional groups over the whole wavelength range of 1200–2400 cm^{-1} were still left. For Maddingley coal, carboxyl and hydroxyl groups decreased significantly in the drying stage, and disappeared by 300 °C, respectively. However, for all Victorian brown coals, some surface functional groups remained at 550 °C, especially for the groups at the wavenumber of 1700–1340 cm^{-1} (carbonyl, carboxylate, aromatic ring, CH_3 and CH_2 groups), suggesting 550 °C is not high enough for the pyrolysis of Victorian brown coal.

The results from ex-situ char pyrolysed at 700–1000 °C shows the concentration of surface functional groups in the samples decreases with the temperature since high temperature can accelerate the secondary pyrolysis, especially the cracking of tar. This indicates a higher char preparation temperature as 1000 °C can advance the quality of chaar from Victorian brown coals with less volatile (mainly from tar condensation) and better reactivity.

Acknowledgements

The authors would like to acknowledge the support from China Scholarship Council, Brown Coal Innovation Australia (BCIA), and the Australian Synchrotron (Experiment ID-M6001 IR beamline). The authors also would like to thank Dr. Mark Tobin for assistance during the experiments and data analysis.

References

[1] IEA, World Energy Outlook 2014, IEA, 2014.
[2] S. Bhattacharya, K.B. Kabir, K. Hein, Dimethyl ether synthesis from Victorian brown coal through gasification – Current status, and research and development needs, Prog. Energy Combust. Sci. 39 (2013) 577–605.
[3] M.A. Serio, D.G. Hamblen, J.R. Markham, P.R. Solomon, Kinetics of volatile product evolution in coal pyrolysis: experiment and theory, Energy Fuels 1 (1987) 138–152.
[4] C.-Z. Li, J.-i Hayashi, K. Miura, Chapter 4 – pyrolysis of victorian brown coal, in: C.-Z. Li (Ed.), Advances in the Science of Victorian Brown Coal, Elsevier Science, Amsterdam, 2004, pp. 134–222.
[5] H.Y. Cai, A.J. Güell, I.N. Chatzakis, J.Y. Lim, D.R. Dugwell, R. Kandiyoti, Combustion reactivity and morphological change in coal chars: effect of pyrolysis temperature, heating rate and pressure, Fuel 75 (1996) 15–24.
[6] J. Ibarra, E. Muñoz, R. Moliner, FTIR study of the evolution of coal structure during the coalification process, Org. Geochem. 24 (1996) 725–735.
[7] J.V. Ibarra, R. Moliner, Coal characterization using pyrolysis-FTIR, J. Anal. Appl. Pyrolysis 20 (1991) 171–184.
[8] V. Calemma, R. Rausa, R. Margarit, E. Girardi, FT-i.r. study of coal oxidation at low temperature, Fuel 67 (1988) 764–770.
[9] A. Tahmasebi, J. Yu, Y. Han, F. Yin, S. Bhattacharya, D. Stokie, Study of chemical structure changes of chinese lignite upon drying in superheated steam, microwave, and hot air, Energy Fuels 26 (2012) 3651–3660.
[10] X. Lin, C. Wang, K. Ideta, J. Miyawaki, Y. Nishiyama, Y. Wang, S. Yoon, I. Mochida, Insights into the functional group transformation of a chinese brown coal during slow pyrolysis by combining various experiments, Fuel 118 (2014) 257–264.
[11] L. Zhang, T. Li, D. Quyn, L. Dong, P. Qiu, C.-Z. Li, Formation of nascent char structure during the fast pyrolysis of mallee wood and low-rank coals, Fuel 150 (2015) 486–492.
[12] K. Kirtania, J. Tanner, K.B. Kabir, S. Rajendran, S. Bhattacharya, In situ synchrotron IR study relating temperature and heating rate to surface functional group changes in biomass, Bioresour. Technol. 151 (2014) 36–42.
[13] N.H. Zainan, S.C. Srivatsa, S. Bhattacharya, Catalytic pyrolysis of microalgae Tetraselmis suecica and characterization study using in situ Synchrotron-based Infrared Microscopy, Fuel 161 (2015) 345–354.
[14] K. Miura, K. Mae, W. Li, T. Kusakawa, F. Morozumi, A. Kumano, Estimation of hydrogen bond distribution in coal through the analysis of OH stretching bands in diffuse reflectance infrared spectrum measured by in-Situ technique, Energy Fuels 15 (2001) 599–610.
[15] G. Dou, D. Wang, X. Zhong, B. Qin, Effectiveness of catechin and poly(ethylene glycol) at inhibiting the spontaneous combustion of coal, Fuel Process. Technol. 120 (2014) 123–127.
[16] X. Qi, D. Wang, H. Xin, G. Qi, An In situ testing method for analyzing the changes of active groups in coal oxidation at low temperatures, Spectrosc. Lett. 47 (2014) 495–503.
[17] D. Wang, G. Dou, X. Zhong, H. Xin, B. Qin, An experimental approach to selecting chemical inhibitors to retard the spontaneous combustion of coal, Fuel 117 (2014) 218–223.
[18] G. Xiong, Y. Li, L. Jin, H. Hu, In situ FT-IR spectroscopic studies on thermal decomposition of the weak covalent bonds of brown coal, J. Anal. Appl. Pyrolysis 115 (2015) 262–267.
[19] L.L. Baxter, T.H. Fletcher, D.K. Ottesen, Spectral emittance measurements of coal particles, Energy Fuels 2 (1988) 423–430.
[20] R.M. Silverstein, G.C. Bassler, Spectrometric identification of organic compounds, J. Chem. Educ. 39 (1962) 546–553.
[21] P.R. Solomon, D.G. Hamblen, R.M. Carangelo, M.A. Serio, G.V. Deshpande, General model of coal devolatilization, Energy Fuels 2 (1988) 405–422.
[22] J. Yu, A. Tahmasebi, Y. Han, F. Yin, X. Li, A review on water in low rank coals: the existence, interaction with coal structure and effects on coal utilization, Fuel Process. Technol. 106 (2013) 9–20.
[23] Y. Sato, S. Kushiyama, K. Tatsumoto, H. Yamaguchi, Upgrading of low rank coal with solvent, Fuel Process. Technol. 85 (2004) 1551–1564.
[24] P.R. Solomon, M.A. Serio, E.M. Suuberg, Coal pyrolysis: experiments, kinetic rates and mechanisms, Prog. Energy Combust. Sci. 18 (1992) 133–220.
[25] M. Sakaguchi, K. Laursen, H. Nakagawa, K. Miura, Hydrothermal upgrading of Loy Yang Brown coal – effect of upgrading conditions on the characteristics of the products, Fuel Process. Technol. 89 (2008) 391–396.
[26] P.R. Solomon, T.H. Fletcher, R.J. Pugmire, Progress in coal pyrolysis, Fuel 72 (1993) 587–597.

Chapter 5 Entrained flow gasification behaviour at low temperatures (<1000 °C)

After examining the pyrolysis behaviour of four Victorian brown coals in Chapter 4, their gasification behaviour is investigated at low temperature for study of these coals. Entrained flow gasifiers are most attractive for commercial applications and dominate the world market due to their flexibility to handle different feedstock. Therefore, gasification using entrained flow gasifiers, also known as entrained flow gasification, is selected and examined for Victorian brown coals.

As Victorian brown coals are quite reactive, these may obtain good gasification performance, carbon conversion and gas composition, at low temperatures below 1000 °C. To understand if Victorian brown coal is suitable for low temperature gasification, one needs to know optimal entrained flow gasification performance at low temperatures. The other important information is to assess the residence time required for 100% carbon conversion at low temperature. So far, only one study has reported the entrained flow gasification behaviour of one Victoria brown coal, Morwell coal, at low temperatures. This study was conducted at temperatures up to 1000°C and concluded that 6 second residence time at 1000°C and 20% CO_2 resulted in only 56% carbon conversion. However, the entrained flow gasification behaviour of other Victorian brown coals and the residence time for complete carbon conversion at low temperatures were not investigated.

In this chapter, the entrained flow gasification behaviour of two Victorian brown coals, Yallourn and Morwell, at the temperature of 700-1000 °C and at the CO_2 concentration of 5-30% is reported, including their char properties and reactivity, carbon conversion, and gas composition. As part of this study, a quantitative explanation for the effect of residence time on carbon conversion and gas composition at 1000 °C is also developed by gasifying the chars in the same reactor until 100% carbon conversion was obtained.

This chapter reproduces the following submitted paper to the Journal of Fuel.

Entrained flow gasification behaviour of Victorian Brown coal at low temperature

Tao Xu and Sankar Bhattacharya

Department of Chemical Engineering, Monash University, VIC 3800, Australia

*Corresponding author. E-mail address: sankar.bhattacharya@monash.edu

Phone: +61 3 99059623 Fax: +61 3 99055686

Abstract

This paper presents a study of the behaviour of entrained flow gasification data was generated for two Victorian brown coal chars (Yallourn and Morwell coal char) in CO_2 at temperatures between 700-1000 °C. The effect of temperature, total gas flow, reactant gas concentration and residence time on char reactivity, carbon conversion, and syngas yield and composition was investigated. The results indicate that at a higher temperature and CO_2 concentration, carbon conversion increases as expected, along with syngas yield and concentration. It is found that gasification under entrained flow condition achieves higher carbon conversion and gas yield than that under dropping flow condition, even if with a shorter residence time. The finding suggests that the gasification experiments should be conducted under entrained flow condition (the gas velocity > the particle velocity) for better gasification performance. At 1000 °C, with an increase in residence time, the carbon conversion and syngas yield gradually increases to nearly 100% and an estimated equilibrium value, respectively. The experimental data establishes that for a complete char conversion, 17.4 seconds and 21.4 seconds residence times are required for Yallourn and Morwell, respectively, if gasification is conducted at 1000 °C in an environment of 20% CO_2. This finding indicates that Victorian brown coals need to be gasified at a higher temperature above 1000 °C to shorten the residence time considering that the typical residence time of industrial entrained-flow gasifier is 6-10 s.

Keywords: Entrained flow, Gasification, Victorian brown coal, residence time, low temperature

1. Introduction

Coal is still the most important fuel for primary energy production in the world, and it will continue to dominate the global power sector in the foreseeable future [1]. The latest BP statistical report indicates that current coal resources (1139 billion tons) can largely meet the world's coal demand until 2170 at current consumption rates [2]. Low rank coals, including sub-bituminous and brown coals, make up approximately 30 of the coal reserves worldwide. In Australia, Victorian brown coals represent a significant, low cost energy resource with reserves of 430 billion tons [3]. However, its utilization is limited to mine-mouth power generation using conventional pulverized coal-fired combustion units at relatively low efficiencies. Therefore, it is necessary to assess and develop alternative utilization techniques for this vast resource, such as the production of high-value chemicals.

Gasification is an alternative mode of coal utilization. Coal gasification is a thermochemical conversion method that produces syngas, consisting of carbon monoxide, hydrogen, and methane, by reacting coal with gasification mediums like steam, carbon dioxide, and oxygen. A variety of chemicals and liquid fuels can be obtained from the syngas produced from coal gasification [4].

The major gasifier types currently used in large scale include fixed bed, fluidized bed, and entrained flow gasifiers [5]. Of these, the entrained flow gasifier is attractive for commercial plants due to its flexibility of feedstock handling. For syngas production, entrained flow gasifiers dominate the world gasification market [6], but specific technological information for gasification of brown coals is limited.

Several studies on entrained flow gasification of coal have been reported in the literature. The numerical simulation on coal gasification performance in oxygen was developed by Wang et al. [7]. The effect of temperature on the carbon conversion and gas quality of a German lignite during gasification at high temperature (1000-1400°C) under oxygen atmosphere was investigated by Tremel et al. [8]. While the gasification characteristics, including gas compositions and carbon conversion, of coke and bituminous coal under oxygen atmosphere was studied by Lee et al. [9]. Under oxygen atmosphere, investigations on gasification behaviour of Victorian brown coal are limited, although there are some studies assessing alkali and alkaline earth metal (AAEM) emissions and their catalytic effects during pyrolysis and gasification of Victorian brown coals [10-12]. There has been one study reporting on pressurized fluidized bed gasification of Victorian brown coals at a pilot scale [13]. This study concluded that fluidized bed gasification may not be suitable for

Victorian brown coals and recommended entrained flow gasification from low to high temperature ranges. Only one study [14] is reported in the literature on entrained flow pyrolysis and gasification of one Victoria brown coal (Morwell coal) at low temperature. This study was conducted at temperatures up to 1000°C and concluded that 6 second residence time at 1000 °C in an atmosphere of 20% CO_2 and 80% N_2 resulted in only 56% carbon conversion. It was not known what residence would be required for ~100% carbon conversion..

In this study, the gasification behaviour of two Victorian brown coal chars, Yallourn and Morwell coal char, is reported including their char properties and reactivity, carbon conversion, and gas quality during CO_2 gasification. As part of this study, the relation between 100% carbon conversion and residence time was examined based on regasifying the chars after every run of 5-6s residence time. This study generates fundamental information that will be useful for the development of commercial entrained-flow gasifiers using Victorian brown coals.

2. Experimental

2.1 Sample preparation

The coal samples used in this study are Yallourn (YL) and Morwell (MW) coals, two brown coals from the Latrobe Valley, Victoria, Australia. Proximate analysis was carried out in a Thermo-Gravimetric Analyser (Model STA 449 F3 Jupiter®, NETZSCH-Gerätebau GmbH, Germany), according to Australian standards -AS 2434.2, 2434.7-2434.8. The ultimate analysis was conducted by an analyser (Model 2400, Perkin-Elmer, USA). The proximate and ultimate analysis of Yallourn and Morwell coal are listed in Table 1.

For the preparation of char, coal samples were firstly grounded, air-dried, and sieved to 90-106 μm. Then, char was generated from the prepared samples by pyrolysis at 1000°C in nitrogen in an entrained flow reactor. The char properties are listed in Table 1. The average size of the char is around 100 μm.

Table 1: Proximate and ultimate analysis of coal and char samples

Items	YL coal	YL char	MW coal	MW char
Proximate analysis (wt%)				
Moisture (as received)	5.82	0.59	14.92	3.01
Volatile matter (d.b.)	48.18	7.61	49.31	9.94
Fixed carbon (d.b.)	51.82	79.71	48.65	82.91
Ash (d.b.)	2.32	12.68	2.04	7.13
Ultimate analysis (d.b., wt%)				
Carbon	62.99	86.46	60.42	88.12
Hydrogen	4.98	0.45	4.59	0.82
Nitrogen	0.54	0.2	1.54	0.2
Sulfur	0.40	0.21	0.86	0
Ash	2.32	12.68	2.04	7.13
Oxygen (by difference)	28.77	0	30.55	3.73

d.b. = dry basis

2.2 Apparatus and procedure

An electrically heated entrained flow reactor was employed for the gasification experiments, as described elsewhere [14]. The furnace is of 2 m length and consists of six separately controllable heating zones. Thus, an isothermal gas-temperature zone in the entire reactor tube can be obtained. Inside of the quartz reactor is designed to have two layers with an inner diameter of 50 and 80 mm, respectively. The pyrolyzed coal char was fed continuously from the top of the reactor at an average rate of 600 mg/min by a piezoelectric feeder and introduced into the inner chamber through a water-cooled injector. For each run, primary gas of N_2 was fed from the top of the reactor at a rate of 0.5 L/min entraining the coal char into the reactor. The majority of the secondary gas used for gasification was introduced from the bottom of the reactor at a total rate of 4.5 L/min into the external chamber. Therefore, it was heated up to the furnace temperature before entering into the inner reaction chamber along with the mixture of the coal and primary gas at the top of the reactor.

In the downstream piping, a glass beaker connecting the quartz reactor was used to collect solid products like ash and char residue. A water-ice box was used to condense the volatile matter in the produced gas. To remove the moisture and small particles mixed in the produced gas, a thimble filter was installed before the gas analyzer.

The reactor was heated up to the desired temperature before feeding the sample. To avoid reaction of other reactant gas with coal inside the reactor and downstream piping, inert gas N_2 was fed for at least 30 minutes until the micro-GC showed that there was only N_2 in the outlet gas. Then, reactant gas CO_2 at controlled flow rate was introduced into the reactor. After stable CO_2 composition had been measured by micro-GC, the coal char was fed at the top of the reactor. At the end of the experiment, the solid products were collected.

The experiments were conducted at various, and temperatures (700 - 1000°C), gas flow rate (2 – 5 L/min), CO_2 concentrations (5 - 20%) in $N_2$and residence time (6 - 24s). Therefore, their effects on gasification behaviour of Victorian brown coals were investigated in this study.

2.3 Data analysis

2.3.1 Solid and liquid phase analysis

Both proximate and ultimate analysis were performed on the solid residues - gasified chars. The morphology change of the solid products is observed by an emission scanning electron microscope (FEI Nova NanoSEM 450).

To investigate the gasification reactivity of the gasified chars with different residence time, the thermo-gravimetric analyzer (Model STA 449 F3 Jupiter®, NETZSCH-Gerätebau GmbH, Germany) was used for isothermal gasification at 800°C. Around 10mg was used for each reactivity test. Under N_2 atmosphere, the temperature was raised to 110°C at a heating rate of 5 K/min and then to 800°C at a heating rate of 10 K/min. CO_2 was then introduced to the furnace and gasification was conducted for 2 hours at 800°C. According to our previous study [14], little or no tar is generated from entrained flow gasification, so it is negligible and not discussed in this study.

2.3.2 Gas phase analysis

The produced gas was analyzed by a micro gas chromatograph (Varian 490-GC). During each experiment, a sequence of at least 30 consecutive gas sampling runs was set, and each consisting of 210 s measurement and 40 s equilibration time. After the gas composition had reached a steady state, the data were selected and averaged to give the final result. According to the gas composition, carbon conversion was calculated.

Carbon conversion represents the amount of carbon in the char that has reacted, i.e. is present in the gas phase. Here, the main char-gas reaction during CO_2 gasification of char is the Boudouard reaction, given below:

$$C_{(s)} + CO_2 \longrightarrow 2CO \quad \text{(R 1)}$$

As CO is the carbon from char the gas phase, carbon conversion (X) is calculated by using the following equation:

$$\mathrm{X}(\%) = \frac{0.5 \times 12 X_{CO}}{m_C} \times 100 \quad \text{(E 1)}$$

Where X_{CO} is the molar concentration of produced CO from char gasification, and m_C is the mass of carbon in the feed coal. As the mass of carrier gas N_2 is kept constant during the gasification process, the X_{CO} can be calculated based on the given equation:

$$x_{CO} = \frac{V_{N_2} X'_{CO}}{24.5 X'_{N_2}} \quad \text{(E 2)}$$

Where V_{N_2} is the inlet flow rate of N_2 in L/min, X'_{CO} is the CO concentration of the produced gas, X'_{N_2} is the N_2 concentration of the produced gas, and 24.5 is a constant for the molar volume of an ideal gas at 1 atmosphere of pressure and 25 °C.

2.4 Residence time

According to Rhodes' and Kawnish's studies [15, 16], the residence time (t) is determined by particle velocity (U_P) and gas velocity (U_g):

$$t = \frac{H}{U_P + U_g} \quad \text{(E 3)}$$

$$U_P = \frac{x^2(\rho_p - \rho_g)g}{18\mu} \quad \text{(E 4)}$$

$$U_g = \frac{4F_g}{\pi D^2} \quad \text{(E 5)}$$

Where x is the particle size (m), ρ_p is the particle density (kg/m^3), ρ_g is the density of reactant gas (g/L), μ is the viscosity of reactant gas (PI), F_g is the total gas flow rate (m^3/s), D is the diameter of the inside chamber (m). This calculation of the residence time is based on two assumptions: a) the size of the particle does not change during the gasification; b) the density of the particle does not

change during gasification. The total gas flow rate in the furnace is affected by the operating temperature, and it is calculated by the following equation:

$$F_g = \frac{T_1 F_{g,0}}{T_0} \quad \text{(E 6)}$$

Where T_0 is the room temperature (297.6K), T_1 is the furnace temperature (K), and $F_{g,0}$ is the inlet total gas flow rate at room temperature (m^3/s).

2.5 Thermodynamic equilibrium calculation

Factsage 6.4 was used for equilibrium calculations to estimate the gas composition and gas yield of produced gas based on the thermodynamic equilibrium in the temperature ranges from 700°C to 1000°C. The input file included all components of coal char expressed in grams together with the gasification conditions including temperature (700-1000 °C), pressure (1 atm.), and reactant gas (20% CO_2/80% N_2).

3. Results and discussion

3.1 Combined effect of temperature and residence time

According to the residence time calculation model, the total gas flow rate (Fg) can affect the gas velocity and change the residence time. Here, two different values for Fg (5 L/min and 2 L/min) were used to obtain different residence times, when other operating parameters were kept the same. The corresponding residence times at various temperatures is presented in Table 2.

Table 2: Experimental conditions for the study of the combined effect of residence time and temperature

Experimental Condition					
Fuel	**T (°C)**	**F_g (L/min)**	**U_p (m/s)**	**U_g (m/s)**	**t(s)**
YL char	700	5	0.13	0.15	6.71
	800	5	0.13	0.17	6.36
	900	5	0.13	0.18	6.04
	1000	5	0.13	0.20	5.76
	700	2	0.17	0.06	9.88
	800	2	0.16	0.07	9.57
	900	2	0.14	0.07	9.28
	1000	2	0.14	0.08	9.01

Figure 1 shows the comparison of carbon conversion and syngas yield of Yallourn char at various temperatures under the total gas flow rate of 2 L/min and 5 L/min. As seen in Figure 1(A) and 1(B), regardless of gas flow rate change, the increase of temperature from 700 °C to 1000 °C resulted in a significant increase in carbon conversion from 3.5 wt% to 63.5 wt%. Likewise, the CO yield of YL char increased significantly from 0.2 L/g coal to 4.5 L/g coal, with increasing reaction temperatures from 700 °C to 1000 °C. As expected, the high temperature facilitated the endothermic Boudouard reaction (equation 1), thus improving the carbon conversion and CO yield. According to Tanner's study [14], carbon conversion and CO yield of MW char also increased with increasing temperatures, as well. Therefore, it can be concluded that high temperature has a positive effect on the carbon conversion and CO yield of Victorian brown coals. As the maximum temperature, 1000 °C (the maximum capability of the reactor) was chosen for the further experiments.

When the total gas flow rate decreased from 5 L/min to 2 L/ min, the residence time increased by around 3 seconds. However, the increasing residence time at a given temperature did not give rise to an increase in carbon conversion and syngas yield. Instead, carbon conversion significantly decreased by 59% at 800 °C, by 49% at 900 °C, and by 38% at 1000 °C. The CO gas yield also decreased by 58% at 800 °C, by 47% at 900 °C, and by 36% at 1000 °C, respectively. This is because the decrease in total gas flow rate to 2 L/min decreases the gas velocity (Ug) and makes it slower than the particle velocity (Up), which results in a change in the particle moving mode from "entrained" to "dropping". More specifically, as shown in Figure 2, when Ug > Up, the particle is entrained by the fluid and the voidage between particles increases ($H_2 > H_1$). This means char particles are reacted with more reactant gas (CO_2) and, therefore, char gasification rate increases correspondingly. By contrast, when Ug < Up, the particle gravity dominates the whole particle moving. The voidage between particles is smaller so that char gasification rate decreases. The results suggest that the gas flow rate affect the particle moving mode in the reactor by changing the gas velocity.

Here, the entrained flow gasification is defined as when Ug > Up, the particle is entrained and dominated by the fluid gas in the reactor during gasification and dropping flow gasification is when Ug < Up, the particle is controlled by its own gravity in the system. The findings indicate that the entrained-flow gasification with a shorter residence time achieves better gasification performance than the dropping flow gasification. Consequently, further gasification experiments were conducted under entrained flow condition.

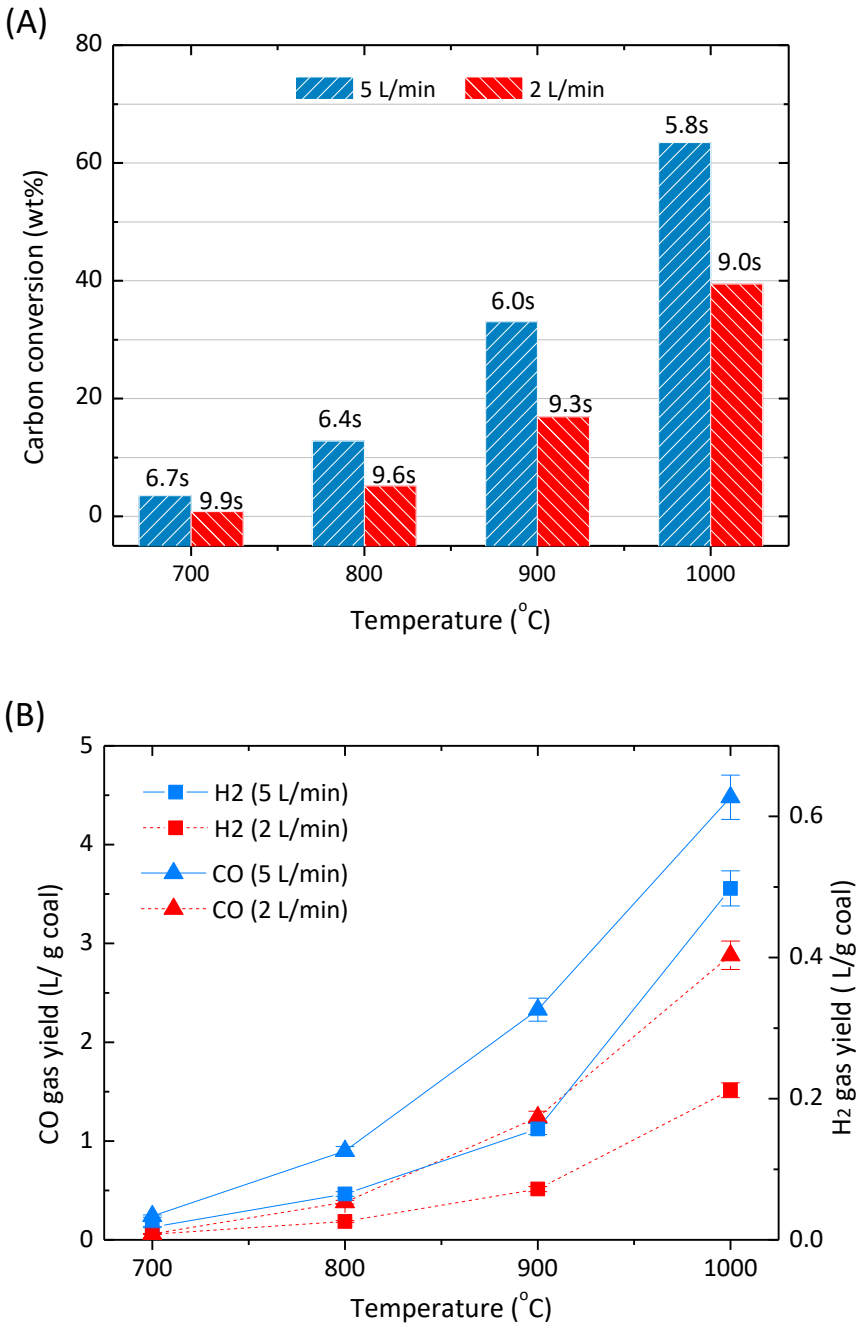

Figure 1: Comparison of carbon conversion and syngas yield of YL char at various temperatures using the total gas flow rate of 2 L/ min and 5 L/min (A: carbon conversion; B: syngas yield)

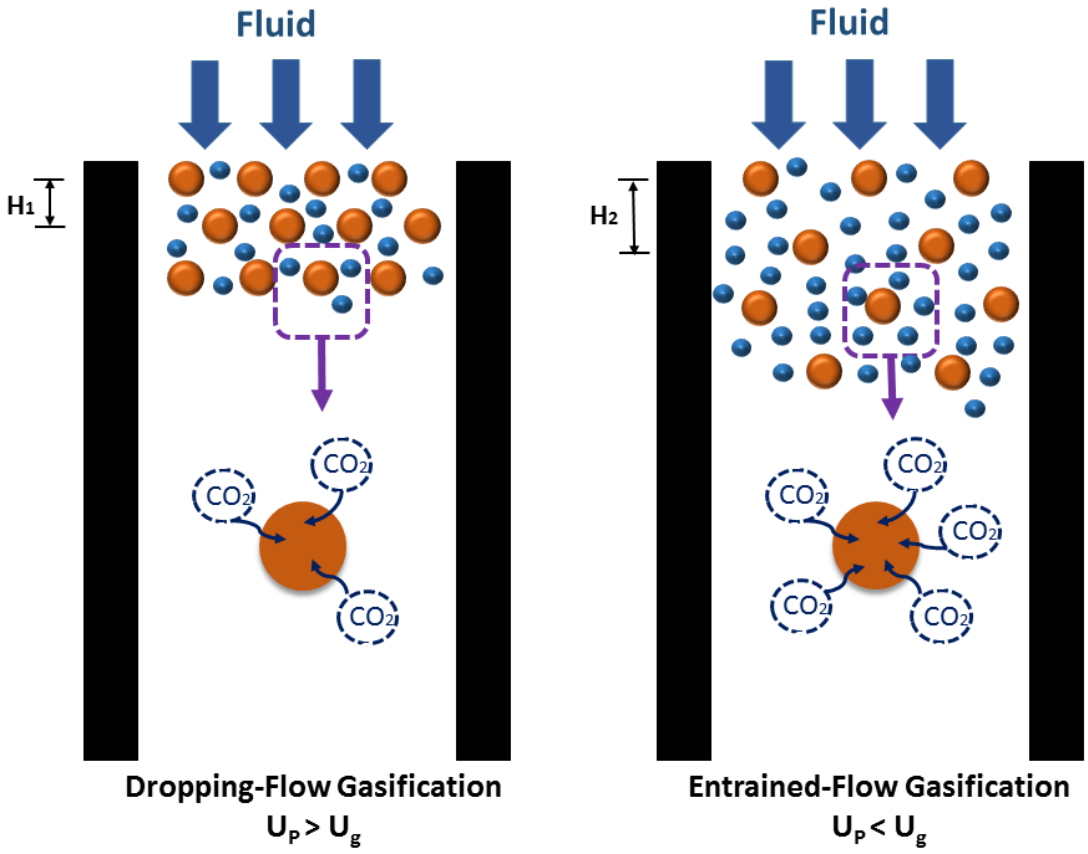

Figure 2: Particle moving mode in the dropping-flow gasification and entrained-flow gasification

3.2 Effect of CO_2 concentration

Table 3 shows the influence of input CO_2 concentration on the gasification behaviour of YL char at 1000°C. It can be seen that with increasing input CO_2 concentration from 5 vol.% to 20 vol.%, generated CO yield increased from 1.52 L/g coal to 4.48 L/g coal., and the CO concentration on N_2 and CO_2 free basis correspondingly increased from 92.87 vol.% to 94.91 vol.%. The carbon conversion also went up by 15.16 % with input CO_2 concentration. As expected, carbon content in gasified char decreased with the increase of CO_2 concentration because of the increased carbon conversion. Similar trends for the syngas yield and quality, and carbon conversion could be found with Morwell char in the literature. In Tanner's study [14], the CO gas yield and carbon conversion of MW char increased by 3.3 L/g coal and 16.3 wt.% respectively, with input CO_2 concentration increasing from 5 vol.% to 20 vol.%. The results show that higher CO_2 concentration improves the gasification performance of Victorian brown chars with an increased syngas yield and carbon conversion. This because the higher CO_2 concentration boosts Boudouard reaction (equation 1) to generate more CO. For a maximum CO_2 concentration, 20% CO_2 was chosen as the optimal concentration for further experiments.

Table 3: Gasification behaviour of YL char at various input CO_2 concentration and 1000 °C

Fuel	**YL char**		
Atmosphere	**5%CO_2**	**10%CO_2**	**20%CO_2**
Temperature (°C)	**1000**	**1000**	**1000**
Syngas yield (L/ g coal)			
H_2	0.12	0.14	0.24
CO	1.52	2.42	4.48
Total	1.64	2.56	4.72
Syngas composition (N_2 and CO_2 free basis, vol.%,)			
H_2	7.13	5.39	5.09
CO	92.87	94.61	94.91
Carbon conversion (wt.%)	35.31	37.97.56	50.47
Ultimate analysis (dry basis, wt.%)			
C	75.73	74.82	73.01
H	1.43	1.39	0.57
N	0.55	0.61	0.57
S	0.34	0.35	0.40
O (by difference)	7.77	6.66	6.45
ash	14.18	16.17	18.32

3.3 Effect of residence time

To study the effect of residence time, the gasification experiments were conducted at 1000 °C under 20% CO_2/80% N_2 with a total gas flow rate of 5 L/min. The coal chars of 50 g were initially placed in the piezoelectric feeder and fed at a frequency of 70 Hz. The gasified char was then collected and recycled three times in total to increase the residence time. The corresponding gasified chars of MW and YL prepared at different times of gasification process were marked as YL1, YL2, YL3, YL4, MW1, MW2, MW3, and MW4. The residence time of each char gasification is presented in Table 4.

Table 4: Experimental conditions for the study of the effect of residence time

Experimental Condition					
Fuel	**T (°C)**	**F_g (L/min}**	**U_p (m/s)**	**U_g (m/s)**	**t(s)**
YL1	1000	5	0.13	0.2	5.75
YL2	1000	5	0.12	0.2	6.04
YL3	1000	5	0.09	0.2	6.66
YL4	1000	5	0.07	0.2	7.02
MW1	1000	5	0.17	0.2	5.18
MW2	1000	5	0.16	0.2	5.37
MW3	1000	5	0.14	0.2	5.55
MW4	1000	5	0.14	0.2	5.58

3.3.1 Gasified char properties and reactivity

The YL and MW gasified chars with different gasification times were analysed by using proximate analysis and ultimate analysis. For YL samples, as shown in Table 4, with increased residence time, the fixed carbon value for gasified chars decreased from 73.5 wt% to 52.1 wt%. Likewise, the ultimate analysis results show a steady decrease in carbon content in the char samples from 86.5 wt% to 61.4 wt% with increased gasification time. For MW char, after three recycling gasification, the fixed carbon and carbon content decreased to 76.0 wt% and 71.0 wt%, respectively. As expected, a longer residence time leads to a higher carbon release from char, converting more char to CO.

YL and MW gasified char samples contained low volatile matter at around 10 wt% and 7 wt%, respectively. By contrast, the ash content of YL and MW gasified chars was significantly increased with the residence time. This is because when the carbon in the char was increasingly converted to the gas phase, more ash would be left and accumulated.

Table 5: Property of gasified char samples of Yallourn and Morwell

Fuel	t (s)	*Proximate analysis (wt%)*				*Ultimate analysis (d.b., wt%)*				
		Moisture (a.r.)	**Volatile matter (d.b.)**	**Fixed carbon (d.b.)**	**Ash (d.b.)**	**C**	**H**	**N**	**S**	**O (by difference)**
YL char	0	0.59	7.61	79.71	12.68	86.46	0.45	0.2	0.21	0
YL1	5.7	0.48	10.38	73.45	16.17	82.71	0.41	0.48	0.23	0
YL2	11.6	0.24	9.68	65.79	24.53	74.38	0.39	0.45	0.25	0
YL3	17.5	0.46	10.68	57.34	31.98	67.10	0.31	0.35	0.26	0
YL4	23.4	0.59	10.27	52.07	37.66	61.42	0.32	0.32	0.28	0
MW char	0	3.01	9.94	82.93	7.13	84.73	2.75	0.46	0.42	4.51
MW1	5.2	1.82	7.00	81.06	11.94	82.67	1.60	0.68	0.45	2.66
MW2	10.6	1.88	7.38	81.08	11.32	81.76	1.59	0.71	0.46	4.16
MW3	16.1	1.64	7.05	70.57	22.38	71.01	1.42	0.74	0.47	3.98
MW4	21.7	1.59	8.44	67.11	24.45	67.01	1.21	0.75	0.47	6.11

t= residence time, a.r.= as receive, d.b.= dry basis

Figure 3 shows the comparison of carbon conversion of YL and MW chars gasified in 90% CO_2 at 800 °C using a TGA. The comparison was based on t_{50}, the time needed for 50% carbon conversion. As expected, the t_{50} of YL gasified chars also increased by 14 mins when the gasification time increased from 6s to 23s. The t_{50} of MW gasified chars increased by 9 mins (48%) with the increasing gasification time from 5s to 22s. This considerable increase in t_{50} indicates the reactivity of MW and YL chars decreased with the increased gasification time. According to the findings of Hattingh and Everson's study [17], the gasification reactivity of coal in CO_2 decreased with the increased ash content. This confirms that when gasification time increases, more carbon is released, and more ash is accumulated in the residues.

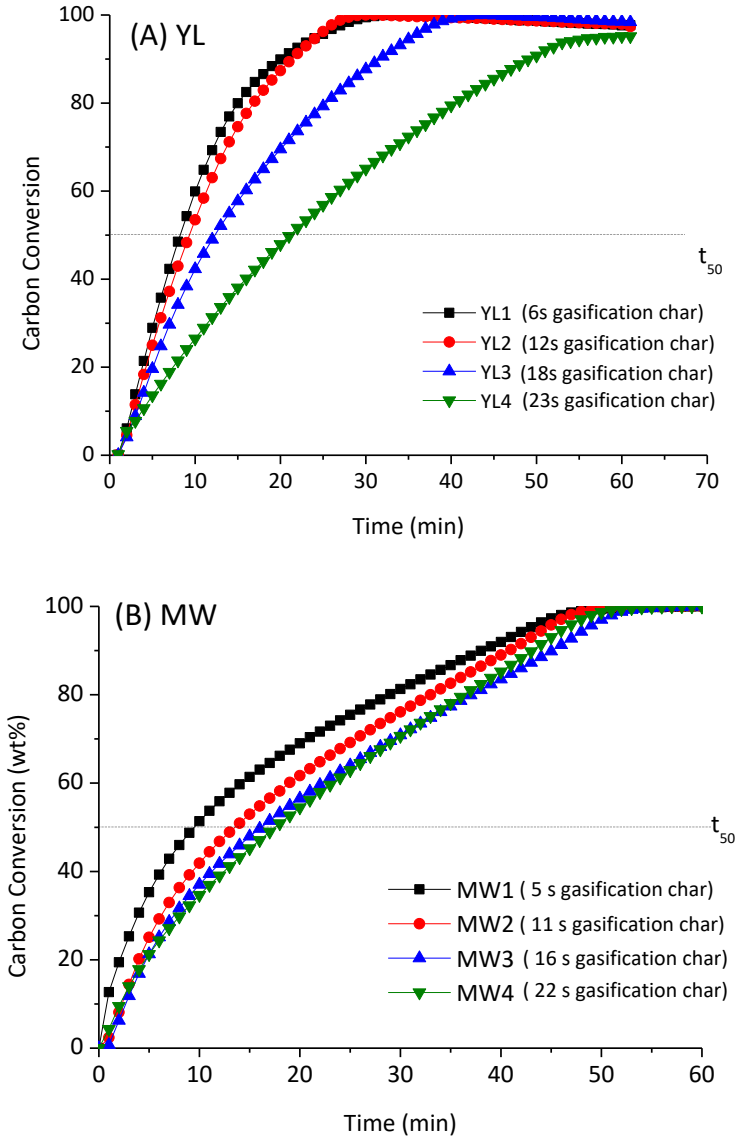

Figure 3: Comparison of carbon conversion of progressing gasification of the YL and MW chars at 90% CO_2 and 800 °C

3.3.2 Carbon Conversion

Figure 4 shows the influence of residence time on the carbon conversion of YL and MW char at an atmosphere of 20% CO_2/80% N_2 and 1000 °C. As seen, with the increasing residence time, the carbon conversion of YL char steadily increased 96.2 wt% (17.5 s), then sightly increased to 99.6 wt% (23.4 s). For MW char, the carbon conversion also increased steadily from 46.5 wt% (5.2s) to 98.1 wt% (21.7s) with the residence time. The results show that the increase of residence time improves carbon conversion of YL and MW char. It is found that under 20% CO_2/80% N_2 and 1000 °C, nearly 100% carbon conversion can be obtained for YL and MW char at a minimum residence time of 17.4s and 21.7s, respectively. In comparison with YL char, MW char needs four more seconds residence time than YL coal char to obtain nearly 100% carbon conversion. This finding indicates that YL char has better gasification reactivity than MW char. Considering that the typical residence time for a commercial-scale entrained flow gasifier is 6-10 s [18-20], it indicates that the residence time of YL and MW char for complete conversion at low temperature is too long so that a higher temperature above 1000 °C is required for the entrained flow gasification of YL and MW char shorten the residence time.

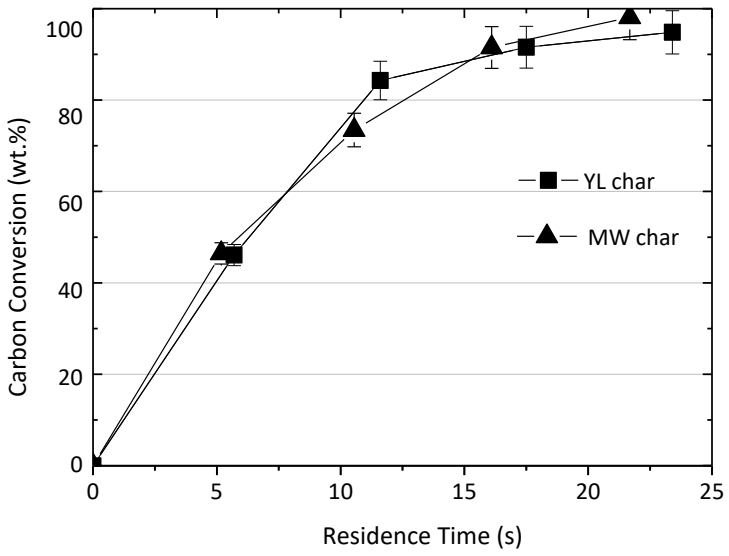

Figure 4: Influence of residence time on carbon conversion of YL and MW char at an atmosphere of 20% CO_2/80% N_2 and 1000 °C.

3.3.3 Syngas yield and quality

Figure 5 and Figure 6 show the influence of residence time on syngas yield and gas quality during CO_2 gasification of YL and MW char. For MW char, CO gas yield and concentration significantly increased from 4.1 L/ g coal and 15.5 vol% to 7.93 L/ g coal and 30.6 vol%, respectively, when the residence time increased from 5.1s to 21.7s. At the same range of residence time, H_2 gas yield also increased from 0.19 L/ g coal to 0.29 L g coal, and H_2 concentration increased from 0.7 vol% to 1.1 vol%.

For YL char, CO concentration increased significantly from the 16.1 vol% to 28.6 vol%, when residence time increased from 5.8s to 17.5s. However, the increase of residence time from 17.5s to 23.4s resulted in CO concentration increase from 31.9 vol% to 33.0 vol% only. Likewise, the CO gas yield firstly increased considerably from 4.0 L/g coal (5.8s) to 7.2 L/ g coal (17.5s), and then slightly increased to 7.3 L/ g coal (23.4s). The results show that the increasing residence time increases the syngas yield and concentration of YL and MW char. This is a result of increased char-CO_2 reaction (Boudouard reaction) with residence time.

The "estimated syngas (H_2/CO) concentration" shown in Figure 6 was calculated by Factsage 6.4. As seen, with the increasing residence time, the value of experimental syngas yield and concentration gradually climbed and was getting closer to the equilibrium concentration value. At nearly complete carbon conversion, the experimental value of MW and YL char was nearly the same as the equilibrium concentration. The results demonstrated that the YL and MW char were completely converted at 23.4 s and 21.7 s respectively.

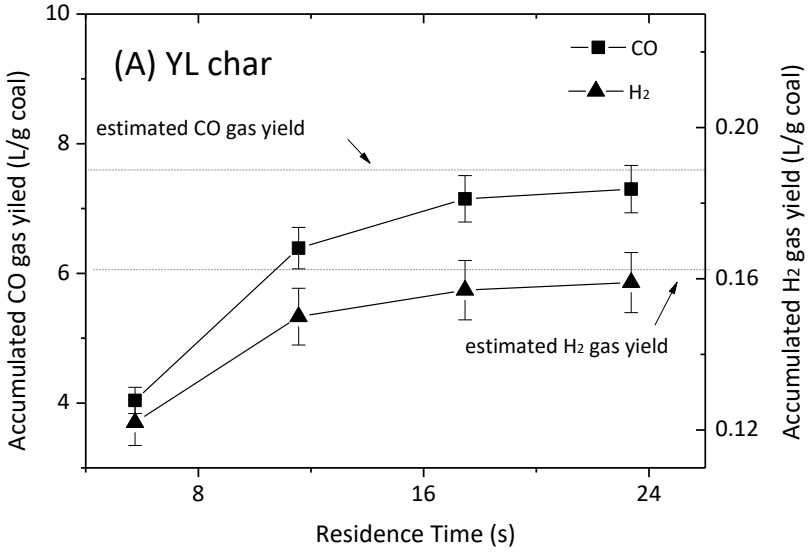

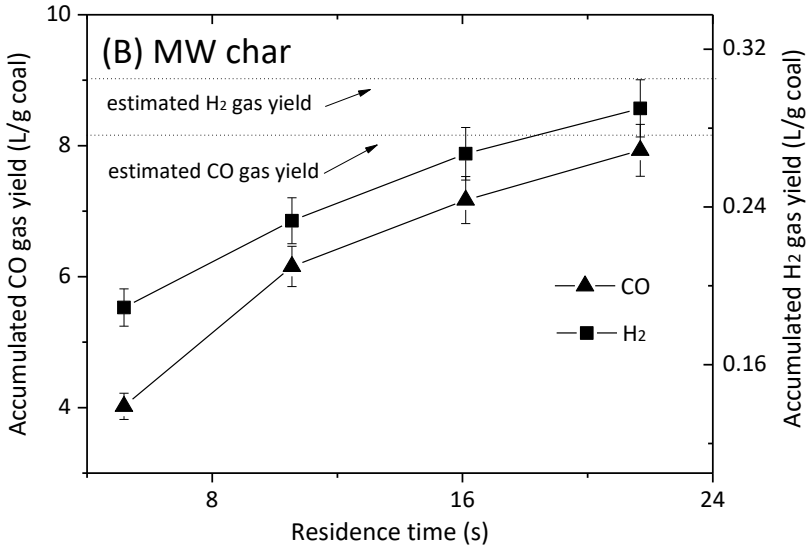

Figure 5: Influence of residence time on syngas yield of YL and MW char under 20% CO_2/80%N_2 at 1000 °C

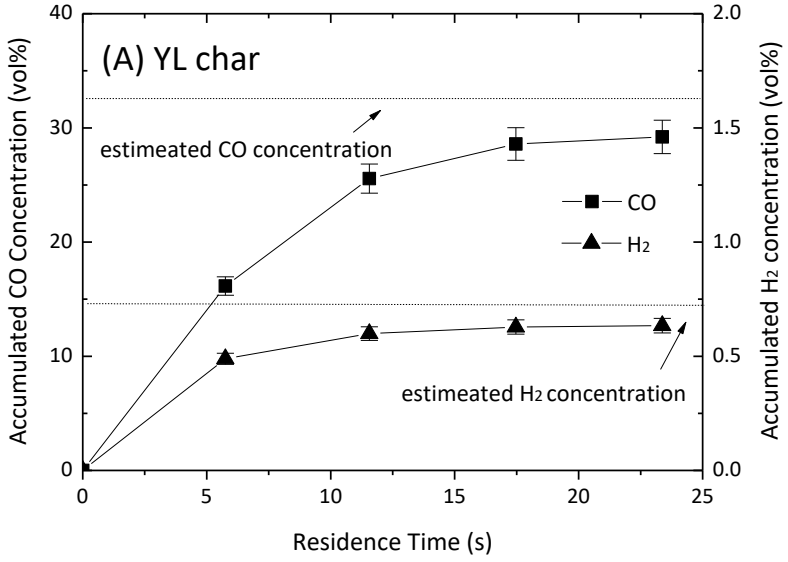

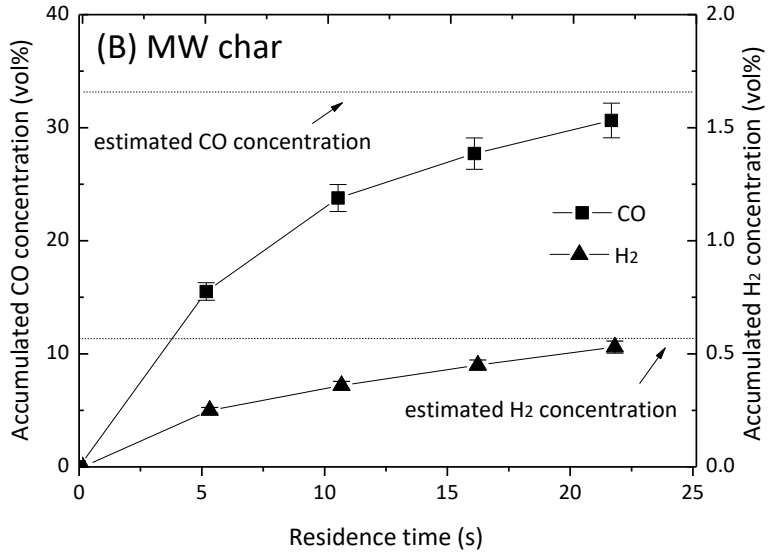

Figure 6: Influence of residence time on syngas composition of YL and MW char under 20% CO_2/80%N_2 at 1000 °C

3.3.4 Char morphology change

To gain a better understanding of the morphology change during char gasification, the morphology observations were measured by the SEM. Figure 7 shows the SEM photographs of YL char at carbon conversion of 0, 45%, 88%, 96%, and 99% at 1000 °C. As seen, no significant changes in overall particle size were found with the increasing carbon conversion. This finding demonstrates the hypothesis of the residence time calculation that particle size does not change during the gasification and ensure the accuracy of the calculated residence time. As the carbon conversion increased, more small-diameter particles were observed in the SEM pictures, suggesting the fragmentation of the char particle because of the particle collision between particles or with the reactor wall, and the formation of the ash because of the Boundary reaction. In terms of the morphology change of the single particle, mineral constituents were found on the surface of the pyrolysed YL char at 1000 °C. With the progress of the gasification, more small pores were observed on the particle surface at carbon conversion of 45% and 88%, a result of increased Boudouard reaction between carbon in char with CO_2. At high carbon conversions of 96% and 99%, a smooth surface was found for the particle which can be contributed by the melting of mineral constituents on the surface.

Figure 8 shows the SEM photographs of MW char at carbon conversion of 0, 47%, 73%, 92%, and 98% at 1000 °C. Like YL char, with the increasing residence time, the overall particle size of MW chars does not significantly change and more pores were observed on the

surface of the char particle. By contrast, no significant melting of mineral constituents was found on the surface of MW gasified char at higher carbon conversions of 92% and 98%. These are because the gasified MW chars at high conversions have less mineral content (12-14% mineral content) compared to the rich-mineral YL samples (32-37% mineral content).

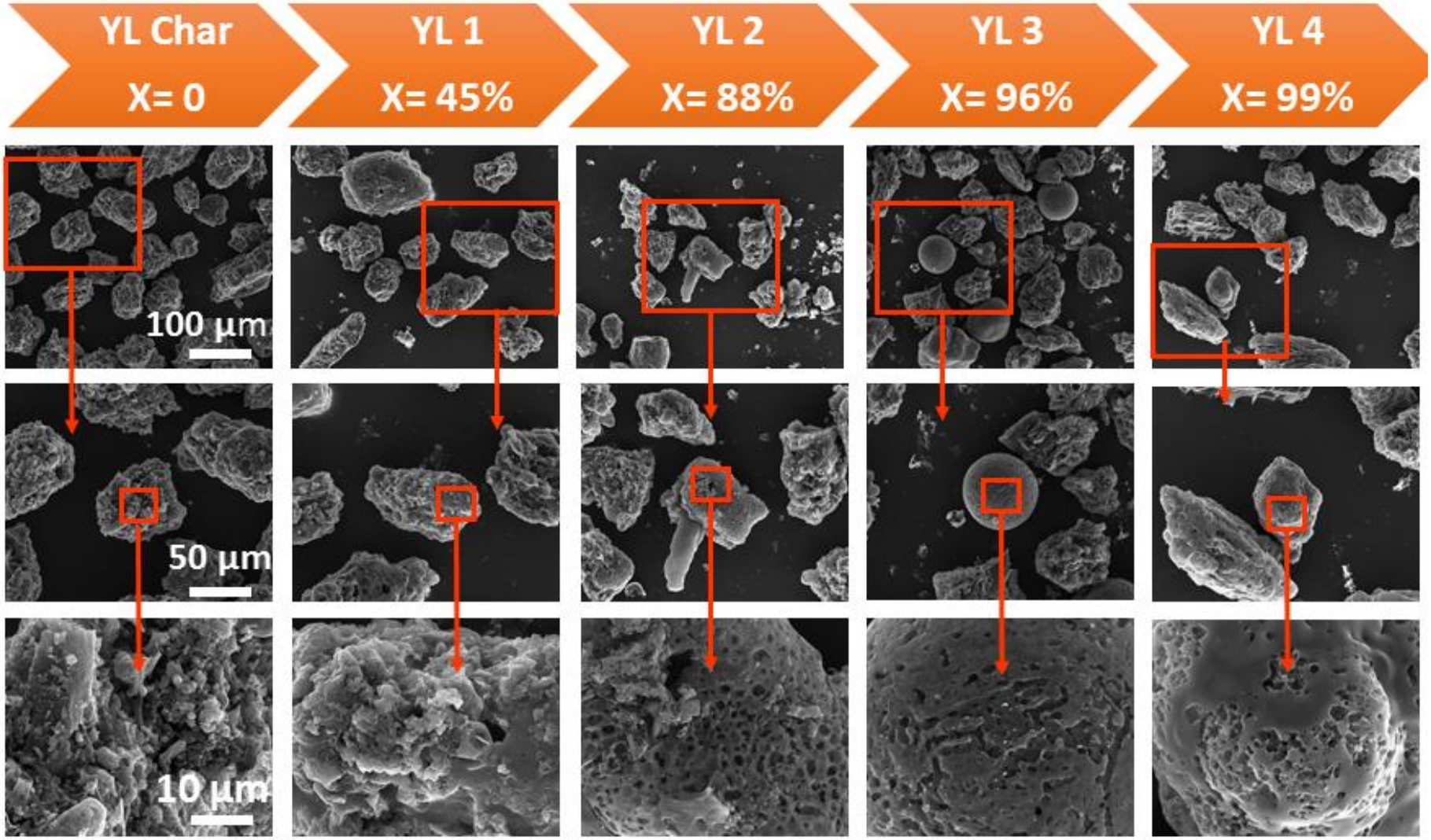

Figure 7: SEM photographs of YL char at carbon conversion of 0, 55%, 85%, 98%, and 99%, respectively (1000 °C)

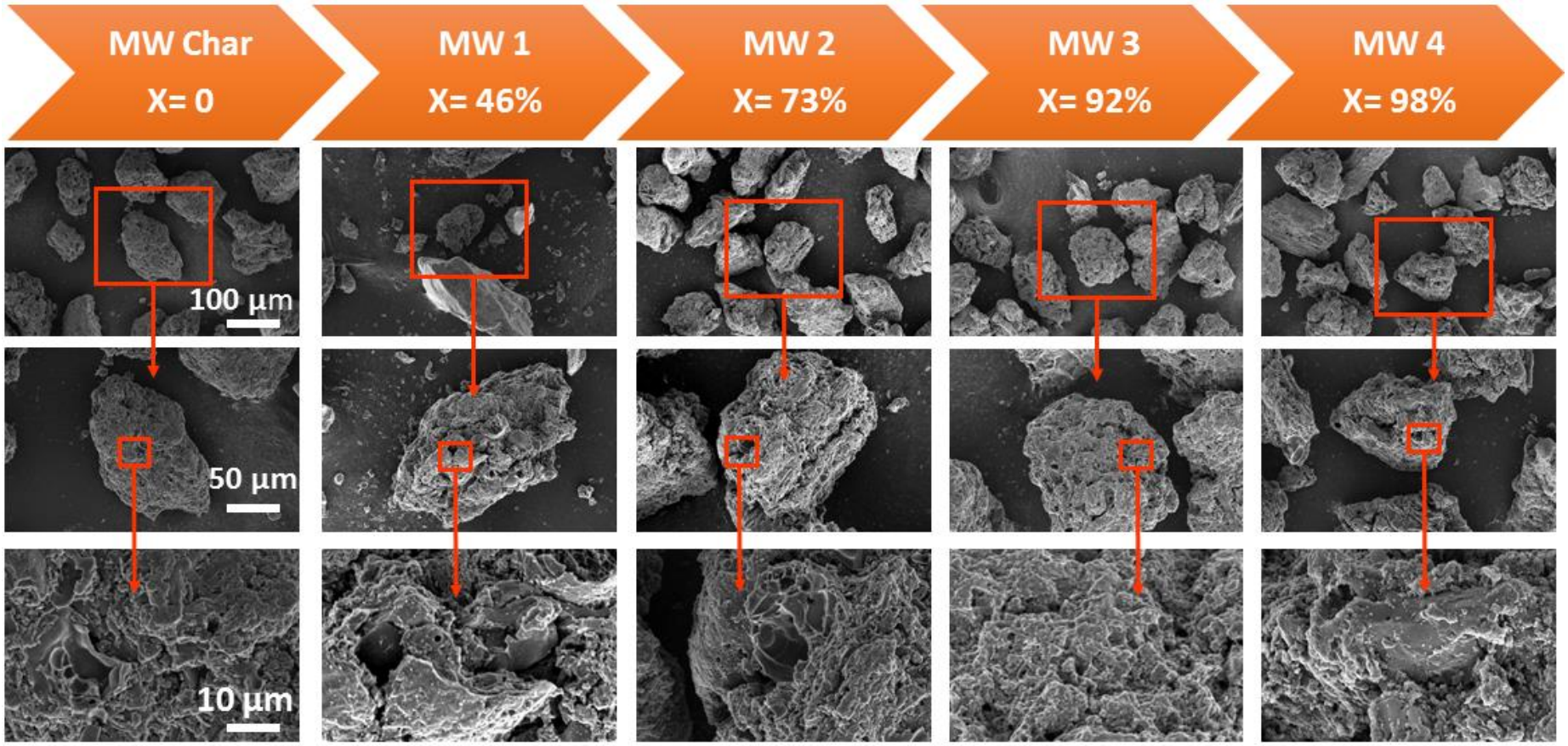

Figure 8: SEM photographs of MW char at carbon conversion of 0, 47%, 73%, 89%, and 96%, respectively (1000 °C)

SEM photographs of MW char with carbon conversion of 99% are shown in Figure 9. As seen, at nearly complete carbon conversion, MW char presented mainly four morphology change:

(1) The particle fragmentation. As shown in Figure 9(A) and (B), the observed hemisphere particle is generated through the self-fragmentation of the particle during gasification, and the small sphere particle can be from the fragmentation of one large particle. The particle fragmentation results in the decrease of the particle size [21].

(2) Unconverted char. Some unconverted particles have a porous surface, as shown in Figure 9(C).This finding indicates that carbon in char releases from outside and inside of the particle, but does not change particle size. Some particles with a smooth surface are also observed, as shown in Figure 9(D). This smooth surface is resulted by the melting of the mineral constituents of the rich-mineral particle.

(3) The particle agglomeration, as shown in Figure 9(E). This agglomeration can be derived from the melting of the mineral constituents and results in the increase of the particle size.

(4) Tiny ash particle, as shown in Figure 9(F). In the end, the char particle is completely converted to form the ash particle. Compared to the particle shape mentioned above, the dimeter of the ash is much smaller (around 1μm).

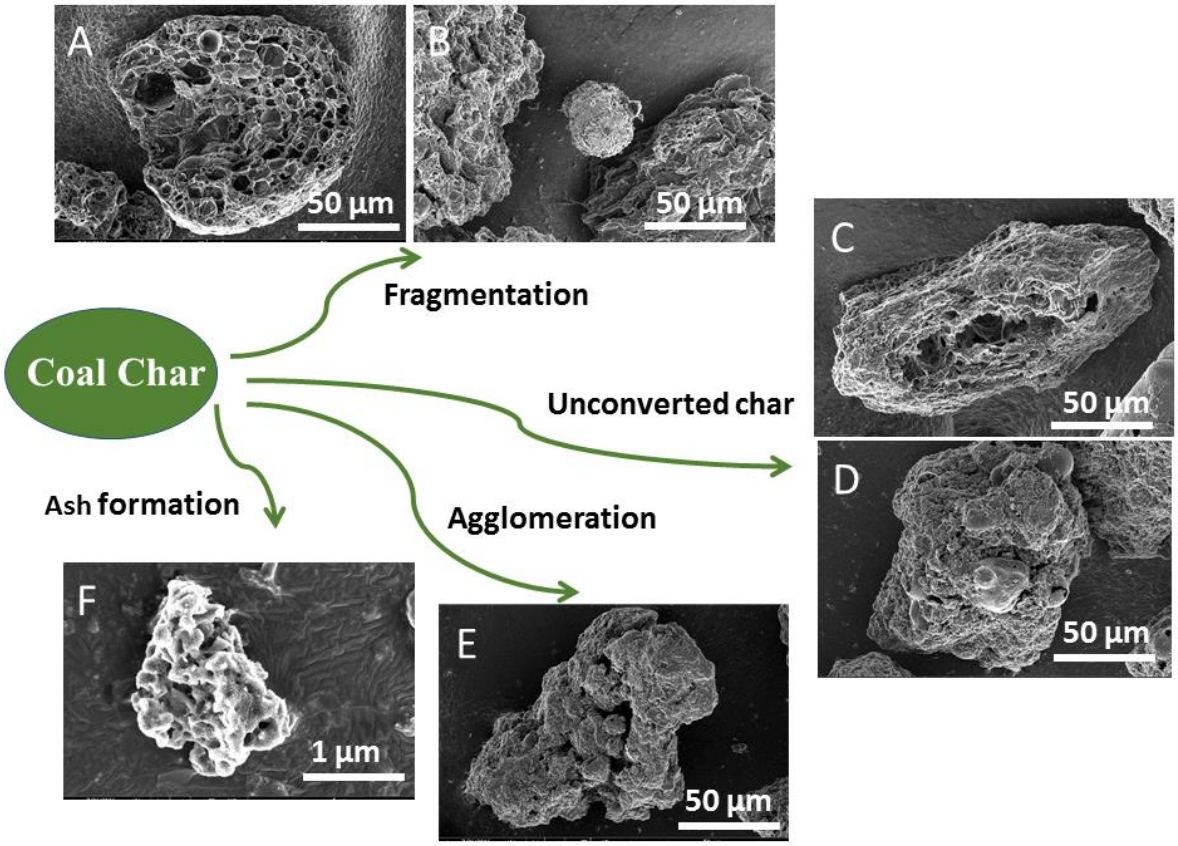

Figure 9: SEM photographs of MW char at carbon conversion of 99%

4 Conclusions

This study provides fundamental data on the effect of temperature, input CO_2 concentration, and residence time on entrained flow gasification behaviour of YL and MW chars in CO_2. The findings show that an increase of temperature and input CO_2 concentration results in an increase in carbon conversion and syngas yield. By contrast, the increase of residence time by decreasing the total gas flow rate from 5 L/min to 2 L/min results in lower carbon conversion and syngas yield. This is because a decrease in total gas flow rate decreases Ug. When Ug < Up, the moving mode of particles in the reactor changes from entrained to falling. Comparing the two conditions, entrained flow gasification (Ug > Up) with a shorter residence time attains better gasification performance in terms of higher carbon conversion and syngas yield than dropping flow gasification (Ug < Up) at the same temperature and CO_2 concentration. This finding suggests, as expected, that entrained flow condition can achieve better gasification performance than the fixed-bed or dropping flow condition.

As expected, when the residence time increases, the carbon conversion and syngas yield of YL and MW char improve, and the carbon content and gasification reactivity of their gasified char decrease.

The experimental data establish that the residence time required for complete conversion of the YL and MW char at 1000 °C and 20% CO_2 is 17.4s and 21.7s, respectively. At the reaction time, the measured syngas yield and concentration of YL and MW char also approximately equals the equilibrium concentration value, demonstrating the completion of the conversion. As the residence time for complete conversion of YL and MW char is almost double longer than that for the typical commercial-scale entrained flow gasifier (6-10s), it is recommended that the gasification of Victoria brown coal is carried out at a higher temperature above 1000 °C to shorten the residence time for complete carbon conversion.

No significant change in the overall particle size of YL and MW chars was found during the gasification progress at 1000 °C. At a high carbon conversion above 98%, the melting of mineral constituents on the particle surface was only found in YL gasified char, not MW gasified char. At the carbon conversion of MW char at 98%, four major changes were observed in the samples: the particle fragmentation, particle agglomeration, unconverted chars and tiny ash.

5 Acknowledgements

The authors would like to gratefully acknowledge the support from China Scholarship Council, Brown Coal Innovation Australia (BCIA), and Monash University for their financial support. The authors also acknowledge the Australian Research Council's Linkage Infrastructure, Equipment and Facilities Scheme ((FEI Nova NanoSEM 450) and the use of facilities within the Monash Centre for Electron Microscopy.

6 References

[1] IEA, Coal market outlook, in: World Energy Outlook 2016, IEA, 2016, pp. 203-239.

[2] BP, BP statistical review of world energy in, BP Global, https://www.bp.com/content/dam/bp/en/corporate/pdf/energy-economics/statistical-review-2017/bp-statistical-review-of-world-energy-2017-full-report.pdf, 2017, pp. 36-38.

[3] Department of State Development, Brown coal-Victoria, Australia: a principal brown coal province, in, Department of State Development, Business and Innovation, http://www.energyandresources.vic.gov.au/earth-resources/victorias-earth-resources/coal, 2014.

[4] E.I. Koytsoumpa, K. Atsonios, K.D. Panopoulos, S. Karellas, E. Kakaras, J. Karl, Modelling and assessment of acid gas removal processes in coal-derived SNG production, Appl. Therm. Eng., 74 (2015) 128-135.

[5] R. Mota, G. Krishnamoorthy, O. Dada, S.A. Benson, Hydrogen rich syngas production from oxy-steam gasification of a lignite coal – A design and optimization study, Appl. Therm. Eng., 90 (2015) 13-22.

[6] U.S. Department of Energy, 2010 Worldwide Gasification Database, in: DOE National Energy Technology Laboratory (Ed.), Pittsburg, PA, 2010.

[7] L. Wang, Y. Jia, S. Kumar, R. Li, R.B. Mahar, M. Ali, I.N. Unar, U. Sultan, K. Memon, Numerical analysis on the influential factors of coal gasification performance in two-stage entrained flow gasifier, Appl. Therm. Eng., 112 (2017) 1601-1611.

[8] A. Tremel, J. Stemann, M. Herrmann, B. Erlach, H. Spliethoff, Entrained flow gasification of biocoal from hydrothermal carbonization, Fuel, 102 (2012) 396-403.

[9] S.H. Lee, S.J. Yoon, H.W. Ra, Y.I. Son, J.C. Hong, J.G. Lee, Gasification characteristics of coke and mixture with coal in an entrained-flow gasifier, Energy, 35 (2010) 3239-3244.

[10] K Kirtania, J Joshua, MA Kassim, S Bhattacharya, Comparison of CO2 and steam gasification reactivity of algal and woody biomass chars, Fuel Processing Technology, 117 (2014) 44-52.

[11] X. Zou, J. Yao, X. Yang, W. Song, W. Lin, Catalytic Effects of Metal Chlorides on the Pyrolysis of Lignite, Energy & Fuels, 21 (2007) 619-624.

[12] J. Tanner, M. Bläsing, M. Müller, S. Bhattacharya, Influence of Temperature on the Release of Inorganic Species from Victorian Brown Coals and German Lignites under CO2 Gasification Conditions, Energy & Fuels, 28 (2014) 6289-6298.

[13] S.P. Bhattacharya, Gasification Performance of Australian Lignites in a Pressurized Fluidized Bed Gasifier Process Development Unit Under Air and Oxygen-enriched Air Blown Conditions, Process Saf. Environ. Prot., 84 (2006) 453-460.

[14] J. Tanner, K.B. Kabir, M. Müller, S. Bhattacharya, Low temperature entrained flow pyrolysis and gasification of a Victorian brown coal, Fuel, 154 (2015) 107-113.

[15] M. Rhodes, Single Particles in a Fluid, in: Introduction to Particle Technology, John Wiley & Sons, Ltd, 2008, pp. 29-49.

[16] K. Umeki, K Kirtania, L Chen, S Bhattacharya, Fuel particle conversion of pulverised biomass during pyrolysis in an entrained flow reactor, Industrial and Engineering Chemistry Research, 51(2012), pp. 13973-13979.

[17] B.B. Hattingh, R.C. Everson, H.W.J.P. Neomagus, J.R. Bunt, Assessing the catalytic effect of coal ash constituents on the CO2 gasification rate of high ash, South African coal, Fuel Process. Technol., 92 (2011) 2048-2054.

[18] K. Liu, Z. Cui, T.H. Fletcher, Coal Gasification, in: Hydrogen and Syngas Production and Purification Technologies, John Wiley & Sons, Inc., 2009, pp. 156-218.

[19] C. Higman, M. van der Burgt, Chapter 4 - Feedstocks and Feedstock Characteristics, in: Gasification (Second Edition), Gulf Professional Publishing, Burlington, 2008, pp. 47-90.

[20] J.E. Preciado, J.J. Ortiz-Martinez, J.C. Gonzalez-Rivera, R. Sierra-Ramirez, G. Gordillo, Simulation of Synthesis Gas Production from Steam Oxygen Gasification of Colombian Coal Using Aspen Plus®, Energies, 5 (2012) 4924-4940.

[21] P.P. Sripada, T. Xu, M.A. Kibria, S. Bhattacharya, Comparison of entrained flow gasification behaviour of Victorian brown coal and biomass, Fuel, 203 (2017) 942-953.

Chapter 6 Entrained flow gasification behaviour at high temperatures (>1000 °C)

According to the findings of low temperature gasification in chapter 5, Victorian brown coals required more than 16 s, almost double the residence time used in large scale commercial gasifiers, for complete carbon conversion at 1000 ºC. Entrained flow gasification behaviour at high temperatures (>1000 ºC) was, therefore, investigated and is discussed in this chapter. Only one study is reported in the literature on the high temperature gasification behaviour of Victoria brown coal in an entrained flow reactor [6]. It was found that char conversion and syngas yield increased with increasing temperature and CO_2 concentration. Nonetheless, it is limited to only one Victorian coal - Morwell coal, and only two-step gasification (meaning coal pyrolysis followed by gasification of the pyrolysis char). Therefore, the effect of high-temperature and input CO_2 on parent Victorian brown coals under two different gasification processes, direct and two-step coal gasification, has not been investigated.

In this study, the effect of high temperature and CO_2 concentration on gasification behaviour of three Victorian brown coals, Maddingley, Loy Yang, and Yallourn coal, is investigated in a high temperature atmospheric entrained flow reactor. Two coal gasification processes – direct and two-step coal gasification – are compared in gasification performance and emission of air pollutants (H_2S, HCN, and NH_3). In particular, the following information is generated:

- gas composition and carbon conversion under different pyrolysis and gasification conditions,
- emission of H_2S, HCN, and NH_3 during direct and two-step gasification at different temperatures and CO_2 concentration,
- the morphological change and particle size change of gasification residues at different temperatures.

This chapter reproduces the following submitted paper to the Applied Energy.

Entrained flow gasification of Victorian brown coals and chars using CO_2: gasification behaviour & pollutant gas emission

Tao Xu, Sankar Bhattacharya *

Department of Chemical Engineering, Monash University, VIC 3800, Australia

Corresponding author. Email: Sankar.Bhattacharya@monash.edu

Graphical abstract

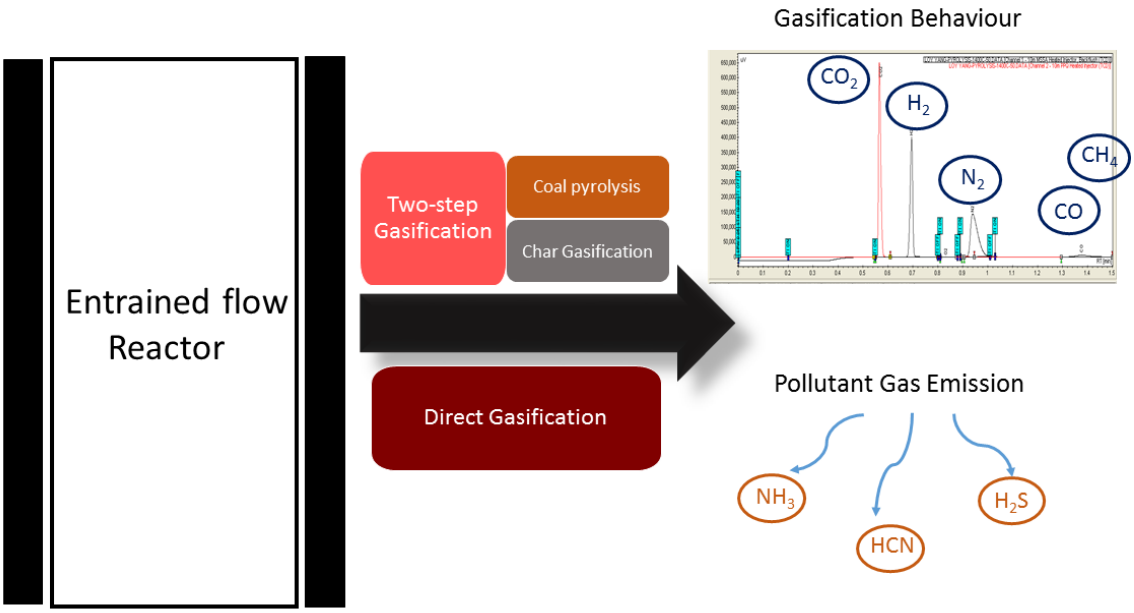

Abstract

This study assesses the gasification behaviour and pollutant gas emission of three Victorian brown coals in CO_2 using a bench - scale entrained flow reactor by comparing two gasification processes - firstly using coal and secondly using two steps of producing char through pyrolysis and then using this char for gasification. The effect of temperature (1000-1400 °C) and input CO_2 (10-40 vol.%) concentration was investigated. Higher temperature and input CO_2 concentration increased CO concentration and carbon conversion. Higher temperature increased H_2S and HCN emissions, but higher CO_2 concentration decreased the H_2S and HCN emissions. The gasification process (direct and two-step gasification) had little effect on the overall carbon conversion but had a significant effect on the gas composition of the product gases. Direct gasification generated little H_2 and more

CO in the product gases than two-step gasification. During two-step gasification, coal pyrolysis contributed to around 65% carbon conversion, 50-80% HCN emission and almost all H_2S emission. It was found that entrained flow gasification achieved very high carbon conversion (~ 98%) for Victorian brown coals at 1200 °C with around 7s residence time for the particle size of 90-106 microns. No NH_3 emissions were detected during the entrained flow gasification but HCN and H_2S emissions were still high in the ppmv level.

Keywords

Gasification, Pollutant gas emission, Entrained flow, Two-step gasification, Direct gasification, Brown coal

1. Introduction

In Australia, Victorian brown coals represent a significant, low cost energy resource with reserves of 430 billion tonnes. These brown coals are the primary energy source in the state of Victoria, supplying approximately 85% of the state's electricity [1]. However, brown coal utilisation is limited to mine-mouth power generation using conventional pulverised coal-fired combustion units at relatively low efficiency and high greenhouse gas emission [2]. Therefore, beyond its direct combustion, great effort is being made by the industry and academia to develop low-emission coal technologies, to utilise such vast resources for higher value products with low emission[3]. As one clean coal technology, gasification is a thermochemical conversion method where fuel reacts with reactants like steam and carbon dioxide to produce syngas (CO/H_2) which can be used for generation of power and a variety of chemicals and liquid fuels [4-7]. Among three major gasifier types - fixed bed, fluidized bed, and entrained flow gasifiers -, the entrained flow gasifiers dominate the world gasification market for syngas production, and is potentially the only gasification process for reliable co-production of power and chemicals using brown coals [8]. However, fundamental understanding of the process and information on the gaseous products of entrained flow gasification using brown coals is limited.

Relatively few experimental studies on entrained flow gasification of low-rank coals have been reported in the literature. Tremel et al. investigated pyrolysis and gasification behaviour of a German lignite in an entrained flow reactor [9]. They found that with the increase of temperature and residence time, the carbon conversion increased. Harris et al. examined entrained flow gasification behaviour of Australian sub-bituminous coals at high temperature and pressure [10], and assessed the effect of temperature and coal types on coal conversion. Cristina et al. [11] and Guo et al. [12] found

that high CO_2 concentration improved carbon conversion of sub-bituminous and bituminous coal in an entrained flow reactor. However, since the quality and composition of coal vary considerably from one coal to another, the influence of high temperature and CO_2 concentration on different brown coal type can be different, especially for Victorian brown coal with several unique physical and chemical characteristics - high moisture content (50-66%) in the as-received coal, low minerals content (<4%) varying mineral composition, and high oxygen content (>25%) [13].

There have been some studies assessing alkali and alkaline earth metal (AAEM) emissions and their catalytic effects during pyrolysis and gasification of Victorian brown coals in a fixed bed [14, 15], and one study reporting on pressurised fluidised bed gasification of Victorian brown coals at a 1.6 MW scale [16]. The latter study suggested that fluidised bed gasification may not be suitable for Victorian brown coals and recommended entrained flow gasification from low to high temperature ranges. In entrained flow gasification, use predominantly of CO_2 is of interest as this can lower or avoid the use of steam and oxygen which are expensive to produce. However, investigations on entrained flow gasification behaviour of Victorian brown coals are limited. Only one study [17] is reported in the literature on the high-temperature pyrolysis and gasification behaviour of Victoria brown coal in an entrained flow reactor. It was found that char conversion and syngas yield increased with increasing temperature and CO_2 concentration. Nonetheless, it is limited to only one Victorian coal - Morwell coal, and only two-step gasification (meaning coal pyrolysis followed by gasification of the pyrolysis char) [17]. The effect of high-temperature and input CO_2 on parent Victorian brown coals and their chars under different gasification processes - two-step and direct coal gasification - has never been investigated.

In this study, the effect of high temperature and CO_2 on gasification behaviour and pollutant gas emission of three Victorian brown coals - Maddingley, Loy Yang, and Yallourn coal- is investigated. Two gasification processes – direct and two-step coal gasification – are compared. This study offers new insight on entrained flow gasification of Victorian brown coals and their chars comparing the performance of coal and char gasification. In particular, the following information is generated:

a) gas quality and carbon conversion under different pyrolysis and gasification conditions;

b) the release of NH_3, HCN, and H_2S under various pyrolysis and gasification conditions;

c) the particle size evolution and morphology change during pyrolysis and gasification process.

The resulting data is useful to examine the further use of the fuel gas for chemical products and power generation.

2. Experimental

2.1 Sample

The three Victorian brown coal samples used in this study are Yallourn (YL) and high-ash Loy Yang (LY) coal from the Latrobe Valley, and Maddingley (MD) coal from the Maddingley mine. As these dried coals can reabsorb moisture to some extent, the moisture content was determined immediately prior to the experiments. The proximate analysis, ultimate analysis and ash composition of these three coals are listed in Table 1. Coal samples were ground, oven-dried, and sieved to 90-106 μm for the experiments.

Table 1: Proximate analysis, ultimate analysis and ash composition of Maddingley, high-ash Loy Yang, and Yallourn coal

Items	Maddingley coal	High-ash Loy Yang coal	Yallourn coal
Moisture (oven dried, wt.%)	1.01-1.50	0.49-1.50	0.64-2.72
Proximate analysis (dry basis, wt.%)			
Volatile matter	47.50	48.00	48.18
Fixed carbon	37.26	43.58	51.82
Ash	15.24	8.42	2.32
Ultimate analysis (dry basis, wt.%)			
Carbon	50.91	60.01	62.99
Hydrogen	4.56	4.68	4.98
Nitrogen	0.51	0.58	0.54
Sulfur	3.34	0.70	0.40
Ash	15.24	8.42	2.32
Oxygen (by difference)	25.44	25.61	28.77
Ash composition (dry basis, wt %)			
SiO_2	19.02	47.16	1.36
Al_2O_3	15.24	22.11	1.75
BaO	0.02	0.01	0.28
CaO	9.24	2.05	8.29
Fe_2O_3	20.55	4.11	51.59
K_2O	0.08	0.61	0.18
MgO	7.58	5.51	17.69
Na_2O	8.92	7.87	5.78
SO_3	19.02	7.41	12.55
TiO_2	0.34	3.17	0.54

2.2 Apparatus and procedure

An electrically heated entrained flow reactor was used for the gasification experiments. The furnace is of 3 m length and consists of nine separately controllable heating zones. The fused alumina reactor has an inner diameter of 89 mm. The samples were fed continuously from the top of the reactor by a screw feeder and introduced into the chamber through a water-cooled injector. For each run, primary

gas of N_2 was fed from the isolation box within the screw feeder at a rate of 4 L/min, entraining the samples into the reactor. The majority of the secondary gas used for gasification was introduced from the top of the reactor at a total rate of 12 L/min into the chamber, after heating to 500 °C through a gas preheater.

A stainless steel solid collector was used to collect the solid products - ash and char residue. After passing through the gas cleaning and cooling system consisting of three impinger vessels, the outlet gas was analysed by Dräger tubes for pollutant gas emission and a micro-gas chromatograph (Varian 490-GC) for composition of the major gases - H_2, CO, CO_2, CH_4, and N_2. The solid products were collected, weighed and analysed offline. A schematic drawing of the entrained flow reactor is available in our previous paper [17].

As mentioned earlier, two gasification processes were investigated: (1) two-step coal gasification, oven-dried coal samples were pyrolysed in N_2 to prepare char under entrained flow conditions, then the char was gasified with CO_2. (2) direct coal gasification, oven-dried coal samples were directly gasified with CO_2. The experiments were conducted at various input CO_2 concentrations (10-40 vol.%) and temperatures (1000-1400 °C), to investigate the effect of input CO_2 and temperature on gas composition and carbon conversion. The residence time of two-step gasification is around 14s (coal pyrolysis: ~7s, char gasification: ~7s), and the residence time of direct gasification is approximately 7s.

2.3 Data collection

The operating parameters of the reactor - furnace temperature, pressure, feeding rate and gas flow rate - are controlled, monitored and recorded by a custom LabVIEW CompactDAQ system. The reactor was heated up to the desired temperature before feeding the sample. Inert gas N2 was fed for at least 1 hour until very low oxygen level (<0.3 vol.%) was achieved in the outlet gas. Then, reactant gas CO_2 at controlled flow rate was introduced into the reactor. After the CO_2 composition had been measured by micro-GC, the samples were fed at a controlled rate from the top of the reactor. The pressure of the system is strictly controlled at atmospheric pressure by manually adjusting the power of the vacuum pump. The steady state is defined when the major gas composition measured by the micro-GC stabilised, as shown in Figure 1. The Micro-GC can determine the vol. % of H_2, CO, N_2, CH_4, and CO_2. The Micro-GC data in the steady state operation were collected and presented here. The NH_3, HCN, and H_2S level during gasification process were also measured three times respectively using Dräger tubes during steady state.

In terms of the solid products, those were collected from the main solid collector and weighed by a precision balance. The particle size distribution and morphology were examined by Mastersizer 2000 and emission scanning electron microscope (FEI Nova NanoSEM 450 FEGSEM), respectively. The impinger vessels were used for tar collection during the run.

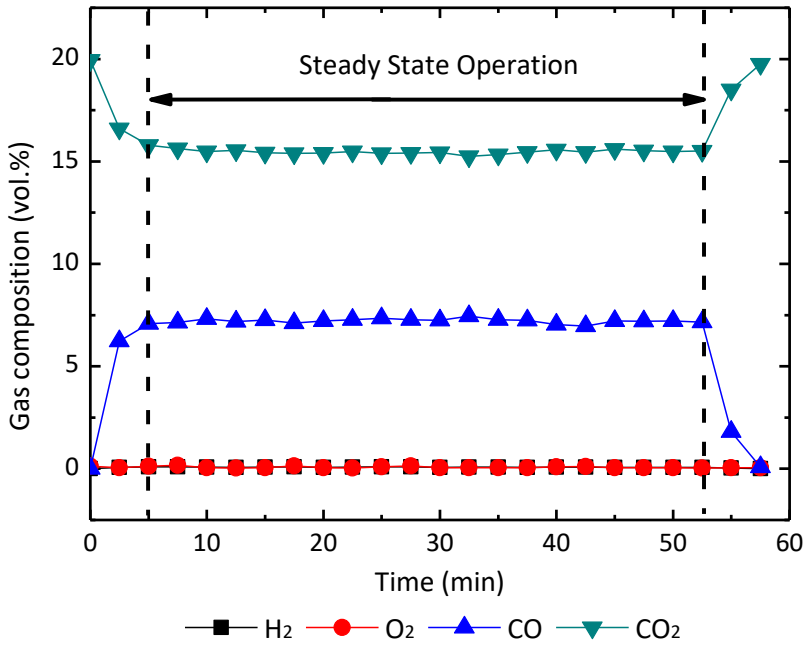

Figure 1: Typical gas composition profile of gasification for LY char at 1200 °C and 20 vol.% CO_2 in N_2 during steady state operation.

2.4 Data analysis

2.4.1 Gasification behaviour

The gasification behaviour of Victorian brown coals and chars is evaluated through fuel gas composition, its calorific value, and carbon conversion.

The data of fuel gas composition from micro-GC were averaged and presented here. Typically, little or no N_2 is generated from coal pyrolysis, the gas composition for coal pyrolysis is shown on a N_2-free basis. According to the gas composition, its calorific value is calculated from the respects of low heating value (LHV) and high heating value (HHV) as follow:

$$\mathrm{LHV}(\mathrm{MJ}/m^3) = x_{H2} \times 10.78 + x_{CO} \times 12.63 + x_{CH4} \times 35.81 \quad \text{(E 1)}$$

$$\mathrm{HHV}(\mathrm{MJ}/m^3) = x_{H2} \times 12.76 + x_{CO} \times 12.63 + x_{CH4} \times 39.75 \quad \text{(E 2)}$$

Where x_{CO}, x_{CO}, x_{CH4} is gas concentration of CO, CO_2, and CH_4, vol.%.

Carbon conversion represents the amount of carbon in the feedstock that has reacted. It can be calculated using ash (solid phase) or carbon-containing produced gas (gas phase) as a tracer, and their calculations are given below:

Solid-phase carbon conversion: $X(\%) = \frac{m_{C,feed} - m_{C,ash}}{m_{C,feed}} \times 100$ (E 3)

Gas-phase carbon conversion: $X(\%) = \frac{(X_{CO} + X_{CH4} + X_{CO2,out} - X_{CO2,in}) \times 12}{m_{C,feed}} \times 100$ (E 4)

Where $m_{C,feed}$ is the mass of carbon in the feeding inlet, $m_{C,ash}$ is the mass of carbon in solid residuce collected from the outlet, $X_{CO}, X_{CO2,out}, X_{CH4}$ is the molar flowrate of CO, CO_2 and CH_4 in the outlet gas, $X_{CO2,in}$ is the molar flowrate of CO_2 in the inlet, $m_{C,feed}$is the mass flowrate of the carbon including the feed coal/char in the inlet.

However, both the calculations have their own uncertainty. The uncertainty of solid-phase method includes the incomplete solid recovery at the outlet and due to ash evaporation; the uncertainty of the gas-phase method is mainly from the inaccuracy of the gas analysis by the micro-GC analyzer. The variations in results of the two methods ranged 0.4-7.6%. In this study, the carbon conversion was calculated in both solid and gas basis.

2.4.2 Pollutant gas emission

The NH_3, HCN, and H_2S level during gasification process were also measured three times respectively using Dräger tubes during steady state. The concentration of NH_3, HCN, and H_2S was averaged from measurements and presented here. The measurement accuracy of NH_3 is ± 10-15%, HCN is ± 10-15%, and H_2S is ± 5-10%. Because the gas temperature in the impingers, approximately 40°C, is higher than the boiling temperature of NH_3 (35.6°C), HCN (25.6°C) and H_2S (- 60°C), these species are unlikely to have condensed in the impingers.

3. Results

3.1 Two-step coal gasification

Coal gasification is a mix of heterogeneous and homogeneous reactions. Pyrolysis and gasification steps take place simultaneously which makes the gasification reactions too complicated to study. Two-step gasification simplifies and separates the gasification process into two stages: 1) coal

pyrolysis; 2) gasification of char from pyrolysis, which allows us to have a better understanding for each stage. After knowing what happened at each stage, two-step gasification can be compared with direct gasification which enables a better understanding of the overall products from coal pyrolysis and char gasification.

3.1.1 Step 1-coal pyrolysis

Pyrolysis experiments were conducted at 1000 °C, 1200 °C and 1400 °C using oven-dried pulverised YL, LY and MD coal with a particle size (90-106 μm) at a feeding rate of 2.6 ± 0.3 g/min. Fuel gas composition was measured online, and the solid char was analysed after experiments. The pyrolysis behaviour regarding producer gas composition, char yield, LHV and HHV, and char property is presented in Table 2.

The three Victorian brown coals have a similar trend in pyrolysis behaviour with temperature. With increasing pyrolysis temperature, the concentration of H_2 and CO increased sharply from 46-50% and 36-46% (1000 °C) to 51-59% and 40-49% (1200 °C), respectively, then gradually increased to 52-59% and 41-48% (1400 °C), respectively. However, the gas composition of the CH_4 and CO_2 correspondingly decreased. The concentration of CH_4 and CO_2 firstly significantly decreased from 2.9-5.4% and 2.9-7.4% (1000 °C), respectively, to 0.1-0.9% and 0-0.4% (1200 °C), respectively, and then both decreased to 0 (1400 °C). The very low concentration of CH_4 and CO_2 can be a result of 1) in-situ gasification (R1) between the nascent char and the CO_2 generated from pyrolysis (R2) [18]; 2) gas-phase reactions between CH_4 and steam from coal moisture (R3), and between CH_4 and CO_2 (R4) above 1000 °C [19, 20].

Boudouard reaction: $$C_{(s)} + CO_2 \longrightarrow 2CO \quad \text{(R 1)}$$

Pyrolysis: $$\text{Coal} \xrightarrow{heat} H_2 + CO + CO_2 + CH_4 + \text{others} \quad \text{(R 2)}$$

Steam - methane reforming: $$CH_4 + H_2O \rightarrow CO + 3H_2 \quad \text{(R 3)}$$

Dry methane reforming: $$CH_4 + CO_2 \rightarrow 2CO + 2H_2 \quad \text{(R 4)}$$

Reverse water-gas shift reaction: $$CO_2 + H_2 \rightarrow \text{CO} + H_2O \quad \text{(R 5)}$$

These are endothermic reactions and their rates increase with an increase of temperature, which results in the increase of the H_2 and CO yield and the corresponding decrease of CO_2 and CH_4 yield. [21]. When the available CO_2 and H_2O are completely consumed, the H_2 and CO yield reached a peak at 1400 °C. As expected, the carbon conversion of the three Victorian brown coals increased

with increasing temperature. The char yields at three pyrolysis temperatures are similar, ranging from 29% to 37%. However, a slight decrease in char yield was seen with increasing temperature because of the in-situ gasification. The value of LHV and HHV decreased slightly with the rising temperature, ranging from 11.6-12.5 MJ/m^3 (LHV) and 12.7-13.6 MJ/m^3 (HHV), as the methane content (which has higher calorific value) decreased.

Regarding char composition, the volatile matter content in three Victorian brown coal char steadily decreased with the increase of the pyrolysis temperature, and the carbon content increased as expected. However, the change of the ash content was different depending on the coal type. A sharp decrease of ash content by 38.6% was observed for YL char from 1200 °C to 1400 °C, which can be attributed to the evaporation of ash above 1200 °C. This suggests that YL ash cannot be used as a tracer for C-conversion calculation above 1200 °C, and, therefore, C-conversion of YL coal/ char above 1200°C is presented using the gas-phase method. On the contrary, the ash content of LY and MD coal increased when pyrolysis temperature increased. Clearly, high temperature has a large influence on pyrolysis behaviour of Victorian brown coals especially on gas composition and char composition. However, above 1200 °C, this influence becomes limited.

Table 2: Pyrolysis behaviour of MD, LY and YL coal at various temperatures in the entrained flow reactor

Sample	**MD coal**			**High-ash LY coal**			**YL coal**		
Atmosphere	**100% N_2**	**100% N_2**	**100% N_2**	**100% N_2**	**100% N_2**	**100% N_2**	**100% N_2**	**100% N_2**	**100% N_2**
Temperature (°C)	**1000**	**1200**	**1400**	**1000**	**1200**	**1400**	**1000**	**1200**	**1400**
Gas composition (N_2 free basis, vol.%)									
H_2	46.75	51.35	52.25	50.28	58.95	59.35	48.52	53.72	53.78
CO	45.57	48.52	47.75	36.72	39.99	40.65	43.66	45.4	46.22
CH_4	2.95	0.11	0	5.40	0.64	0	4.90	0.88	0
CO_2	4.73	0	0	7.41	0.43	0	2.92	0	0
Carbon conversion (wt.%)	60.64	63.06	63.90	59.37	61.66	64.64	60.59	69.85	68.45
Char yield (wt.%)	34.44	33.81	29.19	36.96	34.26	30.66	32.15	29.19	30.52
LHV (MJ/m^3)	11.85	11.70	11.66	11.99	11.63	11.53	12.50	11.84	11.64
HHV (MJ/m^3)	12.89	12.72	12.70	13.20	12.83	12.71	13.65	12.94	12.70
Char property									
Proximate analysis (dry basis, wt.%)									
Volatile matter	19.56	17.68	8.62	8.92	7.47	5.74	11.50	6.14	5.14
Fixed carbon	51.84	50.13	61.99	79.93	77.34	76.95	80.60	86.28	89.01
Ash	28.60	32.19	29.39	11.15	15.19	17.31	7.90	7.58	5.85
Ultimate analysis (dry basis, wt.%)									
C	59.86	61.34	63.48	70.94	72.22	74.46	83.17	88.62	89.28
H	1.09	1.36	1.35	1.38	1.24	0.87	1.42	1.24	0.82
N	0.45	0.44	0.48	0.68	0.56	0.59	0.61	0.78	0.66
S	5.35	4.45	5.30	0.71	0.57	0.43	0.39	0.34	0.30
O (by difference)	4.65	0.22	0	15.14	10.23	6.34	6.51	1.42	3.07
Ash	28.60	32.19	29.39	11.15	15.18	17.31	7.90	7.58	5.85

3.1.2 Step 2-char gasification

After pyrolysis, the effect of temperature and CO_2 on gas composition and carbon conversion during the gasification of Victorian brown coal char is presented in this sub-section. The char samples were fed to the reactor at a feeding rate of 1 ± 0.3 g/min. To compare the carbon conversion calculated by the gas-phase and solid-phase method, a carbon mass balance was conducted for each experiment, which is in the range of 92-98%. It is found that the error of the gas composition was within 2%, and the difference between solid-phase and gas-phase carbon conversion was 0.4-6.5%. Because of the relatively small difference, carbon conversion is presented based on solid-phase calculation in the subsequent sections.

3.1.2.1 Effect of temperature

The char generated at 1000, 1200, and 1400 °C were subsequently gasified at their corresponding pyrolysis temperatures under 20 vol.% CO_2 in N_2. The effect of temperature on entrained flow gasification behaviour is shown in Figure 2. The overall trend of three Victorian brown chars is almost the same. As expected, higher temperature enhances the Boudouard reaction (R1) and char gasification rate, which results in higher CO concentration and higher carbon conversion. When the temperature increased from 1000 °C to 1400 °C, CO concentration increased significantly from 4.6-8.8% to 9.4-12.9%, and solid-phase carbon conversion also largely increased from 84-91% to 99-100%. As expected, CO-rich syngas ($CO\&H_2$) is generated from CO_2 gasification, and CO concentration and CO/H_2 ratio on N_2 & CO_2 free basis account for 95-99% and > 35:1 respectively. Therefore, this syngas ratio is not suitable for direct chemical synthesis (typical 2:1 for methanol) and will have to lower the ratio by water-gas shift reaction. Nearly 100% carbon conversion was observed for YL char at 1200 °C, and for MD and LY char at 1400 °C after 7-second gasification. This indicates that the YL char has the highest reactivity among the three Victorian coal chars. However, the decrease of H_2 by 55-81% was shown for all Victorian brown chars with the increasing temperature. This decrease can arise from the reverse water-shift reaction (R5) above 400°C: the reverse water-shift reaction is favoured by a higher temperature [22].

Clearly, a higher temperature enhances the CO concentration and carbon conversion from gasification of Victorian brown coal chars, and by 1400 °C, Victorian brown coal chars achieve nearly 100% carbon conversion after 7 seconds gasification under 20 vol.% CO_2.

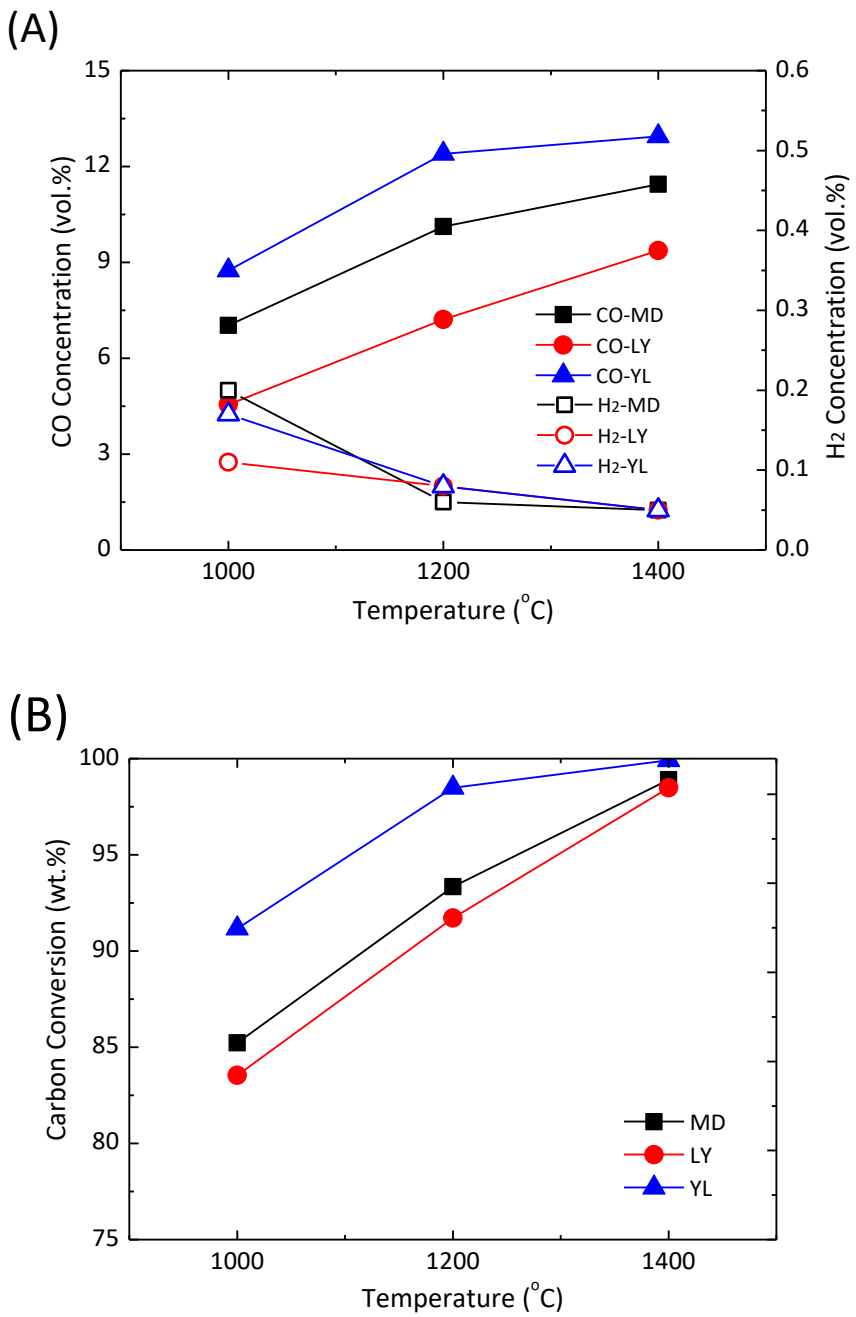

Figure 2: Effect of temperature on gasification behaviour of MD, LY, and YL char at 20 vol.% CO_2: (A) syngas composition, (B) solid-phase carbon conversion

3.1.2.2 Effect of input CO_2 concentration

To investigate the influence of input CO_2, the char generated at 1200 °C were gasified at the same temperature under a variety of input CO_2 concentrations (10-40 vol.%) at a total feed gas flowrate of 16 L/min. As the main reaction of the coal/char gasification is Boudouard reaction (R1), in essence, the change of the input CO_2 concentration affects the CO_2/C ratio of the R1 which is defined as:

$$CO_2 : \text{C ratio} = \frac{N_{CO2,input}}{N_{C,feed}} \quad \text{(E 5)}$$

Where $N_{CO2,input}$ is the molar flowrate of the input CO_2 in mol./min, $N_{C,feed}$ is the molar flowrate of the carbon in feed coal or char in mol. /min. A molar ratio of CO_2/C equals to 1, meaning enough CO_2 from all sources convert the carbon fed in coal or char to CO.

Figure 3 shows the influence of CO_2/C ratio on gas composition and carbon conversion. As is evident, enough CO_2 was fed based on the CO_2/C ratio (>1), the input CO_2 showed a positive effect on gasification performance of three Victorian brown coals with the increasing CO_2/C ratio. When CO_2/C ratio increased from 1.4-1.8 (10% CO_2) to 5.5-7.1(40% CO_2), CO concentration and carbon conversion significantly increased by 1.6-3.4% and 5-16%, respectively.

The optimal input CO_2 at 1 CO_2/C ratio would ideally result in highest CO concentration if infinite time was allowed for the Boudouard reaction to occur. However, in our experiments, the residence time of Victorian brown chars is limited to 7-8 s. Therefore, the observed trend of the increased CO concentration and carbon conversion with increasing CO_2/C ratio is contributed by the increase of char reactivity. Higher CO_2 concentration facilitates the char-CO_2 reaction rate at a given temperature because the reaction rate is proportional to the CO_2 concentration [17]. By contrast, the hydrogen gas concentration steadily decreased from 1.4-2% to 0.4-0.6%, with increasing CO_2/C ratio. The generated hydrogen should mainly evolve from the very low amount of hydrogen in char sample itself, considering that dry coal char is used in this study with a low moisture content below 1 wt.%. The decrease of hydrogen is due to the high input CO_2 promoting the reverse water-gas shift reaction (R5) converting H_2 to CO. Overall, the majority of syngas generated is CO whose concentration on N_2 & CO_2 free basis makes up 98-99%, and H_2 concentration accounts for 2-0.4%.

.It was found that YL char reached a high carbon conversion (95.48%) at a CO_2/C stoichiometry of 1.4, and the higher CO_2/C ratio (>6.2) was required for MD and LY char to reach at a similarly high carbon conversion at 1200 °C. These results indicate that YL char has the highest reactivity, followed by MD char and LY char, respectively. The results also indicate that MD and YL chars achieve complete conversion at a higher CO_2 input as 40% CO_2 and at 1200 °C, but LY char requires a higher CO_2 input for complete conversion.

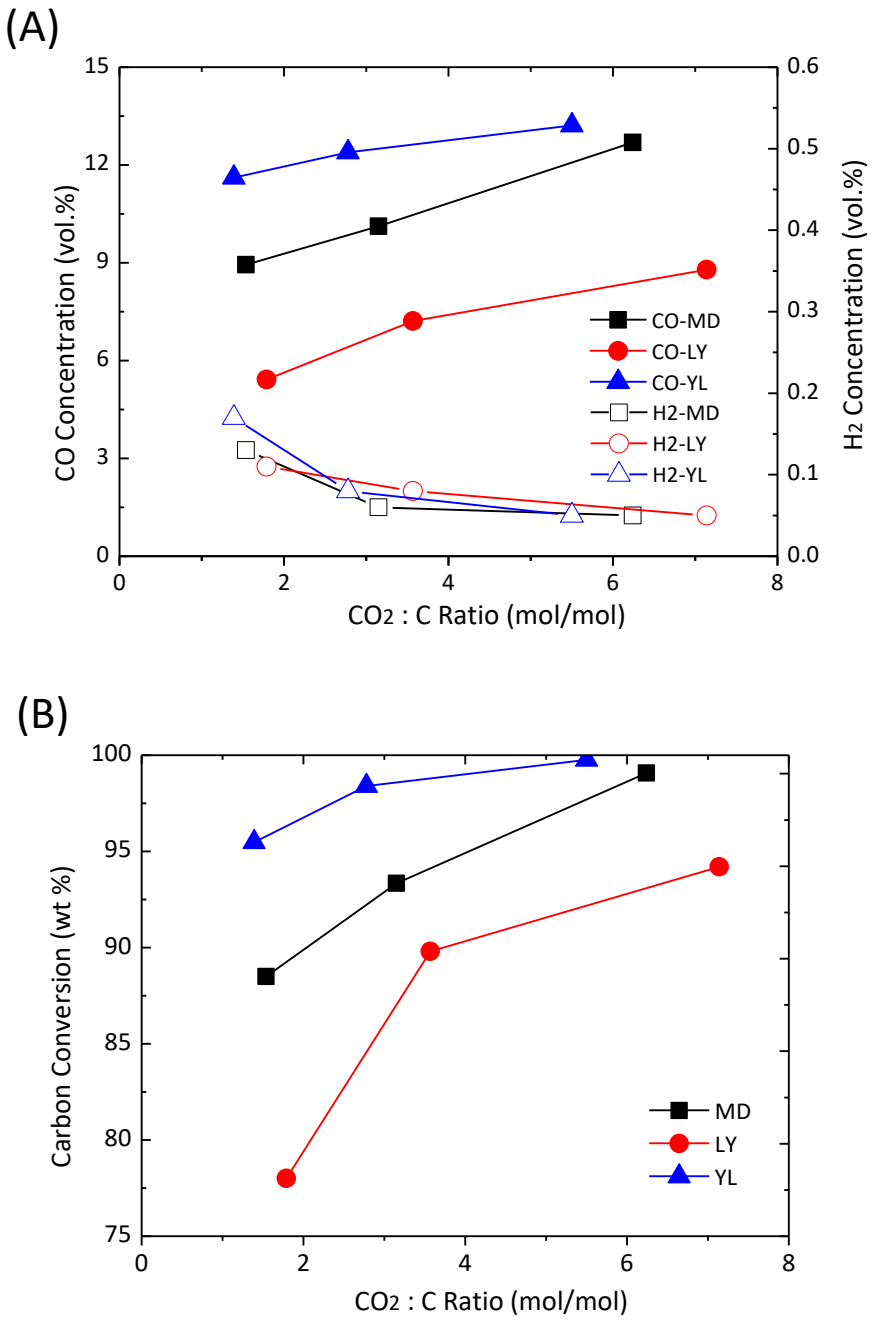

Figure 3: Effect of CO_2/C ratio on gasification behaviour of MD, LY, and YL char at 1200 °C: (A) syngas composition (B) solid-phase carbon conversion.

3.2 Direct coal gasification

This section presents the effect of temperature (1200-1400 °C) and input CO_2 concentration (10%-40%CO_2) on gas quality and carbon conversion by direct gasification of Victorian brown coals. The coal samples were fed directly to the reactor at a feeding rate of 1 ± 0.3 g/min. The carbon balance was carried out for each experiment to calculate carbon conversion by both the solid-phase and gas-

phase method; the C-conversion generally ranged around 91-95%. Gas composition of each experiment varied by 3%, and solid-phase and gas-phase carbon conversion varied by 2.2-7.6%.

3.2.1 Effect of temperature

Direct coal gasification of MD, LY, and YL coal was conducted at 1200 °C and 1400 °C by directly using oven-dried coal having a sieved particle size (90-106 µm) under 20% CO_2 in N_2. The effect of temperature on coal gasification is shown in Figure 4. As expected, the CO concentration and carbon conversion increased steadily for the three Victorian brown coals with temperature. It was found that CO concentration slightly increased from 9.36-10.25% (1200 °C) to 9.61-12.64% (1400 °C), and carbon conversion steadily increased from ~91% (1200 °C) to 100% (1400 °C). This is because that both coal pyrolysis and char gasification are thermodynamically favoured at the elevated temperatures. It was found that YL coal reached nearly 100% carbon conversion at 1200 °C, but MD and LY coal required a higher temperature of 1400°C for complete carbon conversion. This indicates the YL coal has the highest reactivity during both coal pyrolysis and char gasification among three coals. Incidentally, YL coal contains high-level Fe-based minerals (51.59%) which are known to significantly improve the gasification reactivity. Not unexpectedly, high temperature has a positive effect on direct gasification of Victorian brown coal resulting in higher CO gas concentration and carbon conversion. A comparison of the effect of temperature on gas composition and carbon conversion between direct and two-step gasification is presented in section 3.3.

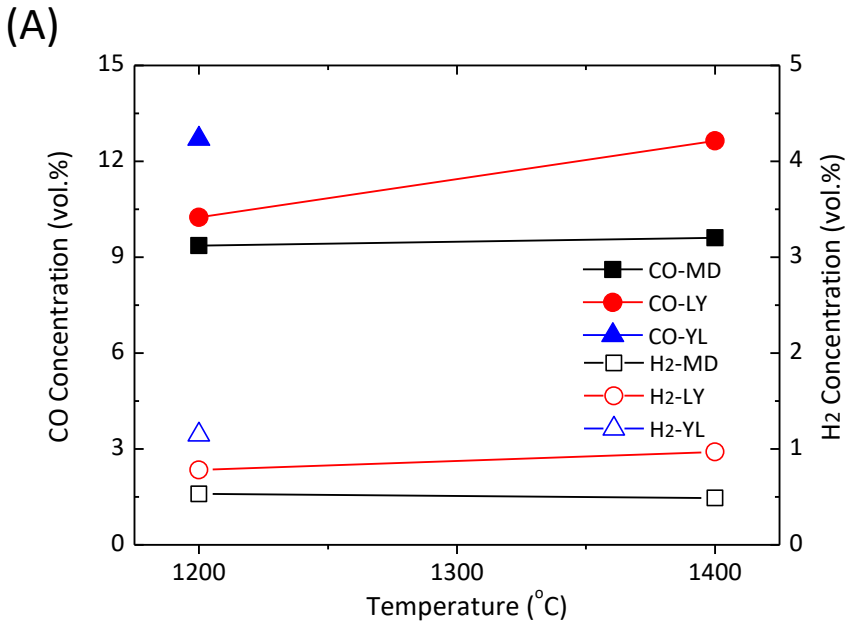

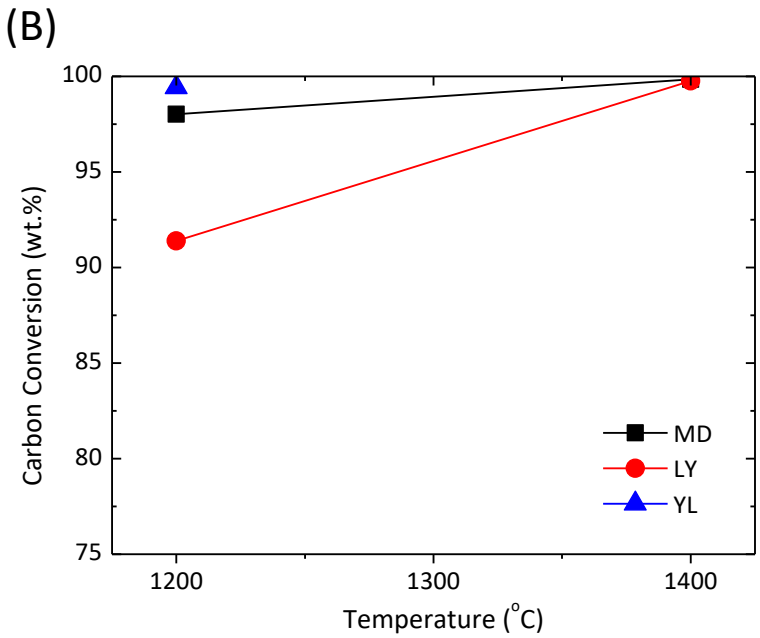

Figure 4: Effect of temperature on gasification behaviour of MD, LY, and YL coal at 20 vol.% CO_2: (A) syngas composition, (B) solid-phase carbon conversion.

3.2.2 Effect of input CO_2 concentration

To investigate the influence of input CO_2, the coal samples were gasified at 1200 °C under a range of input CO_2 concentrations (10-40 vol.%) at a total feed gas flowrate of 16 L/min. The different carbon content in each coal results in the different ratio of feed CO_2 and feed carbon (CO_2/C ratio), although using the same input CO_2 concentration. Figure 5 shows the effect of CO_2/C ratio on coal gasification behaviour at 1200 °C. As seen, the same upward trend in CO gas concentration and carbon conversion was found for all Victorian brown coals, with an increasing CO_2/C ratio. More specifically, CO gas concentration increased from 7.5-12% (1.1-1.2 CO_2/C ratio) to 10.3-12.6% (5.1-6.7 CO_2/C ratio). In addition, the carbon conversion increased from 85-99% (1.1-1.2 CO_2/C ratio) to 95-100% (5.1-6.7 CO_2/C ratio).This is because the increased input CO_2 can accelerate char gasification in the direct coal gasification process. However, it was found that at 1200°C, YL coal obtained nearly 100% carbon conversion at 1.1 CO_2/C ratios, and MD and LY coal required 6.7 and > 6.7 CO_2/C ratios, respectively, to reach such high carbon conversion. This different requirement of CO_2/C ratio determined by the reactivity consequence of Victorian brown coal chars in CO_2: YL> MD> LY. The results show that increased input CO_2 improves CO concentration and carbon conversion of Victorian brown coals because higher input CO_2 increases char gasification reactivity. A comparison of the effect of input CO_2 on carbon conversion between direct and two-step gasification is presented in section 3.3.

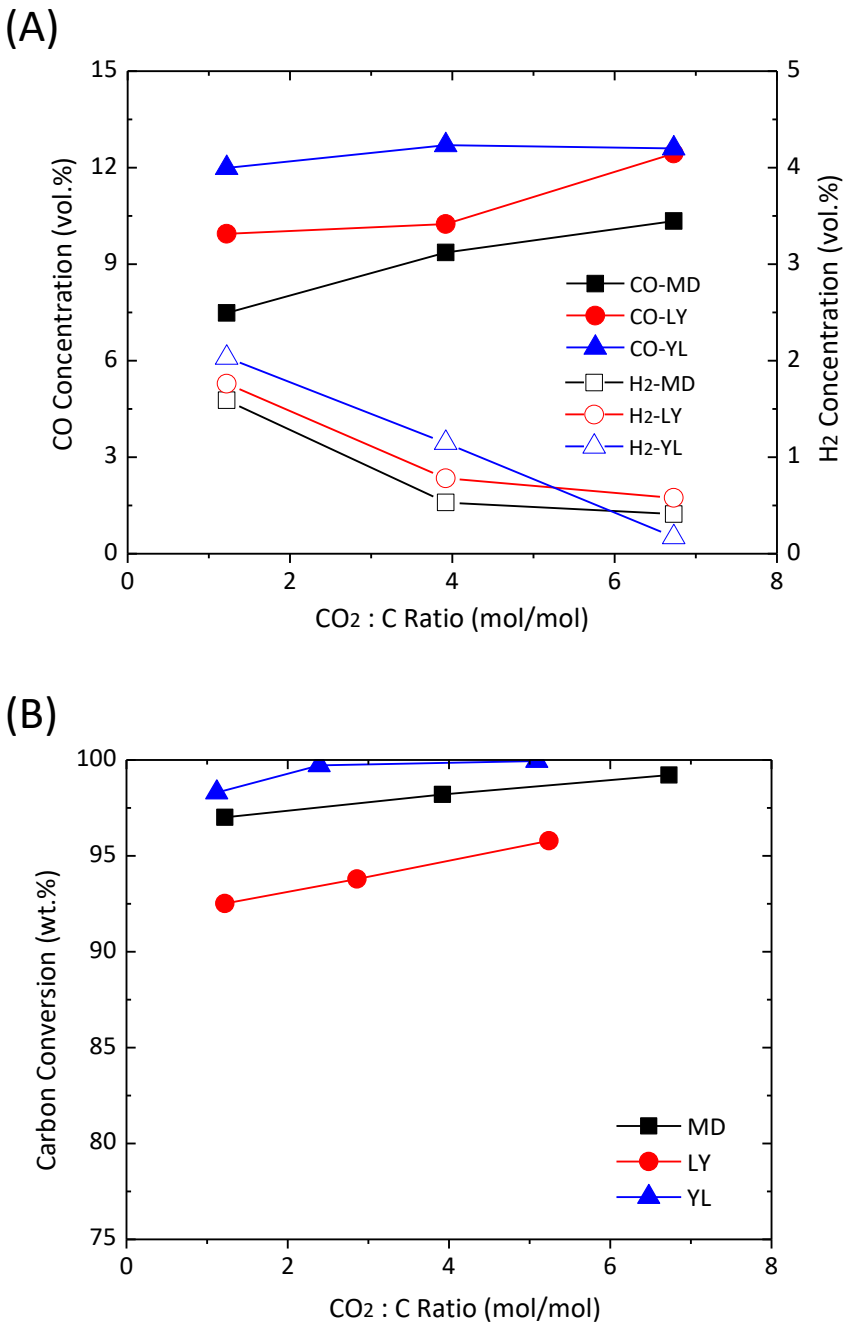

Figure 5: Effect of CO_2/C ratio on gasification behaviour of MD, LY, and YL coal at 1200 °C: (A) syngas composition (B) solid-phase carbon conversion.

3.3 Comparison of direct and two-step coal gasification

3.3.1 Gas composition

As discussed in section 3.1 and 3.2, at a high temperature above 1200°C, the gas products of direct coal gasification is CO and H_2. The gas products of two-step gasification are derived from coal pyrolysis (H_2, CO, and very little CH_4) and char gasification (CO and H_2). Hence, the gas

composition (N_X) of direct and two-step gasification above 1200 °C was calculated by the following equation:

Direct gasification: $N_X(\%) = \frac{V_X}{V_{CO}+V_{H2}} \times 100$ (E 6)

Two-step gasification: $N_X(\%) = \frac{V_X}{V_{CO,S1}.+V_{H2,S1}+V_{CH4,S1}+V_{CO,S2}.+V_{H2,S2}} \times 100$ (E 7)

Where Vx is the gas yield of the gas species of X in L/ g coal, V_{CO} and V_{H2} is the gas yield of CO and H_2 in L/ g coal; $V_{CO,S1}$, $V_{H2,S1}$, and $V_{CH4,S1}$ are the gas yield of CO, H_2, and CH_4 during coal pyrolysis in L/ g coal, $V_{CO,S2}$ and $V_{H2,S2}$ the gas yield of CO and H_2 during char gasification in L/ g coal. The gas composition and total gas yield of direct and two-step gasification is shown in Table 3.

As seen, the gas composition of MD, LY, and YL coal during two-step gasification is consists of 73.1-78.8% CO and 21.2-26.8% H_2 at 1200-1400°C. Of these, coal pyrolysis contributed to almost all H_2 and 22.4-30.5% CO, and char gasification contributed to 69.5-77.6% CO. By comparison between direct and two-step gasification, it is found that the decreased H_2 yield during direct gasification almost equalled the increased CO yield. The results indicated that during direct gasification, the reverse water-gas shift (R5) occurred at 1200-1400 °C which converted H_2 from pyrolysis to CO. Moreover, little or no CH_4 was observed during entrained flow pyrolysis and gasification at above 1200 °C. It is very likely that dry methane reforming (R4) happened in which CH_4 reacted with CO_2 from pyrolysis or environment to generate more CO and H_2, considering the low moisture content of feed coal and char ((< 1%). Therefore, during direct gasification, the CO of three coals was generated from coal pyrolysis (18.8-24.2%), Boudouard reaction (55.1-66.5%), and the reverse water-gas shift reaction (13.1-19.3%). The total gas yield of direct and two-step gasification is similar within 8% and gradually increased with temperature because of increased carbon conversion.

Table 3: Gas composition and total gas yield of direct and two-step gasification at 20% CO_2

Fuel	Temperature (°C)	Direct gasification			Two-step gasification				
					Coal pyrolysis		Char gasification		Total gas yield (L/g coal)
		H_2 (%)	CO (%)	Total gas yield (L/g coal)	H_2 (%)	CO (%)	H_2 (%)	CO (%)	
MD	1200	4.98	95.02	1.63	24.36	22.99	0.32	52.31	1.76
	1400	4.98	95.02	1.67	23.89	21.80	0.35	53.97	1.77
LY	1200	6.99	93.01	1.86	25.72	17.46	0.60	56.24	1.78
	1400	7.34	92.66	2.18	26.56	18.18	0.31	54.95	2.03
YL	1200	8.10	91.90	2.10	20.79	17.67	0.40	61.12	2.15

The equilibrium calculation for gas composition and total gas yield was performed by Factsage 6.4. In the calculations, all reactants including coal (C, H, N, and S content of coal) and reactant gas (20% CO_2 in N_2) were input and calculated under the same experimental condition (1 atm and various temperatures of 1200-1400 °C).The predicted results is shown in Table 4. It was found that the gas composition of direct gasification is much closer to the predicted equilibrium gas composition than that of two-step gasification. However, the experimental gas yield of direct and two-step gasification was both below the predicted gas yield.

Table 4: The predicted gas composition and total gas yield by equilibrium calculations

Fuel	Temperature (°C)	Equilibrium		
		H_2	CO	Total gas yield (L/g coal)
MD	1200	6.67%	93.36%	2.39
	1400	5.63%	94.37%	2.42
LY	1200	6.97%	93.03%	2.75
	1400	5.89%	94.11%	2.76
YL	1200	7.44%	92.56%	2.90

3.3.2 Carbon conversion

Figure 6 shows the comparison of two-step and direct coal gasification in overall carbon conversion for MD, LY, and YL coal. As seen in Figure (A), (B) and (C), for three Victorian brown coals, the overall carbon conversions of direct and two-step coal gasification were both high as 91.4-99.4% at 1200 °C and almost 100% at 1400 °C. Their differences decreased as the temperature was increased from 1200°C (0.1-2.8%) to 1400°C (0.2-0.5 %). The results indicate that at a high temperature above 1200 °C, a high overall carbon conversion (>91%) is obtained for both direct and two-step gasification of Victorian brown coals, and their differences become smaller with increasing temperature. It is clear from two-step gasification that pyrolysis contributed ~65% carbon conversion and char gasification only contributed ~35% carbon conversion at 1000-1400 °C

Regarding the effect of input CO_2, the results of Figure (D), (E) and (F) indicated that direct and two-step coal gasification achieved similar carbon conversion regardless of the input CO_2. When the value of CO_2/C ratio increased from 1.1-1.8 (10 vol.% CO_2) to 5.1-7.1 (40 vol.% CO_2), their differences in overall carbon conversion decreased from 3.6% to 0.4% for MD coal, decreased from

2.3% to 1.9% for LY coal, decreased from 3.6% to 0.4% for YL coal. It was also found that YL coal reached nearly 100% carbon conversion at a CO_2/C ratio of 1.1-1.4 (10% CO_2), but MD and LY coal required a higher CO_2/C ratio of more than 5.2-7.1 (40% CO_2) for complete carbon conversion. This is due to the fact that YL coal/char has higher reactivity than the other two coals, presumably due to the high Fe concentration.

Overall, the gasification process, direct and two-step gasification, had little effect on the overall carbon conversion but had a significant effect on the gas composition of the product gases. Compared to two-step gasification, direct gasification generated little H_2 and more CO in the product gases. Moreover, the decreased H2 yield almost equalled the increased CO yield. It was very likely that the reverse water-gas shift reaction occurred during direct gasification in which CO_2 reacts with H_2 from coal pyrolysis to form CO. The dry methane reforming was also very likely to occur during pyrolysis and CO_2 gasification, considering the very little amount of CH_4 formed and the low moisture of feed coal (< 1%).

Both direct and two-step gasification achieved similar high carbon conversion (~ 98%) for Victorian brown coals at 1200 °C. However, two-step gasification obtained a better H2 /CO ratio (around 1:3) in the product gases than direct gasification, so it was more suitable for downstream synthesis of some chemicals. It is clear that 1200 °C temperature is sufficient to achieve high carbon conversion for the brown coals tested in this study for gasification using CO_2 up to 40% concentration.

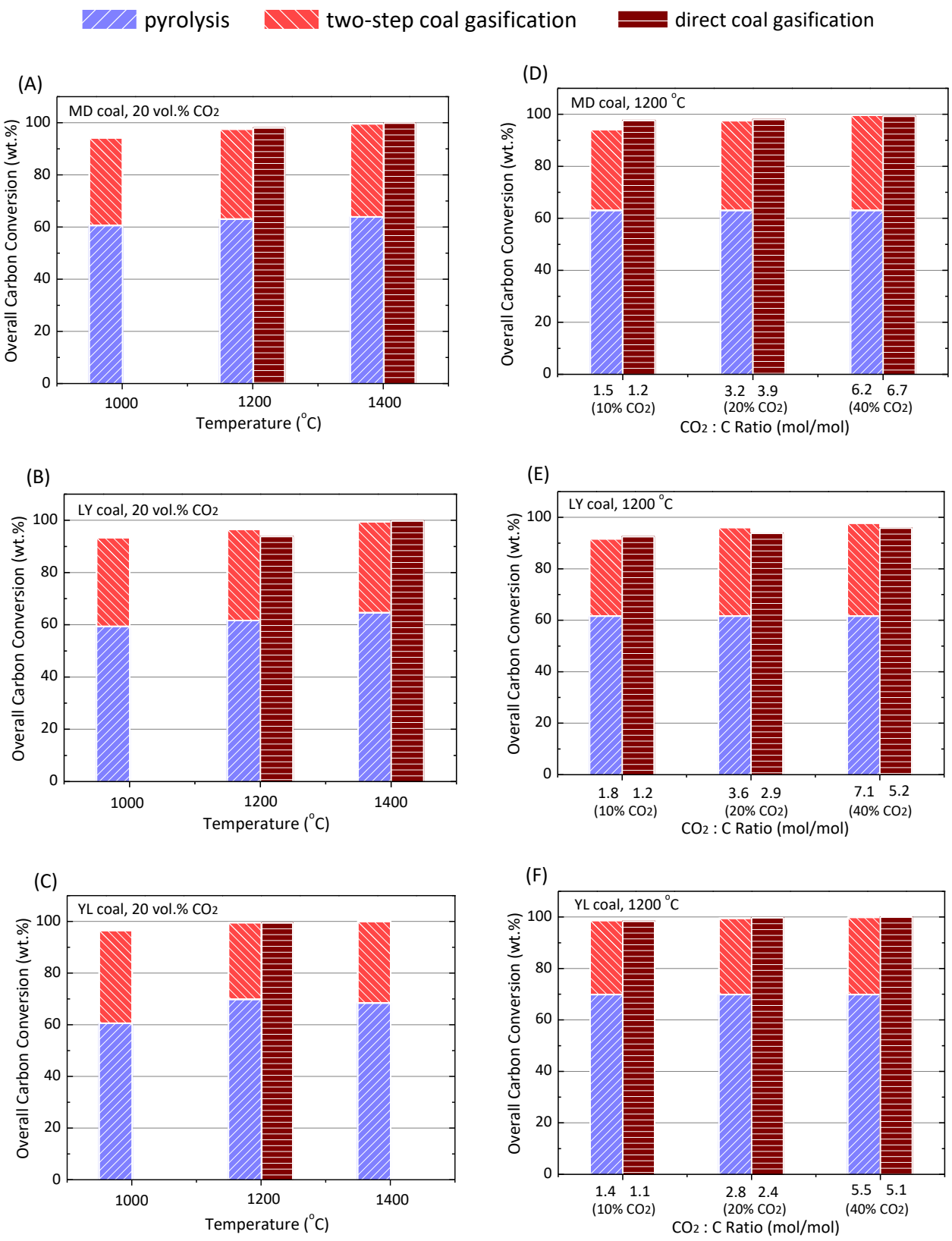

Figure 6: Comparison of direct and two-step coal gasification for MD, LY, and YL coal in overall carbon conversion on solid basis: (1) effect of temperature on overall carbon conversion of MD coal (A), LY coal (B), and YL coal (C); (2) effect of CO_2/C ratio on overall carbon conversion of MD coal (D), LY coal (E), and YL coal (F) at 10%, 20% and 40% CO_2 in the feed gas.

3.4 NH_3, HCN, and H_2S release during gasification

N and S are the major pollutant-forming elements in coals. NH_3 and HCN are known to be the main N-containing gaseous products from heteroaromatic ring systems which have been reported to be the main source of coal-N for Victorian brown coals [20]. H_2S is a principal S-containing gasification product from coal gasification [23]. Therefore, to assess the extent of the emission of the NH_3, HCN, and H_2S from MD, LY, and YL coal during gasification was measured by Dräger tubes under the two different gasification processes, over a range of temperature (1000-1400°C) and CO_2 concentration (10-40 vol%).

3.4.1 Effect of temperature

The influence of the temperature on the H_2S emission of three Victorian brown coals at 20%CO_2 in N_2 is shown in Figure 7 (A), (B) and (C). As is evident, for two-step coal gasification, the H_2S emission from coal pyrolysis comprised the majority of the total gas concentration, and by contrast, only a small concentration (less than 10.31%) are from char gasification. This indicates that the H_2S emission during two-step coal gasification is determined by coal pyrolysis. In the coal pyrolysis, the measurements of MD coal at 1000 °C and 1200 °C is limited by the maximum measurement range of the Dräger tube-200 ppmv. However, the H_2S emission of LY and YL coal slightly increased with temperature increasing from 1000 °C (116 and 11 ppmv, respectively) to 1200 °C (145 and 21 ppmv, respectively).

Sulfur in the Victorian brown coal is nearly 70% organic sulphur, and it exists as thermally unstable organic sulphur (such as aliphatic structures and small S-containing heteroaromatic ring systems), and thermally stable organic sulphur (such as thiophenes) [23]. As LY coal for example, it consists of around 50% unstable sulphur and 50% stable sulphur [24]. Thermally unstable sulphur is completely released at low temperatures around 600 °C. However, the thermally stable sulphur is not released until 1000 °C. Therefore, this increase of H_2S emission is due to the increased decomposition of thermally stable sulphur which is released at a higher temperature [23]. However, when the temperature was increased from 1200 °C to 1400 °C, the H_2S emission from different coals showed a different trend. The H_2S emission of YL coal steadily increased by 18 ppmv because of the increased decomposition of thermally stable sulphur. In contrast, the H_2S emission of MD and LY coal decreased to 180 and 64 ppmv, respectively. This is attributed to the gas phase reaction between produced H_2S and CO_2 from pyrolysis (R6) [15, 25].

$$H_2S_{(g)} + CO_{2_{(g)}} \leftrightarrow COS_{(g)} + H_2O_{(g)} \quad \text{(R 6)}$$

Compared to two-step gasification, direct coal gasification showed lower H_2S concentration in the gas phase. This is because more gas-phase reactions get involved especially for reaction 8 which decrease the H_2S gas concentration by reacting with the CO_2 from pyrolysis and input. Comparing the three Victorian brown coals, it is found that the sequence of H_2S emission is MD > LY > YL. This corresponds to sulphur content in their coals because H_2S is derived from the sulphur in coal.

The influence of temperature on HCN emission at 20% CO_2 in N_2 is shown in Figure 7 (D), (E) and (F). As seen, like the H_2S emission, HCN is mostly released from coal pyrolysis during two-step coal gasification. It is found that during the coal pyrolysis, the measurements of MD coal (1000-1400 °C), LY coal (1200-1400 °C), and YL coal (1200-1400 °C) are limited to the maximum measurement range of the Dräger tube - 50 ppmv. However, it is clear that HCN emission of LY and YL coal from coal pyrolysis increased significantly, by at least 17.5 and 15.5 ppmv respectively, when temperature increased to 1200 °C. This increase can be attributed to the increased thermal decomposition of N-heterocyclic rings in coal and increased thermal cracking of tar-N and char-N at high temperature [26]. During char gasification, the HCN emission steadily increased with increasing temperature because of the positive effect of temperature on the decomposition of heteroaromatic ring systems of char-N. However, the HCN concentration from char gasification was comparably smaller than that in pyrolysis. Overall, the HCN emission during the two-step gasification increased with temperature.

In contrast, HCN concentration decreased by 11.5-53 ppmv at 1200 °C during direct coal gasification. Moreover, the HCN emission of MD and LY coal significantly decreased to near-zero with temperature increasing to 1400 °C. There are two reasons for this. Firstly, it is the inhibition of CO_2 on the formation of HCN where CO_2 from pyrolysis and atmosphere consumes the H-radicals on the surface of the nascent char and inhibits the formation of the HCN [27]. More importantly, this can be attributed to increased gas-phase reactions as the oxidation of HCN with O-radicals and OH-radials from coal pyrolysis at a higher temperature. For the three Victorian brown coals, it is found that the sequence of HCN emission during direct coal gasification is MD > LY > YL.

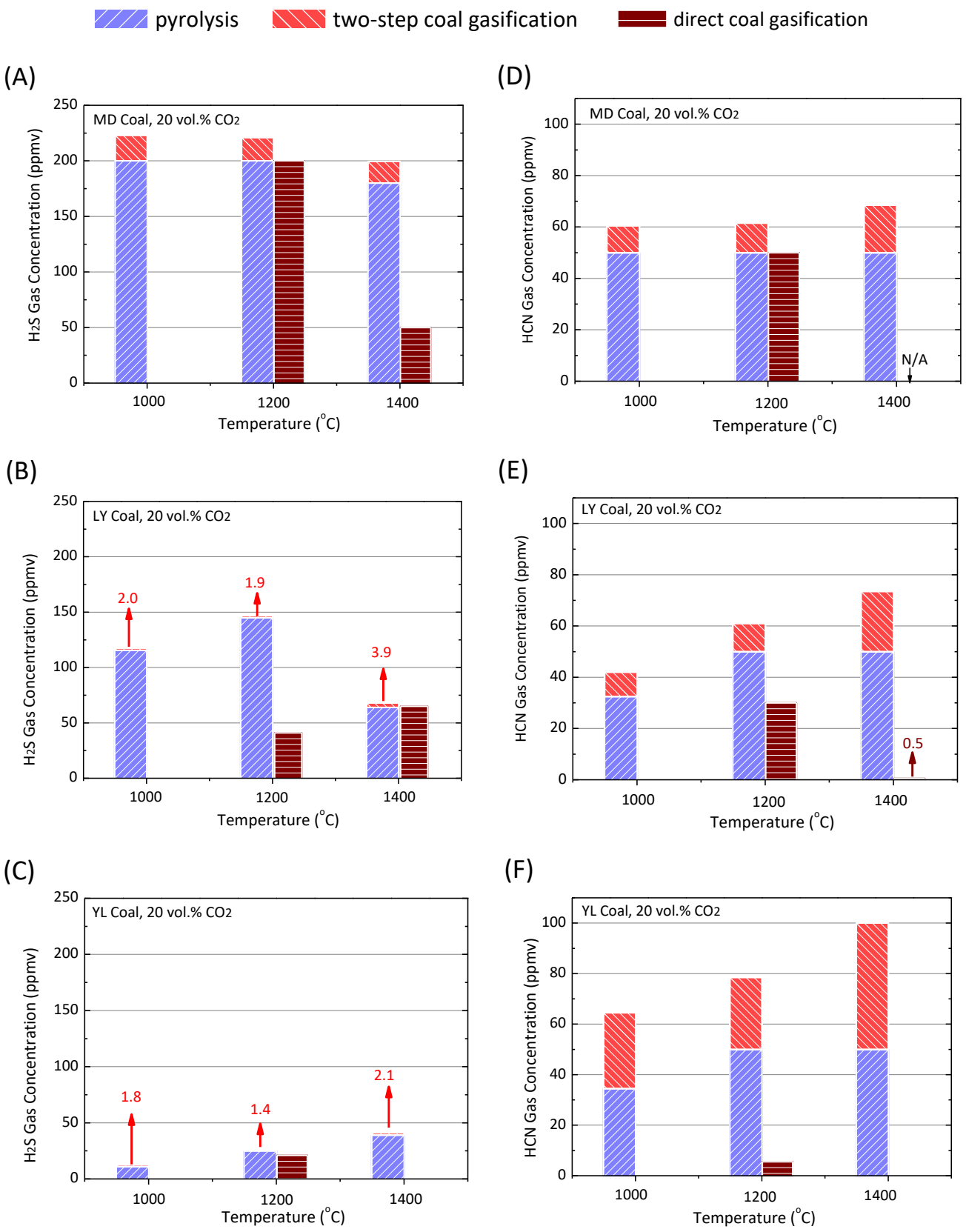

Figure 7: The influence of temperature on the gas concentration of the H_2S and HCN during direct and two-step coal gasification of MD, LY, and YL coal under 20 vol.% CO_2: (1) effect of temperature on the H_2S emission of MD coal (A), LY coal (B), and YL coal (C); (2) effect of temperature on HCN emission of MD coal (D), LY coal (E), and YL coal (F)

3.4.2 Effect of input CO_2

The influence of input CO_2 on H_2S emission for three Victorian brown coals at 1200 °C are shown in Figure 8 (A), (B) and (C). As seen, for two-step coal gasification, the input CO_2 has a significant effect on H_2S emission during char gasification. For three Victorian brown coals, they have a similar trend of H_2S emission. The H_2S emission decreased steadily when the input CO_2 concentration increased from 10% to 40%. This reduction is due to increased input CO_2 promoting the gas-phase reaction between H_2S and CO_2 (R6).

Like two-step coal gasification, the H_2S emission during direct coal gasification also decreased with the increase of CO_2 concentration, although the measurement of MD coal is limited by the maximum measurement range of the Dräger tube-200 ppmv. This reduction confirmed, to some extent, that increasing CO_2 concentration can shift the H_2S-COS equilibrium of R6 to the products side. Overall, it can be concluded that higher CO_2 concentration inhibits H_2S emission during entrained flow gasification.

Figure 8 (D), (E) and (F) show the influence of input CO_2 concentration on HCN emission from three Victorian brown coals at 1200 °C. As seen, for two-step coal gasification, the CO_2 has a significant effect on HCN emission during char gasification. The HCN emission decreased steadily for all three Victorian brown coals when input CO_2 concentration increased. This decrease confirmed that presence of high CO_2 concentration inhibits the emission of HCN (R7) [28].

Similarly, a significant drop of HCN emission was found for MD and YL coal during direct coal gasification with the increase of the CO_2 concentration, due to the inhibition by CO_2. Interestingly, for LY coal, the HCN concentration remained steady at 29-30 ppmv. The result shows the CO_2 concentration does not significantly affect HCN emission of LY coal during direct coal gasification. Compared with the two-step gasification, HCN concentration decreased by more than 30.5 ppmv during the direct coal gasification.

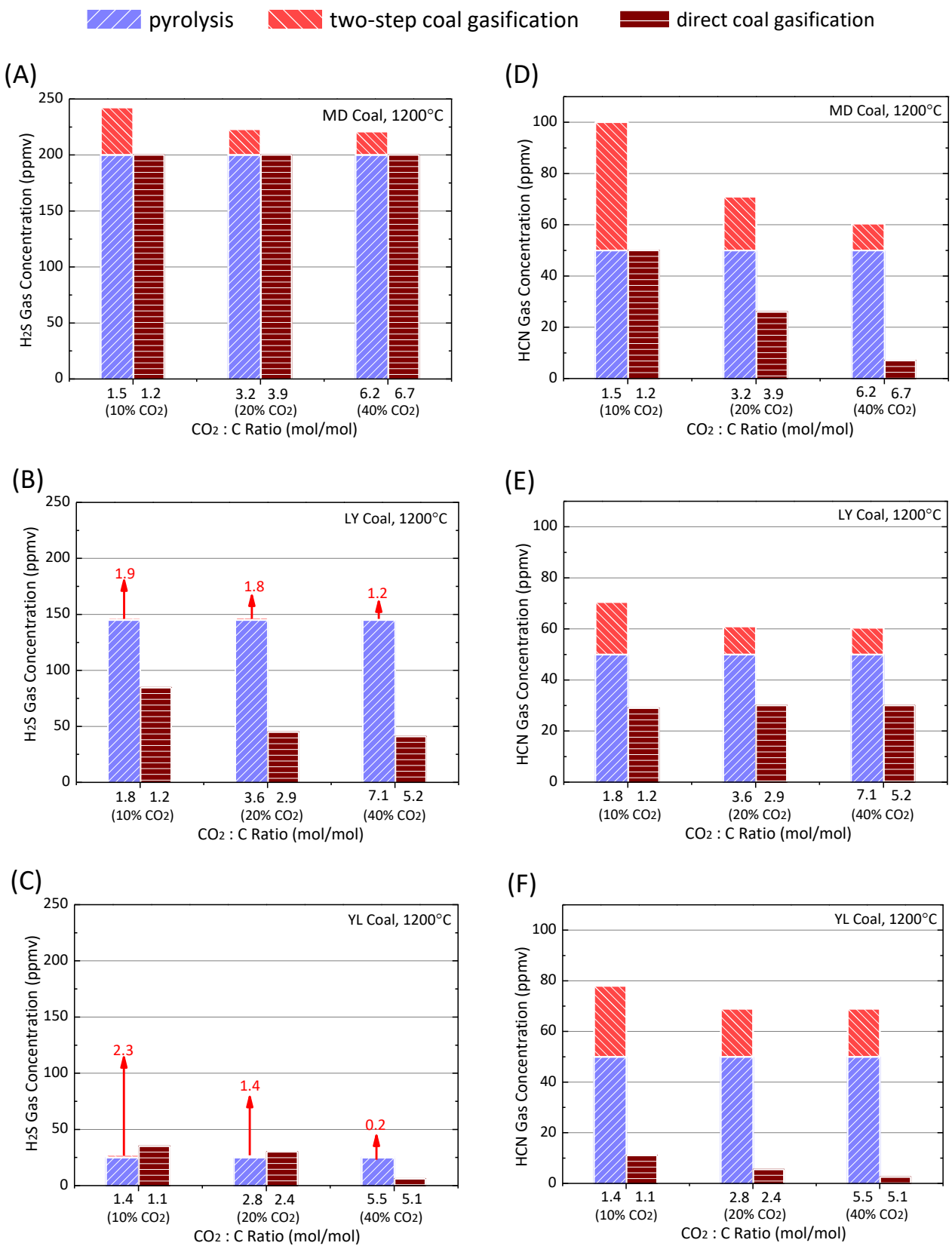

Figure 8: The influence of input CO_2 on the gas concentration of the H_2S and HCN during direct and two-step coal gasification of MD, LY, and YL coal at 1200°C: (1) effect of input CO_2 concentration on H_2S emission of MD coal (A), LY coal (B), and YL coal (C); (2) effect of input CO_2 concentration on HCN emission of MD coal (D), LY coal (E), and YL coal (F)

However, no NH_3 was detected during coal pyrolysis and gasification experiments. There are two reasons for this result. Firstly, the majority of NH_3 in the coal gasification is usually from amine functional groups in the coal [29, 30]. However, the amine functional groups are very low in the Victorian brown coals [31], and their char-N are typically heteroaromatic which leads to the formation of HCN, not NH_3 [17]. In addition, the absence of NH_3 can arise from the secondary gas-phase reactions between NH_3 and CO_2 from coal pyrolysis or gas inlet (R7)-(R9) [30] are following:

$$2NH_3 + CO_2 \leftrightarrow NH_2COONH_4 \quad \text{(R 7)}$$

$$2NH_3 + CO_2 + H_2O \leftrightarrow (NH_4)_2CO_3 \quad \text{(R 8)}$$

$$NH_3 + CO_2 + H_2O \leftrightarrow NH_4HCO_3 \quad \text{(R 9)}$$

The above reactions (R7)-(R9) can occur slowly at room temperature and atmospheric pressure but favoured at the high temperature. Therefore, entrained flow pyrolysis and gasification at a high temperature above 1000°C can increase the extent of the secondary gas-phase reactions between NH_3 and CO_2, resulting in lower NH_3.

The total concentration of gaseous polluting species in the syngas is generally required to be ppbv range for power or chemical products [6]. Given the high level of pollutants in the fuel gas identified from these experiments, it will be necessary to remove HCN, and H_2S from syngas of Victorian brown coals by installing gas cleaning system following gasification.

3.5 Evolution of particle physical characteristics during gasification

As is well known, the gasification process is divided into coal pyrolysis and char gasification. To understand the evolution of particle physical characteristics during CO_2 gasification, the raw coals, chars and gasified chars from two-step coal gasification were examined for particle size distribution and morphology. The MD, LY, and YL coal were sieved with a particle size between 90 and 106 µm. Their chars from coal pyrolysed at 1000°C, 1200°C, and 1400°C were examined to investigate the effect of temperature on particle physical characteristics during coal pyrolysis. The above chars were gasified at the corresponding pyrolysis temperatures using 20% CO_2 in N_2 to investigate the influence of temperature on particle size distribution and morphology change during char gasification. For the effect of input CO_2 during char gasification, the chars generated at 1200°C were gasified at the same temperature using 10% CO_2, 20% CO_2, and 40% CO_2.

3.5.1 Evolution of particle physical characteristics during coal pyrolysis

According to results from the Mastersizer, the volume mean diameter (D_{50}) of MD, LY, and YL chars generated at 1000-1400 °C was in the range of 91-105 µm which is almost the same as the coal particle size (90-106 µm). The results indicate that the pyrolysis temperature had no significant effect on particle size distribution of MD, LY, and YL char and particle size did not significantly change after coal pyrolysis. The particle size of the char depends primarily on particle swelling, particle agglomeration, and particle fragmentation. Particle swelling during devolatilization is a result of fluidity and volatile yield [32] and contributes to the increase in particle size. Particle agglomeration results from the melting mineral constituents, which also account for the increase in particle size. Conversely, particle fragmentation is due to the inter-particle collision or the reactor wall, resulting in the reduction of char particles.

From the SEM images of MD, LY, and YL chars, it was found that the size of char particles was similar and the average particle size was ~95 µm. There was also no significant particle swelling, fragmentation and agglomeration observed in the chars. At 1400 °C, inorganic constituents were found to be migrated on the surface of porous chars,as shown in Figure 9. The SEM results demonstrate that particle size did not significantly change after coal pyrolysis, possibly due to no particle swelling, fragmentation, and agglomeration occurring during pyrolysis.

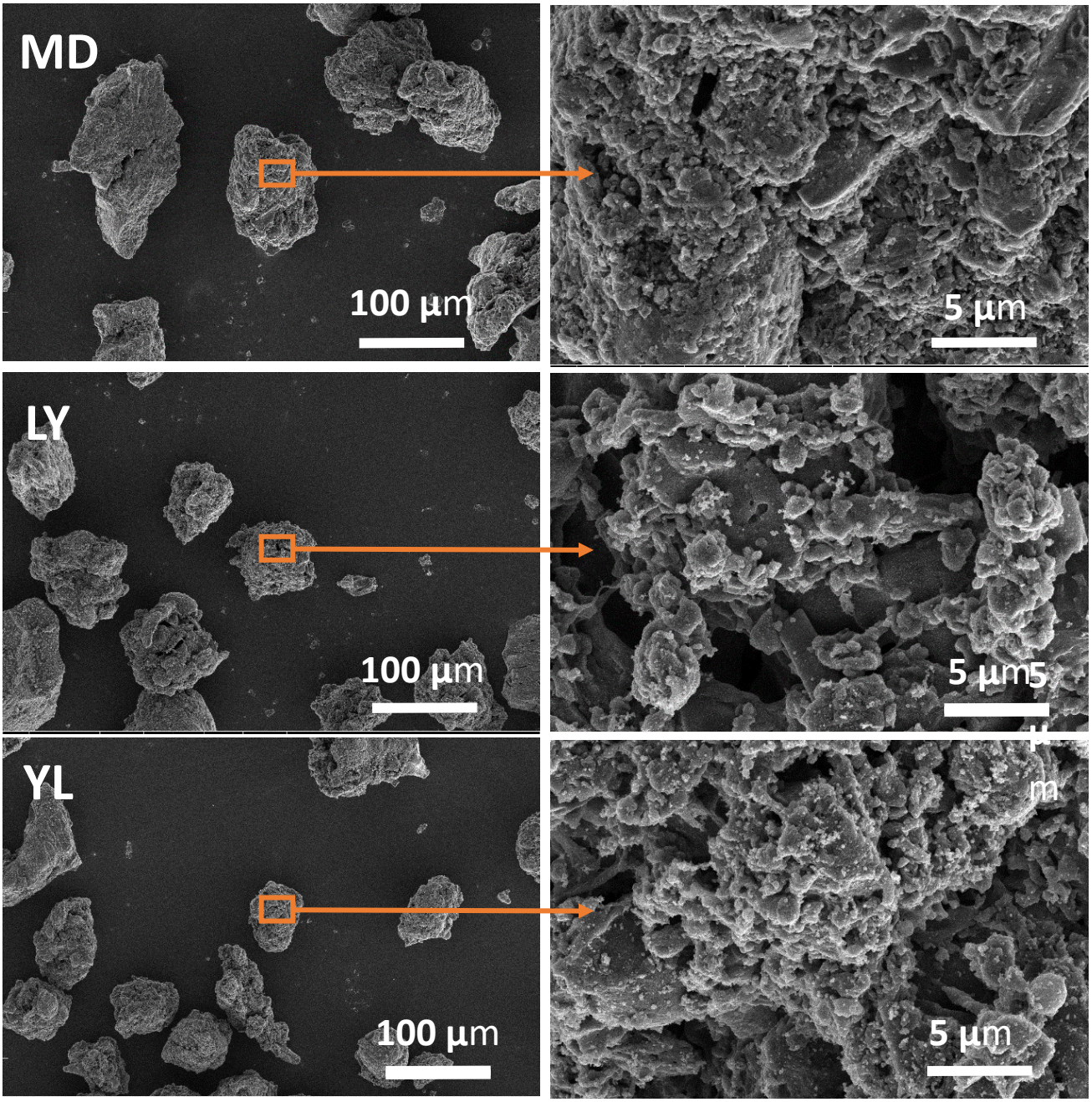

Figure 9: SEM images of MD, LY and YL char at 1400 °C

3.5.2 Evolution of particle physical characteristics during char gasification

During char gasification, the temperature shows a significant effect on particle size distribution. As seen in Figure 10, the D_{50} of MD and YL char decreased significantly by 39%, with the temperature increasing to 1400 °C. In theory, the char, both inside and outside, reacts with the gas. With the progress of the reaction, the particle becomes smaller in size and form the fine ash particle at the end. Therefore, the char particle size decreases because carbon conversion increases with the increasing

temperature. At 1400°C and 20% CO_2, the SEM images of MD and YL gasified chars in Figure 11 show that average particle size dramatically decreased to ~50 µm and the majority of particles were small ash particles (< 10 µm), a result of high carbon conversion. The agglomerations between ash and ash, ash and gasified char were observed from the SEM images as well, which accounts for the increase in the particle size.

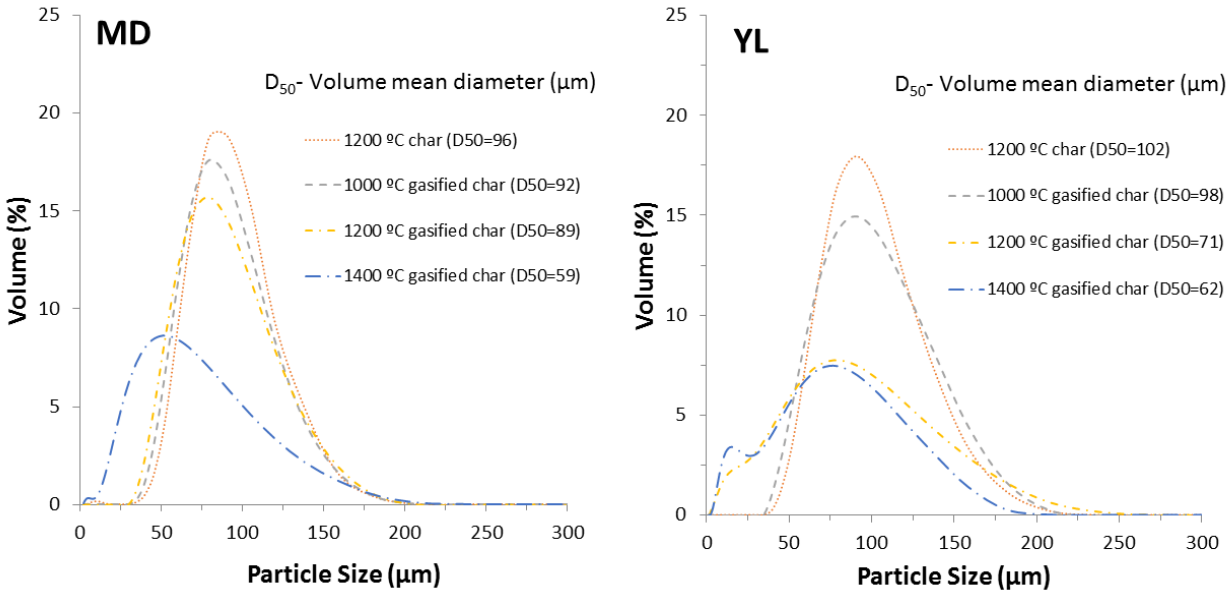

Figure 10: Effect of temperature on particle size distribution of MD and YL char at 20%CO_2 in the char gasification. In the figure, the D_{50} (volume mean diameter) was presented for chars prepared at 1200 °C, and gasified chars at 1000°C, 1200°C, and 1400°C (using char produced at the same temperature).

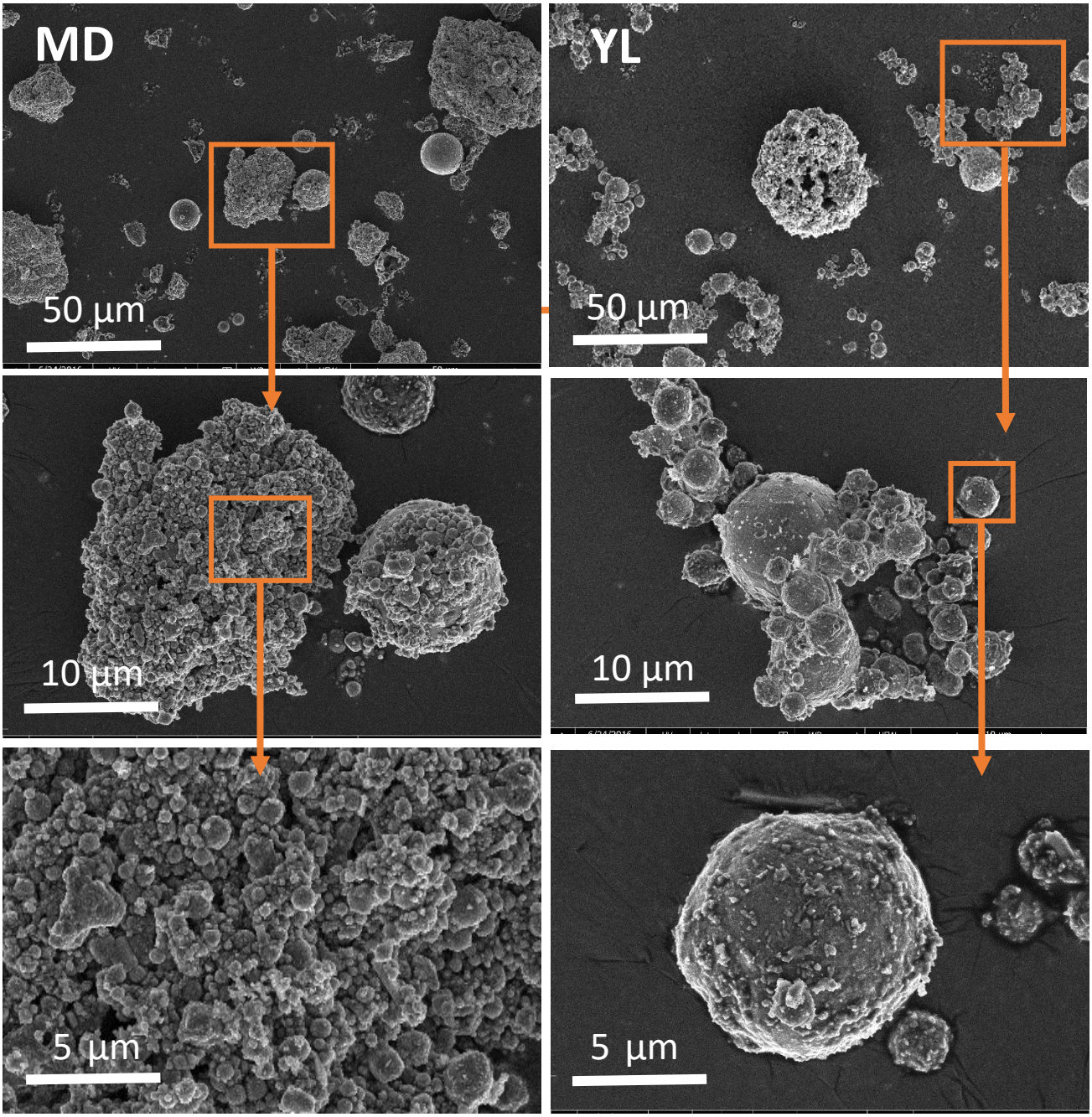

Figure 11: SEM images of MD and YL gasified chars at 1400 °C and 20%CO_2.

Figure 12 presents the influence of CO_2 concentration on particle size distribution of MD and YL gasified chars at 1200 °C during char gasification. As seen, with the increasing CO_2 concentration to 40% CO_2, Volume mean diameters (D_{50}) of MD and YL chars decreased steadily by 30.2% and 64.7%, respectively. This decrease is attributed to the positive effect of increased CO_2 concentration on carbon conversion. More carbons are converted, smaller particle size becomes.

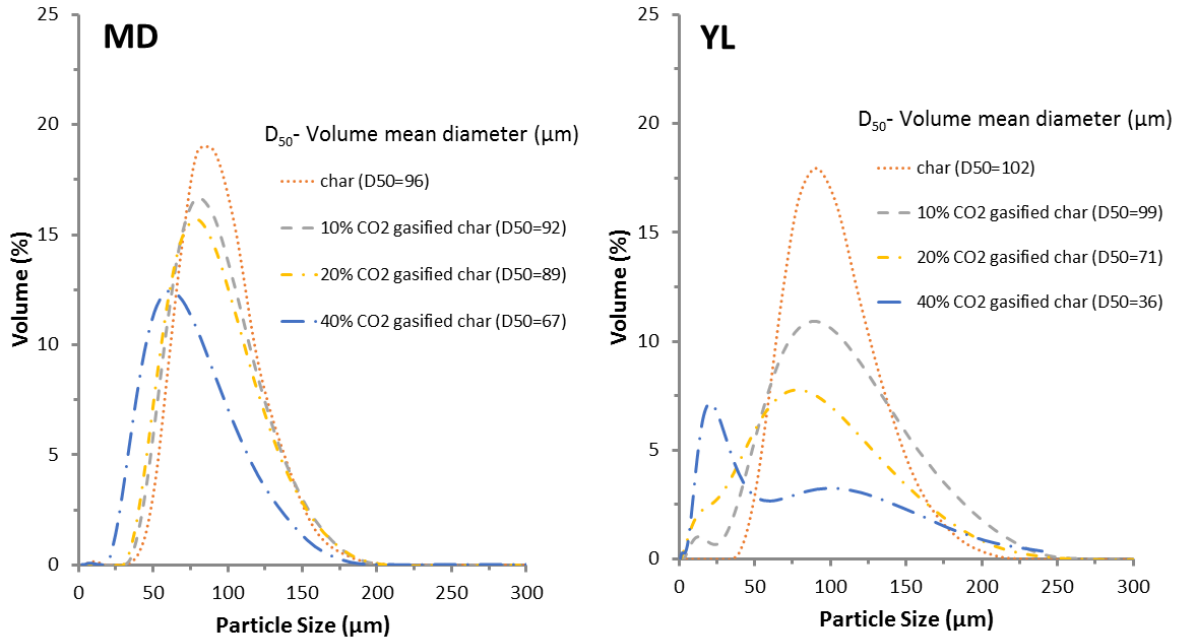

Figure 12: The influence of CO_2 concentration on particle size distribution of MD and YL char at 1200 °C during char gasification. In the figure, the D_{50} (volume mean diameter) was presented for chars prepared at 1200 °C, and gasified chars at 10% CO_2, 20% CO_2, and 40% CO_2.

Interestingly, the effect of temperature and CO_2 concentration on the particle size distribution of LY char was not significant during the char gasification, even though the carbon conversion increased sharply with temperature and CO_2 concentration. The possible reason is that most of the fine particles from char gasification escape with the exhaust gas and not efficiently collected by the main solid collector and impingers. This hypothesis is verified by the SEM images of LY gasified char where the particle size of LY gasified char remained stable after 97% char conversion at 1400 °C and 20% CO_2.

4 Conclusions

This study investigated the influence of temperature and input CO_2 on gasification behaviour and pollutant gas emission of three Victorian brown coals in a high-temperature entrained flow reactor. Two gasification processes were investigated: a) gasification of coal in a single step, b) pyrolysis of coal followed by gasification of the char in two steps. Regardless of the gasification process, high temperature and CO_2 input improved CO concentration and carbon conversion, due to the increased char gasification reactivity. Among the three Victorian brown coals, YL coal achieved the highest carbon conversion, followed by MD coal and LY coal.

The gasification process, direct and two-step gasification, had little effect on the overall carbon conversion but had a significant effect on the gas composition of the product gases. Compared to two-step gasification, direct gasification generated little H_2 and more CO in the product gases because the reverse water-gas shift reaction happened. Very little CH_4 was found during pyrolysis and gasification above 1200 °C because of the dry methane reforming, considering the low moisture of feed coal (< 1%). Both direct and two-step gasification achieved similar high carbon conversion (~ 98%) for Victorian brown coals at 1200 °C. However, two-step gasification obtained a better H_2 /CO ratio (around 1:3) in the product gases than direct gasification, so it was more suitable for downstream synthesis of some chemicals.

Regarding pollutant gas emission, the pyrolysis process is the primary source of H_2S emission as evident from the results of two-step gasification. Higher temperature increased H_2S and HCN emission because of the thermal decomposition of stable sulphur and heteroaromatic ring systems in coal. However, Higher CO_2 concentration reduced the H_2S and HCN emission due to the gas phase reaction with CO_2. Compared with two-step gasification, direct coal gasification released less H_2S and HCN. Interestingly, NH_3 was not detected during pyrolysis and the gasification experiments. Given the high-level emission of H_2S and HCN, the gas cleaning system is essential for entrained flow gasification of Victorian brown coals.

Coal gasification is divided into coal pyrolysis and char gasification. During entrained flow gasification of Victorian brown coals at 1000-1400 °C, pyrolysis played a crucial role, contributing to around 65% carbon conversion, 50-80% HCN emission and almost all H_2S emission. In contrast, char gasification resulted in around 35% carbon conversion, 20-50% HCN emission and very little H_2S emission.

Overall, entrained flow gasification achieved very high carbon conversion (~ 98%) for Victorian brown coals at 1200 °C with around 7s residence time for the particle size of 90-106 microns. No visible tar was found downstream of the entrained flow gasifier. There was also no NH_3 emission during the entrained flow gasification. However, the emission of HCN and H_2S is still high in the ppmv level. It is clear that 1200 °C temperature is sufficient to achieve high carbon conversion for the Victorian brown coals tested in this study for gasification using CO_2 up to 40% concentration.

Acknowledgements

The authors gratefully acknowledge the support from China Scholarship Council, Brown Coal Innovation Australia (BCIA), and Monash University for their financial assistance. The authors also acknowledge the Monash Centre for Electron Microscopy for using the facilities.

References

[1] Department of State Development BaI. Brown coal-Victoria, Australia: a principal brown coal province. http://www.energyandresources.vic.gov.au/earth-resources/victorias-earth-resources/coal: Department of State Development, Business and Innovation; 2014.

[2] DPI. Victoria's energy future. In: Industries DoP, editor. www.dpi.vic.gov.au/energyfuture: The State of Victoria Government; 2010.

[3] Bhattacharya S, Kabir KB, Hein K. Dimethyl ether synthesis from Victorian brown coal through gasification - Current status, and research and development needs. Progress in Energy and Combustion Science. 2013:1-29.

[4] Li S, Ji X, Zhang X, Gao L, Jin H. Coal to SNG: Technical progress, modeling and system optimization through exergy analysis. Applied Energy. 2014;136:98-109.

[5] Tanaka Y, Mesfun S, Umeki K, Toffolo A, Tamaura Y, Yoshikawa K. Thermodynamic performance of a hybrid power generation system using biomass gasification and concentrated solar thermal processes. Applied Energy. 2015;160:664-72.

[6] Koytsoumpa EI, Atsonios K, Panopoulos KD, Karellas S, Kakaras E, Karl J. Modelling and assessment of acid gas removal processes in coal-derived SNG production. Appl Therm Eng. 2015;74:128-35.

[7] Kirtania K, Tanner J, Kabir KB, Rajendran S, Bhattacharya S. In situ synchrotron IR study relating temperature and heating rate to surface functional group changes in biomass. Bioresour Technol. 2014;151:36-42.

[8] Energy USDo. Worldwide gasification plant databases. June 2016 ed. https://www.netl.doe.gov/research/coal/energy-systems/gasification/gasification-plant-databases: National Energy Technology Laboratory; 2016.

[9] Tremel A, Haselsteiner T, Kunze C, Spliethoff H. Experimental investigation of high temperature and high pressure coal gasification. Applied Energy. 2012;92:279-85.

[10] Harris DJ, Roberts DG, Henderson DG. Gasification behaviour of Australian coals at high temperature and pressure. Fuel. 2006;85:134-42.

[11] Gonzalo-Tirado C, Jiménez S, Ballester J. Gasification of a pulverized sub-bituminous coal in CO2 at atmospheric pressure in an entrained flow reactor. Combust Flame. 2012;159:385-95.

[12] Guo X, Dai Z, Gong X, Chen X, Liu H, Wang F, et al. Performance of an entrained-flow gasification technology of pulverized coal in pilot-scale plant. Fuel Process Technol. 2007;88:451-9.
[13] Bhattacharya S, Tsutsumi A. An Overview of Advanced Power generation Technologies Using Brown Coal A2 - Li, Chun-Zhu. Advances in the Science of Victorian Brown Coal. Amsterdam: Elsevier Science; 2004. p. 360-400.
[14] Zou X, Yao J, Yang X, Song W, Lin W. Catalytic Effects of Metal Chlorides on the Pyrolysis of Lignite. Energy & Fuels. 2007;21:619-24.
[15] Tanner J, Bläsing M, Müller M, Bhattacharya S. Influence of Temperature on the Release of Inorganic Species from Victorian Brown Coals and German Lignites under CO2 Gasification Conditions. Energy & Fuels. 2014;28:6289-98.
[16] Bhattacharya SP. Gasification Performance of Australian Lignites in a Pressurized Fluidized Bed Gasifier Process Development Unit Under Air and Oxygen-enriched Air Blown Conditions. Process Saf Environ Prot. 2006;84:453-60.
[17] Tanner J, Bhattacharya S, Bläsing M, Müller M. High-temperature pyrolysis and CO2 gasification of Victorian brown coal and Rhenish lignite in an entrained flow reactor. AlChE J. 2016;62:2101-11.
[18] Tanner J, Bhattacharya S, Blasing M, Muller M. High-Temperature Pyrolysis and CO2 Gasification of Victorian Brown Coal and Rhenish Lignite in an Entrained Flow Reactor. AlChE J. 2016;62:2101-11.
[19] Sripada PP, Xu T, Kibria MA, Bhattacharya S. Comparison of entrained flow gasification behaviour of Victorian brown coal and biomass. Fuel. 2017;203:942-53.
[20] Hernández JJ, Aranda-Almansa G, Bula A. Gasification of biomass wastes in an entrained flow gasifier: Effect of the particle size and the residence time. Fuel Process Technol. 2010;91:681-92.
[21] Bai H, Yeh AC. Removal of CO2 Greenhouse Gas by Ammonia Scrubbing. Industrial & Engineering Chemistry Research. 1997;36:2490-3.
[22] Bustamante F, Enick RM, Cugini AV, Killmeyer RP, Howard BH, Rothenberger KS, et al. High-temperature kinetics of the homogeneous reverse water–gas shift reaction. AlChE J. 2004;50:1028-41.
[23] Systems WtE. Syn-gas: a versatile and renewable fuel. Gasification. Waste to Energy Systems

2015.
[24] Zhiguang S, Batts BD, Smith JW. Hydrous pyrolysis reactions of sulphur in three Australian brown coals. Org Geochem. 1998;29:1469-85.
[25] Tanner J, Bläsing M, Müller M, Bhattacharya S. The temperature-dependent release of volatile inorganic species from Victorian brown coals and German lignites under CO2 and H2O gasification conditions. Fuel. 2015;158:72-80.
[26] Mota R, Krishnamoorthy G, Dada O, Benson SA. Hydrogen rich syngas production from oxy-steam gasification of a lignite coal – A design and optimization study. Appl Therm Eng. 2015;90:13-22.
[27] Giménez-López J, Millera A, Bilbao R, Alzueta MU. HCN oxidation in an O2/CO2 atmosphere: An experimental and kinetic modeling study. Combust Flame. 2010;157:267-76.

[28] BP Statistical Review of World Energy 2010. ENP Newswire2010.

[29] GSTC. The gasification industry. the Gasification & Syngas Technologies Council; 2017.

[30] Liu J, Wang S, Zhao B, Tong H, Chen C. Absorption of carbon dioxide in aqueous ammonia. Energy Procedia. 2009;1:933-40.

[31] Xu T, Srivatsa SC, Bhattacharya S. In-situ synchrotron IR study on surface functional group evolution of Victorian and Thailand low-rank coals during pyrolysis. J Anal Appl Pyrolysis. 2016;122:122-30.

[32] Yu J, Lucas J, Strezov V, Wall T. Swelling and Char Structures from Density Fractions of Pulverized Coal. Energy & Fuels. 2003;17:1160-74.

Chapter 7 The behaviour of mineral matter during pyrolysis and gasification

It is widely acknowledged in literature that the behavior of the inorganic minerals of lignites during gasification is just as important, perhaps even more important, than the entrained flow gasification performance and efficiency, especially for the commercial application of lignites in gasification In practice, the minerals in coal will eventually form the slag in the gasifier. It is crucial for the gasifier to efficiently remove the generated slag in terms of the gasifier operation and maintenance. Therefore, the behaviour of the minerals during gasification is necessary to be understood for the gasifier design. Extensive research on mineral transformation during combustion and fixed-bed gasification of coal has been conducted in the past. However, investigations of mineral transformation during entrained flow gasification are sparse. Only one study has been conducted for the Victorian brown coal, but it is limited to one Victorian brown coal, Morwell coal [75].

In this chapter, mineral transformation and morphology change of three Victorian brown coals, Yallourn, Maddingley, and Loy Yang coal, were investigated in a two-stage process under entrained flow pyrolysis and CO_2 gasification conditions. The parent coals were pyrolyzed at 700-1400°C in nitrogen, and then the pyrolysis chars were gasified at a corresponding temperature with CO_2 in the entrained flow reactor. The low temperature (700-900 ºC) chars and gasified chars were generated from low temperature entrained flow gasification experiments described in Chapter 5, and the high temperature (1000-1200 ºC) chars and gasified chars were obtained from high temperature entrained flow gasification experiments described in Chapter 6. The coals, pyrolysed chars, and gasified chars were characterised by the X-ray powder diffraction (XRD) and the scanning electron microscopy with energy dispersive X-ray spectroscopy (SEM/EDX) to investigate the reaction and transformation of the minerals during entrained flow pyrolysis and gasification process. This study offers a better understanding of behaviour of the selected major minerals (i.e. Al_2O_3, CaO, Fe_2O_3, MgO, SiO_2 and silicates) that are 1.) found in char and 2.) crystalline in nature which can be detected by XRD. Alkalis normally vaporize at studied temperatures and therefore have not been investigated here.

7.1 Mineral transformation and reaction during pyrolysis

This section investigated the transformation and reaction of inorganic components including mineral and non-mineral matters during pyrolysis of Victorian brown coals. The low temperature pyrolysis, 700-900 ºC, was conducted in N_2 by using the low temperature entrained flow reactor in Chapter 5, and the high temperature pyrolysis, 1000-1400 ºC, was carried out in N_2 by using the high

temperature entrained flow reactor in Chapter 6. The effect of the temperature has been investigated and discussed in the following sections.

7.1.1 Coal characterization

Three Victorian brown coals, Yallourn, Maddingley, and Loy Yang, were used in this study. The proximate analysis and ultimate analysis of these coals are presented in Table 3.1, Chapter 3. As evident, Yallourn coal was low ash coal (2.32% ash content), Loy Yang coal was medium ash coal (8.34% ash content), and Maddingley coal was high ash coal (15.24% ash content).

The raw coal ash was prepared at 550 ºC after 6 hours combustion in a muffle furnace. The ash fusion temperature of the coal was measured by SGS Australia according to ISO 540. The results of these measurements by XRF are generally accurate to less than 0.01%. The ash composition and ash fusion temperature of three coals are shown in Table 7.1 and 7.2. As can be seen, three coals differed widely in their ash composition. Yallourn (YL) coal was Fe-rich with 51.59% Fe_2O_3 in coal ash; Maddingley (MD) coal was rich of Fe, Si and S with around 20% Fe_2O_3, SiO_2, and SO_3 respectively; and Loy Yang (LY) coal was Si-rich with 47.16% SiO_2.

Table 7.1: Ash compositions of Yallourn, Maddingley, and Loy Yang coal (%)

Items	Yallourn	Maddingley	Loy Yang
Al_2O_3	1.75	15.24	22.11
BaO	0.28	0.02	0.01
CaO	8.29	9.24	2.05
Fe_2O_3	51.59	20.55	4.11
K_2O	0.18	0.08	0.61
MgO	17.69	7.58	5.51
Na_2O	5.78	8.92	7.87
P_2O_3	ND	ND	ND
SiO2	1.36	19.02	47.16
SO_3	12.55	19.02	7.41
TiO_2	0.54	0.34	3.17
Total	100	100	100

Table 7.2: Ash fusion temperature at reduction atmosphere

Items	Yallourn	Maddingley	Loy Yang
Deformation (°C)	>1560	1120	1250
Sphere (°C)	>1560	1150	1400
Hemi-sphere (°C)	>1560	1160	1440
Flow (°C)	>1560	1170	> 1560

7.1.2 Mineral reaction

The mineral transformation in chars was examined by XRD. Figure 7.1 shows the XRD patterns of YL, MD, and LY ash samples from raw coal and chars prepared at different temperatures. According to Bhattacharya and Harttig [81], the minerals detected in the XRD patterns can be classified as the following by the intensity of the X-ray peak: dominant >60%; Co-dominant >50%; sub-dominant, 20-50%; minor, 5-20%. The mineralogical composition of coal ash and char ash of YL, MD, and LY is presented in Tables 7.3, 7.4, and 7.5.

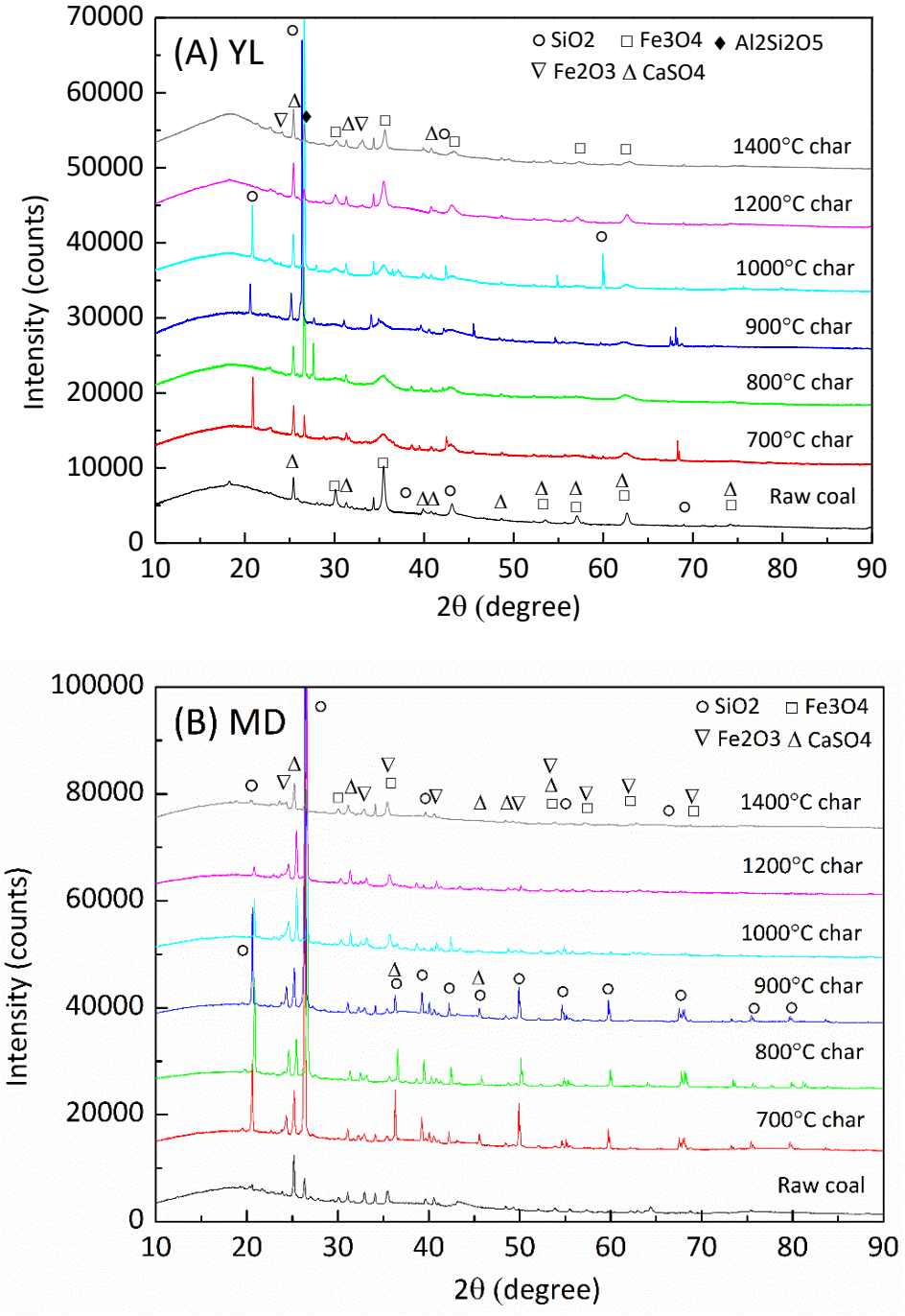

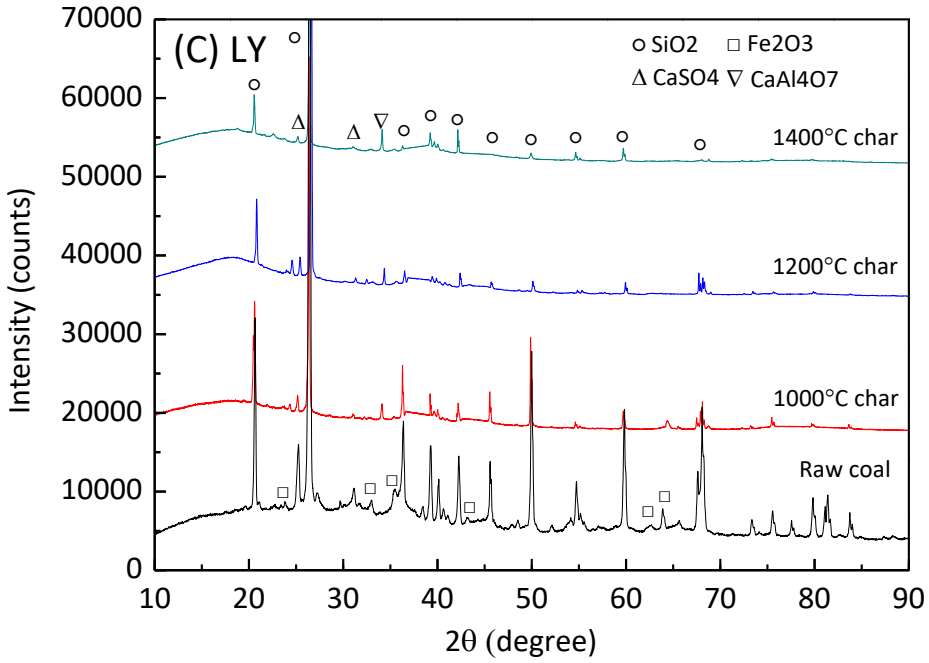

Figure 7.1: XRD pattern of char pyrolyzed at various temperatures: (A) YL, (B) MD, and (C) LY

Table 7.3: Mineralogical composition of YL coal ash and char ash samples by XRD*

Sample	Mineralogical Composition			
	Dominant Phase(s)	**Co-Dominant Phase(s)**	**Sub-Dominant Phase(s)**	**Minor Phase(s)**
Coal Ash	Fe_3O_4		$CaSO_4$	
700°C char Ash	$CaSO_4$		SiO_2 Fe_3O_4	
800°C char Ash	SiO_2	$CaSO_4$	Fe_3O_4	
900°C char Ash	SiO_2	$CaSO_4$	Fe_3O_4	
1000°C char Ash	SiO_2	$CaSO_4$	Fe_3O_4	
1200°C char Ash	$CaSO_4$	Fe_3O_4	Fe_2O_3 Al_2SiO_5	$MgAl_2O_4$
1400°C char Ash	$CaSO_4$	Fe_3O_4	Fe_2O_3 Al_2SiO_5	$MgAl_2O_4$

*Listed in decreasing order of X-ray peak intensity

Table 7.4: Mineralogical composition of MD coal ash and char ash samples by XRD*

Sample	Mineralogical Composition			
	Dominant Phase(s)	**Co-Dominant Phase(s)**	**Sub-Dominant Phase(s)**	**Minor Phases(s)**
Coal Ash	$CaSO_4$	SiO_2	Fe_3O_4 Fe_2O_3	
700°C char Ash	SiO_2		$CaSO_4$	Fe_2O_3 Fe_3O_4
800°C char Ash	SiO_2		$CaSO_4$	Fe_2O_3 Fe_3O_4
900°C char Ash	SiO_2		$CaSO_4$	Fe_2O_3 Fe_3O_4
1000°C char Ash	SiO_2		$CaSO_4$	Fe_2O_3 Fe_3O_4
1200°C char Ash	SiO_2		$CaSO_4$	Fe_3O_4 Fe_2O_3
1400°C char Ash	$CaSO_4$	Fe_3O_4	SiO_2	Fe_2O_3 $Al_2Si_2O_5$

*Listed in decreasing order of X-ray peak intensity

Table 7.5: Mineralogical composition of LY coal ash and char ash samples by XRD*

Sample	Mineralogical Composition			
	Dominant Phase(s)	**Co-Dominant Phase(s)**	**Sub-Dominant Phase(s)**	**Trace Phase(s)**
Coal Ash	SiO_2			$CaSO_4$ Fe_2O_3
1000°C char Ash	SiO_2			$CaSO_4$ $CaAl_4O_7$ Fe_2O_3
1200°C char Ash	SiO_2			$CaSO_4$ $CaAl_4O_7$ Fe_2O_3
1400°C char Ash	SiO_2			$CaSO_4$ $CaAl_4O_7$ Fe_2O_3

*Listed in decreasing order of X-ray peak intensity

All the possible mineral reactions were evaluated by the thermodynamic software (FactSage) in terms of gibbs energy (ΔG) and enthalpy (ΔH) as listed in Table 7.6. ΔG was used to evaluate the possibility of mineral reactions under different conditions.

Table 7.6: Gibbs energy and enthalpy for reactions among minerals at high temperature

Reactions		ΔG (kJ)			ΔH (kJ)		
		1000 °C	1200 °C	1400 °C	1000 °C	1200 °C	1400 °C
$SiO_2 + Al_2O_3 = Al_2SiO_5$	(R 7.1)	-2.48	-1.86	-1.32	-6.59	-6.23	-5.43
$2Fe_3O_4 + 0.5\ O_2 = 3Fe_2O_3$	(R 7.2)	-70.02	-42.66	-14.89	-243.31	-245.6	-249.03
$Fe_3O_4 = 3FeO + 0.5O_2$	(R 7.3)	162.21	140.91	117.73	297.66	298.32	394.66
$3Fe_2O_3 + CO = 2Fe_3O_4 + CO_2$	(R 7.4)	-102.17	-112.42	-123.22	-38.37	-34.97	-30.54
$Fe_2O_3 + MgO = MgFe_2O_4$	(R 7.5)	9.07	15.9	22.95	-33.07	-35.48	-36.49
$CaSO_4 = CaO + SO_2 + 0.5O_2$	(R 7.6)	153.09	103.27	54.95	475.12	464.99	448.86
$CaSO_4 + CO = CaO + SO_2 + CO_2$	(R 7.7)	-19.09	-51.82	-83.17	193.61	184.42	169.29
$2CaO + SiO_2 = Ca_2SiO_4$	(R 7.8)	-131.24	-137.19	-143.32	-93.91	-92.71	-91.37
$CaO + MgO + SiO_2 = CaMgSiO_4$	(R 7.9)	-107.61	-107.26	-107.03	-110.24	-109.42	-108.35
$CaO + Al_2O_3 + 2SiO_2 = CaAl_2Si_2O_8$	(R 7.10)	-131.64	-135.62	-139.86	-106.98	-105.39	-103.18

As one Fe-rich coal, the Fe_3O_4 was found to be the dominant phase in raw coal of YL, followed by the $CaSO_4$. After coal pyrolysis, the intensity of SiO_2 peaks increased with increasing temperature, and SiO_2 became the dominant phase in char at 800-1000 °C. However, when the temperature increased from 1200 °C to 1400°C, the intensity of SiO_2 peaks significantly decreased while the intensity of Al_2SiO_5 peaks increased. This change may be a result of Al_2O_3 reacting with the SiO_2. The Fe_3O_4 peaks were found in YL chars at 700-1400 °C. Interestingly, the Fe_2O_3 peaks were found at 1200-1400 °C and the intensity increased with temperature, which may be a result of the oxidation of Fe_3O_4 (R 7.2). It is clear that the decomposition of Fe_3O_4 as R 7.3 in Table 7.6 can not occur at 1000-1400 °C because of thermodynamical limitation, so the source of oxygen for R 7.2 could be derived from pyrolysis.

For MD coal, the $CaSO_4$ and SiO_2 were found to be the dominant phase in raw coal. In contrast to YL, in which no Fe_2O_3 and only the Fe_3O_4 was observed in the raw coal and low temperature chars (700-1000 °C), both the Fe_2O_3 and Fe_3O_4 peak were observed in MD coal and chars (700-1400 °C). At 1200-1400 °C, with increasing temperature, the intensity of Fe_2O_3 peaks decreased but the intensity of Fe_3O_4 peaks increased. This change can be associated with the reaction (R 7.4) between Fe_2O_3 and CO from pyrolysis. Similar to YL, the intensity of SiO_2 peaks in MD chars increased with

increasing temperature, and SiO_2 became the dominant phase in char at 800-1200 °C. At 1400 °C, the intensity of SiO_2 peaks dramatically decreased while the intensity of Al_2SiO_5 peaks increased possibly because of the reaction between SiO_2 and Al_2O_3.

The $CaSO_4$ was the major phase in raw coal and chars of YL and MD. The intensity of $CaSO_4$ peaks in chars increased with the temperature and became the dominant phase at high temperature as 1400 °C due to the decrease of the SiO_2 intensity. For LY samples, it was found that the SiO_2 is the only major and dominant phase in raw coal and chars pyrolysed at 1000-1400 °C as the LY coal ash is Si-rich with 47.16% SiO_2.

The results indicated that the mineral transformation of Victorian brown coals during pyrolysis mainly happened at a high temperature between 1000 °C and 1400 °C, and no mineral reaction was observed below 1000 °C. The behaviour of mineral matters during coal pyrolysis also widely differed in each coal due to the significant difference of mineral components among coals. The major crystalline minerals in chars and mineral reaction during coal pyrolysis are summarized in Table 7.7.

Table 7.7: Major crystalline minerals in YL, MD and LY chars and mineral reaction during coal pyrolysis

YL	MD	LY
Major Minerals		
SiO_2 (Quartz) $CaSO_4$ (Anhydrite) Fe_3O_4 (Magnetite)	SiO_2 (Quartz) $CaSO_4$ (Anhydrite)	SiO_2 (Quartz)
Mineral Reactions		
$SiO_2 + Al_2O_3 \xrightarrow{1000-1400\,^{\circ}C} Al_2SiO_5$	$3Fe_2O_3 + CO \xrightarrow{1000-1400\,^{\circ}C} 2Fe_3O_4 + CO_2$	n.d.
$Fe_3O_4 + 0.5O_2 \xrightarrow{1200-1400^{\circ}C} 3\,Fe_2O_3$	$SiO_2 + Al_2O_3 \xrightarrow{1000-1400\,^{\circ}C} Al_2SiO_5$	n.d.

n.d.: not detected

7.2 Mineral transformation during char gasification

This section presents the mineral transformation during char gasification in CO_2. The gasified chars, generated from low temperature (700-900 ºC) entrained flow gasification in Chapter 5, and the gasified chars, generated from high temperature (1000-1400 ºC) entrained flow gasification in Chapter 6, were examined by the XRD and are discussed in the following sections.

7.2.1 Char characterization

The chars of YL, MD, and LY were prepared by using two entrained flow reactors. The low temperature chars (700-900 ºC) were generated in N_2 using the low temperature entrained flow gasifier. The high temperature chars (1000-1400 ºC) were generated in N_2 using the high temperature entrained flow gasifier. The ultimate analysis and proximate analysis of chars prepared at various temperatures are presented in Table 7.8.

Table 7.8: Properties of chars pyrolysed at various temperatures on a dry basis, wt%

Fuel	Pyrolysis Temperature(°C)	VM	FC	C	H	N	S	O*	Ash
YL	700	17.3	71.05	73.04	2.46	0.87	0.35	11.63	11.65
	800	8.25	83.24	72.68	2.63	0.82	0.29	15.07	8.51
	900	5.17	84.25	77.1	1.89	0.71	0.29	9.43	10.58
	1000	11.50	80.6	83.17	1.42	0.61	0.39	6.51	7.90
	1200	6.14	86.28	88.62	1.24	0.78	0.34	1.44	7.58
	1400	5.14	89.01	89.28	0.82	0.66	0.30	3.09	5.85
MD	700	16.25	49.53	74.97	1.26	0.57	0.26	0	34.22
	800	13.08	52.27	53.46	1.59	0.62	3.67	6.01	34.65
	900	10.90	54.44	52.35	1.32	0.61	4.07	6.99	34.66
	1000	19.56	51.84	59.86	1.09	0.45	5.35	4.65	28.6
	1200	17.68	50.13	61.34	1.36	0.44	4.45	0.22	32.19
	1400	8.62	61.99	63.48	1.35	0.48	5.30	0	29.39
LY	1000	8.92	79.93	70.94	1.38	0.68	0.71	15.14	11.15
	1200	7.47	77.34	72.22	1.24	0.56	0.57	10.22	15.19
	1400	5.74	76.95	74.46	0.87	0.59	0.43	6.34	17.31

*****: by difference

The gasified chars generated from entrained flow gasification (700-1400 ºC) were burned at 550 ºC for 6 hours in a muffle furnace to prepare ash samples for the XRD analysis. The results of XRD analysis are presented and discussed in the following section.

7.2.2 Mineral transformation

The mineral transformations in gasified chars were examined by the XRD. Figure 7.2 shows the XRD patterns of YL, MD, and LY ash samples from raw coal, char prepared at 1200 ºC, and gasified chars generated at different temperatures. The mineralogical composition of coal ash and gasified char ash of YL, MD, and LY is presented in Tables 7.9, 7.10, and 7.11.

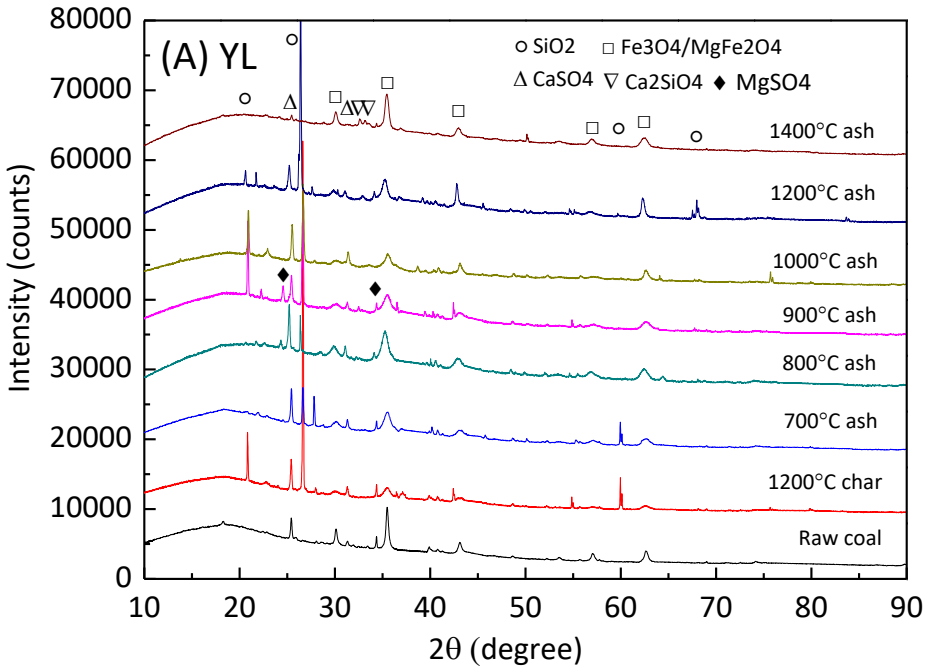
(A) YL
○ SiO2 □ Fe3O4/MgFe2O4
Δ CaSO4 ▽ Ca2SiO4 ♦ MgSO4
1400°C ash
1200°C ash
1000°C ash
900°C ash
800°C ash
700°C ash
1200°C char
Raw coal
Intensity (counts)
2θ (degree)

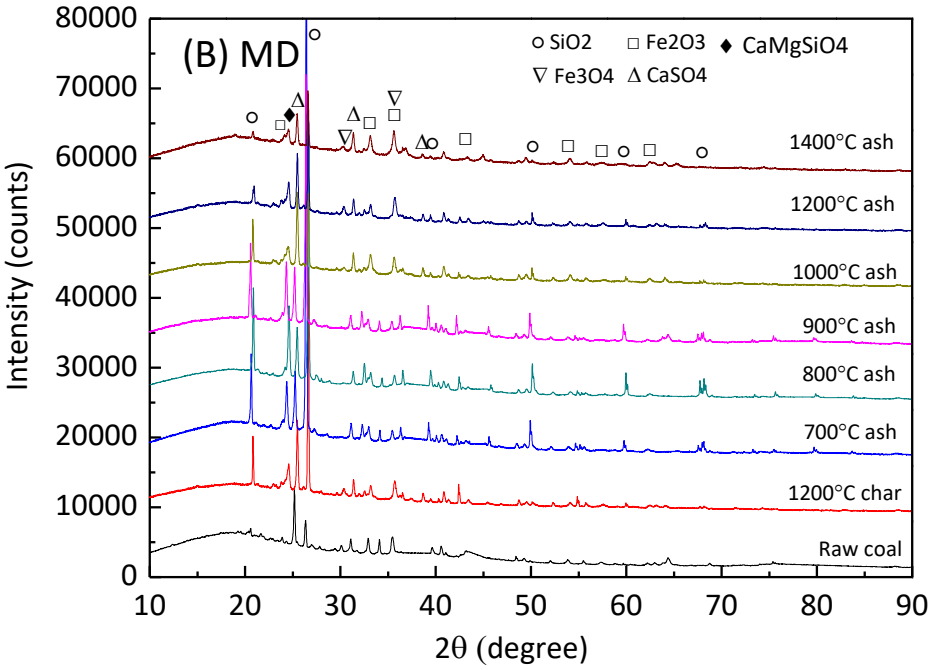
(B) MD
○ SiO2 □ Fe2O3 ♦ CaMgSiO4
▽ Fe3O4 Δ CaSO4
1400°C ash
1200°C ash
1000°C ash
900°C ash
800°C ash
700°C ash
1200°C char
Raw coal
Intensity (counts)
2θ (degree)

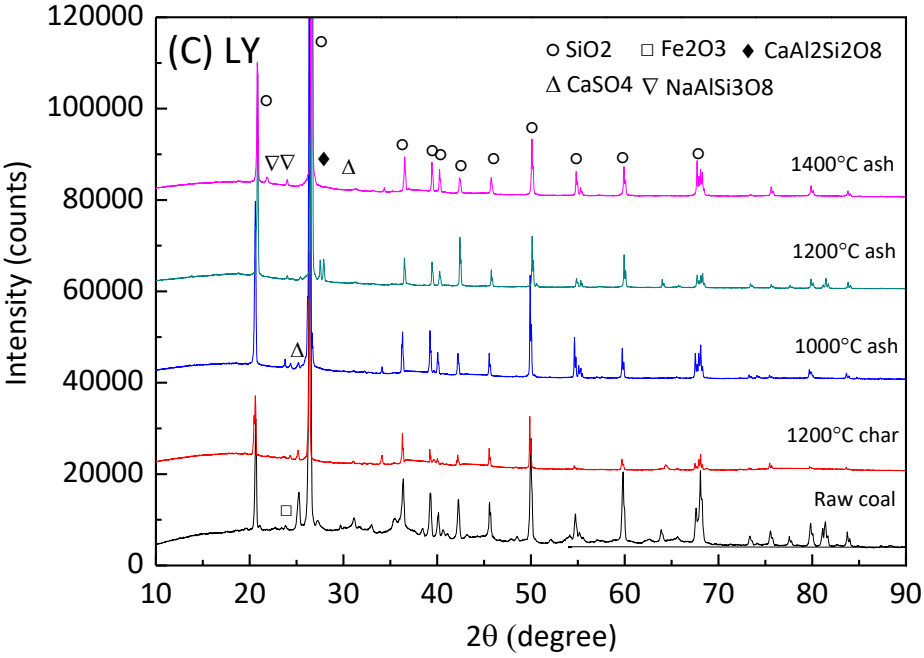

Figure 7.2: XRD pattern of sample series at various temperatures: (A) YL, (B) MD, and (C) LY

Table 7.9: Mineralogical composition of YL coal ash and gasified char ash samples by XRD*

Sample	Mineralogical Composition			
	Dominant Phase(s)	**Co-Dominant Phase(s)**	**Sub-Dominant Phase(s)**	**Minor Phases(s)**
Coal Ash	Fe_3O_4/ $MgFe_2O_4$		CaSO4	
700°C Ash	SiO_2	Fe_3O_4/ $MgFe_2O_4$ $CaSO_4$		$MgSO_4$ Na_2SO_4
800°C Ash	SiO_2	$CaSO_4$ Fe_3O_4/ $MgFe_2O_4$		$MgSO_4$ Na_2SO_4
900°C Ash	SiO_2		$CaSO_4$ Fe_3O_4/ $MgFe_2O_4$ $MgSO_4$	Na_2SO_4
1000°C Ash	SiO_2		$CaSO_4$ Fe_3O_4/ $MgFe_2O_4$	Na_2SO_4
1200°C Ash	SiO_2		Fe_3O_4/ $MgFe_2O_4$ $CaSO_4$	Ca_2SiO_4
1400°C Ash	Fe_3O_4/ $MgFe_2O_4$			Ca_2SiO_4 $CaSO_4$

*Listed in decreasing order of X-ray peak intensity

Table 7.10: Mineralogical composition of MD coal ash and gasified char ash samples by XRD*

Sample	Mineralogical Composition			
	Dominant Phase(s)	**Co-Dominant Phase(s)**	**Sub-Dominant Phase(s)**	**Minor Phases(s)**
Coal Ash	$CaSO_4$	SiO_2	Fe_2O_3	
700°C Ash	SiO_2			$CaSO_4$ Fe_2O_3
800°C Ash	SiO_2			$CaSO_4$ Fe_2O_3
900°C Ash	SiO_2			$CaSO_4$ Fe_2O_3
1000°C Ash	SiO_2	$CaSO_4$	$Fe_3O_4/MgFe_2O_4$ Fe_2O_3	$CaMgSiO_4$
1200°C Ash	SiO_2		$CaSO_4$ $Fe_3O_4/MgFe_2O_4$ Fe_2O_3	$CaMgSiO_4$
1400°C Ash	SiO_2		$Fe_3O_4/MgFe_2O_4$ Fe_2O_3	$CaSO_4$ $CaMgSiO_4$

*Listed in decreasing order of X-ray peak intensity

Table 7.11: Mineralogical composition of LY coal ash and gasified char ash samples by XRD*

Sample	Mineralogical Composition			
	Dominant Phase(s)	**Co-Dominant Phase(s)**	**Sub-Dominant Phase(s)**	**Trace Phases(s)**
Coal Ash	SiO_2			$CaSO_4$ Fe_2O_3
1000°C Ash	SiO_2			$NaAlSi_3O_8$ $CaAl_2Si_2O_8$
1200°C Ash	SiO_2			$NaAlSi_3O_8$ $CaAl_2Si_2O_8$
1400°C Ash	SiO_2			$NaAlSi_3O_8$ $CaAl_2Si_2O_8$

*Listed in decreasing order of X-ray peak intensity

The mineral reaction occurring in the Victorian brown coals and their ashes are shown below:

Anhydrite ($CaSO_4$) was a major mineral phase in YL and MD ashes from coal and gasified chars at 700-1200 ºC. Anhydrite was found to be chemically stable from 700 ºC to 1000 ºC in gasified char ashes of YL and MD. However, above 1000 ºC, with the increasing temperature, the intensity of $CaSO_4$ peaks decreased. It is clear from Table 7.6 that the self-decomposition of $CaSO_4$ (R 7.6) can not happen at high temperature because of thermodynamic limitation. Therefore, this decreased can rise from the reaction (R 7.7) between $CaSO_4$ and CO from the CO_2 gasification.

At 1200-1400 ºC, the calcium made by above reactions reacted with other available species to form bredigite (Ca_2SiO_4) in YL gasified char ashes, form monticellite ($CaMgSiO_4$) in MD samples, and form anorthite ($CaAl_2Si_2O_8$) in LY samples. The results agreed with the findings of the American lignites that the calcium oxide made by decomposition of $CaSO_4$ reacted with other available species such as silicates or magnesium oxides or alumina silicates to form different minerals such as bredigite and members of the gehlenite-akermanite solid solutions [82].

Quartz (SiO_2) was a dominant mineral phase in gasified char ashes generated at 700-1200 ºC from YL, MD, and LY. Moreover, quartz was the only major and dominant mineral phase for LY ashes from coal, char, and gasified chars, because of the abundance of Si in LY coal ash (around 50% SiO_2). Quartz will undergo structure transformation with increasing temperature, converting from trigonal α-quartz to hexagonal β-quartz at 573 ºC, to hexagonal β-tridymite at 870 ºC, and to cubic β-cristobalite at 1470 ºC. Despite the thermal structure change, quartz is generally chemically stable to at least 1000 ºC [82]. In the YL and MD gasified ash samples, quartz was stable at 700-1000 ºC and still present at 1200 ºC in all samples. However, at high temperature, >1000 ºC, the intensity of the SiO_2 peaks decreased with increasing temperature, and the intensity of calcium silicates peaks increased. Two recent research also has found the same change of SiO_2 at high temperature in Morwell and Loy Yang coal during gasification in CO_2 [75, 78].

Magnetite, Fe_3O_4, and Magnesioferrite, $MgFe_2O_4$, have very similar X-ray pattern, which makes them difficult to distinguish. Since YL and MD coal ash were Fe-rich, containing 51.6% and 20.6% Fe_2O_3 respectively, members of magnetite- magnesioferrite series were the major mineral phase in all YL ash samples from coal and gasified chars at 700-1400 ºC, and also presented in MD ashes from gasified chars at 1000-1400 ºC. It was found that the intensity of Fe_3O_4/ $MgFe_2O_4$ peaks in YL and MD ashes increased with increasing temperature at 1000-1400 ºC. The results indicated that only Fe_3O_4, not $MgFe_2O_4$, could be formed at high temperatures. It can form from the reduction of hematite (Fe_2O_3) by CO which is discussed in the following content.

Hematite (Fe_2O_3) was a major mineral phase in MD coal ash, and it was presented in its ashes from chars gasified at 700-1400 ºC. The Fe_2O_3 was chemically stable at low temperatures, 700-900 ºC. However, with the increasing temperature, the intensity of Fe_2O_3 peaks significantly decreased and the intensity of Fe_3O_4/ $MgFe_2O_4$ peaks, by contrast, increased. According to Table 7.6, the formation of $MgFe_2O_4$ (R 7.5) is impossible at high temperature due to thermodynamic limitation. Therefore, this change can be rose from the Fe_2O_3 reacting with CO from CO_2 gasification, reaction (R 7.4)

Bredigite (Ca_2SiO_4) forms at 1000-1200 ºC due to R 7.8. It formed in ashes of YL gasified coal which had 5.78% Na_2O, but not in MD and LY ashes with greater than 7.87% Na_2O. Some research found that low-sodium ashes, such as Beulah-Zap lignite and Morwell coal, formed Ca_2SiO_4, as high-sodium ashes tended to form sodium sulphates rather than sodium silicates at high temperatures [75, 82, 83]. The detected mineral phases during char gasification are summarized in Table 7.12.

Table 7.12: The melting point of the detected mineral phases

Phase	Chemical Formula	Temperature Predicted (ºC)							Melting point (ºC)
		coal	700	800	900	1000	1200	1400	
Albite	$NaAlSi_3O_8$					3	3	3	1100
Anhydrite	$CaSO_4$	1,2,3	1,2	1,2	1,2	1,2	1,2	1,2	1450
Anorthite	$CaAl_2Si_2O_8$					3	3	3	1274
Hematite	Fe_2O_3	2,3	2	2	2	2	2	2	1538
Larnite	Ca_2SiO_4							1	1540
Magnesium Ferrite	$MgFe_2O_4$	1	1	1	1	1,2	1,2	1,2	1713 [84]
Magnesium Sulfate	$MgSO_4$		1	1	1				1124
Magnetite	Fe_3O_4	1	1	1	1	1,2	1,2	1,2	1590
Monticellite	$CaMgSiO_4$					2	2	2	1503
Quartz	SiO_2	2,3	1,2	1,2	1,2	1,2,3	1,2,3	2,3	1670
Sodium sulfate	Na_2SO_4		1	1	1	1			884

1: YL; 2: MD; 3: LY

Overall, it was found that mineral reactions during gasification of Victorian brown coals happened at high temperatures between 1000 ºC and 1400 ºC, and major mineral phases were chemically stable at low temperatures. Evidently, there were significant differences for different coals in the behaviour of mineral matters because of the wide difference in minerals. The mineral reactions during CO_2 gasification of YL, MD, and LY chars are summarized in Table 7.13. At high temperature, the mineral transformation from high melting point SiO_2 (1670 °C) to low melting point minerals such as Ca_2SiO_4 (1540 °C), $CaMgSiO_4$ (1503 °C), and $CaAl_2Si_2O_8$ (1274 °C) decreased the operating temperature required for the liquid slag formation and reduced the operational cost. By contrast, the formation of Fe_3O_4 with high melting point (1590 °C) at 1000 -1400 ºC had a detrimental effect on the operational cost of an entrained flow gasifier.

YL and MD coal ash had high Fe content (51% and 21%, respectively) which works as catalyst for gasification and improves coal/char reactivity [85]. At 1000-1400 ºC, mineral reactions of Fe containing minerals in YL and MD samples are quite different. More Fe_3O_4 from the decomposition

of Fe_2O_3 was formed in YL samples, but more Fe_2O_3 was formed in MD samples because of oxidation of Fe_3O_4. Suzuki et al. found that a lower oxidation state of iron, Fe_3O_4, seems to be more reactive than Fe_2O_3 and results in better gasification rate [86]. By contrast, LY coal ash had high SiO_2 content (~48%) which has no catalytic effect on gasification [87]. At high temperature, the carbon conversion of YL is largest, followed by MD and then LY. Certainly, ash content and mineral reactions are two of the most important factors accounting for the different gasification behaviour of Victorian brown coals.

Table 7.13: Mineral reaction during char gasification of YL, MD, and LY

YL	MD	LY
$CaSO_4+CO \xrightarrow{1000\text{-}1400°C} CaO+SO_2+CO_2$	$CaSO_4+CO \xrightarrow{1000\text{-}1400°C} CaO+SO_2+CO_2$	$CaO+Al_2O_3+2SiO_2 \xrightarrow{1000\text{-}1400°C} CaAl_2Si_2O_8$
$2CaO+SiO_2 \xrightarrow{1200\text{-}1400°C} Ca_2SiO_4$	$CaO+MgO+SiO_2 \xrightarrow{1000\text{-}1400°C} CaMgSiO_4$	
$3Fe_2O_3+CO \xrightarrow{1000\text{-}1400\ °C} 2Fe_3O_4+CO_2$	$3Fe_2O_3+CO \xrightarrow{1000\text{-}1400\ °C} 2Fe_3O_4+CO_2$	

7.3 Modelling of mineral transformation during coal-CO_2 gasification

The FactSage 6.4, a well-known thermodynamic software package, was used to predict the reaction and transformation of inorganic matters during coal gasification at various temperatures and 20% CO_2. Based on the experimental coal feeding rate (1 g/min) and inlet gas flow rate (3.2 L/min CO_2 and 12.8 L/min N_2), the weight of coal elements, determined by ultimate analysis and ash composition, and the weight of the reactant gas, CO_2, were input into the Reaction module in the FactSage. The composition of inorganic matters after coal gasification at 1 atm and various temperatures was then determined by the Equilib module in the FactSage. The predicted inorganic compositions of YL, MD, and LY after coal gasification at various temperatures are presented in Tables 7.13, 7.14, and 7.15.

Table 7.14: Predicted inorganic compositions after YL coal gasification

Phase	Inorganics Matters (wt%)	Temperature (°C)					
		700	800	900	1000	1200	1400
Magnesioferrite	$MgFe_2O_4$	49.26 (2)	55.64 (2)	60.85 (3)	67.97 (3)	58.04 (3)	52.32 (1)
Anhydrite	$CaSO_4$	17.61 (2)	18.09 (2)	18.95 (3)	21.16 (3)	(3)	(4)
Sodium Sulfate	Na_2SO_4	11.53 (4)	11.77 (4)	9.77 (4)	2.02 (4)		
Magnesium Sulfate	$MgSO_4$	9.32 (4)	6.55 (4)	3.05 (4)	0.08		
Hematite	Fe_2O_3	5.81	1.95				
Forsterite	Mg_2SiO_4	2.78	2.86	2.99	3.34		
Spinel	$MgAl_2O_4$	2.14	2.2	2.3	2.57	3.15	3.02
Periclase	MgO			0.76	1.96	10.23	9.92
Calcium Iron Oxide	$CaFe_2O_4$					27.16	28.99
Perovskite-A	$CaTiO_3$					0.87	0.86
Merwinite	$Ca_3MgSi_2O_8$						4.58

(1): dominant mineral phase found in XRD measurements
(2): co-dominant mineral phase found in XRD measurements
(3): sub-dominant mineral phase found in XRD measurements
(4): minor mineral phase found in XRD measurements

Table 7.15: Predicted inorganic compositions after MD coal gasification

Phase	Inorganics Matters (wt%)	Temperature (°C)					
		700	800	900	1000	1200	1400
Cordierite	$Mg_2Al_4Si_5O_{18}$	27.29					
Anhydrite	$CaSO_4$	21.29 (4)	23.1 (4)	23.04 (4)	22.87 (2)	(3)	(4)
Hematite	Fe_2O_3	19.51 (4)	21.16 (4)	21.28 (4)	21.51 (3)	25.48 (3)	(3)
Sodium Sulfate	Na_2SO_4	18.79	5.01	4.64	3.61	4.27	
Sapphirine	$Mg_4Al_{10}Si_2O_{23}$	7.05	6.36	6.09			
Forsterite	Mg_2SiO_4	3.49	11.36	11.22	11.59		6.61
Nepheline	$NaAlSiO_4$		32.08	33.04	35.35	30.58	32.21
Spinel	$MgAl_2O_4$				4.55	11.06	11.63
Monticellite(s)	$CaMgSiO_4$				(4)	20.89 (4)	(4)
Merwinite	$Ca_3MgSi_2O_8$					7.18	22.98
Magnetite	Fe_3O_4				(3)	(3)	25.94 (3)

(1): dominant mineral phase found in XRD measurements
(2): co-dominant mineral phase found in XRD measurements

(3): sub-dominant mineral phase found in XRD measurements
(4): minor mineral phase found in XRD measurements

Table 7.16: Predicted composition of inorganic matters after LY coal gasification

Phase	Inorganics Matters (wt%)	Temperature (°C)		
		1000	1200	1400
High-Albite	$NaAlSi_3O_8$	52.37 (5)	53.79 (5)	45.06 (5)
Anorthite	$CaAl_2Si_2O_8$	10.98 (5)	10.98 (5)	11.55 (5)
Nepheline	$NaAlSiO_4$	10.68	8.91	
Sapphirine	$Mg_4Al10Si_2O_{23}$	8.18	8.84	1.41
Forsterite	Mg_2SiO_4	7.54	7.28	2.64
Ilmenite	$(FeO)(TiO_2)$	4.68	4.85	6.68
Leucite(RHF)-B	$KAlSi_2O_6$	3.03	2.67	
Ulvospinel	$(FeO)_2(TiO_2)$	2.74	2.5	0.29
Cordierite	$Mg_2Al_4Si_5O_{18}$			32.59

(5): minor mineral phase found in XRD measurements

Compared with the XRD patterns in Figure 7.2, it was found that the equilibrium predictions for YL and MD samples reasonably agreed with the experimental results. The major minerals in YL and MD samples were successfully predicted by FacSage modelling. However, one major deficiency of the FacSage modelling was found to be that it could not predict the actual change of SiO_2 which was thermally stable below 1000 ºC and the dominant mineral phase, in most cases, in gasification residues. Because of this deficiency, predictions for Si-rich LY samples turned out to disagree with the XRD results. There was other predicted mineral which was not found in XRD measurements. This could be contributed by three reasons: 1) no crystalline structure of the predicted mineral phases which was not detected by the XRD [78]; 2) the thermal change of coal minerals during ashing procedure or inaccurate mineral [82]; 3) incorrect mineral input for equilibrium calculations where some metal element may exist in the form of organic matters, not minerals.

7.4 Morphology change

The morphology change in gasification residues of YL, MD, and LY between 800 ºC and 1400 ºC was examined by using a field-emission scanning electron microscope (FE-SEM) (Hitachi SU8010) which had secondary electron microscopy (SEM), backscattered electron microscopy (BSEM), and energy dispersive X-ray spectroscopy (EDX). In this study, The SEM was used to identify the sample surface morphology, the BSEM was used to detect the distribution of inorganic matters in the sample, and the EDX was used to provide the detailed information on the molten part and mineral-rich part.

7.4.1 The SEM analysis

It can be seen from SEM images in Figures 7.3, 7.4 and 7.5, with the increasing temperature and carbon conversion, the particle size of YL and MD gasification residues significantly decreased to ~ 20 μm and ~ 50 μm respectively at 1400 °C (Figures 7.3O and 7.4O). By contrast, the particle size of LY samples did not significantly change with temperature, and its size was ~100 μm at 1400 °C, seen in Figure 7.5K. The change of particle size during char gasification indicated that reaction mode of the sample, which provides useful information for the reaction model selection in kinetic studies [58]. The final particle morphology suggested that the YL and MD chars may be suitable for the volumetric model and modified volumetric model in which it is assumed that the sample reacts homogeneously with the gasifying agent. The LY chars may be suitable for the grain model in which it is assumed that the internal of the particle does not react.

The morphology of mineral matters in gasified chars of YL and MD showed differently at different temperatures. At a low temperature below 1000 °C, no morphology change was observed in minerals. The mineral constituents started to appear and were observed on the sample surface at 1000 °C, seen in Figures 7.3G and 7.4G. With temperature increased, minerals aggregated and melted seriously, and developed a smooth surface of char at 1200 °C, seen in Figures 7.3L and 7.4L. At 1400 °C, the minerals developed to smooth sphere particles and aggregated with each other to form larger particles, seen in Figures 7.3P and 7.4P, resulting in the increase of the particle size.

7.4.2 The BSEM and EDX analysis

As can be seen in the BSEM images, the distribution of mineral matters also changed with the temperature and carbon conversion. In the BSEM images, the mineral-rich area generally looks brighter than the other area because of more metal elements. The EDX analysis of YL, MD, and LY samples showed and indicated that the area A, a bright part in the particle, contained less carbon and more inorganic minerals than the area B, a dark part. The YL and MD gasification residues had a very similar morphological change in mineral matters at various temperatures. It was found that minerals disperse homogeneously in the gasified char at 800 °C, and no evidence of mineral aggregation was found in particles, seen in Figures 7.3C and 7.4C. As the temperature and carbon conversion increased, inorganic minerals stated to aggregate and adhered to the char surface, seen in Figures 7.3H and 7.4H. The EDX analysis shows mineral constituents of YL samples contained high Fe content (~16%), seen Figure 7.3I, and MD samples contained high Si & Al content, seen in Figure 7.4I.

At 1200 °C, the minerals aggregated and melted seriously, and covered the majority of the particle surface (Figures 7.3M and 7.4M). The EDX analysis (Figures 7.3N and 7.4N) showed that carbon content in the particle decreased largely and the particle contained more minerals with high Fe content (>13%). Therefore, the melting of minerals is because YL and MD samples contained high Fe-content ash which melts at temperature lower than 1200 °C [88]. At 1400 °C and carbon conversion of 99%, the particles were almost comprised of inorganic minerals, seen in Figures 7.3R and 7.4R. The EDX analysis at 1400 °C (Figures 7.3S and 7.4S) showed that very little carbon (<4.2%) was left and the particle was formed by high Fe content minerals.

By contrast, the LY samples showed different morphology change. Unlike YL and MD samples, mineral constituents were observed at a higher temperature as 1200 °C (Figure 7.5G). There was also no melting of minerals observed on the particles at high temperatures. This is because LY coal ash has high SiO_2 content (~47%) which is thermal stable below 1200 °C and makes behaviour of mineral matters less reactive. At 1400 °C and carbon conversion of 98%, minerals aggregated and developed to small spheres which coated the whole large particle, seen in Figure 7.5M. The EDX analysis at 1400 °C (Figures 7.5O) indicated that the gasification residues contained a considerable amount of carbon (approximate 25%). In other word, there were a certain amount of char particles which had not been completely converted, even though the overall carbon conversion was around 98%.

Overall, with the increasing temperature, carbon conversion increased, and therefore, less carbon and more minerals were left in the particles. At carbon conversion of 99%, almost only mineral spheres can be observed in the samples of YL and MD. The morphological results demonstrated that the mineral transformation took place at high temperatures between 1000 °C and 1400 °C. With the increasing temperature and carbon conversion, mineral constituents with high Fe content were found in YL and MD samples at 1000 °C, followed by mineral melting at 1200 °C. Compared to high Fe content YL and MD samples, high Si-content LY samples acted more stable in the behaviour of mineral matters.

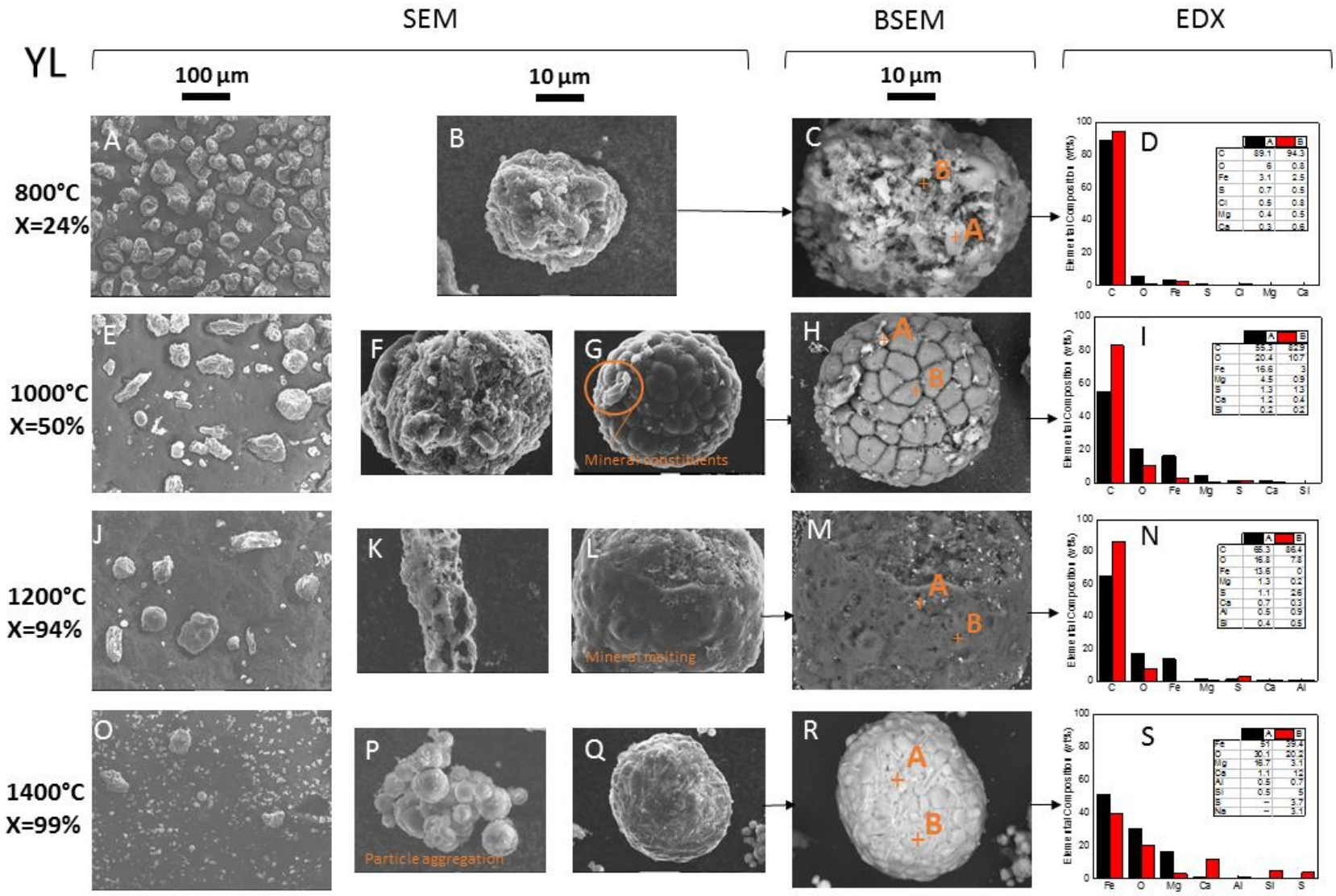

Figure 7.3: The SEM, BSEM, and EDX analysis of YL gasification residues at 800-1400 °C and 20% CO_2

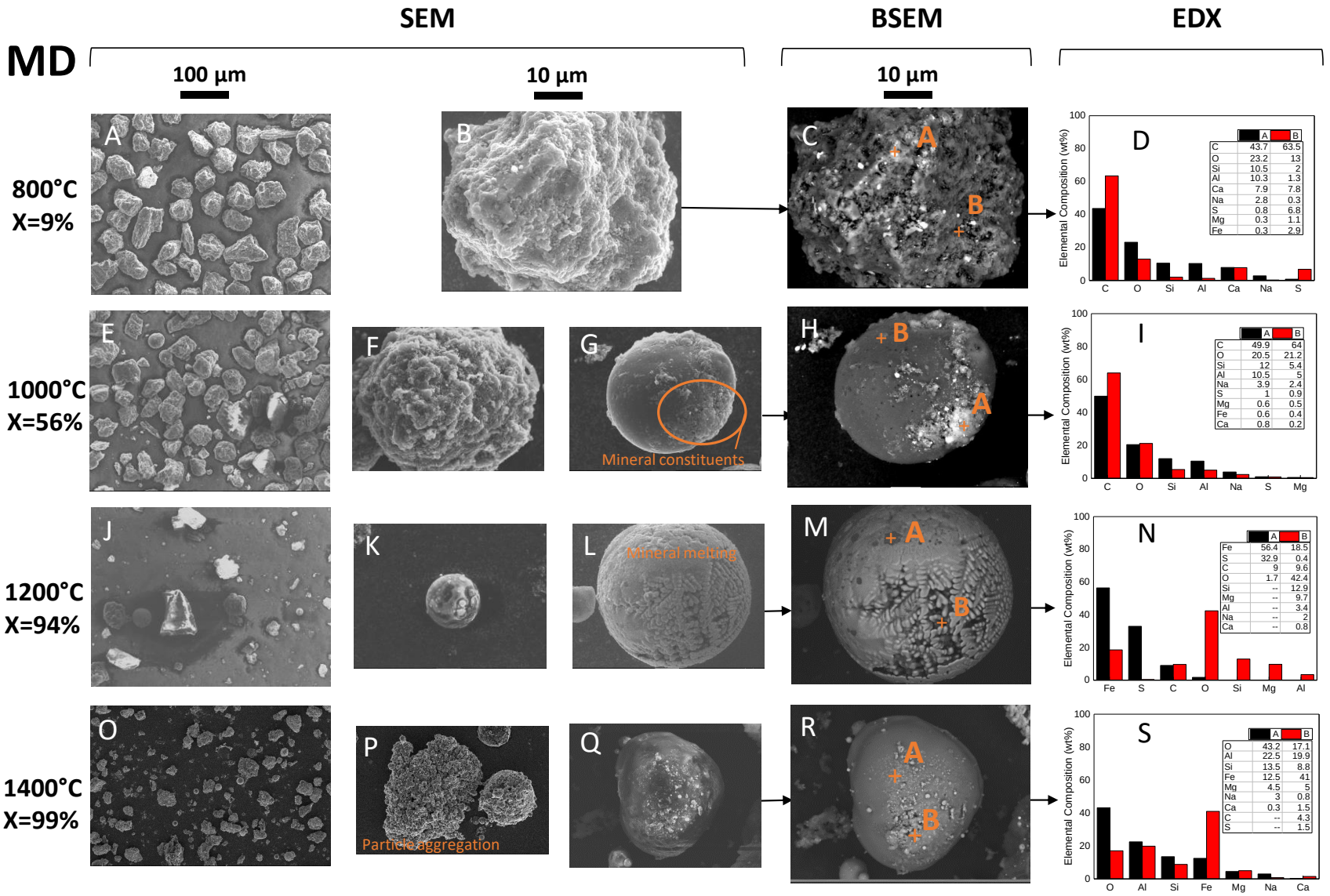

Figure 7.4: The SEM, BSEM, and EDX analysis of MD gasification residues at 800-1400 °C and 20% CO_2

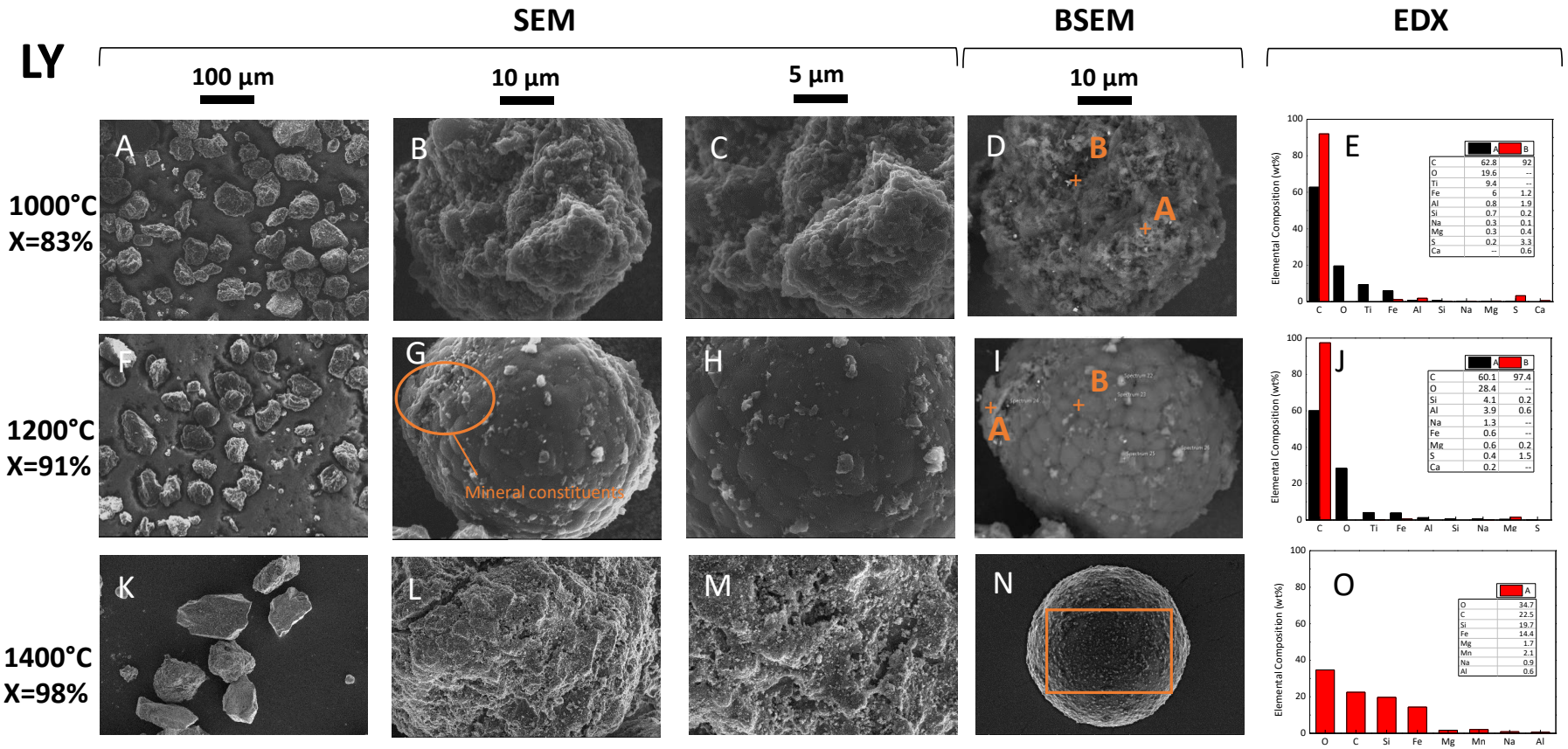

Figure 7.5: The SEM, BSEM, and EDX analysis of LY gasification residues at 1000-1400 °C and 20% CO_2

7.5 Chapter summary

This chapter investigated the mineral behaviour of YL, MD, and LY during entrained flow pyrolysis and CO_2 gasification between 700 ºC and 1400 ºC by the XRD and SEM-EDX. The effect of temperature on mineral transformation and morphology change during the two-stage entrained flow gasification was discussed in detail.

The mineral reactions during coal pyrolysis and char gasification happened at high temperatures between 1000 ºC and 1400 ºC, not low temperatures. There were significant differences for parent coals in mineral reactions during coal pyrolysis and char gasification. During coal pyrolysis, the formation of Al_2SiO_5 was both found in YL and MD chars at 1000-1400 ºC. The decomposition of Fe_3O_4 and the increase of the Fe_2O_3 intensity were found in YL chars at 1200-1400 ºC, whereas the MD chars showed the opposite change in Fe_3O_4 because of the oxidation of Fe_2O_3 by CO from pyrolysis.

During char gasification, the decomposition of $CaSO_4$ and the increase of Fe_3O_4/ $MgFe_2O_4$ intensity were observed in both YL and MD gasification residues at 1000-1400 ºC. The SiO_2 decreased to form the Ca_2SiO_4 in YL samples and form $CaMgSiO_4$ in MD samples at 1200-1400 ºC. The SiO_2 was also the only major mineral phase in YL chars and gasification residues, so few mineral reactions were observed during coal pyrolysis and char gasification.

YL and MD samples showed a very similar morphological change in gasification residues at 1000-1400 ºC. The mineral constituents with high Fe content started to be found on the surface at 1000 ºC, and then minerals melted and coated the particle at 1200 ºC. At 1400 ºC, minerals developed the smooth spheres and aggregated with each other. By contrast, high Si-content LY samples showed more stable in particle morphology in terms of particle size and the behaviour of mineral matters.

At 1400 ºC and high carbon conversion of 98-99%, the YL and MD gasification residues eventually became small particles, but the size of LY particles was almost stable. The final particle morphology indicated that YL and MD may be suitable for the volumetric model and modified volumetric model, which is discussed in Chapter 9.

Chapter 8 Comparison of entrained flow gasification behaviour of Victorian brown coals and biomass

After a comprehensive experimental investigation on entrained flow gasification of Victorian brown coals in chapter 5-7, it is necessary to evaluate their gasification performance by comparing with other solid fuels, such as biomass. Therefore, the entrained flow gasification behaviour of Victorian brown coals and biomass is investigated and compared in this chapter to understand the difference between two fuels.

In this study, the gasification performance of Loy Yang coal and pine park is comprehensively assessed by direct coal gasification. The gasification experiments were conducted in the temperature range of 1000-1200 °C and CO_2 concentration range of 10-40% using a high temperature entrained flow reactor. The comparison among the fuels includes gas composition, carbon conversion, the emission of air pollutants (H_2S, HCN, and NH_3), and mineral transformation with the temperature and CO_2 concentration.

This chapter reproduces the following published paper in Fuel.

Fuel 203 (2017) 942–953

Contents lists available at ScienceDirect

Fuel

journal homepage: www.elsevier.com/locate/fuel

Full Length Article

Comparison of entrained flow gasification behaviour of Victorian brown coal and biomass

Pavan Pramod Sripada, Tao Xu, M.A. Kibria, Sankar Bhattacharya *

Department of Chemical Engineering, Monash University, VIC 3800, Australia

GRAPHICAL ABSTRACT

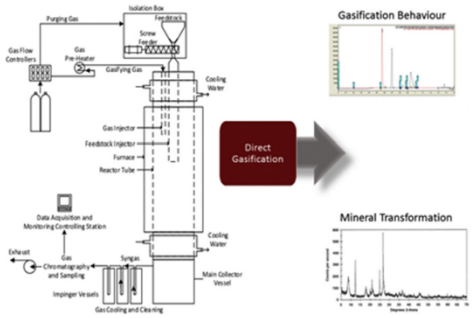

ARTICLE INFO

Article history:
Received 2 September 2016
Received in revised form 5 April 2017
Accepted 11 April 2017
Available online 20 April 2017

Keywords:
Entrained-flow gasification
Biomass
Victorian brown coal
Gasification
Pollutant gas emission
Mineral transformation

ABSTRACT

This study assesses and compares the gasification performance of a Victorian brown coal (Loy Yang) and Pine bark in the temperature range of 1000–1400 °C with CO_2 (10–40% in N_2) as the gasifying agent in a bench-scale atmospheric entrained flow reactor. The effect of temperature and CO_2 concentration in the feed gas on the carbon conversion, syngas composition, and emission of polluting species such as HCN, NH_3 and H_2S has been investigated. In addition, complementary char analysis such as the particle size distribution and char morphology have been performed in order to characterize the fragmentation behaviour. Further, the mineral matter transformation at elevated temperatures has been analyzed through X-ray diffractograms of the chars and comparing with the thermochemical equilibrium predictions. As expected, the carbon conversion increased with increasing temperature and CO_2 concentration. For both the fuels, ~98% conversion was achieved at 1200 °C. The products included the solid residue and the gaseous components such as CO, H_2, CO_2, and CH_4. No tar was observed during the gasification runs. The pollutant gases were in the ppmv range with NH_3 and H_2S negligible amounts being detected for Loy Yang coal and Pine bark, respectively.

1. Introduction

The utilization of coal and its substitution with renewable options has been debated widely over the past few years. However, coal is expected to dominate the world energy market until 2030 and contribute to energy production until the end of 2100 [1–3].

* Corresponding author.
E-mail address: Sankar.Bhattacharya@monash.edu (S. Bhattacharya).

http://dx.doi.org/10.1016/j.fuel.2017.04.058
0016-2361/

Gasification is a well-known and a more sustainable utilization option with higher efficiency and significantly lower NO_x and SO_X emissions compared to the traditional combustion process [4,5]. Of the many gasification techniques available, entrained flow gasification dominates the gasification market, accounting for more than 70% of worldwide syngas production, predominantly due to the flexibility of feedstock handling and higher carbon conversion [6,7]. In particular, the feedstock flexibility aspect allows for at least the partial substitution of coal with a renewable carbonaceous fuel such as biomass. However, the 'compatibility' of fuels for co-gasification has to be investigated through fuel specific gasification performance data under industrially relevant conditions in order to enable the design and optimization of the process. In this study, a Victorian brown coal (Loy Yang coal) and a biomass (Pine bark) have been compared in terms of carbon conversion and mineral matter behaviour during entrained flow gasification.

Biomass holds tremendous potential to meet the global energy and chemical needs. The technical potential of biomass for energy is significant and is estimated to be 1500 EJ/year by 2050 [8]. Particularly, biomass derived from forestry, agriculture and municipal wastes and residues is an attractive fuel for gasification owing to large abundance and low cost. Several carbon-rich industrial refuse, for example, the rejects of the local pulp and paper industries, such as wood bark are potential feedstock because of their typically lower ash and sulfur contents.

Entrained flow gasification is an industrially mature technology with several investigations on a variety of coals [9–13]. However, limited data exists on the gasification performance of Victorian brown coal that are one of the largest reserves of lignites in Australia and the world [6]. The investigations of Tremel et al. and Harris et al. on the pyrolysis and gasification behaviour of a German lignite and Australian sub-bituminous coals in an entrained flow reactor demonstrate the influence of the coal property and the gasification conditions on the carbon conversion achieved [14,15]. Similar studies on a variety of biomass by Qin et al. [16] demonstrate the effects of the gasification medium (steam and O_2 mixtures) on the outlet gas quality and carbon conversion.

The use of steam and oxygen for gasification in an industrial setting is cost intensive. On the other hand, the use of air lowers the cost, however, the product gas is dilute with nitrogen resulting in a lower heating value. Instead, the utilization of CO_2 as a gasifying agent reduces carbon footprint and the heat requirement for phase change compared to steam gasification [17]. Recently, Billaud et al. investigated the CO_2 gasification performance of sawdust in a lab-scale entrained flow gasification rig [18]. For the char samples used in their study, a temperature of 1200 °C was required. Tanner et al. investigated the entrained flow gasification of German lignite and Victorian brown coal, and suggest that ~100% carbon conversion was achieved at 1400 °C [19]. However, the gasification conditions required in large scale gasification would be governed by both the carbon conversion and the mineral matter behaviour. The mineral composition would affect the slag formation temperature in the gasifier [20]. This, in fact, reinforces the need for fuel specific experimental data at industrially relevant gasification conditions.

In this paper, the comprehensive assessment of entrained flow gasification performance of Loy Yang coal and pine bark is presented. The Loy Yang brown coal is currently used for mine-mouth power generation in conventional pf boilers. The pine bark is a reject from the paper mills. Both these solid fuels are currently assessed for entrained flow gasification with a view of producing chemicals and liquid fuels. The comparison between the fuels is drawn in terms of carbon conversion, syngas composition, emission of syngas contaminants such as H_2S, HCN, and NH_3; mineral matter characteristics and their transformation as a function of temperature. The results from this study contribute to the overall objective of the feasibility analysis of the co-gasification of the biomass along with Victorian brown coals to be undertaken later.

2. Experimental

2.1. Sample selection and preparation

In this study, Loy Yang coal from Loy Yang mine in Victoria, and Pine bark (*Pinus Radiata*) sourced from Norske Skog were selected as the coal and biomass subject. In this paper, Loy Yang coal and Pine bark with henceforth be referred to as LY and PB respectively. These fuels have been selected for comparison due to their similar carbon and ash contents. Both samples were firstly air-dried and ground and then sieved to a particle size of 90–106 μm using a Tyler sieve shaker machine. A range of fuel characterization such as the proximate, ultimate analysis, ash fusibility, and composition have been carried out and are presented in Table 1.

2.2. Apparatus and procedure

The gasification tests were conducted on the HELENA (High temperature, electrically heated, entrained flow apparatus), shown in Fig. 1. The HELENA, located at Monash University Clayton, was custom designed to mimic industrial gasifier residence times; a detailed description of the capabilities and process parameter ranges of the apparatus is covered by Tanner et al. (2016) [19]. At atmospheric pressure, the furnace of HELENA is heated to the desired temperature at a rate of approximately 1 °C/min using the temperature control panel. The slow heating rate preserves the condition of the alumina reactor tube and the molybdenum disilicide heating elements. The cooling water system is turned on prior to heating and remains switched on throughout the duration of the experiment. The impingers (gas cleaning and cooling section) and the solids collector are air-blown, cleaned with water and dried prior to use to ensure accurate ash collection and weighing. The gasifying agent was pre-heated to 500 °C and the Varian

Table 1
Proximate, ultimate and ash fusibility analysis of fuels.

Parameter	Loy Yang	Pine Bark
Moisture (oven dried, wt%)	1.0	5.0
Proximate analysis (dry basis, wt%)		
Volatile matter	50.63	59.78
Fixed carbon	35.33	23.91
Ash	14.02	16.30
Ultimate analysis (dry basis, wt%)		
C	57.38	53.47
H	3.89	5.47
N	0.14	0.15
S	0.12	0.13
O	24.44	24.49
Ash fusibility (reducing atmosphere) (°C)		
Deformation	1250	1148
Sphere	1400	1166
Hemi-sphere	1440	1218
Flow	>1500	1236
Ash composition (dry basis, wt%)		
SiO_2	38.6	60.69
Al_2O_3	36.7	14.38
Fe_2O_3	5.64	6.78
CaO	1.26	6.18
MgO	7.85	2.74
Na_2O	6.33	1.12
K_2O	0.59	5.47
TiO_2	2.19	0.90
SO_2	0.04	0.69
P_2O_5	0.28	0.97
BaO	0.05	0.03

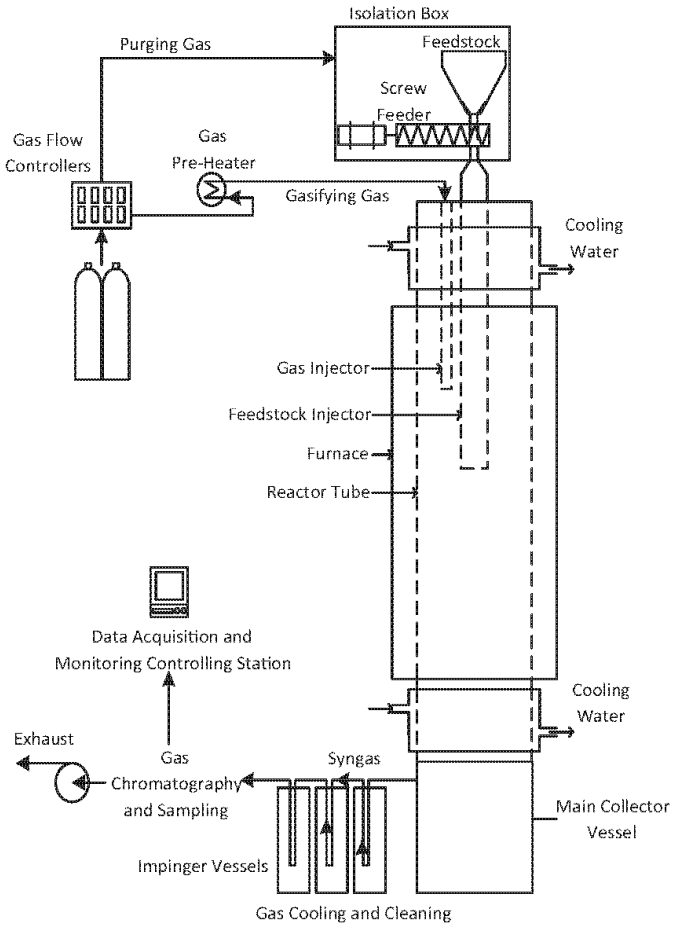

Fig. 1. Schematic of the high-temperature entrained flow reactor.

490-GC micro-gas chromatography (μGC) analyzer was calibrated using an external standard gas.

Following sample preparation, the raw feed material was dried overnight in an oven at 105 °C. This ensured that the moisture content of the material entering the HELENA was minimized and uniform, hence, reducing the likelihood of the raw sample agglomerating and blocking the feeding mechanism of the entrained flow reactor. Approximately 150 g of the feed material, measured by the Mettler Toledo XP10002S Precision Balance Toploading Scale, was placed in the feed system at the top of the HELENA. The reactor was purged with nitrogen at a flowrate of 16 L/min (4 L/min purge gas and 12 L/min carrier gas) until the oxygen concentration was approximately 0.5% or below as determined by the μGC. Subsequently, the CO_2 atmosphere as required for the experiment is fed in the reactor gas. The screw feeder was switched on and samples were fed slowly at around 1 g/min, which ensures entrained flow conditions. Under the above conditions, the residence times for both the fuels is in the range of 7–8 s, replicating the conditions closer to industrial gasifiers. The residual gasification char is collected in the jacketed solids collector, and the particles and moisture are removed from the gas by the impingers prior to gas composition analysis. Control of the exhaust vacuum pump allowed the system to be continuously maintained at atmospheric pressure (±0.01 bar gauge). The fuel feed rates, gas flowrates and internal pressure were monitored/controlled by using a custom National Instruments LabVIEW CompactDAQ system. The composition of H_2, O_2, CO, CO_2, CH_4 and N_2 in the product gas were analyzed online approximately every 3 min using the μGC. After steady state was attained, approximately after 15 min of feeding, the compositions of pollutant gas (NH_3, HCN, and H_2S) were measured by a Dräger gas sampling tubes. Following completion of the gasification run, the solids were collected, weighed, sealed and labeled in a container.

2.3. Data collection and analysis

The μGC instrument was calibrated based on a three-point calibration curve prior to the start of the experimental run. The gas composition of the outlet gas during the experiments was measured on-line by the μGC to determine the vol.% of N_2, O_2, H_2, CO, CH_4, and CO_2. The steady state gas composition data were collected, averaged and presented in terms of gas composition (N_2 and CO_2 free basis), carbon conversion and its calorific values i.e., lower heating value (LHV) and higher heating value (HHV). The gas

composition is shown in the N_2 and CO_2 free basis, as they are not the product of gasification reaction. The LHV and HHV for the product gases (N_2 and CO_2 free basis) are calculated by the following equation:

$$\text{LHV } (\text{MJ/m}^3) = x_{H2} \times 10.78 + x_{CO} \times 12.63 + x_{CH4} \times 35.81 \quad (1)$$

$$\text{HHV } (\text{MJ/m}^3) = x_{H2} \times 12.76 + x_{CO} \times 12.63 + x_{CH4} \times 39.75 \quad (2)$$

where x_{H2}, x_{CO}, x_{CH4} is the volume fraction of H_2, CO and CH_4 respectively.

Carbon conversion (χ) was calculated based on solids basis that considers the carbon in solid feed and the carbon in the obtained chars as shown in Eq. (3).

$$\chi\ (\%) = \left(1 - \frac{m_{C,char}}{m_{C,feed}}\right) \times 100 \quad (3)$$

where $m_{C,feed}$ is the mass of carbon in the solid fuel fed and $m_{C,char}$ is the mass of carbon in the chars recovered. Gas basis-based on the C-containing gas phase products such as CO, CO_2, and CH_4 is calculated using Eq. (4).

Gas basis-based on the C-containing gas phase products such as CO, CO_2, and CH_4 is calculated using Eq. (4).

$$\chi\ (\%) = \frac{(X_{CO+}X_{CO2} + X_{CH4}) \times 12}{m_{C,feed+CO2}} \times 100 \quad (4)$$

where X_{CO}, X_{CO2}, X_{CH4} is the molar concentration of CO, CO_2 and CH_4 from in the outlet gas, and $m_{C,feed+CO2}$ is the mass of carbon including feed CO_2 in the feeding inlet.

The composition of NH_3, HCN, and H_2S was examined using a Dräger tube with an accuracy of NH_3 (±10–15%), HCN (±10–15%), and H_2S (±5–10%). Each gas was measured three times and averaged number is presented here. Further, condensation of these species is unlikely due to the fact that the gas temperature in the impingers (approx. 40 °C) is higher than the respective boiling points.

The particle size distribution of the raw fuels and the chars was measured using a Malvern Mastersizer 2000 instrument that has upper detection limit of 2000 μm. The measurements were obtained from a wet cell with a suction pressure of 1.5 bar, vibratory feed rate of 50% and an average obscuration of 0.8%. For each sample, three sub-samples were drawn from different positions in the lot and each of the sub-samples was analyzed in triplicates.

The crystalline mineral matter in the solid products was evaluated by a MiniFlex 600 XRD. The parent fuel and the chars could not be analyzed directly due to the large presence of amorphous carbon that masks most of the peaks. Therefore, before measurement, the solid products were burned at relatively lower temperature 600 °C for 2 h in a muffle furnace to remove the carbon while minimizing further devolatilization of the minerals. Subsequently, ash samples were packed into an aluminum sample holder and scanned in a step-scan mode (0.2°/step) over the angular range of 2–100° (2θ). The diffractogram was then collected and analyzed for the crystalline mineral phases by the MDI Jade software. Replicates were performed when required.

The morphology change of the solid products is observed by a JEOL 7001F field emission gun scanning electron microscope mounted with an Oxford Instruments X-Max 80 EDS detector, located at the Monash center for electron microscopy. The scanning electron microscopy (SEM) images were obtained at an accelerating voltage of 15 kV and a working distance of 10 mm. The images were obtained after focusing at the desired magnification and correcting for astigmatism.

3. Results and discussion

3.1. Mass balance

There was no visible trace of tar in the impingers under entrained flow conditions and the temperatures used during the experiments. Incidentally, the same observation was made in gasification of Australian lignites in a pressurized fluidized bed gasifier at a relatively lower temperature range of 750–920 °C [21]. Furthermore, the same observation was made by Qin et al. for the entrained flow gasification of biomass with air as the oxidizing medium [22]. The chars in the gasification runs were deposited in the main collection pot and the first impinger. Although fines were captured in the fines trap, they could not be recovered in the experiments. The carbon balance is the range of 75–90%. The unaccounted carbon may be because the unrecovered char/ash deposited on the reactor walls and the gas lines or the soot that escapes the traps. The majority of the carbon is accounted distributed in the gas phase between CO, CO_2, and CH_4. CH_4 was observed in limited quantities <0.1% only for PB at 1000 °C at all CO_2 concentrations. On the other hand, the char particles account for less than 6.5 and 4.5% of the total carbon at the lowest gasification temperature of LY and PB respectively. As expected, the contribution of the chars to the total carbon decreases with increasing temperature and CO_2 concentration-hence conversion, for both LY and PB.

3.2. Gasification performance

3.2.1. Carbon conversion

The carbon conversion in the samples has been calculated on a solids basis. The solid basis calculation considers the ratio between to the total carbon content in the chars recovered to the total carbon in the fuel fed by making use of the ultimate analysis of the chars and the fuels respectively.

Carbon conversion during gasification is a function of the temperature and CO_2 concentration in the feed gas. The conversion trends were consistent between the solid basis and gas basis calculations. However, the solid basis and gas basis conversion is varying by 5–10% in most cases and by about ~17% in the case of PB 1000 °C and 1200 20% CO_2. The difference between these calculations may be due to a range of factors including incomplete solid recovery or the overestimation of CO_2 fed or inaccuracy of the gas analysis. The observations and inferences drawn from Fig. 2 are as follows:

- The carbon conversion is a stronger function of temperature than CO_2 concentration. As observed in the case of LY and PB, the increase in CO_2 concentration results only in a maximum increase of 6%-points at lower temperatures, but the temperature rise results in the increase of 8%-points in the case of LY and 10%-points in the case of PB. The conversion values for PB is significantly higher compared to LY at 1200 °C, based on the solids basis calculations.
- The CO_2 requirement for gasification is an industrially relevant parameter that is to be obtained from lab-scale gasification studies. Considering equilibrium conditions, pure CO_2 feed under the reaction conditions (residence time and temperature) approximately, 2 LCO_2/g carbon fed is required. As seen from Fig. 2, except for 10% CO_2 concentration, the CO_2 is fed in excess. The excess CO_2 released from downstream applications can either be recirculated into the feed stream or be used for chemical synthesis.

3.2.2. Syngas composition

The influence of the temperature and the feed CO_2 concentration on syngas composition (N_2 free basis) from LY and PB gasification is

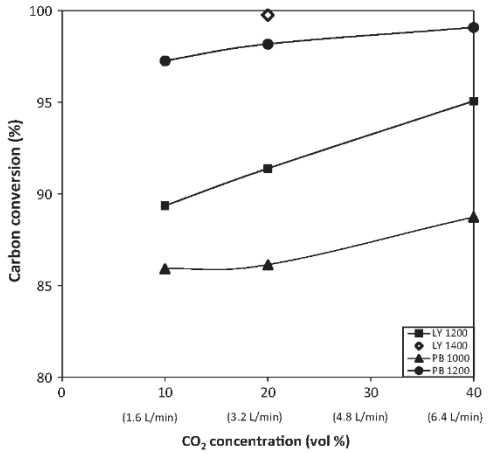

Fig. 2. Carbon conversion on solids basis obtained for LY coal and PB biomass at different temperatures represented as a function of CO_2 concentration in the feed gas. Figures in parenthesis indicate the amount of CO_2 in the feed gas in L/min.

presented in Fig. 3. The CO concentration increases with temperature and decreases with CO_2 concentration in the feed. On the other hand, the production of H_2 decreases with both temperature and CO_2 concentration in feed. With increase in CO_2% in the feed stream, the proportion of unreacted feed CO_2 increases, thus leading to a corresponding decrease in CO and H_2 concentration.

The evolution of the gas composition is due to the following reactions.

Devolatilization $\quad Coal\ or\ biomass \xrightarrow{heat} H_2 + CO + CO_2 + CH_4 + others$

Boudouard reaction $\quad C + CO_2 \leftrightarrow 2CO$

Steam gasification $\quad C + H_2O \leftrightarrow CO + H_2$

Water Gas Shift Reaction $\quad CO + H_2O \leftrightarrow CO_2 + H_2$

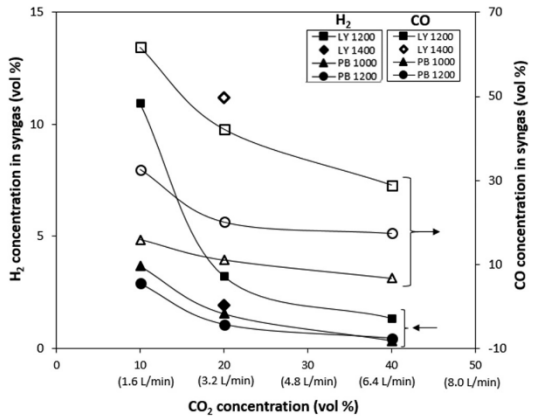

Fig. 3. Syngas composition (N_2 free basis) obtained for LY coal and PB biomass at different temperatures represented as a function of CO_2 concentration in the feed gas. Figures in parenthesis indicate the amount of CO_2 in the feed gas in L/min.

The devolatilization of the fuels results in the formation of gaseous species including H_2, CO, CO_2, CH_4 and several other organic components. The consumption of the carbon in the fuels occurs predominantly through the Boudouard reaction and the steam gasification reaction that consume CO_2 and H_2O. The higher CO with increasing temperature in Fig. 4 is due to higher carbon conversion. However, qualitatively the steam gasification component is minor due to the low moisture content in the feed. In addition, the contribution of water gas shift is significant in altering the overall gas composition [16]. At higher CO_2 concentration in the feed, the equilibrium favours the reverse reaction that results in the further formation of CO and H_2O.

The net concentration of CO_2 in the outlet stream is a consequence of various phenomena such as the CO_2 generation during devolatilization, consumption in the Boudouard reaction and the reverse water gas shift reaction, and as unreacted feed. It is not possible to decouple these effects in an entrained flow gasifier of this scale. However, the influence of pyrolysis on the overall gas composition has to be investigated. Moreover, the CO_2 released during pyrolysis does result in further gasification in-situ, thereby increasing the CO concentration in the product gas. Further investigations using analytical techniques such as the TG-FTIR/TG-MS under controlled conditions are required to assess the contribution of each of these factors individually.

Comparison between the fuels on the overall gas composition indicates that CO/H_2 ratio of the fuels is lower for LY sample (13:1) compared to the PB (18:1) at 1200 °C 20%CO_2. The CO/H_2 ratio for LY varied between in the range of 5:1–21:1 whereas for PB the ratio ranged between 4:1 and 38:1. The lower syngas ratios are at the lowest temperature i.e., 1000 °C for PB and 1200 °C for LY at 10% CO_2 in N_2 as the gasifying agent. However, these conditions do not result in conversions ~100%. Therefore, the realistic CO/H_2 ratio to be expected from CO_2 gasification of these fuels under entrained flow conditions is in the range of 20:1–30:1.

The syngas generated from CO_2 gasification is expected to be CO-rich. If the gasification is planned for chemical synthesis, this ratio may not be suitable. Therefore, the syngas ratio will have to be adjusted using the water gas shift reaction to lower the syngas ratio typically down to 2:1 (for methanol) [23,24].

However, on the other hand, if power generation is the objective of gasification, then the heating values for the syngas generated are to be considered. The heating values presented in Table 2 are in N_2 free basis. The heating values (HHV) for the LY (3.58–8.48 MJ/m^3) are higher than for PB (0.89–4.24 MJ/m^3). Considering the fact that the exit gas composition are dilute with CO_2, the low heating values are expected. Therefore, even for power generation, the water gas shift reaction has to be carried out to improve the heating value of syngas.

3.3. Pollutant gas emission

The influence of the temperature and CO_2 concentration on H_2S, HCN, and NH_3 release is shown in Tables 3 and 4 respectively. The concentration of these pollutants in the ppmv range both the fuels. However, there is a significant difference between the concentration of these pollutants released during the gasification of LY and PB. The findings are summarized below:

- Considering H_2S, the LY sample releases significantly higher H2S compared to PB. The concentration range is between 40 and 80 ppmv; whereas for PB, the concentration is relatively negligible at 2.5 ppmv. The result is interesting since both LY and PB have very low sulfur contents around 0.12 and 0.13 wt %. Therefore, the large difference in H_2S release profiles has to be attributed to the nature of the sulfur in the organic matrix. In LY coal, about 60% of the sulfur is known to be organically

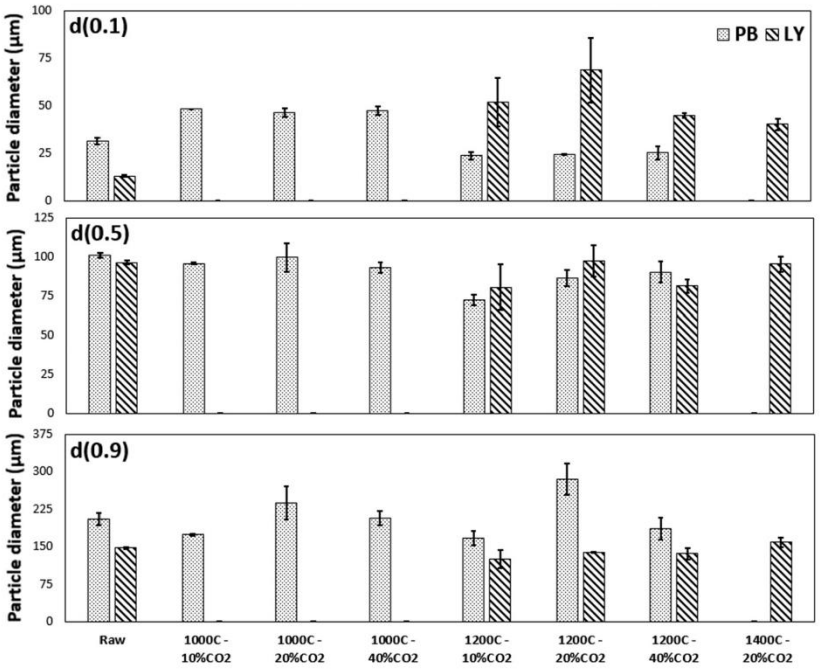

Fig. 4. Particle size distribution for the raw sample and the chars of (a) LY (b) PB.

Table 2
LHV and HHV in (N_2 free basis) of LY and PB.

Fuel	Temperature (°C)	Atmosphere	LHV (MJ/m^3)	HHV (MJ/m^3)
LY	1200	10% CO_2	8.68	8.48
	1200	20% CO_2	5.42	5.36
	1200	40% CO_2	3.60	3.58
	1400	20% CO_2	6.16	6.13
PB	1000	10% CO_2	2.59	2.70
	1000	20% CO_2	1.56	1.60
	1000	40% CO_2	0.88	0.89
	1200	10% CO_2	4.18	4.24
	1200	20% CO_2	2.48	2.50
	1200	40% CO_2	2.12	2.13

Table 3
The effect of temperature on the H_2S, HCN, and NH_3 release of Loy Yang coal and pine bark.

Fuel	LY		PB	
CO_2 concentration in N_2 (vol.%)	20		20	
Temperature (°C)	1200	1400	1000	1200
Pollutant gas (ppmv)				
HCN	30	0.5	12.5	15.33
H_2S	45	65	2.5	2.5
NH_3	0	0	>3	>3

bonded resulting in H_2S release. In PB, on the other and, most of the sulfur is inorganically bonded. In PB and in biomass in general, the sulfur produced mainly through the thermal cracking and hydrogenation of the sulfur-containing molecules [25]. Moreover, the S present in the mineral matter can contribute to the H_2S release. The H_2S release in coals may be due to two factors; the thermal decomposition of organic sulfur at higher temperatures [26] and the consumption of H_2S to form COS by the reaction given below.

$$H_2S_{(g)} + CO_{2_{(g)}} \leftrightarrow COS_{(g)} + H_2O_{(g)}$$

The former explains the increase in H_2S release with temperature and the latter explains the decrease in H_2S with increasing CO_2 in the feed gas.

- The HCN evolution from LY did not change with CO_2 concentration at 1200 °C. However, at a constant CO_2 concentration, when the temperature was increased from 1200 °C to 1400 °C the

Table 4
The influence of the CO_2 concentration on H_2S, HCN, and NH_3 release of Loy Yang coal and pine bark.

Fuel	LY			PB		
Temperature (°C)	1200			1200		
CO_2 concentration in N_2 (vol.%)	10	20	40	10	20	40
Pollutant gas emission (ppmv)						
HCN	29	30	30	15.3	10	5
H_2S	84.5	45	41	2.5	2	1
NH_3	0	0	0	>3	20	7

HCN evolution reduced drastically. On the other hand, for PB, the increase in CO_2 concentration significantly reduced the HCN evolution while the temperature increase from 1000 °C to 1200 °C resulted only in a marginal increase in HCN concentration. The formation of HCN is due to the thermal cracking of the nitrogen containing compounds such as pyridines and pyrroles in the volatiles. In the case of the PB and other biomass, the nitrogen is majorly released into the volatile phase that possibly results in the formation of HCN where as in the case of LY some of the nitrogen may be retained in the char. The HCN formed may then be oxidised at higher temperatures with O-radicals and OH-radials at a higher temperature through the following reactions to cause a decrease in HCN with temperature for LY.

$$HCN + O \leftrightarrow NH + CO$$

$$HCN + OH \leftrightarrow CN + H_2O$$

- No NH_3 was detected for the LY whereas NH_3 was detected in larger quantities in PB·NH_3 is the dominant contaminant released during biomass gasification that is formed due to thermal cracking and the steam reforming of N-containing organics. However, in the case of LY, the char bound N is typically heteroatomic that results in the formation of HCN [19]. Further, it is also observed that NH_3 decreases with CO_2 concentration in PB. This is due to the destruction of NH_3 under oxygen to release nitrogen and steam [27].

The results presented in Tables 3 and 4 indicate that level of pollutants in this study is much higher than the tolerance limits (typically in the ppbv range) for the chemical synthesis applications [28]. This fact necessitates the removal of HCN, NH_3, and H_2S from syngas of LY and PB through the installation of gas cleaning systems.

3.4. Char characterization

3.4.1. Particle size distribution

Fig. 4 summarizes the particle size distributions of the various chars of LY and PB samples. The comparison has been made in terms of $d(0.1)$, $d(0.5)$, and $d(0.9)$ which have been defined as the particle size at 10, 50 and 90% of the total volume distribution. For the LY samples in Fig. 4, the chars have the similar $d(0.9)$ values of around 150 μm compared to the parent coal. Further, a similar trend is observed in the d(0.5) values that are consistently in the mean particle size range of 90–106 μm. However, in the case of $d(0.1)$, there is a significant increase in the size of the chars compared to the parent coal. From Fig. 4, no conclusive trend for evolution of particle size for the LY chars with both CO_2 concentration and temperature is evident. However, the d(0.1) of reduced by 10–15 μm when the temperature increased from 1200 to 1400 °C at 20% CO_2.

On the other hand, in the case of PB, all the observations made for the LY coal are consistent; however, a large variance is observed in the d(0.9) values. The large variance may be due to the char particle agglomeration at higher temperatures resulting in particles with much larger sizes. Another observation that is not consistent with LY is that the d(0.1) values at the higher temperature are lesser than the raw biomass.

The particle sizes of chars are primarily a result of three factors, namely, particle agglomeration/sintering, swelling and particle fragmentation. Agglomeration/coalescence of the char particles occurs due to the melting mineral constituents. The ash composition and fusion plays an important role in determining the agglomeration between char particles. Agglomeration has been observed for both coal and biomass in fluidized bed gasifiers which result in particle de-fluidization problems [9]. The swelling of the fuel matrix at high temperatures is a result of the rapid devolatilization. Victorian brown coals are not known to swell or develop plasticity. On the other hand, biomass (wood bark), is known to swell upon devolatilization [30]. However, the swelling properties of biomass under entrained flow gasification (temperatures and heating rate), to our knowledge, has not been determined yet.

Conversely, the fragmentation/disintegration phenomenon results in the particle size reduction of the relatively softer char particles. The char particle fragmentation occurs due to the inter-particle collision and collision of the particles with the reactor walls as the particles descend down the reactor.

While the particle agglomeration and swelling generally account for the increase in the particle size of the chars with respect to the parent fuel, the particle fragmentation explains for the decrease in the d(0.1) for PB with an increase in temperature. Although from this study it is not possible to conclusively state which one of the above phenomena are more dominant for coal and biomass, it can be speculated that the biomass char particles are more susceptible to agglomeration (higher d(0.9) values shown in Fig. 4) compared to the coal due to its significantly lower AFT. The fragmentation of the chars is also validated by the scanning electron microscopy (SEM) presented in Fig. 5.

3.4.2. Morphology

The SEMs of the char samples were obtained in both the secondary electron and the backscatter mode. However, in Fig. 5, only the backscatter images of chars are shown as they depict the internal pore structure and the mineral matter presence with greater contrast as opposed to the secondary electron images where only the topological information is obtained. The particles selected for analysis include the carbon rich and the mineral-rich particles. Some of the general observations are as follows.

- The particle size for the char samples is significantly lower than the parent fuel as observed from a relatively lower magnification of 150×. The images are shown in Fig. 5(b), (c) and (e), (f) obtained at 2500× magnification demonstrate the decreasing particle size with temperature.
- In the parent fuel, the PB sample had a fibrous structure whereas the LY was characteristic of a dense smooth surface. A large variation was observed in the appearance of the char particles of these fuels. The carbon-rich char particles were distorted in appearance compared to the mineral rich ones which appeared to retain their original shape or take a spherical shape due to the mineral melting. The mineral constituents in the chars at the highest temperatures were found on the surface of the particle.

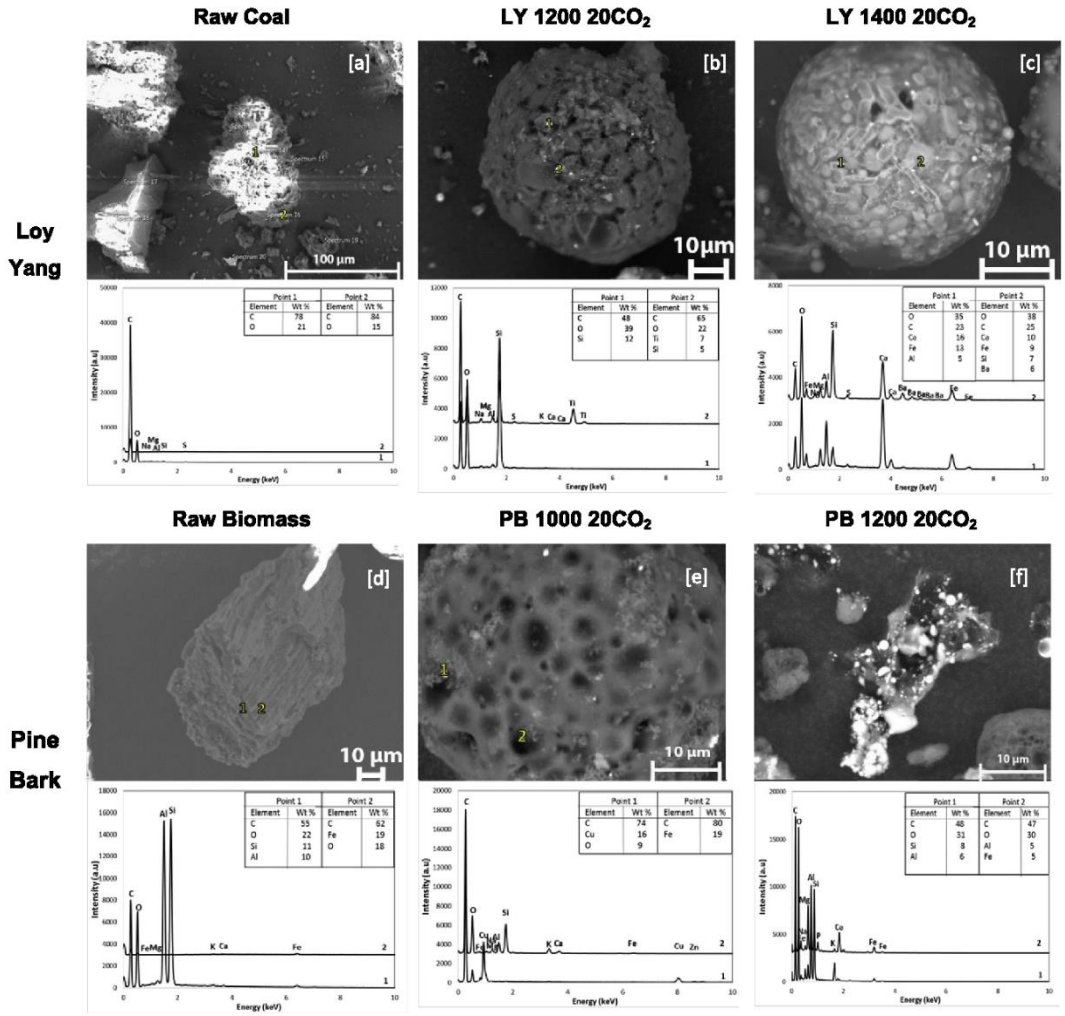

Fig. 5. Scanning electron micrographs and EDX spectra for the raw sample and the chars. The elements with less than 5 wt% are not reported in the EDX spectra.

The EDX results aid in indicating the possible mineral composition at specific locations within the particles. For all the samples, the EDX spectra qualitatively indicate the presence of alkali/alkaline earth metal based (K, Na, Ca, Mg) aluminosilicates. Moreover, in certain locations of the biomass chars, the presence of Fe and *trace* Cu and Zn was detected. On the other hand, for coal, the presence of Na and Ti were more frequently detected, as expected from their higher inherent presence in the LY compared to PB. The detail examination of the mineral matter composition is presented in the next section.

3.5. Mineral matter characteristics

3.5.1. Thermochemical calculations

Thermochemical calculations were performed in the 'equilib' module in the FACTSAGE software version 6.4 in order to predict the possible equilibrium products for the fuels under all the reaction conditions. The calculations were compared qualitatively with the XRD patterns. However, it is expected that only the crystalline phases of the predicted minerals would match with the diffractograms.

The inputs for the calculations were the ultimate analysis and the mineral composition of the raw fuels, and the reacting conditions such as the reactant gas composition (10, 20, 40%CO_2 in N_2), pressure of 1 atm and a temperature of (1000, 1200 and 1400 °C). For the raw fuel, however, the predictions were made at a temperature of 600 °C under air atmosphere at 1 atm pressure, to account for the possible mineral interactions/transformation during the ashing procedure. The list of predicted solid phases is summarized in Table 5.

From the calculation results, it was observed that there was no significant difference in the equilibrium predictions with increasing CO_2 concentration. Further, from stoichiometry, as the CO_2 in the feed is in excess for all the CO_2 concentrations used, the effect of CO_2 on the diffractograms is expected to be insignificant.

Therefore, only the effect of temperature is emphasized in further discussion. For all the samples, there is a reasonable qualitative agreement between the equilibrium predictions and the diffraction patterns as shown in Fig. 6. However, some of the compounds that were predicted could not be detected in the diffractograms, possibly due to their amorphous or weak crystalline nature. For the raw LY samples, major minerals predicted include albite, cordierite, sodium sulfate, anhydrite, hematite, rutile, sapphirine whereas for the raw PB sample the list included the kaliophilite, monticellite, comberite, potassium aluminate, merwinite, and fairchildite. The differences in the predictions for LY and PB are consistent with the mineral composition presented in Table 1. In LY samples, the greater sodium content is in the form of sodium-alumino silicates and sodium sulfate, where as in the case of PB, Na was predicted to be present along with Ca in combeite and to some extent in sodium titanate that was not detected in the diffractograms. Due to the larger Ca content in PB, the majority of the compounds predicted had calcium in silicates and carbonates; where as in LY, Ca was predicted only to be present as $CaSO_4$ (anhydrite).

3.5.2. Crystalline constituents and mineral transformation

The peaks detected in the XRD patterns and the corresponding match with the pure mineral have been classified as the following in accordance with Bhattacharya and Harttig [29]: dominant >60%; Co-dominant-sum of phase >60%; sub-dominant, 20–50%; minor, 5–20%; trace, <5%. As the CO_2 concentration in the reactant gas, did not have any effect on the thermochemical calculations, the mineral identification in the XRD patterns was carried out only for 20%CO_2 concentration across all the char samples for effective comparison. The results of the classification are presented in Table 6. The salient observations are as follows:

- Silica species are the dominant phase for both the coal and the biomass samples. β-quartz was the detected phase for both the raw fuels and all the samples post-gasification.
- Negligible change in the high melting minerals was detected as they were observed consistently (in the same concentration range) in both chars at both the temperatures for LY and PB. However, in some of the lower melting minerals, structural changes were observed. For instance, in the coal samples, albite a sodium alumino-silicate with a melting point of 1100 °C undergoes a structural transformation from an ordered structure in 1200 °C chars to a disordered structure in 1400 °C chars.
- The sodium in the crystalline minerals of the coal is mainly in the form of albite, aphthitalite and sodium sulfate. Aphthitalite and sodium sulfate, both low melting minerals (880–890 °C), do not occur in any of the char samples. However, in the char samples, two other sodium alumino-silicates were detected. Na released from the organic matrix may be captured and retained in the ash by charge compensation with the Al-Si matrix [20]. In LY, at 1200 °C, nepheline was detected, at 1400 °C the nepheline phase was absent and low-carnegieite was detected. In the case of raw PB, the sodium is present only in combeite as shown in the diffraction patterns, whereas in the chars, nepheline is the only mineral phase that appears to contain Na.
- The potassium in the crystalline phases in raw PB is present predominantly as kaliophilite and fairchildite phase. Kaliophilite that does not appear to transform in the chars as well. Potassium occurring in clays is considered inert as it does not tend to participate in reactions. This helps explain the predominant occurrence of K in the chars only in kaliophilite. In LY too, the potassium is present in a high melting alumino-silicate (leucite), however, only in trace quantities.
- The majority of the calcium in the crystalline phases of PB occurs in combeite, merwinite, monticillite, and calcite. The calcium presence is noticed in most of the minerals. At higher

Table 5
Chemical formula and the melting point of the detected mineral phases.

Phase	Chemical formula	Temperature predicted				Melting point (°C)
		600 °C	1000 °C	1200 °C	1400 °C	
Al_2O_3	Al_2O_3	LY PB				–
Albite	$Na(AlSi_3O_8)$	LY		LY	LY	1100
Alumina	Al_2O_3					2072
Anhydrite	$CaSO_4$	LY				1450
Anorthite	$Ca(Al_2Si_2O_8)$			LY	LY	1274
Aphthitalite	$(K,Na)_3Na(SO_4)_2$	LY				888
Calcite	$CaCO_3$	PB		PB		1339
Combeite	$Na_2Ca_2Si_3O_9$	PB				–
Cordierite	$(Mg,Fe)_2Al_3(AlSi_5O_{18})$	LY				1470
Fairchildite	$K_2Ca(CO_3)_2$	PB				809
Forsterite	Mg_2SiO_4			LY	LY	1890
Hematite	Fe_2O_3	LY				1538
Ilmenite	$Fe^{2+}TiO_3$			LY	LY	1800
Kaliophilite	$KAlSiO_4$	PB	PB	PB		1800
Potassium aluminate	$KAlO_2$	PB				–
Leucite	$K(AlSi_2O_6)$			LY	LY	1686
Low-carnegieite	$NaAlSiO_4$				LY	1526
Merwinite	$Ca_3Mg\ (SiO_4)_2$	PB	PB	PB		1575
Monticellite	$Ca(Mg,Fe)SiO_4$	PB		PB		1503
Nepheline	$NaAlSiO_4$		PB	LY PB		1250
Periclase	MgO		PB			2800
Perovskite	$CaTiO_3$			PB		1975
Pyrite	FeS_2	LY				1180
Quartz	SiO_2	LY PB	LY PB	LY PB	LY PB	1670
Rutile	TiO_2	LY				1843
Sapphirine	$Mg_4Al_{10}Si_2O_{23}$	LY		LY	LY	1475°
Sodium sulfate	Na_2SO_4	LY				884
Spinel	$MgAl_2O_4$			PB		2135
Ulvospinel	Fe_2TiO_4			LY		1395
Vaterite	$CaCO_3$		PB	PB		1339
Wustite	FeO		PB	PB		1377

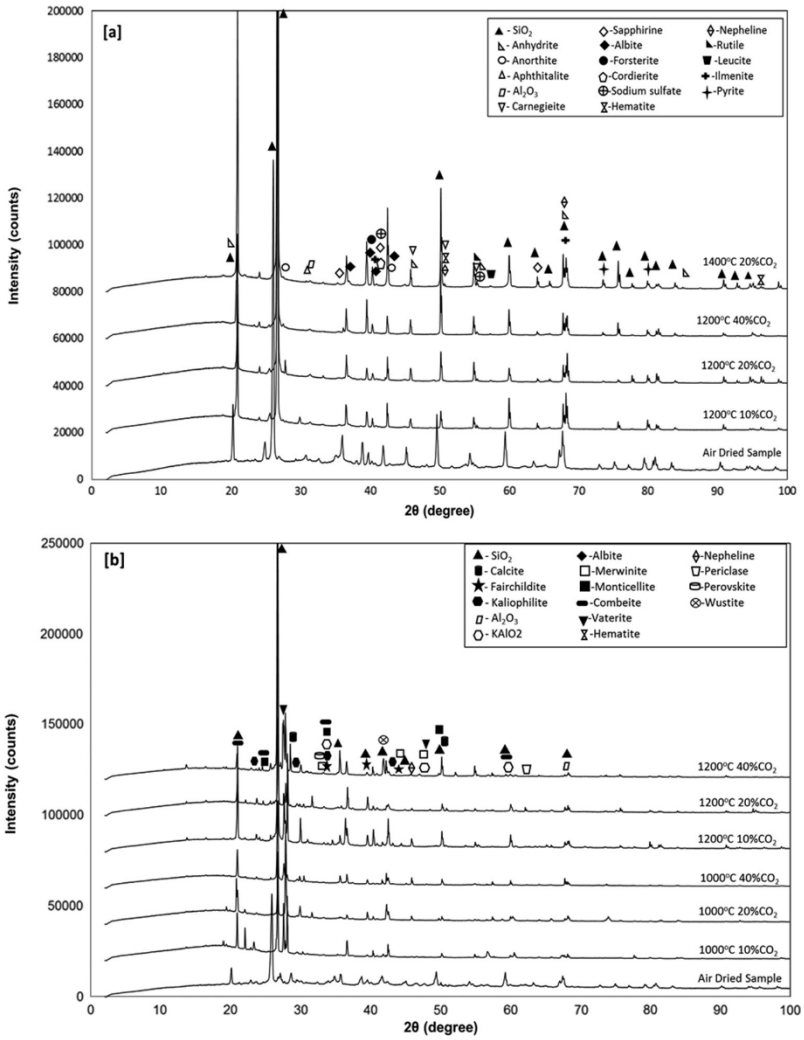

Fig. 6. X-ray diffractograms for the ash prepared from the raw sample and the chars of (a) LY (b) PB.

temperatures, however, the majority of the Ca exists as monticellite and calcite. On the other hand, in LY coal, the Ca in anhydrite ($CaSO4$) is possibly incorporated into anorthite ($CaAl_2Si_2O$) apart from forming calcite (although not detected in the XRD pattern). The calcite at high temperatures form as a result of the recarbonation reaction that occurs between the CaO (produced by oxidation of Ca released at low temperatures) with CO_2 in the gas atmosphere.

$$CaO(s) + CO_{2(g)} \leftrightarrow CaCO_{3(s)}$$

The re-carbonation reaction is known to cause fouling on the reactor walls in some cases (600 °C < T < 800 °C) [31].

- In PB, it is observed that the Mg is typically contained in the form of silicates such as monticellite and merwinite. In the chars samples of biomass periclase (MgO) is present at 1000 °C chars. Due to decomposition, the Mg released may have been incorporated into the Al matrix resulting in the formation of spinel ($MgAl_2O_4$) in the 1200 °C chars. In the LY coal and chars, the Mg content is in the form of sapphirine ($Mg_4Al_{10}Si_2O_{23}$), a stable, high melting alumino-silicate.

3.5.3. Implications on ash fusibility and slag viscosity

The differences in the mineral matter composition influences the ash deposition, slag formation, slag viscosity, and the refractory life [32]. As shown in Table 1, flow temperature of LY > 1500 °C is higher than that of PB by at least 264 °C. One of the common indices to correlate the AFT to the ash composition is the alkali index determined by Eq. (5) [20]. In general, higher the alkali index, higher the AFT.

$$Alkali\ Index = Ash\ (\%)\frac{Fe_2O_3 + CaO + MgO + Na_2O + Fe_2O}{SiO_2 + Al_2O_3} \quad (5)$$

Table 6
Mineral composition in the chars of LY and PB samples.

Fuel	Sample	Mineralogical composition				
		Dominant phase(s)	Co-dominant phase(s)	Sub-dominant phase (s)	Minor phases (s)	Trace phase (s)
LY	Coal ash	β-Quartz			Albite (ordered) Anhydrite Hematite Sodium sulfate Sapphirine FeS_2	Cordierite Reutile Aphthitalite Al_2O_3
	1200 20CO_2 ash	β-Quartz		Anorthite	Albite (ordered) Nepheline	Forsterite Ilmenite Leucite Ulvospinel (amorphous)
	1400 20CO_2 ash	β-Quartz				Albite (disordered) Anorthite Sapphirine Forsterite Ilmenite Low carnegieite Leucite
PB	Biomass ash	β-Quartz		Combeite	Alumina Kaliophilite $KAlO_2$ Merwinite Monticellite	Calcite Fairchildite Vaterite
	1000 20CO_2 ash	β-Quartz			Merwinite Periclase Wustite	Kaliophilite Nepheline
	1200 20CO_2 ash	β-Quartz			Calcite	Kaliophite Merwinite Monticellite Nepheline Perovskite

However, for the fuels investigated, both LY (0.041) and PB (0.044) have similar alkali index. Therefore, the alkali index is not sufficient to explain the large difference in AFT in this case.

Possible reasons for the larger AFT for LY may be obtained from a deeper analysis of the ash composition. From the analysis of 43 ash samples, Vassilev et al. suggest the relative influence of the oxides for increasing hemi-spherical temperature is in the order $TiO_2 > Al_2O_3 > SiO_2$ and decreasing hemispherical temperature is in the order of $SO_3 > CaO > MgO > Fe_2O_3 \geq Na_2O$; and K_2O shows intermediate behaviour [33]. The larger presence of Al_2O_3 and TiO_2 in LY samples may explain the higher AFT in LY and the lower AFT in PB may be due to the larger presence of CaO and K_2O. Further, the origin of mineral matter was also found to correlate with the hemi-spherical temperatures [33]. It is evidenced from the XRD analysis that the LY ash consists of mineral phases such as quartz and feldspars such as albite and anorthite that lead to higher AFT. On the other hand, PB is characteristic of minerals such as calcites and fairchildite that possibly result in a lower AFT.

During the gasification of the fuels, the minerals undergo various physico-chemical changes to result in an extremely heterogeneous and complex mixture. Among the various minerals, the presence of silicates increases the AFT; on the contrary, the presence of oxides, carbonates, sulfates, sulfide and partly oxide proportions decreases the AFT [33]. The role of sulfur in coal is critical as it leads to the formation of sulfate minerals of Ca and Mg at high temperature ashes that possess fluxing action. In S-deficit fuels such as the Victorian brown coal and biomass, Ca and Mg are expected to form oxides-hydroxides and silicates that rise AFT. In general, it has been observed that higher AFT ashes contain minerals with high melting temperature and low AFT ashes contain lower melting minerals [33]. However, from the observations made in the previous section, it is evident that both the LY and PB char samples consists of minerals with a wide range of melting points. While the LY ashes consists predominantly alumino-silicates and the PB ash contains carbonates, silicates, and alumino-silicates to a lesser extent. The low melting minerals such as sodium sulfate and fairchildite in PB would not cause problems as they are expected to form slag in the operating temperature range of entrained flow gasifiers. In addition, the high melting minerals would not contribute to slag formation. However, the interaction and behaviour of the various minerals resulting in the formation of secondary reaction products and eutectic mixtures whose melting temperature is a function of composition are to be investigated in greater depth.

Apart from the ash fusibility characteristics, it is critical to determine the slag viscosity as a function of temperature for the operation of a slagging gasifier. The slag viscosity is acceptable in the range of 15–25 Pa s in an entrained flow gasifier to ensure reliable continuous slag tapping [34]. In attempts to correlate the rheological properties of the slag to the chemical composition, Higman and van der Burgt suggest the correlation between T_{25} and the base-acid ratio [35]. T_{25} is the temperature at which the slag viscosity is 25 Pa s. The base-acid ratio is defined as in Eq. (6).

$$Base{-}acid\ ratio = \frac{Fe_2O_3 + CaO + MgO + Na_2O + Fe_2O}{SiO_2 + Al_2O_3 + TiO_2} \quad (6)$$

Both LY (0.28) and PB (0.29) have close base-acid ratios. The T_{25} values for this base-acid range are expected to be around 1250–1450 °C. However, the correlations based on the various oxides are usually only indicative since the influence of mineral interactions are not accounted, therefore, rheological studies on the slags have to be performed. Moreover, the slag behaviour might be affected by particulate C content, content of iron and operating temperatures in the gasifier [34]. Furthermore, synergistic effects between the blended ashes pertaining to the co-gasification prospects have to be explored.

4. Conclusions

The gasification runs were carried out in the temperature range of 1000–1400 °C and under varying CO_2 concentrations of 10–40% in N_2 in an atmospheric entrained flow reactor. Both the biomass (PB) and the coal (LY) had a residence time of 7–8 s within the reactor under entrained flow conditions. Carbon balance on the system was performed and approximately 75–90% of the carbon was accounted for during the runs.

Both the fuels had similar carbon conversion levels of ~98% at 1200 °C. The conversion increased with temperature and CO_2 concentration in the feed gas. The products included the residual char and the product gases CO, H_2, CO_2, and CH_4. CH_4 was detected only for PB gasification runs at 1000 °C. The product gases were CO-rich as the gasification predominantly occurred through the Boudouard reaction. The CO/H_2 ratios (on N_2 free basis) were approximately 38:1 and 21:1 for PB and LY at 1200 °C and 20%CO_2 in N_2 as the gasifying agent. No tar was visible during all the gasification runs. The emission characteristics of the polluting gases (detected in ppm levels) varied for the fuels. For LY, no NH_3 was detected whereas for PB, no H_2S was detected.

The particle size distributions particularly for PB indicate a decrease in the size of fines with increasing temperature. The same observation was made from the scanning electron micrographs. The mineral composition of the fuels at high temperature was predicted using Factsage. The predictions matched reasonably well with the crystalline minerals identified in the X-ray diffractograms. The mineral identified had a wide range of melting points. However, the melting point and the viscosity of the slag formed is expected to be a function of the interaction between the various minerals. Such parameters have to be investigated in future to comprehensively assess the co-gasification possibility of LY and PB samples.

Acknowledgements

The authors would like to gratefully acknowledge the financial support received from *Australian Research Council*, *Australian Paper*, *Carter Holt Harvey, Orora, Circa, Norske Skog and Visy through the Industry Transformation Research Hub* Grant IH130100016; China Scholarship Council, and Brown Coal Innovation Australia (BCIA). The authors also acknowledge the Australian Research Council's Linkage Infrastructure, Equipment and Facilities Scheme (LIEF 120100141) and the use of facilities within the Monash Centre for Electron Microscopy. The authors would like to thank the undergraduate students Mitchell Fly and Sean McKellar for their assistance during gasification experiments.

References

[1] IEA. World energy outlook 2014. IEA; 2014.
[2] BP. BP statistical review of world energy in: BP, BP Global; 2014. <http://www.bp.com/en/global/corporate/about-bp/energy-economics/statistical-review-of-world-energy/review-by-energy-type/coal/coal-reserves.html>.
[3] Thielemann T, Schmidt S, Peter Gerling J. Lignite and hard coal: energy suppliers for the world needs until the year 2100—an outlook. Int J Coal Geol 2007;72:1–14.
[4] Qi X, Wang D, Xue H, Jin L, Su B, Xin H. Oxidation and self-reaction of carboxyl groups during coal spontaneous combustion. Spectrosc Lett 2015;48:173–8.
[5] Qi X, Wang D, Xin H, Qi G. An in situ testing method for analyzing the changes of active groups in coal oxidation at low temperatures. Spectrosc Lett 2014;47:495–503.
[6] Bhattacharya S, Kabir KB, Hein K. Dimethyl ether synthesis from Victorian brown coal through gasification – current status, and research and development needs. Prog Energy Combust Sci 2013;39:577–605.
[7] U.S. Department of Energy. 2010 worldwide gasification database. Pittsburg, PA: DOE National Energy Technology Laboratory; 2010.
[8] Bauen A, Berndes G, Junginger M, Vuille F. Bioenergy – a sustainable and reliable energy source. IEA Bioenergy; 2009.
[9] Lee JG, Kim JH, Lee HJ, Park TJ, Kim SD. Characteristics of entrained flow coal gasification in a drop tube reactor. Fuel 1996;75:1035–42.
[10] Crnomarkovic N, Repic B, Mladenovic R, Neskovic O, Veljkovic M. Experimental investigation of role of steam in entrained flow coal gasification. Fuel 2007;86:194–202.
[11] Guo X, Dai Z, Gong X, Chen X, Liu H, Wang F, et al. Performance of an entrained-flow gasification technology of pulverized coal in pilot-scale plant. Fuel Process Technol 2007;88:451–9.
[12] Vascellari M, Arora R, Pollack M, Hasse C. Simulation of entrained flow gasification with advanced coal conversion submodels. Part 1: pyrolysis. Fuel 2013;113:654–69.
[13] Vascellari M, Arora R, Hasse C. Simulation of entrained flow gasification with advanced coal conversion submodels. Part 2: char conversion. Fuel 2014;118:369–84.
[14] Tremel A, Haselsteiner T, Kunze C, Spliethoff H. Experimental investigation of high temperature and high pressure coal gasification. Appl Energy 2012;92:279–85.
[15] Harris DJ, Roberts DG, Henderson DG. Gasification behaviour of Australian coals at high temperature and pressure. Fuel 2006;85:134–42.
[16] Qin K, Lin W, Jensen PA, Jensen AD. High-temperature entrained flow gasification of biomass. Fuel 2012;93:589–600.
[17] Butterman HC, Castaldi MJ. CO_2 as a carbon neutral fuel source via enhanced biomass gasification. Environ Sci Technol 2009;43:9030–7.
[18] Billaud J, Valin S, Peyrot M, Salvador S. Influence of H_2O, CO_2 and O_2 addition on biomass gasification in entrained flow reactor conditions: experiments and modelling. Fuel 2016;166:166–78.
[19] Tanner J, Bhattacharya S, Bläsing M, Müller M. High-temperature pyrolysis and CO_2 gasification of Victorian brown coal and Rhenish lignite in an entrained flow reactor. AIChE J 2016;62:2101–11.
[20] Tanner J, Bläsing M, Müller M, Bhattacharya S. Reactions and transformations of mineral and nonmineral inorganic species during the entrained flow pyrolysis and CO_2 gasification of low rank coals. Energy Fuels 2016;30:3798–808.
[21] Bhattacharya SP. Performance of Australian lignites in a pressurized fluidized bed gasifier process development unit under air and oxygen-enriched air blown conditions. Process Saf Environ Prot 2006;84:453–60.
[22] Qin K, Jensen PA, Lin W, Jensen AD. Biomass gasification behavior in an entrained flow reactor: gas product distribution and soot formation. Energy Fuels 2012;26:5992–6002.
[23] Cao Y, Gao Z, Jin J, Zhou H, Cohron M, Zhao H, et al. Synthesis gas production with an adjustable H_2/CO ratio through the coal gasification process: effects of coal ranks and methane addition. Energy Fuels 2008;22:1720–30.
[24] Wender I. Reactions of synthesis gas. Fuel Process Technol 1996;48:189–297.
[25] Hongrapipat J, Pang S, Saw WL. Removal of NH_3 and H_2S from producer gas in a dual fluidised bed steam gasifier by optimisation of operation conditions and application of bed materials. Biomass Convers Bioref 2016;6:105–13.
[26] Tan LL, Li C-Z. Formation of NO_x and SO_x precursors during the pyrolysis of coal and biomass. Part II. Effects of experimental conditions on the yields of NO_x and SO_x precursors from the pyrolysis of a Victorian brown coal. Fuel 2000;79:1891–7.
[27] McKenzie LJ, Tian F-J, Li C-Z. NH_3 formation and destruction during the gasification of coal in oxygen and steam. Environ Sci Technol 2007;41:5505–9.
[28] Higman C, Tam S. Advances in coal gasification, hydrogenation, and gas treating for the production of chemicals and fuels. Chem Rev 2014;114:1673–708.
[29] Bhattacharya SP, Harttig M. Control of agglomeration and defluidization burning high-alkali, high-sulfur lignites in a small fluidized bed combustor effect of additive size and type, and the role of calcium. Energy Fuels 2003;17:1014–21.
[30] Vähä-Savo N, DeMartini N, Hupa M. Combustion of black liquor-solid biomass mixtures in a single particle reactor—characteristics and fate of nitrogen. Energy Fuels 2011;25:4944–51.
[31] Zevenhoven M, Yrjas P, Skrifvars B-J, Hupa M. Characterization of ash-forming matter in various solid fuels by selective leaching and its implications for fluidized-bed combustion. Energy Fuels 2012;26:6366–86.
[32] Krishnamoorthy V, Pisupati SV. A critical review of mineral matter related issues during gasification of coal in fixed, fluidized and entrained flow gasifiers. Energies 2015;8:10430–63.
[33] Vassilev SV, Kitano K, Takeda S, Tsurue T. Influence of mineral and chemical composition of coal ashes on their fusibility. Fuel Process Technol 1995;45:27–51.
[34] Wang P, Massoudi M. Slag behavior in gasifiers. Part I: influence of coal properties and gasification conditions. Energies 2013;6:784–806.
[35] Higman C, Van der Burgt M. Gasification. 2nd ed. New York, NY, USA: Elsevier; 2008.

Chapter 9 Kinetic modelling and application for the entrained flow gasification

9.1 Introduction

Fundamental data on the reaction kinetics is required to evaluate, compare, model and optimize the coal gasification process. However, data on gasification kinetics of Victorian brown coals are limited. While there are several char gasification models, such as the volumetric model (VM), the grain model (GM), the modified volumetric model (MVM) and the random pore model (RPM), in the literature, these models have not been validated for Victorian brown chars with different particle sizes. Therefore, the gasification kinetics of Victorian brown coal chars with CO_2 were investigated in this study, and a numeric model for carbon conversion of Victorian brown coals under entrained flow gasification condition proposed and evaluated by comparing with the experimental results using the EFR.

In this chapter, the effect of temperature, CO_2 concentration, particle size, and the pyrolysis reactor on CO_2 gasification reactivity was investigated using a thermogravimetric analyzer (TGA). Four models – the VM, GM, MVM, and RPM- were employed and compared with the experimental TGA data of two Victorian brown coal chars (YL and MD), the optimal model was identified. The kinetic parameters of CO_2 gasification of Victorian brown chars were then calculated using the optimal model. Based on these calculated kinetic parameters, a numeric model for predicting the carbon conversion under entrained flow gasification condition was proposed. This model is then further evaluated and modified by comparing with the experimental entrained flow gasification data in chapter 5 and 6.

Such information is important for modelling work involving computational fluid dynamics to study the hydrodynamics of the process and to optimize gasifier operating conditions. This study offers a useful mathematical equation for industry to estimate the conversion of Victorian brown coals under entrained flow gasification without experiments.

9.2 Factors influencing gasification reactivity

This section studied the factors, including the temperature, CO_2 concentration, particle size, and pyrolysis, which influences the gasification reactivity of Victorian brown coal using a TGA. In the

light of the findings, the operation parameters of the TGA experiments were chosen to investigate the kinetic model.

The gasification experiments were carried out on a Netzsch STA model 449 F3 Jupiter analyzer. The typical experimental procedure was as follows: the approximate 10mg coal sample was first heated from 25 °C to 200 °C at 5 °C/min with N_2 to remove the moisture from the coal. The sample was then heated to 1000 °C at 10 °C/min with N_2 and maintained at this temperature for 30 mins to release the volatile matter from the coal and make the coal char. After that, the temperature of the TGA decreased or increased to the reaction temperature at 10 °C/min with N_2. After reaching the reaction temperature, the sample was maintained for 30 mins in N_2, and the gas was then switched to CO_2 for char gasification. The char-CO_2 gasification was performed isothermally for 30 mins. The corrections from blank runs under the same experimental conditions were done to negate the effects of the instrument such as gas buoyancy changes and balance drifts.

Experimental TGA data were collected every 3 s, and the conversion of each point was calculated by using the following equation:

$$X = \frac{m_0 - m_t}{m_0 - m_{ash}} \quad \text{(E 9.1)}$$

where m_0 is the initial mass of the char sample before the gas switches to CO_2, m_t is the sample mass at a particular time during char-CO_2 gasification, and m_{ash} is the remaining mass, corresponding to ash content.

9.2.1 Effect of temperature

The effect of temperature on carbon conversion of YL and MD char at 90% CO_2 is shown in Figure 9.1. As can be seen, the carbon conversion of two chars significantly increased with the increasing temperature within the same residence time. This increasing trend as a function of temperature is expected because the main chemical reaction during char-CO_2 gasification is the Boudouard reaction which is endothermic, and the CO_2 gasification is thermodynamically favored. It is found that the residence time for the complete carbon conversion significantly decreased in the temperature range of 750-1000 °C. The time for 50% conversion (t_{50}) decreased by around 50% with an increase of temperature by 50 °C. However, the residence time for the reaction completion decreased slightly when the temperature increased from 1000 °C to 1100 °C. This difference in the increasing percentage of the conversion with the temperature is associated with the effective reaction rate in temperature zones [40]. At low temperatures (Regime I), the reaction rate is controlled by the

heterogeneous reaction between the char and the gas reagent. When the temperature increases to the medium temperature zone (Regime II), the reaction rate is limited by the internal diffusion of gaseous reactants. Therefore, the results indicated that Regime I, the chemical reaction controlled temperature range, is below 1000 °C and the transition between Regime I and Regime II could occur at 1000-1100 °C. Therefore, the experiments were performed at 750- 1000 °C, in Regime I, to test the other factors affecting the gasification reactivity and to obtain intrinsic gasification kinetics of Victorian brown coals.

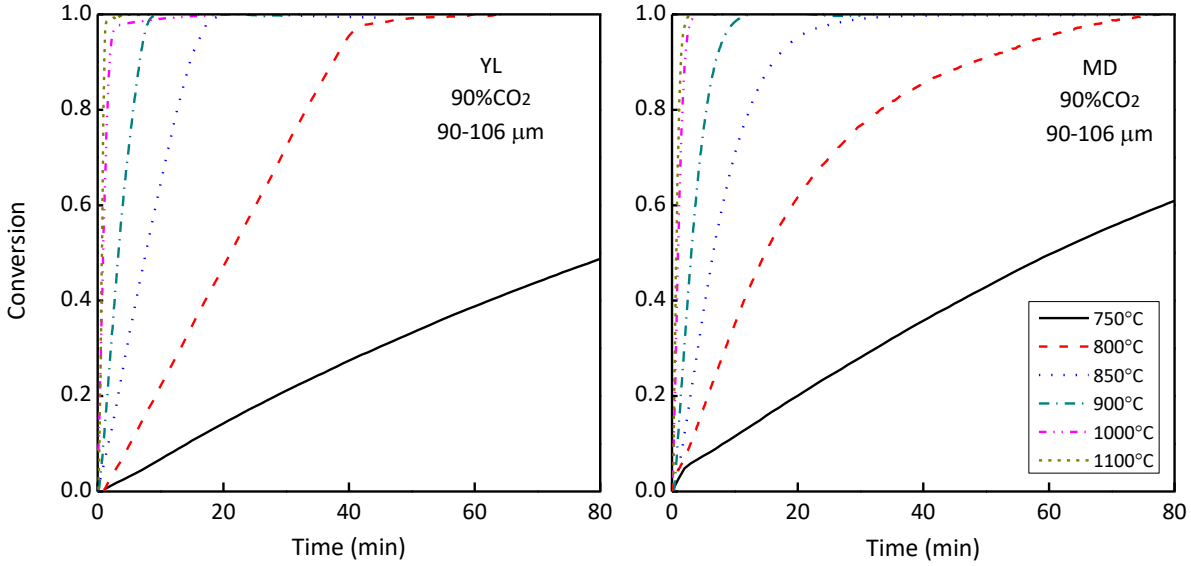

Figure 9.1: Effect of temperature on carbon conversion of YL and MD char at 90% CO_2

9.2.2 Effect of CO_2 concentration

The effect of CO_2 concentration on the carbon conversion of YL and MD char at 800°C is shown in Figure 9.2. As expected, the gasification rate increased with the increasing CO_2 concentration. The t_{50} significantly decreased by 16% when the CO_2 concentration rose from 30% to 50%. As the CO_2 concentration increased to 70%, the gasification rate only increased slightly. The results indicated that increasing CO_2 concentration had a positive effect on the gasification rate of the two chars, especially at low CO_2 concentration. By contrast, the effect of CO_2 concentration can be neglect when the experiments were carried out at a high CO_2 concentration as 90%. The effect of CO_2 concentration on gasification rate is further discussed in section 9.4.

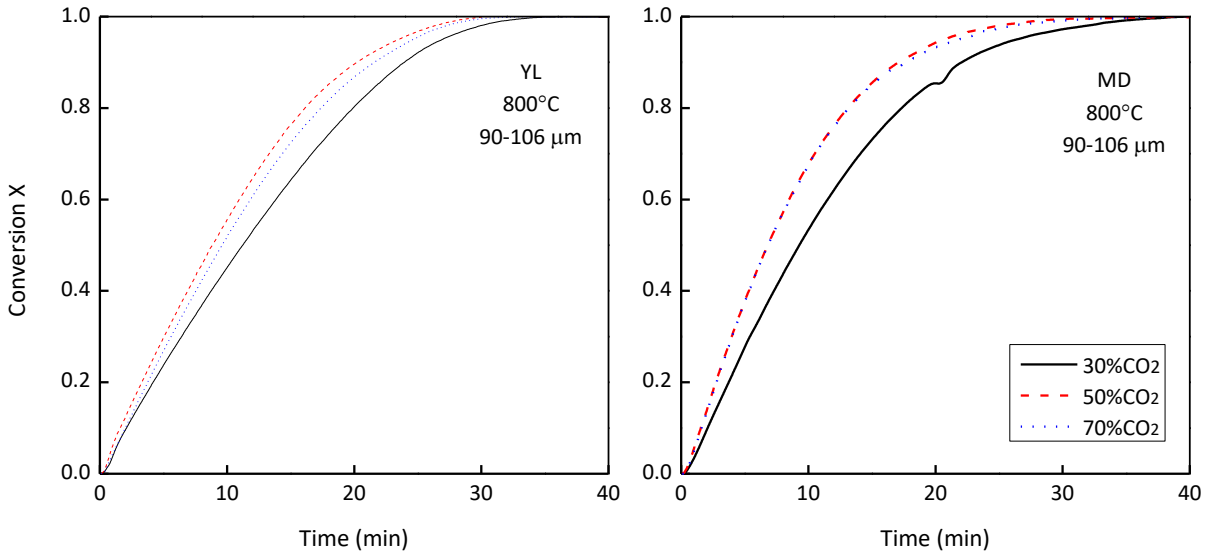

Figure 9.2: Effect of CO_2 on the carbon conversion of YL and MD char at 800 °C

9.2.3 Effect of particle size

The effect of particle size on the carbon conversion of YL and MD chars at 850 °C is shown in Figure 9.3. As can be seen, the carbon conversion of YL and MD chars dramatically increased as the particle size of the chars decreased from 90-106 µm to 63-75 µm. However, when the particle size continued to decrease to 20-38 µm, its effect on the gasification rate showed differently. The carbon conversion of YL chars gradually decreased, whereas the carbon conversion of MD char slightly decreased. Hence, one small particle size (20-38 µm) and one large particle size (90-106 µm) were selected for YL and MD chars to further study the effect of particle size on reaction models in section 9.3 and the gasification rate in section 9.4 at various temperatures.

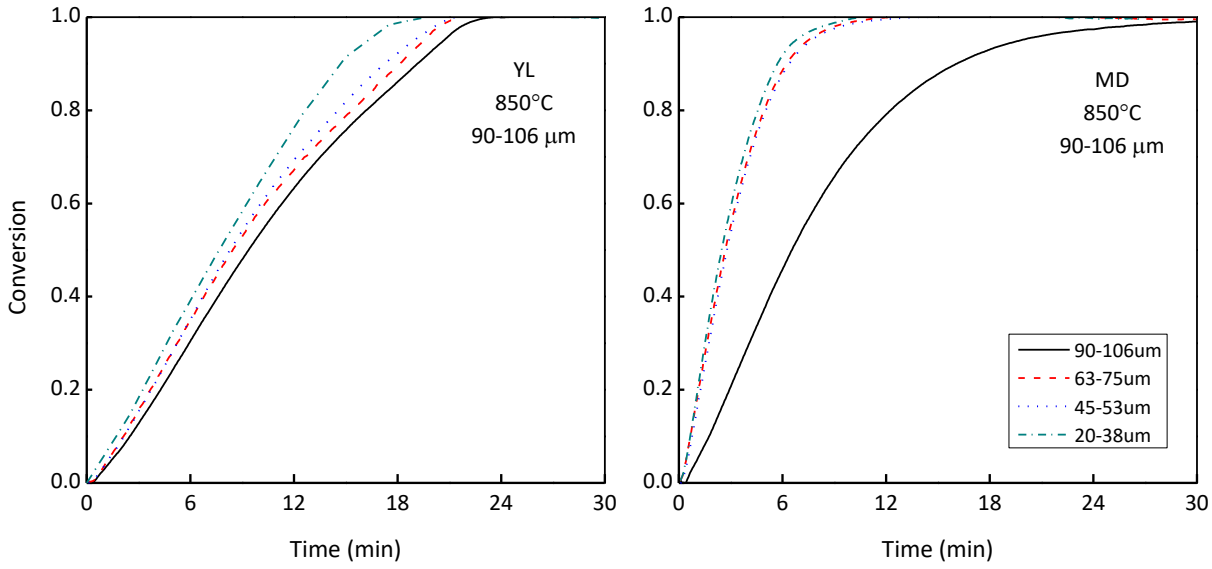

Figure 9.3: Effect of particle size on the carbon conversion of YL and MD chars at 850 °C.

9.2.4 Effect of pyrolysis reactors

Some studies have shown that pyrolysis affects the coal reactivity regarding the pyrolysis temperature, the heating rate, residence time, and gas atmosphere [58, 89, 90]. Different reactors using different heating rate, residence time, and gas atmosphere affect the properties of generated chars, resulting in different gasification reactivity. In this section, the char was generated from two reactors at 1000 °C to test its effect on gasification reactivity. The two reactors and the corresponding char preparation procedure are presented as follows:

- A thermogravimetric analyzer (TGA). The coal samples were loaded into the container of the TGA before the experiments. The coal samples were heated from 25 °C to 1000 °C at a heating rate of 10 °C/min with N_2. The samples were then maintained isothermally at 1000 °C for 1 hour to produce the char.
- Entrained flow reactor (EFR). The coal samples were loaded in the screw feeder outside of the EFR before the experiments. The entrained flow reactor was first electrically heated to 1000 °C with N_2 and maintained at this temperature. Coal samples were then fed and entrained by the inlet gas into the reactor. The coal samples were pyrolyzed in the reactor with a gas residence time of around 7 s, and the generated char was collected from the bottom of the reactor.

The effect of the chars generated from the TGA and EFR on carbon conversion of YL and MD chars at 800 °C is shown in Figure 9.4. As can be seen, the EFR chars of YL and MD had significantly

higher gasification reactivity than the TGA chars. The t_{50} of EFR chars of YL and MD was reduced by around 25% and 67%, respectively, compared with their corresponding TGA chars. The effect of TGA and EFR chars on the gasification rate of YL and MD char is further discussed in section 9. 4.

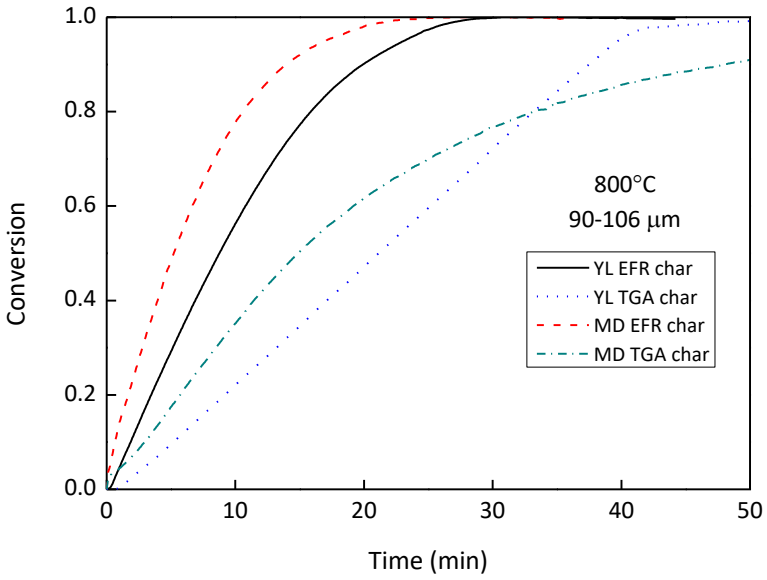

Figure 9.4: The effect of the chars generated from the TGA and EFR on carbon conversion of YL and MD char at 800 °C

In summary, the gasification conversion rate increased with increasing temperature and CO_2 concentration, and decreasing particle size. Chars prepared in the entrained flow gasifier achieved a higher gasification reactivity than that of the thermogravimetric analyser. In order to further investigate the effect of these factors on gasification rate using a reaction model, the TGA experiments were performed at 750-1100°C and 30%-90% CO_2 using the chars generated from the TGA and EFR with particle sizes of 20-38 µm and 90-106 µm.

9.3 Selection and validation of the reaction model

9.3.1 Reaction models

Different models have been proposed to describe the coal char gasification reaction with CO_2. In this section, four models, based on one-step solid-gas reaction, were selected to fit the experimental TGA data.

The first one is the volumetric model (VM), in which it is assumed that the gas reacts homogeneously with the char. The reaction rate is expressed as [89]:

$$\frac{dX}{dt} = k_{VM}(1 - X) \qquad \text{(E 9.2)}$$

The second model is the grain model (GM), also known as the shrinking model, in which the char particle is considered as a spherical grain, and it is assumed that the chemical reaction only occurs on the external surface [58]. The reaction rate is expressed as:

$$\frac{dX}{dt} = k_{GM}(1-X)^{\frac{2}{3}} \quad \text{(E 9.3)}$$

The third model is the modified volumetric model (MVM) developed by Kasaoka et al., in which the volumetric model is modified by adding a new parameter-the time power (b) [75]. The reaction rate is expressed as::

$$\frac{dX}{dt} = k_{MVM}(\mathrm{X})(1-\mathrm{X}) \quad \text{(E 9.4)}$$

$$-\mathrm{In}(1-\mathrm{X}) = \mathrm{a}t^{b} \quad \text{(E 9.5)}$$

where a and b are empirical constant, the $k_{MVM}(\mathrm{X})$ is the kinetic parameter of the model and it is expressed by the following equation:

$$k_{MVM}(\mathrm{X}) = a^{\frac{1}{b}}b\lfloor -In(1-X)\rfloor^{\frac{b-1}{b}} \quad \text{(E 9.6)}$$

The kinetic parameter can be presented using the mean value of the rate constant:

$$\bar{k}_{MVM} = \int_0^1 k_{MVM}(\mathrm{X})\, dX \quad \text{(E 9.7)}$$

The fourth model is the random pore model (RPM) presented by Bhatia and Perlmutter, and it assumed that the random overlapping of pore surfaces [61]:

$$\frac{dX}{dt} = k_{RPM}(1-\mathrm{X})\sqrt{1-\psi In(1-X)} \quad \text{(E 9.8)}$$

$$\psi = \frac{4\pi L_0(1-\varepsilon_0)}{S_0^2} \quad \text{(E 9.9)}$$

where the ψ is the model parameter, S_0, L_0, and ε_0 present the surface area, pore length, and solid porosity, respectively.

Overall, VM and GM do not account for any change in the internal structure. The MVM expression gets closer to the RPM model by adding a reaction order (b), where a two-order polynomial is the power of the time. Of these models, the RPM is the most commonly used model for experimental kinetic data because it can explain a maximum reaction rate during the initial step of gasification. However, a recent study has reported that the maximum reaction rate is a systematic error and is

caused by gas switching [44]. Therefore, in this study, a lower limit of carbon conversion-10%- was selected for fitted experimental data from the TGA. Moreover, at a high conversion, char reactivity is reduced by factors such as annealing, a decrease of pore size, and deactivation of the inherent inorganic species [45], and the experimental TGA data starts to deviate from the ideality of the models. Therefore, an upper limit of carbon conversion of 60% was also chosen for the experimental TGA data.

9.3.2 Model fit

The four models were tested for MD and YL chars with the particle sizes of 20-38 μm and 90-106 μm by comparing with the experimental TGA data at 900 °C and 1000° C. Table 9.1 shows the summarized kinetic and empirical parameters of four models by fitting the experimental TGA data. A bad fit of the GM and VM was found for experimental data of MD and YL chars with a relatively low value of R^2 (0.88- 0.98) between experimental and model prediction. By contrast, the MVM and RPM were both found to quite fit for the different particle sizes of MD and YL chars at 900°C and 1000°C, and the R^2 was in the range of 0.99-1. The MVM was chosen to be further assessed for MD and YL chars at a wider temperature range of 750 -1100 °C.

The correlation between the MVM results and the experimental data of YL and MD chars at various temperatures is shown in Figure 9.5. As evident, the model shows a high correlation (R^2 >0.994) with the experimental data of YL and MD chars from 750 °C to 1100 °C, indicating that the MVM is applicable for both YL and MD chars. The kinetic constants based on the MVM were calculated and is presented in the following section.

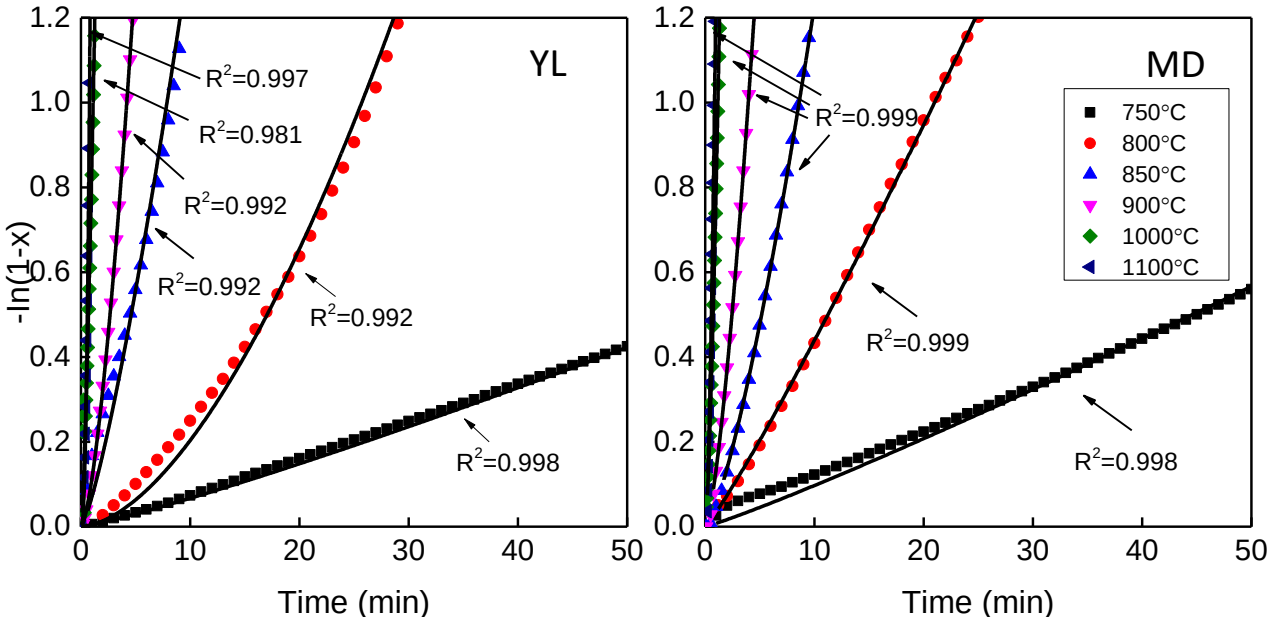

Figure 9.5: Fit of the modified volumetric model to the experimental data of YL and MD chars at various temperatures.

Table 9.1: Summarized kinetic and empirical parameters for the GM, VM, MVM, and RPM kinetic model for Maddingley and Yallourn coal

Sample	Temp./ °C	Particle size./ µm	GM		VM		MVM				RPM		
			K/min^{-1}	R^2/-	K/min^{-1}	R^2/-	a/-	b/-	K/min^{-1}	R^2/-	Ψ	K/min^{-1}	R^2/-
Maddingley	900	20-38	0.265	0.987	0.329	0.954	0.195	1.397	0.380	0.999	3.69	0.207	0.997
	900	90-106	0.219	0.977	0.272	0.939	0.130	1.489	0.333	0.999	2.88	0.171	0.991
	1000	20-38	0.969	0.982	1.174	0.972	1.184	1.203	1.307	0.994	53.65	0.181	0.990
	1000	90-106	0.719	0.961	0.943	0.931	0.819	1.451	1.206	0.999	14.09	0.351	0.999
Yallourn	900	20-38	0.246	0.997	0.310	0.968	0.271	1.035	0.273	0.990	2.35	0.206	0.993
	900	90-106	0.195	0.963	0.254	0.919	0.119	1.479	0.312	1.000	6.39	0.126	0.995
	1000	20-38	0.947	0.924	1.250	0.878	1.232	1.535	1.001	0.993	32.69	0.340	0.997
	1000	90-106	0.739	0.976	0.956	0.942	0.845	1.063	1.161	0.997	6.19	0.481	0.999

9.4 Analysis of kinetic parameters using the MVM

The char gasification rate can be expressed as an nth order reaction rate equation, following the Arrhenius relationship:

$$k = A_0 \exp(-\frac{E_a}{RT}) P^n \quad \text{(E 9.10)}$$

where A_0 is a pre-exponential factor, E_a is the activation energy, R is the gas constant, T is the temperature, P is the partial pressure of the gasifying agent, and n is the reaction order. The activation energy (E_a) represents the minimum energy required to initiate a particular chemical reaction. The pre-exponential factor (A_0) is a constant accounting for collision frequency. It can be seen from equation (E 9.10) that higher pre-exponential factor and lower activation energy results in a higher gasification rate.

Based on the MVM, the k_{MVM} of YL and MD chars at different temperatures was calculated by using the equations (E 9.5) –(E 9.7) to plot the Arrhenius relationship of Ink verse 1/T, shown in Figure 9.6. A_0 and E_a is determined by the y-intercept and the slope of the trend line. As seen, the gasification rate of the TGA YL and MD chars showed a good linear correlation at low temperatures of 750-1000 °C, indicating the temperature range is under the Regime I (chemical reaction controlled zone) and the determined kinetics under 1000 °C is the true kinetics as we intend. It was found that the transition between Regime I and II happened at 1000-1050 °C where the gradient of trend lines was observed to change.

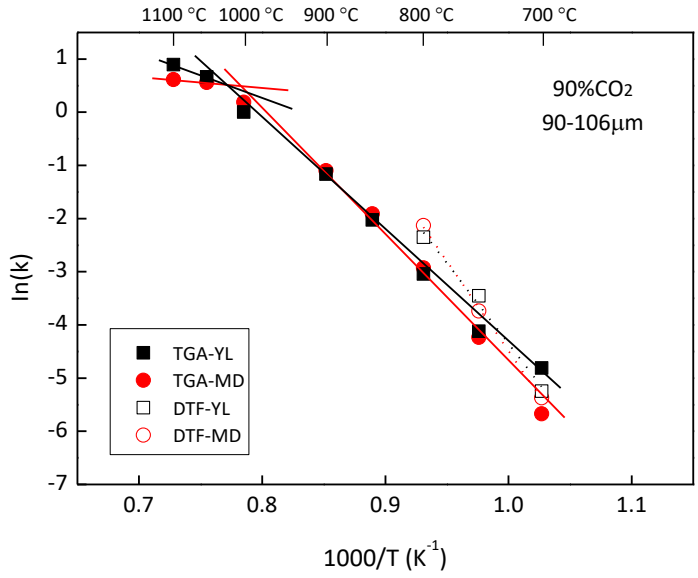

Figure 9.6: Arrhenius plots of the gasification reaction rate of TGA and EFR chars of YL and MD.

The analogous experiments were carried out at 800 °C with various CO_2 concentration to determine the reaction order (n) in equation (E 9.10). The gasification rate at different CO_2 concentrations is shown in Figure 9.7, and the reaction order is determined by the gradient of the linear trend. The calculated kinetic parameters - the activation energy, pre-exponential factor, and reaction order – are presented in Table 9.2 and discussed in the following.

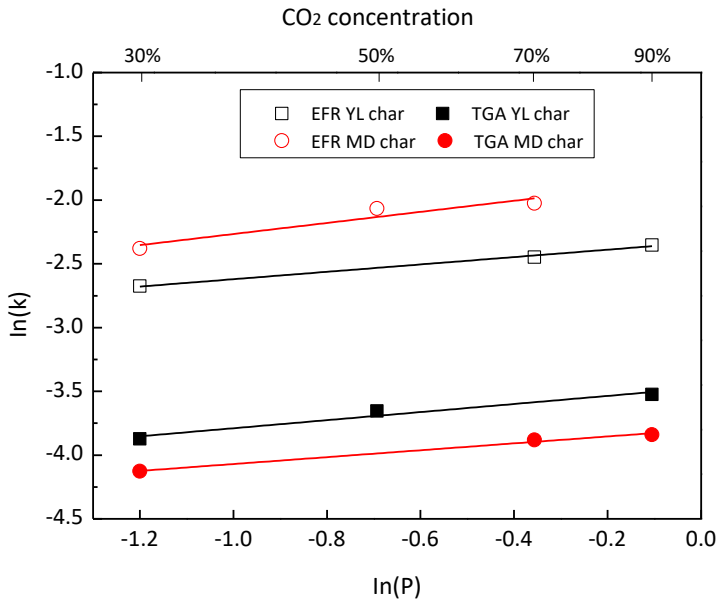

Figure 9.7: Effect of CO_2 concentration on char gasification rate at 800 °C

Table 9.2: Kinetic parameters of TGA and EFR chars using the MVM

Fuel	Char sample	Activation energy (Ea, kJ/mol)	Pre-exponential (A_0,min^{-1})	Reaction order (n)	Regime I to II transition (°C)
Maddingley	*TGA char*				
	90-106µm	219.79	2.27E+09	0.27	1000-1050
	20-38 µm	220.02	2.74E+09	n.d.	1000-1050
	EFR char				
	90-106 µm	281.78	5.85E+12	0.43	1000-1050
Yallourn	*TGA char*				
	90-106 µm	197.76	1.99E+08	0.32	1000-1050
	20-38 µm	208.89	5.62E+08	n.d.	1000-1050
	EFR char				
	90-106 µm	252.64	2.02E+11	0.29	1000-1050

n.d.: not determined

As seen, the decreasing particle size of MD and YL chars resulted in a slight increase in the activation energy and a significant increase in pre-exponential factor. For MD and YL chars prepared

in the TGA, the activation energy slightly increased by 1.7 kJ /mol and 9.1 kJ /mol with the particle size decreased from 90-106 μm to 20-38 μm, possibly due to the distribution of the inorganic species. Conversely, the pre-exponential factor significantly increased with the decrease of the particle size, indicating the increase rate of solid-gas interaction happened during gasification and lead to a higher gasification rate. This explains why smaller particles are more reactive in Figure 9.3. The findings have an agreement with Tanner's study on Victorian brown coal char which reported the slight increase of the activation energy and the dramatic increase of pre-exponential factor with the decreasing particle size [45].

At a particular particle size as 90-106 μm, the EFR char showed a greater gasification rate than the TGA char. As evident, compared to the TGA char, the pre-exponential factor of the EFR char was much greater, which increased gasification rate even though its activation energy was slightly bigger. Chars prepared in the EFR experience higher heating rate and higher steric factors and therefore obtain higher surface area and more carbon active sites, which may result in a greater pre-exponential factor and therefore, a higher gasification rate. The results demonstrated that the char preparation reactors had a significant effect on the char reactivity during CO_2 gasification.

By comparing YL and MD chars at a particular particle size, it was found that for TGA chars, the MD had higher char-CO_2 gasification reactivity than the YL; but for EFR chars, the YL and MD had similar reactivity. These order of the gasification reactivity corresponded to the order of the pre-exponential factor. As the pre-exponential factor is affected by the surface area, porosity and catalytic inorganic components within the char sample, it indicates that the gasification reactivity of the two chars is determined by a combination of these factors. Compared with reported kinetic parameters of other Victorian brow coal chars, it was found that the MD char had the highest reactivity, followed by the MW and YL char , and then the LY char [45].

The reaction order for the CO_2 concentration was determined for the TGA and EFR chars with a particle size of 90-106 μm. As evident, the reaction order, n, for all samples was similar, ranged from 0.27 to 0.43. The positive value of n indicated that the increasing CO_2 concentration increased the gasification rate. When gasification performed at atmospheric pressure ($0<n<1$), higher reaction order also resulted in a lower gasification rate. The results agreed with the previous study which reported that YL chars had a reaction order of 0.48 [45].

In the light of equations (E 9.4) and (E 9.5), the gasification rate based on the modified volumetric model can be explained as follows:

$$\frac{dx}{dt} = A_0 \exp(-\frac{E_a}{RT}) P^n (1 - \mathrm{x}) \quad \text{(E 9.11)}$$

The calculated kinetic parameters in Table 9.2 can be used for the above equation to predict the gasification rate at a particular residence time, temperature, and CO_2 concentration at atmospheric pressure. However, the kinetic parameters were calculated by using the experimental TGA data and the MVM, the validation of the equation using these parameters for entrained flow gasification is still unclear. Hence, the proposed equation (E 9.11) was evaluated for the gasification in the entrained flow reactor (EFR), by comparing the predicted modelling results with experimental entrained flow gasification data (in Chapter 5 and 6), and the results are presented in the following section.

9.5 Model application and evaluation for the EFR

This section evaluates the proposed model expression by using the experimental results in the EFR (Chapter 5 and 6) to verify the validation of the numeric equation for the char gasification in an entrained flow reactor.

It has been stated by many studies that the most common expression for the gasification rate is as follows [58, 59]:

$$\frac{dx}{dt} = \mathrm{k}(1 - \mathrm{x}) \quad \text{(E 9.12)}$$

$$1 - \mathrm{X} = \exp(-\mathrm{kt}) \quad \text{(E 9.13)}$$

$$\mathrm{X} = 1 - \exp(-\mathrm{kt}) \quad \text{(E 9.14)}$$

where k is the normalized gasification rate, t is the time, X is the carbon conversion. In the light of equation (E 9.13), the experimental results of low-temperature entrained flow gasification at 1000 ℃ (in Chapter 5) were firstly plotted in terms of (1-X) verse time, and the experimental gasification rates (K_{EFR}) of YL and MD chars were then determined by fitting an exponential curve, seen in Figure 9.8.

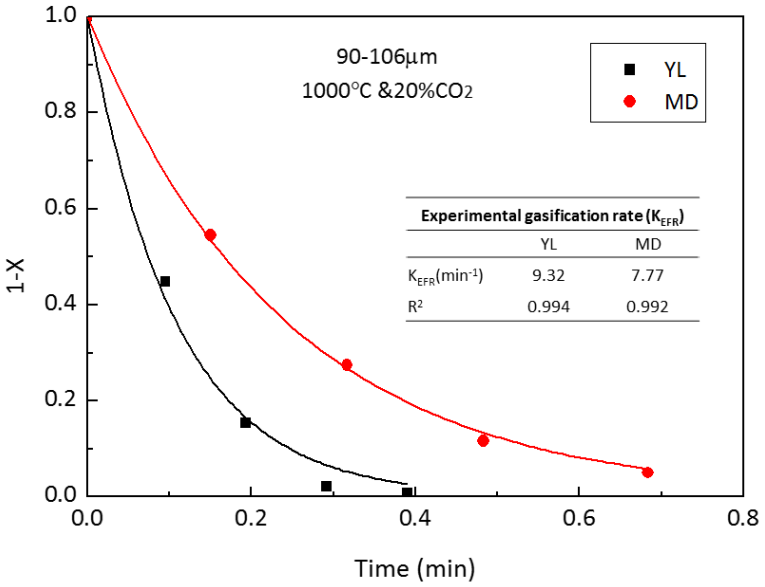

Figure 9.8: The experimental results of low-temperature entrained flow gasification of YL and MD chars at 1000 °C

The corresponding modelling gasification rates were also calculated and presented in Table 9.3, by using equation (E 9.11) and kinetic constants from Table 9.2 and the literature determined by the TGA. As can be seen, the modelling gasification rate using the kinetic parameters of EFR chars was quite similar to the experimental one. By contrast, the modelling gasification rate using the kinetic parameters of TGA chars, calculated by the MVM and RPM, was much lower than the experimental one. The results indicated that the kinetics parameters of the EFR char are more applicable for predicting the gasification rate in the EFR than that of the TGA char. The results also demonstrate that the proposed equation (E 9.11) can be used to predict the gasification rate of YL and MD chars in the EFR at 1000 °C by using the kinetic parameters of the EFR char.

Table 9.3: The experimental and modelling gasification rate (k) at 1000 °C and 20% CO_2

Items	YL	MD
k-experimental	9.32	7.77
k_{MVM}-EFR	8.039991	8.04E+00
k_{MVM}-TGA	0.732973	1.09E+00
k_{RPM}-TGA*	0.720151	n.d.

n.d.: not determined, *: calculated by using the kinetic constants from Tanner's study [91]

In practice, the carbon conversion of coal/char gasification, which represents the conversion efficiency, is more widely used. According to equation (E 9.14), the carbon conversion is expressed and determined by the gasification rate (k) and time (t). Therefore, the experimental and modelling gasification rates were used for equation (E 9.14) to compare the corresponding carbon conversions at 1000 °C and various residence times, seen in Figure 9.9. It is clear that the modelling results of the

EFR char, based on the modified volumetric model, was able to match with the experimental gasification data in the EFR at 1000 °C. The results demonstrate that the proposed equation (E 9.11) can be used to predict the carbon conversion of YL and MD chars in the EFR at 1000 °C with various residence time by using the kinetic constants of the EFR char. Therefore, the proposed equation was further examined to predict the carbon conversion of YL and MD chars at various temperatures from low (800 °C) to high (1400 °C), by using the kinetic constants of the EFR char.

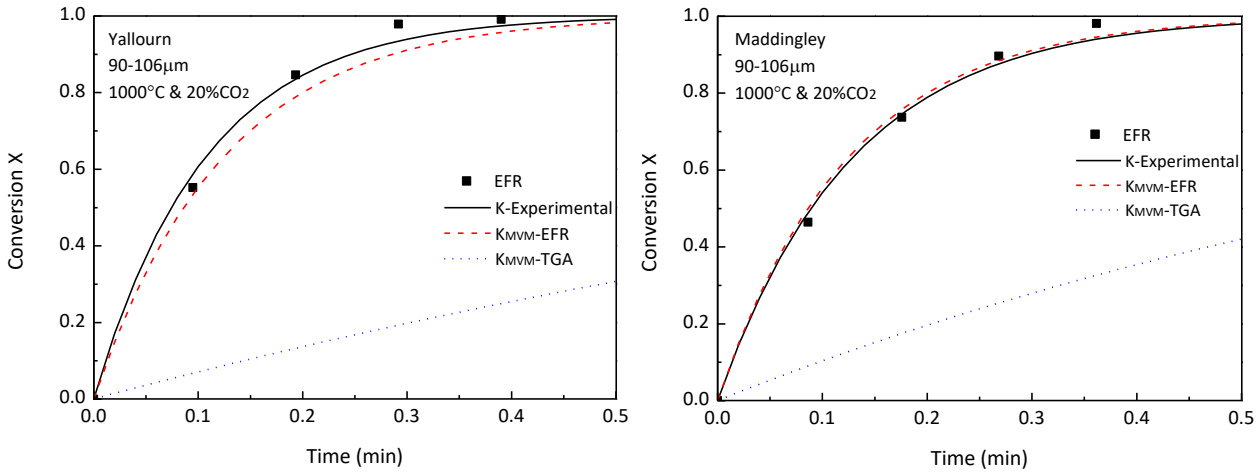

Figure 9.9: The comparison of experimental and modelling results on the gasification conversion of YL and MD chars at 1000 °C and 20%CO_2.

The experimental and estimated carbon conversions of YL and MD chars at 800-1400 °C and 20% CO_2 with a residence time of about 7 s are shown in Table 9.4. The experimental carbon conversion at 800-1000 °C was generated by low-temperature entrained flow gasification (Chapter 5) and the carbon conversion at 1200-1400 °C was generated by high-temperature entrained flow gasification (Chapter 6). The corresponding estimated carbon conversion was calculated by equations (E 9.11) and (E 9.14) using the kinetic constants of the EFR char based on the modified volumetric model. As evident, at high temperature (1000-1400 °C), the estimated carbon conversions quite matched the experimental carbon conversions. In contrast, at low temperature (800-900 °C), the estimated carbon conversions is much lower than the experimental ones. This is because that at low temperatures, the pre-exponential factor determined by the TGA was much lower than that of the EFR, which is a result of the significantly detrimental effect of the internal diffusion resistance on the kinetics determination of the TGA [46, 92]. However, this detrimental diffusion effect reduced and became negligible at high temperatures above 1000 °C in the TGA, so the experimental and modelling results came closer to match at 1000-1400 °C.

Table 9.4: Experimental and estimated carbon conversion at various temperatures and 20% CO_2

Temperature (ºC)	YL		MD	
	Experimental carbon conversion (%)	Estimated carbon conversion (%)	Experimental carbon conversion (%)	Estimated carbon conversion (%)
800	23.85	1.18	9.84	1.30
900	25.38	12.42	21.52	17.61
1000	55.19	59.89	55.60	60.85
1200	99.23	99.96	95.28	100
1400	99.93	100	99.07	100

Therefore, it can be concluded that the proposed mathematical model (E 9.11) is applicable for CO_2 gasification in the EFR at 1000-1400 °C. The carbon conversion of Victorian brown coal chars in the entrained flow reactor can be estimated by the following equation and kinetic parameters, shown in Table 9.5.

Table 9.5: Carbon conversion equation and kinetic parameters for the equation

$X = 1 - \exp\left[-A_0 \exp(-\frac{E_a}{RT}) P^n t\right]$	YL char	MD char
Reaction order, n	0.29	0.43
Activation energy, E_a (kJ/mol)	252.64	281.78
Pre-exponential factor, A_0, (min^{-1})	2.02 E+11	4.85E+12

9.6 Chapter summary

In this chapter, an investigation on the kinetics of CO_2 gasification of Victorian brown coal chars regarding influence factors (temperature, CO_2 concentration, particle size, and pyrolysis reactors) and reaction models is presented. It was found that the gasification conversion rate increased with increasing temperature and CO_2 concentration, and decreasing particle size. Char prepared in the entrained flow reactor was observed to have a higher reactivity than that of the thermogravimetric analyzer at the same temperature.

Four reaction models (the VM, GM, MVM, and RPM) were selected and employed for the experimental TGA data of YL and MD chars. The validation of MVM and RPM was found for both chars with different particle sizes at 900 °C and 1000 °C but the VM and GM were not. The MVM also demonstrated its validation for two chars at various temperatures from 750 °C to 1100 °C.

Based on the MVM, the kinetic parameters of YL and MD chars were calculated using the experimental TGA data. It was found the activation energy of all samples was similar and the gasification rate of the sample was strongly dependent on the pre-exponential factor. Because of a much higher pre-exponential factor, the EFR char achieved higher gasification rate than that of the TGA char. Small particles had a higher pre-exponential factor and became more reactive, but different size particles achieved a similar gasification rate, indicating that the effect of particle size on gasification rate was very limited. The order of increasing char-CO_2 gasification reactivity of the two chars was found to be Maddingley > Yallourn. Based on the MVM and Arrhenius equation, a numeric model was proposed to predict the gasification rate of YL and MD chars under entrained flow gasification.

After comparing with the EFR experimental data in Chapter 5 and 6, it was found that the proposed model was applicable for the entrained flow gasifier to predict the carbon conversion of YL and MD chars at 1000-1400 °C, by using the kinetic parameters of the EFR char based on the MVM and TGA experiments. This model offers a useful mathematical equation for the industry to estimate the conversion behaviour of Victorian brown coals against time in an entrained flow gasifier without any experiments or operation.

Chapter 10 Conclusions and recommendations for future work

This study has focused on the entrained flow pyrolysis and gasification of Victorian brown coals in CO_2 to better understand the gasification performance, emission of air pollutants, and mineral transformation for a wide range of operating conditions such as temperature, residence time, and CO_2 concentration. Although there have been few studies (small to pilot scale) into the gasification of Victorian brown coal using fixed bed and fluidized bed gasifiers, only one study has investigated the entrained flow pyrolysis and gasification behaviour of one Victorian brown coal. This study provides for the first time a detailed investigation of entrained flow gasification of several Victorian brown coals using a combination of experimental and modelling approaches.

This study is divided into four main areas:

- an investigation of a range of temperature and reactant concentration influencing entrained flow gasification of Victorian brown coals regarding the gasification performance and emission of air pollutants (HCN, NH_3, H_2S),
- an investigation of mineral reactions and transformations during entrained flow pyrolysis and gasification of Victorian brown coals,
- a comparison of the entrained flow gasification behaviour of Victorian brown coal and biomass in respect of gasification performance, emission of air pollutants, and mineral transformation,
- the kinetic modelling of char-CO_2 gasification of Victorian brown coals using a validated reaction model and comparison with the experimental entrained flow gasification data.

The major conclusions from each of these areas are summarised in the following sections.

10.1 Gasification performance and emission of air pollutants

The gasification performance and emission of air pollutants of Victorian brown coals in an entrained flow reactor using CO_2 as the gasifying agent are mainly affected by five factors: total gas flow rate, residence time, temperature, CO_2 concentration and the gasification environment (direct using coal vs two-step by first pyrolysing the coal and then gasifying the char).

The effect of total gas flow rate on the gasification performance of Victorian brown coals is significant in terms of changing the mode of gas-particle contact. A lower total gas flow rate decreases the gas velocity (Ug) in the reactor. When Ug deceases below the solid particle velocity (Up) in the reactor, the mode of gas-particle contact in the reactor changes from gas-controlled

entrained flow to solid-controlled falling flow. Gasification under entrained flow condition (Ug > Up) achieves higher carbon conversion and higher CO gas yield than the gasification under falling flow condition (Ug < Up) even with a shorter residence time. This is because under entrained flow condition, fine particles are in constant contact with gaseous reactants and the solids flow with gas together.

The effect of residence time on the gasification performance is also significant as expected. An increasing residence time increases the carbon conversion and CO gas yield during CO_2 gasification. At 1000 °C, the residence time required for the complete conversion of the YL and MW chars (90-106 μm) is around 20 s, which is longer than the typical residence time for commercial applications (4-10s). Hence, it can be concluded that the entrained flow gasification of Victoria Brown coal needs to be carried out at a temperature above 1000°C to reduce the residence time for the conversion completion.

Temperature has a significant effect on gasification performance and emission of HCN. The higher temperature significantly increases carbon conversion and CO concentration in the product gas. Moreover, a higher temperature can largely decrease the residence time for 100% carbon conversion. The increasing temperature also increases the HCN emission during entrained flow gasification.

Additionally, the effect of CO_2 concentration on gasification performance and emission of HCN, NH_3, and H_2S is strong. The higher CO_2 concentration increases carbon conversion and CO concentration during CO_2 gasification possibly because of the increased gasification reactivity of char. A higher CO_2 concentration also decreases the emission of H_2S and HCN during entrained flow gasification.

The gasification process, direct and two-step gasification, has little effect on the overall carbon conversion but has a significant effect on the gas composition of the product gases. Compared to two-step gasification, direct gasification generates little H_2 and more CO in the product gases. Moreover, the decreased H_2 yield almost equals the increased CO yield. It is very likely that the reverse water-gas shift reaction occurs during direct gasification in which CO_2 reacts with H_2 from coal pyrolysis to form CO. The dry methane reforming is also very likely to occur during direct gasification in CO_2, considering the very little amount of CH_4 formed and the low moisture of feed coal (< 1%).

Coal gasification is divided into coal pyrolysis and char gasification. During entrained flow gasification of Victorian brown coals at 1000-1400 °C, pyrolysis plays a crucial role, contributing to

around 65% carbon conversion, 50-80% HCN emission and almost all H_2S emission. In contrast, char gasification results in around 35% carbon conversion, 20-50% HCN emission and very little H_2S emission.

Overall, entrained flow gasification achieves very high carbon conversion (~ 98%) for Victorian brown coals at 1200 °C with around 7s residence time for the particle size of 90-106 microns. No visible tar is found downstream of the entrained flow gasifier. There is also no NH_3 emission during the entrained flow gasification. However, the emission of HCN and H_2S is still high in the ppmv level.

10.2 Mineral transformation

Mineral reactions and transformations of Victorian brown coals during coal pyrolysis and char gasification happen at high temperatures (1000-1400 °C). The behaviour of mineral matter during coal pyrolysis and char gasification shows significant differences for parent fuels. During coal pyrolysis, SiO_2 decreases to form Al_2SiO_5 with SiO_2 in YL and MD chars. YL chars show the oxidation of Fe_3O_4 to form Fe_2O_3, but MD chars show the opposite trend, the increase of Fe_3O_4 and the decrease of Fe_2O_3 .

During char gasification, SiO_2 reacts with the CaO produced from the decomposition of $CaSO_4$ to form Ca_2SiO_4 in YL samples and $CaMgSiO_4$ in MD samples at 1200-1400 ºC. Interestingly, SiO_2 is the only major mineral phase in LY chars and gasification residues, and no significant mineral transformation takes place during coal pyrolysis and char gasification of LY. This study offers a better understanding of the mineral transformation and slag composition formed during entrained flow pyrolysis and gasification, which provides very important information for the design of an entrained flow gasifier to efficiently remove the slag generated during the operation.

10.3 Comparison of entrained flow gasification behaviour between Victorian brown coals and biomass

In this study, entrained flow gasification behaviour of Victorian brown coal (Loy Yang) was compared with one biomass (pine bark) by direct gasification of the fuels. The comparison of the two fuels is drawn in the gasification performance and pollutant gas emission. For Loy Yang coal and pine bark, they have similar carbon conversion at 1200 °C. The product gas of two fuels is CO-rich, and Victorian brown coal has a slightly higher syngas concentration than that of pine bark. The emission of air pollutants varies for the fuels. No NH_3 is detected for Victorian brown coal, and no

H_2S is detected for pine bark during entrained flow gasification in CO_2. This study offers a better understanding of the similarities and differences of entrained flow gasification behaviour between Victorian brown coals and pine bark. Thus, this study provides valuable information for industry to assess the co-gasification possibility of biomass and Victorian brown coal.

10.4 Kinetic modelling of char-CO_2 gasification of Victorian brown coals

Among the volumetric model (VM), grain model (GM) and the modified volumetric model (MVM), the MVM is valid for the TGA experimental data from gasification of Victorian brown coals, and the VM and GM are not. The smaller particle size increases gasification reactivity of Victorian brown coals through significantly increasing the pre-exponential factor. The chars generated in the EFR have higher reactivity than the chars generated in the TGA because of the higher pre-exponential factor. Maddingley coal also has higher reactivity rather than Yallourn coal, possibly because Maddingley coal has high Fe_2O_3 content in its ash which has positively catalytic effect on gasification reactivity.

The carbon conversion of YL and MD chars in an entrained flow reactor at 1000-1400 °C can be predicted by the following equation:

$$X = 1 - \exp\left[-A_0 \exp(-\frac{E_a}{RT}) P^n t\right]$$

where the reaction orders (n) of YL and MD chars are 0.29 and 0.43, respectively; the activation energy (E_a) of YL and MD are 252.6 kJ/mol and 281.8 kJ/mol, respectively; and the pre-exponential factors (A_0) of YL and MD are 2.02 E+11 min^{-1} and 5.85 E+12 min^{-1}, respectively.

10.5 Practical implications of this study

In this study, fundamental gasification data of Victorian brown coals are generated for industry to use in computational fluid dynamics model for an entrained flow gasifier using Victorian brown coals. Both direct and two-step gasification achieve similar high carbon conversion (~ 98%) for Victorian brown coals at 1200 °C. However, two-step gasification obtains a better H_2 /CO ratio (around 1:3) in the product gases than direct gasification, so it is more suitable for downstream synthesis of some chemicals. It is clear that 1200 °C temperature is sufficient to achieve high carbon conversion for the brown coals tested in this study for gasification using CO_2 up to 40% concentration.

This study also offers a better understanding of the similarities and differences of entrained flow gasification behaviour between Victorian brown coals and pine bark. Thus, this study provides valuable information for industry to assess the co-gasification possibility of biomass and Victorian brown coal. Moreover, this study provides a valuable mathematic model for predicting the carbon conversion of Victorian brown coals using an entrained flow reactor with CO_2 at 1000-1400 °C.

10.6 Recommendations for future work

Although this research has conducted experimental and modelling work on entrained flow gasification of Victorian brown coal, there is a number of areas where future work which should be done. Those are listed below.

10.6.1 Experimental

This project has investigated five major factors affecting coal gasification, but there are other important process variables have not been studied because of the limitation of the current facility. In particular,

(i) the effect of pressure on carbon conversion, gas composition, and mineral transformation at high temperature should be determined. It would also be useful to examine the effect of pressure on the gasification kinetics of Victorian brown coals by TGA,

(ii) the effect of residence time at high temperature (>1000 °C) should be investigated as a function of particle size with respect to the specsific surface area and pore size distribution.

Current research investigates the gasification kinetics of two Victorian brown coals, Yallourn and Maddingley, with CO_2. For a comprehensive study,

(iii) the kinetic experiments should be extended to other Victorian brown coals, Loy Yang. This would increase the understanding of the gasification reactivity of a range of Victoria brown coals.

(iv) the effect of steam, as one important gasifying agent, on the kinetics of gasification of Victorian brown coal/char should be studied using TGA. This could be done using the existing equipment by connecting the steam generator.

Based on the current research on entrained flow gasification of Victorian brown coal and of biomass,

(v) using the existing equipment, co-gasification of Victorian brown coal and biomass in CO_2 could be examined to understand the gasification efficiency and performance using a blend of fuels.

(vi) This study only investigated the carbon conversion and gaseous emissions. One important aspect of entrained flow gasification is the viscosity of slags at the bottom of the gasifier. A comprehensive database of the viscosity of the Victorian brown coal ashes should be developed.

10.6.2 Modelling

(i) The developed numerical model is based on the TGA and EFR data of two Victorian brown coals, Yallourn and Maddingley, so the model should be extended to other Victorian brown coal (Loy Yang). This would require further TGA and EFR experiments using the existing experimental equipment. The extra information would further validate and modify the model for entrained flow gasification of Victorian brow coals.

(ii) Current kinetic modelling mainly examines three reaction models: volumetric model, grain model, and modified volumetric model. In addition, the random pore model should be studied for Victorian brown coals to complete the evaluation.

(iii) The developed model is mainly based on TGA data. To obtain a more accurate prediction for entrained flow gasification, a numerical model based on the entrained flow gasification data should be developed. This will require the gasification data as a function of temperature (>1000 °C) and a wide range of residence time.

(iv) Current kinetics is based on isothermal reaction. Non- isothermal reaction kinetics should be studied to compare with current kinetic data.

References

[1] J. Tanner, S. Bhattacharya, Kinetics of CO2 and steam gasification of Victorian brown coal chars, Chem. Eng. J., 285 (2016) 331-340.

[2] D.M. Quyn, H. Wu, S.P. Bhattacharya, C.-Z. Li, Volatilisation and catalytic effects of alkali and alkaline earth metallic species during the pyrolysis and gasification of Victorian brown coal. Part II. Effects of chemical form and valence, Fuel, 81 (2002) 151-158.

[3] D.M. Quyn, H. Wu, C.-Z. Li, Volatilisation and catalytic effects of alkali and alkaline earth metallic species during the pyrolysis and gasification of Victorian brown coal. Part I. Volatilisation of Na and Cl from a set of NaCl-loaded samples, Fuel, 81 (2002) 143-149.

[4] H. Wu, D.M. Quyn, C.-Z. Li, Volatilisation and catalytic effects of alkali and alkaline earth metallic species during the pyrolysis and gasification of Victorian brown coal. Part III. The importance of the interactions between volatiles and char at high temperature, Fuel, 81 (2002) 1033-1039.

[5] D.P. Ross, C.A. Heidenreich, D.K. Zhang, Devolatilisation times of coal particles in a fluidised-bed, Fuel, 79 (2000) 873-883.

[6] J. Tanner, S. Bhattacharya, M. Bläsing, M. Müller, High-temperature pyrolysis and CO2 gasification of Victorian brown coal and Rhenish lignite in an entrained flow reactor, AlChE J., 62 (2016) 2101-2111.

[7] J. Yu, A. Tahmasebi, Y. Han, F. Yin, X. Li, A review on water in low rank coals: The existence, interaction with coal structure and effects on coal utilization, Fuel Process. Technol., 106 (2013) 9-20.

[8] BP, BP statistical review of world energy in, BP Global, https://www.bp.com/content/dam/bp/en/corporate/pdf/energy-economics/statistical-review-2017/bp-statistical-review-of-world-energy-2017-full-report.pdf, 2017, pp. 36-38.

[9] DPI, Victoria's energy future, in: D.o.P. Industries (Ed.), The State of Victoria Government, www.dpi.vic.gov.au/energyfuture, 2010.

[10] C.-Z. Li, Advances in the science of Victorian brown coal, 1 ed., Elsevier, 2004.

[11] B.a.I. Department of State Development, Brown coal-Victoria, Australia: a principal brown coal province, in, Department of State Development, Business and Innovation, http://www.energyandresources.vic.gov.au/earth-resources/victorias-earth-resources/coal, 2014.

[12] S. Bhattacharya, K.B. Kabir, K. Hein, Dimethyl ether synthesis from Victorian brown coal through gasification - Current status, and research and development needs, Progress in Energy and Combustion Science, (2013) 1-29.

[13] P. G. J, A. D. J, K. L. T, The Chemical Characteristics of Victorian Brown Coal, in: The Chemistry of Low-Rank Coals, American Chemical Society, 1984, pp. 3-14.

[14] R.A. Durie, The Science of Victorian brown coal : structure, properties, and consequences for utilization, Oxford : Butterworth-Heinemann, Oxford, 1991.

[15] C. Higman, M. van der Burgt, Chapter 3 - The Kinetics of Gasification and Reactor Theory, in: Gasification (Second Edition) Gulf Professional Publishing, Burlington, 2008, pp. 91-191.

[16] C. Saha, S. Bhattacharya, Chemical looping combustion of low-ash and high-ash low rank coals using different metal oxides – A thermogravimetric analyser study, Fuel, 97 (2012) 137-150.

[17] H.-D. Schilling, Coal gasification : existing processes and new developments, Graham & Trotman London, 1981.

[18] G. Kovacik, Og, M. uztöreli, A. Chambers, B. Özüm, Equilibrium calculations in coal gasification, International Journal of Hydrogen Energy, 15 (1990) 125-131.

[19] H.D. Schilling, B. Bonn, U. Krauss, Coal gasification: existing processes and new developments, Graham and Trotham Ltd, London, UK, 1981.

[20] A. Kristiansen, Understanding Coal Gasification, in, IEA Coal Research, London, 1996.

[21] A. Williams, M. Pourkashanian, J.M. Jones, N. Skorupska, Combustion and Gasification of Coal, Taylor & Francis, New York, 2000.

[22] R. D'Aquino, From coal to chemicals, Chemical Engineering Progress, 99 (2003) 11-11.

[23] G. Ondrey, Coal-to-chemicals: this may be coal's decade, as the number of gasification projects skyrockets, Chemical engineering, 118 (2011) 16-20.

[24] I. Wender, Reactions of synthesis gas, Fuel Processing Technology, 48 (1996) 189-297.
[25] W.t.E. Systems, Syn-gas: a versatile and renewable fuel, in: Gasification, Waste to Energy Systems

2015.
[26] H. Timmermann, Mk Plus™: The Next Generation Lurgi FBDB™ Gasification, in: 5th International Freiberg Conference on IGCC & XtL Technologies, Leipzig, Germany, 2012.
[27] C. Higman, S. Tam, Advances in Coal Gasification, Hydrogenation, and Gas Treating for the Production of Chemicals and Fuels, Chem. Rev., 114 (2013) 1673-1708.
[28] D.J. Harris, D.G. Roberts, ANLECR&D Scoping Study: Black Coal IGCC, in, CSIRO Energy Technology, 2010.
[29] M. Gräbner, B. Meyer, Introduction of a Ternary Diagram for Comprehensive Evaluation of Gasification Processes for High Ash Coals, in: 2011 International Conference on Coal Science and Technology, Oviedo, Spain, 2011.
[30] A. Lowe, L. Juniper, D.J. Harris, N. Simento, CCSD Coal Utilisation Compendium, CRC for Coal in Sustainable Devleopment, 2008.
[31] Y. Ishibashi, O. Shinada, First Year Operation Results of CCP's Nakoso 250 MW Air-Blown IGCC Demonstration Plant, in: Gasification Technologies Conference, Washington DC, 2008.
[32] C. Higman, M. van der Burgt, Gasification, 2nd ed., Gulf Professional Publications, Burlington, MA, 2008.
[33] F. Kapteijn, R. Meijer, J.A. Moulijn, Transient kinetic techniques for detailed insight in gas·solid reactions, Energy and Fuels, 6 (1992) 494 - 497.
[34] N.M. Laurendeau, Heterogeneous kinetics of coal char gasification and combustion, Progress in Energy and Combustion Science, 4 (1978) 221-270.
[35] P.L. Walker Jr., F. Rusinko Jr., L.G. Austin, Gas reactions of carbon, in: D.D. Eley, P.W. Selwood, P.B. Weisz (Eds.) Advances in Catalysts: Volume XI, Academic Press, New York, 1959, pp. 133-221.
[36] S. Ergun, Kinetics of the reactions of carbon dioxide and steam with coke, U.S. Bureau of Mines Bulletin, 598 (1962) 37.
[37] J. Gadsby, F.J. Long, P. Sleightholm, K.W. Sykes, The mechanism of the carbon dioxide-carbon reaction, Proceeding of the Royal Society (London), series A., A193 (1948) 357-376.
[38] S. Ergun, M. Mentser, A study of the carbon dioxide-carbon reaction by oxygen exchange, Bureau of Mines, Bulletin 664 (1973).
[39] P.L. Walker, F. Rusinko, L.G. Austin, Gas Reactions of Carbon, Advances in Catalysis, 11 (1959) 133-221.
[40] C. Higman, M. van der Burgt, Chapter 3 - The Kinetics of Gasification and Reactor Theory, in: Gasification (Second Edition), Gulf Professional Publishing, Burlington, 2008, pp. 33-45.
[41] I.W. Smith, The combustion rates of coal chars: a review, Proceedings of the Combustion Institute, 19 (1982) 1045 - 1065.
[42] J. Adánez, J. Miranda, J. Gavilán, Kinetics of a lignite-char gasification by CO2, Fuel, 64 (1985) 801-804.
[43] S. Kasaoka, Y. Sakata, C. Tong, Kinetic evaluation of the reactivity of various coal chars for gasification with carbon dioxide in comparison with steam, Int. Chem. Eng.; (United States), (1985) Medium: X; Size: Pages: 160-175.
[44] A. Gomez, R. Silbermann, N. Mahinpey, A comprehensive experimental procedure for CO2 coal gasification: Is there really a maximum reaction rate?, Applied Energy, 124 (2014) 73-81.
[45] IEA, Coal market outlook, in: World Energy Outlook 2016, IEA, 2016, pp. 203-239.
[46] P. Ollero, A. Serrera, R. Arjona, S. Alcantarilla, Diffusional effects in TGA gasification experiments for kinetic determination, Fuel, 81 (2002) 1989-2000.
[47] M.F. Irfan, M.R. Usman, K. Kusakabe, Coal gasification in CO2 atmosphere and its kinetics since 1948: A brief review, Energy, 36 (2011) 12-40.
[48] T.-W. Kwon, S.D. Kim, D.P.C. Fung, Reaction kinetics of char-CO_2 gasification, Fuel, 67 (1988) 530 - 535.
[49] G.Ö. Çakal, H. Yücel, A.G. Gürüz, Physical and chemical properties of selected Turkish lignites and their pyrolysis and gasification rates determined by thermogravimetric analysis, J. Anal. Appl. Pyrolysis, 80 (2007) 262-268.
[50] L. Shufen, S. Ruizheng, Kinetic studies of a lignite char pressurized gasification with CO2, H2 and steam, Fuel, 73 (1994) 413-416.
[51] K. Osafune, H. Marsh, Gasification kinetics of coal chars in carbon dioxide, Fuel, 67 (1988) 384 - 388.

[52] K. Asami, P. Sears, E. Furimsky, Y. Ohtsuka, Gasification of brown coal and char with carbon dioxide in the presence of finely dispersed iron catalysts, Fuel Processing Technology, 47 (1996) 139-151.
[53] D. Harris, I.W. Smith, Intrinsic reactivity of petroleum coke and brown coal char to carbon dioxide, steam and oxygen, Proceedings of the Combustion Institute, 23 (1990) 1185 - 1190.
[54] S. Kajitani, S. Hara, H. Matsuda, Gasification rate analysis of coal char with a pressurised drop tube furnace, Fuel, 81 (2002) 539 - 546.
[55] S. Dutta, C.Y. Wen, R.J. Belt, Reactivity of coal and char. 1. in carbon diozide atmosphere, Industrial & Engineering Chemistry Process Design and Development, 16 (1977) 20 - 30.
[56] S. Kajitani, N. Suzuki, M. Ashizawa, S. Hara, CO_2 gasification rate analysis of coal char in entrained flow coal gasifier, Fuel, 85 (2006) 163 - 169.
[57] S. Kajitani, N. Suzuki, M. Ashizawa, S. Hara, CO2 gasification rate analysis of coal char in entrained flow coal gasifier, Fuel, 85 (2006) 163-169.
[58] A. Molina, F. Mondragón, Reactivity of coal gasification with steam and CO2, Fuel, 77 (1998) 1831-1839.
[59] S. Dutta, C.Y. Wen, R.J. Belt, Reactivity of Coal and Char. 1. In Carbon Dioxide Atmosphere, Industrial & Engineering Chemistry Process Design and Development, 16 (1977) 20-30.
[60] J.Y. Park, O. Levenspiel, The crackling core model for the reaction of solid particles, Chem. Eng. Sci., 30 (1975) 1207-1214.
[61] S.K. Bhatia, D.D. Perlmutter, A random pore model for fluid-solid reactions: I. Isothermal, kinetic control, AlChE J., 26 (1980) 379-386.
[62] S. Kasaoka, Y. Sakata, M. Shimada, Effects of coal carbonization conditions on rate of steam gasification of char, Fuel, 66 (1987) 697-701.
[63] T. Adschiri, T. Shiraha, T. Kojima, T. Furusawa, Prediction of CO2 gasification rate of char in fluidized bed gasifier, Fuel, 65 (1986) 1688-1693.
[64] K. Raghunathan, R.Y.K. Yang, Unification of coal gasification data and its applications, Industrial & Engineering Chemistry Research, 28 (1989) 518-523.
[65] D.-K. Zhang, A. Poeze, Variation of sodium forms and char reactivity during gasification of a South Australian low-rank coal, Proc. Comb. Inst., 28 (2000) 2337-2344.
[66] P.J. Ashman, A. Kosminski, S. Button, P. Mullinger, Gasification of Victorian lignite in a laboratory scale fluidised bed gasifier, in: 5th Asia-Pacific Conference on Combustion, 2005.
[67] L. Mckenzie, Formation of NO_X and NO_X precursors during the gasification of Victorian brown coal, in: CRC Annual Report 2004-2005, Cooperative Research Center for Clean Power from Lignite, 2004.
[68] J. Yu, C.-Z. Li, Catalytic gasification of Victorian brown coal-char-supported Nano iron catalyst for water-gas-shift reaction and hydrogen production in: CRC Annual Report 2005-2006, Cooperative Research Center for Clean Power from Lignite, 2005.
[69] S.P. Bhattacharya, Fluidized Bed Pyrolysis and Gasification Tests at the University of North Dakota Using Victorian Low-Rank Coal, in, 1999.
[70] S. Bhattacharya, Comparison of gasification of Australian brown coal and North Dakota lignit in a transport reactor, in: CRC Anuual Report 2006-2007, Cooperative Research Center for Clean Power from Lignite, 2006.
[71] S.P. Bhattacharya, Gasification Performance of Australian Lignites in a Pressurized Fluidized Bed Gasifier Process Development Unit Under Air and Oxygen-enriched Air Blown Conditions, Process Safety and Environmental Protection, 84 (2006) 453-460.
[72] J. Tanner, M. Bläsing, M. Müller, S. Bhattacharya, Influence of Temperature on the Release of Inorganic Species from Victorian Brown Coals and German Lignites under CO2 Gasification Conditions, Energy & Fuels, 28 (2014) 6289-6298.
[73] J. Tanner, M. Bläsing, M. Müller, S. Bhattacharya, The temperature-dependent release of volatile inorganic species from Victorian brown coals and German lignites under CO2 and H2O gasification conditions, Fuel, 158 (2015) 72-80.
[74] J. Tanner, K.B. Kabir, M. Müller, S. Bhattacharya, Low temperature entrained flow pyrolysis and gasification of a Victorian brown coal, Fuel, 154 (2015) 107-113.

[75] E.I. Koytsoumpa, K. Atsonios, K.D. Panopoulos, S. Karellas, E. Kakaras, J. Karl, Modelling and assessment of acid gas removal processes in coal-derived SNG production, Appl. Therm. Eng., 74 (2015) 128-135.
[76] B.G. Miller, Clean Coal Engineering Technology, in, Elsevier, pp. 198-216.
[77] L. Zhang, E. Binner, Y. Qiao, C.-Z. Li, High-Speed Camera Observation of Coal Combustion in Air and O2/CO2 Mixtures and Measurement of Burning Coal Particle Velocity†, Energy & Fuels, 24 (2009) 29-37.
[78] BP Statistical Review of World Energy 2010, in: ENP Newswire, 2010.
[79] M. Ottaway, Use of thermogravimetry for proximate analysis of coals and cokes, Fuel, 61 (1982) 713-716.
[80] L. Lu, V. Sahajwalla, C. Kong, D. Harris, Quantitative X-ray diffraction analysis and its application to various coals, Carbon, 39 (2001) 1821-1833.
[81] S.P. Bhattacharya, M. Harttig, Control of Agglomeration and Defluidization Burning High-Alkali, High-Sulfur Lignites in a Small Fluidized Bed CombustorEffect of Additive Size and Type, and the Role of Calcium, Energy & Fuels, 17 (2003) 1014-1021.
[82] H.H. Schobert, Chapter 6 Behavior of inorganic components of lignites, Coal Science and Technology, 23 (1995) 290-342.
[83] J.C. Nankervis, R.B. Furlong, Phase changes in mineral matter of North Dakota lignites caused by heating to 1200 °C, Fuel, 59 (1980) 425-430.
[84] B. Phillips, S. SÕMiya, A. Muan, Melting Relations of Magnesium Oxide-Iron Oxide Mixtures in Air, J. Am. Ceram. Soc., 44 (1961) 167-169.
[85] Y. Ohtsuka, Y. Tamai, A. Tomita, Iron-catalyzed gasification of brown coal at low temperatures, Energy & Fuels, 1 (1987) 32-36.
[86] T. Suzuki, M. Mishima, T. Takahashi, Y. Watanabe, Catalytic steam gasification of Yallourn coal using sodium hydridotetracarbonyl ferrate, Fuel, 64 (1985) 661-665.
[87] D. Sutton, B. Kelleher, J.R.H. Ross, Review of literature on catalysts for biomass gasification, Fuel Process. Technol., 73 (2001) 155-173.
[88] S. Bhattacharya, S. Pipatmanomai, A. Luxsanayotin, Effect of mineral oxides on slag formation tendency of Mae Moh lignites, 2010.
[89] M. Tomaszewicz, G. Łabojko, G. Tomaszewicz, M. Kotyczka-Morańska, The kinetics of CO2 gasification of coal chars, J. Therm. Anal. Calorim., 113 (2013) 1327-1335.
[90] W. Zhu, W. Song, W. Lin, Effect of the Coal Particle Size on Pyrolysis and Char Reactivity for Two Types of Coal and Demineralized Coal, Energy & Fuels, 22 (2008) 2482-2487.
[91] F. Bustamante, R.M. Enick, A.V. Cugini, R.P. Killmeyer, B.H. Howard, K.S. Rothenberger, M.V. Ciocco, B.D. Morreale, S. Chattopadhyay, S. Shi, High-temperature kinetics of the homogeneous reverse water–gas shift reaction, AlChE J., 50 (2004) 1028-1041.
[92] A. Gómez-Barea, P. Ollero, R. Arjona, Reaction-diffusion model of TGA gasification experiments for estimating diffusional effects, Fuel, 84 (2005) 1695-1704.